# Tribological characterization of greased drive-shaft : Evaluation of constant velocity joint durability

Valentin Ripard

N°d'ordre NNT : 2019LYSEI083

**THESE de DOCTORAT DE L'UNIVERSITE DE LYON**
opérée au sein de
**INSA Lyon**

**Ecole Doctorale MEGA** N°EDA 162
**Mécanique, Energétique, Génie Civil, Acoustique**

**Spécialité : Génie mécanique**

Soutenue publiquement le 25/10/2019, par :
**Valentin RIPARD**

# Tribological characterization of greased drive-shaft: evaluation of constant velocity joint durability

Devant le jury composé de :

| | | | |
|---|---|---|---|
| SEABRA, Jorge | Professeur | University of Porto | Président du jury |
| FABRE, Agnès | Maitre de Conférences HDR | ENSAM Aix en provence | Rapporteure |
| MASSI, Francesco | Professeur | SAPIENZA – Universita Di Roma | Rapporteur |
| MINFRAY, Clotilde | Maitre de Conférences HDR | Centrale Lyon | Examinatrice |
| VILLE, Fabrice | Professeur | INSA Lyon | Directeur de thèse |
| DASSENOY, Fabrice | Professeur | Centrale Lyon | Co-directeur de thèse |
| RUZEK, Michal | Maitre de Conférences | INSA Lyon | Invité |
| CHARLES, Pierre | Docteur | GROUPE PSA | Invité |

## Département FEDORA–INSA Lyon - Ecoles Doctorales–Quinquennal 2016-2020

| SIGLE | ECOLE DOCTORALE | NOM ET COORDONNEES DU RESPONSABLE |
|---|---|---|
| **CHIMIE** | **CHIMIE DE LYON**<br>**http://www.edchimie-lyon.fr** Sec. :<br>Renée EL MELHEM<br>Bât. Blaise PASCAL, 3e étage<br>secretariat@edchimie-lyon.fr<br>INSA : R. GOURDON | M. Stéphane DANIELE<br>Institut de recherches sur la catalyse et l'environnement de Lyon<br>IRCELYON-UMR 5256<br>Équipe CDFA<br>2 Avenue Albert EINSTEIN<br>69 626 Villeurbanne CEDEX<br>directeur@edchimie-lyon.fr |
| **E.E.A.** | **ÉLECTRONIQUE, ÉLECTROTECHNIQUE, AUTOMATIQUE**<br>**http://edeea.ec-lyon.fr**<br>Sec. : M.C. HAVGOUDOUKIAN<br>ecole-doctorale.eea@ec-lyon.fr | M. Gérard SCORLETTI<br>École Centrale de Lyon<br>36 Avenue Guy DE COLLONGUE<br>69 134 Écully<br>Tél : 04.72.18.60.97 Fax 04.78.43.37.17<br>gerard.scorletti@ec-lyon.fr |
| **E2M2** | **ÉVOLUTION, ÉCOSYSTÈME, MICROBIOLOGIE, MODÉLISATION**<br>**http://e2m2.universite-lyon.fr**<br>Sec. : Sylvie ROBERJOT<br>Bât. Atrium, UCB Lyon 1<br>Tél : 04.72.44.83.62<br>INSA : H. CHARLES<br>secretariat.e2m2@univ-lyon1.fr | M. Philippe NORMAND<br>UMR 5557 Lab. d'Ecologie Microbienne<br>Université Claude Bernard Lyon 1<br>Bâtiment Mendel<br>43, boulevard du 11 Novembre 1918<br>69 622 Villeurbanne CEDEX<br>philippe.normand@univ-lyon1.fr |
| **EDISS** | **INTERDISCIPLINAIRE SCIENCES-SANTÉ**<br>http://www.ediss-lyon.fr<br>Sec. : Sylvie ROBERJOT<br>Bât. Atrium, UCB Lyon 1<br>Tél : 04.72.44.83.62<br>INSA : M. LAGARDE<br>secretariat.ediss@univ-lyon1.fr | Mme Emmanuelle CANET-SOULAS<br>INSERM U1060, CarMeN lab, Univ. Lyon 1<br>Bâtiment IMBL<br>11 Avenue Jean CAPELLE INSA de Lyon<br>69 621 Villeurbanne<br>Tél : 04.72.68.49.09 Fax : 04.72.68.49.16<br>emmanuelle.canet@univ-lyon1.fr |
| **INFOMATHS** | **INFORMATIQUE ET MATHÉMATIQUES**<br>**http://edinfomaths.universite-lyon.fr**<br>Sec. : Renée EL MELHEM<br>Bât. Blaise PASCAL, 3e étage<br>Tél : 04.72.43.80.46<br>infomaths@univ-lyon1.fr | M. Luca ZAMBONI<br>Bât. Braconnier<br>43 Boulevard du 11 novembre 1918<br>69 622 Villeurbanne CEDEX<br>Tél : 04.26.23.45.52<br>zamboni@maths.univ-lyon1.fr |
| **Matériaux** | **MATÉRIAUX DE LYON**<br>**http://ed34.universite-lyon.fr**<br>Sec. : Stéphanie CAUVIN<br>Tél : 04.72.43.71.70 Bât.<br>Direction<br>ed.materiaux@insa-lyon.fr | M. Jean-Yves BUFFIÈRE<br>INSA de Lyon<br>MATEIS - Bât. Saint-Exupéry<br>7 Avenue Jean CAPELLE<br>69 621 Villeurbanne CEDEX<br>Tél : 04.72.43.71.70 Fax : 04.72.43.85.28<br>jean-yves.buffiere@insa-lyon.fr |
| **MEGA** | **MÉCANIQUE, ÉNERGÉTIQUE, GÉNIE CIVIL, ACOUSTIQUE**<br>**http://edmega.universite-lyon.fr**<br>Sec. : Stéphanie CAUVIN<br>Tél : 04.72.43.71.70<br>Bât. Direction<br>mega@insa-lyon.fr | M. Jocelyn BONJOUR<br>INSA de Lyon<br>Laboratoire CETHIL<br>Bâtiment Sadi-Carnot<br>9, rue de la Physique<br>69 621 Villeurbanne CEDEX<br>jocelyn.bonjour@insa-lyon.fr |
| **ScSo** | **ScSo***<br>**http://ed483.univ-lyon2.fr** Sec. :<br>Véronique GUICHARD<br>INSA : J.Y. TOUSSAINT<br>Tél : 04.78.69.72.76<br>veronique.cervantes@univ-lyon2.fr | M. Christian MONTES<br>Université Lyon 2<br>86 Rue Pasteur<br>69 365 Lyon CEDEX 07<br>christian.montes@univ-lyon2.fr |

*ScSo : Histoire, Géographie, Aménagement, Urbanisme, Archéologie, Science politique, Sociologie, Anthropologie

"If you want to go fast, go alone. If you want to go far, go together."

African Proverb

# Acknowledgments

Les travaux de thèse présentés dans ce manuscrit représentent l'aboutissement d'une collaboration entre le Groupe PSA à travers son OpenLab VAT@Lyon (Vibro-Acoustic-Tribology@Lyon), le LaMCoS (Laboratoire de Mécanique des Contacts et des Structures) de l'INSA Lyon ainsi que le LTDS (Laboratoire de Tribologie et Dynamique des Systèmes) de Centrale Lyon. Ainsi, c'est de tout cœur que je remercie :

| | |
|---|---|
| **Mes directeurs de thèse** : | Fabrice VILLE<br>Fabrice DASSENOY |
| **Mes encadrants académiques** : | Clotilde MINFRAY<br>Michal RUZEK |
| **Les membres du jury :** | Agnès FABRE<br>Jorge SEABRA<br>Francesco MASSI |
| **Les encadrants du Groupe PSA** : | Moussa DIABY (ex – PSA)<br>Pierre CHARLES<br>Gildas BUREAU |

Au-delà de la patience et la constante bienveillance dans leur soutien technique et scientifique, je tiens aussi à remercier Fabrice V, Fabrice D, Clotilde et Michal pour les qualités humaines dont ils ont fait preuve, faisant de ces 3 années de collaboration une très belle étape de ma vie.

Ces mêmes qualités se retrouvent au sein du Groupe PSA. J'ai donc une pensée pour les nombreuses personnes chez PSA qui ont également contribué à ces travaux. J'adresse des remerciements particuliers à Moussa et Pierre mes deux encadrants lors de ces 3 ans, François PUCHALA, Arnaud LANGLAIS mais aussi Gildas BUREAU pour son expertise précieuse lors des différents blocages techniques dans la thèse. J'inclurais aussi dans ces remerciements l'ensemble des équipes REGL et Stellab qui ont fait que chaque période passée en entreprise soit aussi enrichissante qu'agréable.

Je tiens également à remercier au sein des laboratoires académiques :

- Au LTDS, Thierry LE MOGNE et Jules GALIPAUD qui m'ont permis de comprendre le fonctionnement de l'XPS grâce à leurs longues explications ;
- Au LaMCoS, Sophie DE OLIVEIRA et Emmanuel MONTERO m'ont apporté quotidiennement leur aide administrative sous la direction de Philippe VELEX, Directeur de l'équipe SMC et Daniel NELIAS, Directeur du Laboratoire ;
- A l'INEGI de Porto, David GONCALVES qui m'a notamment aidé avec les mesures EHD;
- les doctorants et post-docs. Tous m'ont fait passé d'excellents moments au laboratoire (il est difficile de n'en oublier aucun, je m'en excuse d'avance si c'est le cas) :

- les anciens : Nina, Marion, Pauline, Grégoire, Pierrick, Arnaud, Stéphane, Romain, Vincent, Dimitri
- les moins anciens : Tommy, Etienne, Guillaume, Thomas, Martial, Loïc, JB, Martin, Pierre, Romain
- et les «bébés» : Pierre et Jean.

D'autre part, je tiens à remercier mes amis pour leur présence durant la thèse, certains membres du corps arbitral de la FFR, mais aussi ma famille qui m'a soutenu tout au long de ma thèse et même plus largement de ma scolarité, ce travail en étant la conclusion. Plus particulièrement, je leur suis reconnaissant du soutien qu'ils ont pu notamment m'apporter lors de l'écriture des dernières pages de cette thèse, au moment de la disparition d'un être qui nous était, à tous, cher.

Enfin, comment ne pas citer Jérôme CAVORET. Sans lui et sans l'aide qu'il m'a apportée au quotidien, cette thèse n'aurait pas été la même. Il aurait été difficile pour moi de produire ces résultats. Pour résumer, merci à tous !

# Abstract

New customer desires are leading car manufacturers to new challenges. Indeed, enhanced vehicles like SUV (Sport Utility Vehicle) becomes more and more popular, especially in Europe. These vehicles involve some modification over the usual mechanical transmissions designs. This vehicle type has a higher angularity than sedans for example. This desire modification has 2 impacts: the increase of slipping in the transmission and its influence on the durability of the components.

The angularity modification remains one of the major lines of research in recent years for car manufacturers. Its increasing influences efficiency. Indeed, this axis of improvement is attractive for manufacturers due to new environmental standards but also an increase in oil price.

In addition, a car must have a reliable transmission that does not require, in the case of constant velocity joints, any maintenance during vehicle life. The following work will focus on this objective.

The main goal of this manuscript is to understand the wear mechanism of the tripod constant velocity joint (CVJ). An analysis of the kinematics was first conducted to reproduce contacts on test rigs. It relied on data from the bibliography but also a simulation of solid dynamics. In addition, the design of a new observation rig using additive manufacturing made it possible to experimentally reproduce slipping in tripod.

Furthermore, a characterization of greases used in Groupe PSA transmissions was performed in order to know the friction coefficients inducing the shudder level of the CVJ. These are also essential in order to judge the efficiency of the component.

Finally, a wear investigation is performed to explain the possible lubrication failure mechanisms with greases proposing different mechanical behaviour. This approaches enables the transmission designer to choose a grease ensuring maximum durability of transmission components.

Looking ahead, a lubricant characterization rig specially designed for tripod joint contacts has been designed. It will thus allow a more complete characterization of further lubricants to this essential vehicle component.

# Résumé

La modification des besoins clients amène les constructeurs automobiles vers de nouveaux challenges. En effet, en Europe notamment, les véhicules rehaussés type SUV (Sport Utility Vehicle) sont de plus en plus populaires. Or, ces véhicules impliquent une modification de l'implantation des transmissions mécaniques. Ces dernières possèdent alors une angularité plus élevée que pour des berlines par exemple. Cette modification a alors 2 impacts : l'augmentation du glissement dans la transmission mais aussi son influence sur la durabilité des composants.

La modification de l'angularité est un des enjeux majeurs de ces dernières années pour les constructeurs. En effet, son augmentation influe sur le rendement des transmissions. Or, avec des normes environnementales de plus en plus contraignantes mais aussi une hausse du prix du pétrole, cet axe d'amélioration représente un facteur d'attractivité pour les constructeurs.

De plus, la durabilité des organes reste primordiale. Une voiture se doit d'avoir une transmission fiable ne nécessitant, pour le cas des joints homocinétiques, aucun entretien durant la vie du véhicule. C'est sur cet axe que les travaux suivants ont majoritairement porté.

L'objectif de ce manuscrit est de comprendre le mécanisme d'usure des joints homocinétiques côté boîte dits tripode. Une analyse de la cinématique a d'abord été menée afin de reproduire les contacts sur des bancs d'essais. Elle s'est appuyée sur des données issues de la bibliographie mais aussi une simulation de la dynamique des solides. De plus, la création en fabrication additive d'un banc d'observation a permis d'évaluer de façon expérimentale le glissement dans cet organe de transmission.

Par la suite, une caractérisation des graisses de transmission utilisée dans le groupe PSA a été effectuée afin de connaître les coefficients de frottement induisant le niveau de vibrations de la transmission pour un client. Ces derniers sont essentiels pour juger l'efficacité énergétique de l'organe.

Enfin, une étude de l'usure a permis d'expliquer les mécanismes de défaillance de la lubrification avec des graisses proposant des propriétés mécaniques. Cela permet alors de comprendre les données-clés afin de choisir une graisse assurant une durabilité maximale des organes de transmission et remplissant alors un des deux enjeux cités ci-dessus.

Pour le futur, un banc de caractérisation des lubrifiants spécialement conçu pour les contacts de joint tripode a été créé. Il permettra ainsi de caractériser de façon plus complète les lubrifiants du futur pour cet organe essentiel d'une voiture.

# TABLE OF CONTENT

# List of figures

# List of tables

# Abbreviation & Nomenclature

| *Abbreviation* | *Complete name* |
|---|---|
| C1 | Grease n°1 |
| C2 | Grease n°2 |
| CVJ | Constant Velocity Joint |
| CAD | Computer Aided Design |
| DPF | Diesel Particulate Filter |
| GAF | Generated Axial Forces |
| HFRR | High Frequency Reciprocating Rig |
| LVE | Linear Visco-Elastic region |
| NEDC | New European Driving Cycle |
| NLGI | National Lubricating Grease Institute |
| NVH | Noise Vibration Harshness |
| MoDTC | Molybdenum dithiocarbamate |
| MoDTP | Molybdenum dithiophosphate |
| MTM | Mini Traction Machine |
| P1 | Grease n°3 |
| P2 | Grease n°4 |
| SCR | Selective Catalytic Reduction |
| SUV | Sport utility vehicle |
| WLTP | Worldwide harmonized Light vehicles Test Procedures |
| XPS | X-Ray Photoelectron Spectroscopy |
| ZDTP | Zinc dithiophosphates |

| *Parameters* | *Description* | *Units* |
|---|---|---|
| a | Semi-axis along x direction | [m] |
| b | Semi-axis along y direction | [m] |
| d | Distance between the rolling track and the rotational axis | [m] |
| $d_{HFRR}$ | Distance of HFRR stroke | [m] |
| $D_{pixel}$ | Distance between 2 straight line | [pixels] |
| $D_{slip12}$ | Constant part of affine function | [pixels] |
| E | Material young modulus | [Pa] |
| $E_b$ | Blinding energy | [eV] |
| $E_k$ | Kinematic energy | [eV] |
| $f_{HFRR}$ | Frequency of HFRR test | [Hz] |
| G' | Storage moduli | [Pa] |
| G'' | Loss moduli | [Pa] |
| $h_{min}$ | Minimum film thickness | [m] |
| $m_{rd}$ | Maximum rolling distance | [m] |
| $P_h$ | Hertz Pressure | [Pa] |
| $P_{h-HFRR}$ | Hertz Pressure for HFRR test | [Pa] |
| $R_q$ | Root mean square roughness | [m] |
| rd | Theoretical rolling distance | [m] |
| R | Radius circle of the spider | [m] |
| $R_x$ | Reduced radius of curvature in x direction | [m] |
| $R_y$ | Reduced radius of curvature in y direction | [m] |
| R' | Reduced radius of curvature in elliptical contacts | [m] |
| S | Slope in rheological flow curves | [-] |
| S | Slipping difference | [%] |
| S_oil | Separated Oil | [%] |
| sd | Slipping distance after X turns | [m] |
| $slope_{12}$ | Slope used in observation rig calculation | [-] |
| SRR | Slide-to-Roll Ratio | [%] |
| $\nu$ | Poisson's ratio | [-] |
| $\alpha$ | Articulation angle | [°] |
| $\tan(\delta)$ | Damping factor | [-] |
| $\omega$ | Rotational speed of CVJ | [Hz] |
| $\omega_R$ | Rotational speed for Rheometer | [Hz] |
| φ | Plate diameter of rheology measurements | [m] |
| $\tau$ | Shear stress | [Pa] |
| $\tau_{CO}$ | Cross over stress (flow point) | [Pa] |
| $\tau_s$ | Slip ratio | [%] |
| $\theta$ | Rotation angle of the CVJ | [°] |

# Introduction

The component durability and the mechanical efficiency improvements remain major requirements when designing automotive products. It should be noted that in the mechanical industry, the innovative technologies used in recent years to reduce car fuel consumption and $CO_2$ emissions have been mainly oriented towards engine components and gearboxes.

As far as transverse transmissions are concerned, most of the effort aims at reducing vibrations and reinforcing materials to avoid transmission joint breakages. However, the transverse transmission does more than just transmitting torque and speed from the gearbox to the wheels. Indeed, it also enables the suspension to move freely, regardless of the wheel steering. But the transmission is also subject to wear (abrasive, adhesive, or even contact fatigue) due to system kinematics. These wear mechanisms are the result of friction and have a negative impact on efficiency and thus consumption. It is therefore necessary here to take these aspects into account when designing components of the transmission in order to comply with the future Euro 6.d emission standard.

The tripod transmission joints on the gearbox side are known to produce wear and reliability problems for customers. Wear occurs on a recurring basis, especially for SUV, which have the peculiarity of having higher articulation angles. For the same transmission, this higher articulation angle induces more severe operating conditions, in particular with rolling sliding contact conditions. The literature and the expertise carried out by Groupe PSA reveal the abrasive and / or adhesive wear of the tracks as well as the pitting phenomena of the spider trunnions.

The consequence of these failures is the appearance of vibrations (or shudder). It seems to arise from a complex set of factors. The lateral transmission, also called the constant velocity joint, is a component possessing a very particular kinematics. Indeed, this joint has been preferred to the cardan joint for its capacity to transfer the torque with an input speed equal to the output speed and a displacement possibility on the "gearbox side" which is necessary for suspension. This particularity, however, causes tribological problems on the "transmission-side" joint. It could lead to lubrication defects in the contact zone. These problems are due to the system architecture which prevents contact re-lubrication, due to the very high contact conformity, but also to the grease properties.

So, the thesis goal will be to solve these problems in order to reduce wear and friction in tripod transmission joint.

**Chapter one** presents a bibliographic study of different standards and phenomena which will be encountered in the present work. It also shows how an automotive transmission works. **Chapter two** exposes experimental methodologies used during this work. It presents the different tribometers and also the analyses used to characterize and quantify wear. The present work is decomposed in three different steps. The first one, **chapter three** takes root in automotive transmission and characterizes the contact which will be investigated. The actual contact conditions are derived from experimental observations and Hertz' theory. After this step, **chapter four** investigates the performance of greases used by Groupe PSA inside the constant velocity joint. It shows industrial tests led on grease to quantify their properties. The vehicle operating conditions from chapter three are transferred to the laboratory test rig to quantify the grease performances under such conditions. The final step completes wear investigations performed in **chapter five.** It proposes the wear mechanism of constant velocity joint tracks based on friction measurements, rheology results and film thickness measurements.

Chapter one

# State of the Art

*The first chapter proposes a state of the art.*

*In the first section automotive transmission is presented. A description of it composition and disposition on vehicle is done. Environmental regulations which lead automotive industry since decades are explained. Finally, a focus on tripod joint used during this work is done.*

*In the second section, the basic concepts of tribology, which is the study of friction, wear and lubrication, are presented. The lubrication theory is exposed to understand the following work. The rheological concepts used in this study are presented. The last section presents the Hertz theory in order to calculate contact pressure.*

*The third section describes what a grease is and what are its main components: base oils, thickeners and additives.*

As conclusion, objectives of this PhD work will be highlighted.

## 1.1. Automotive transmission

### 1.1.1.Constant velocity Joint function

In the automotive industry, transmission includes different systems of the vehicle likes braking system, steering system, hydraulic system, steering knuckle or transmissions itself (figure 1.1).

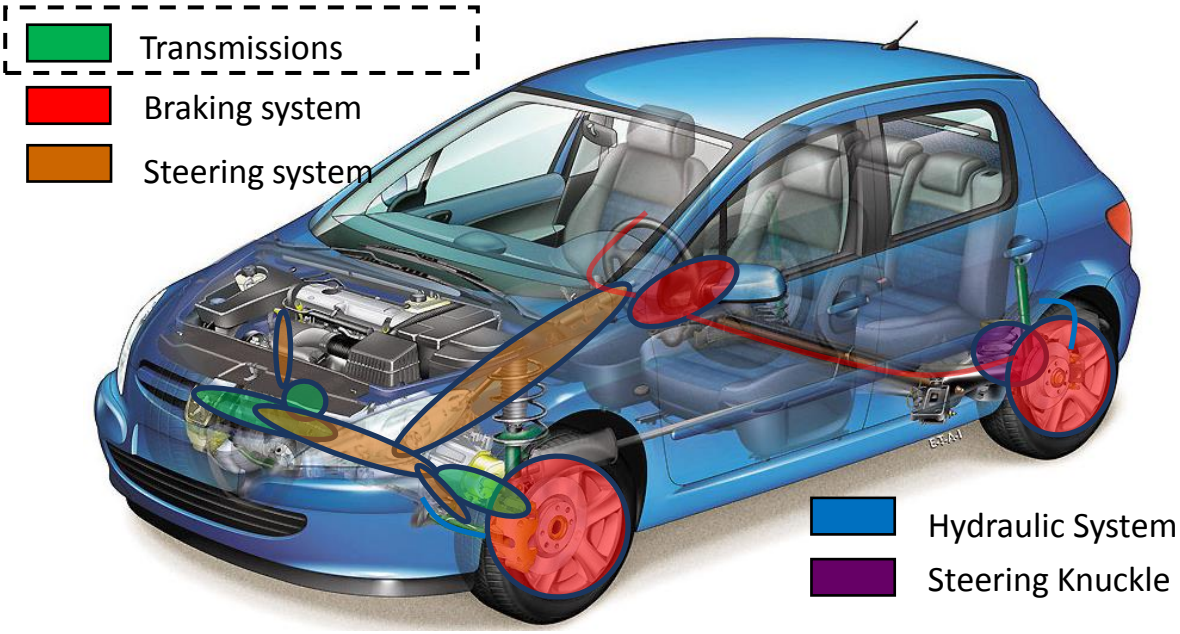


*Figure 1.1: Cars transmission parts (courtesy of Groupe PSA)*

Constant velocity joint (CVJ) is a transmission part. Its goal is to transmit torque and velocity from the gearbox to the steering knuckle and wheel. But CVJ has to transmit this movement with different angularity in function of steering directions and wheel positions with respect to the differential and gearbox. Also it permits the variable geometry between the wheel and the gearbox in order to absorb the suspension displacement without any angular gap whatever the articulation angle (figure 1.2).

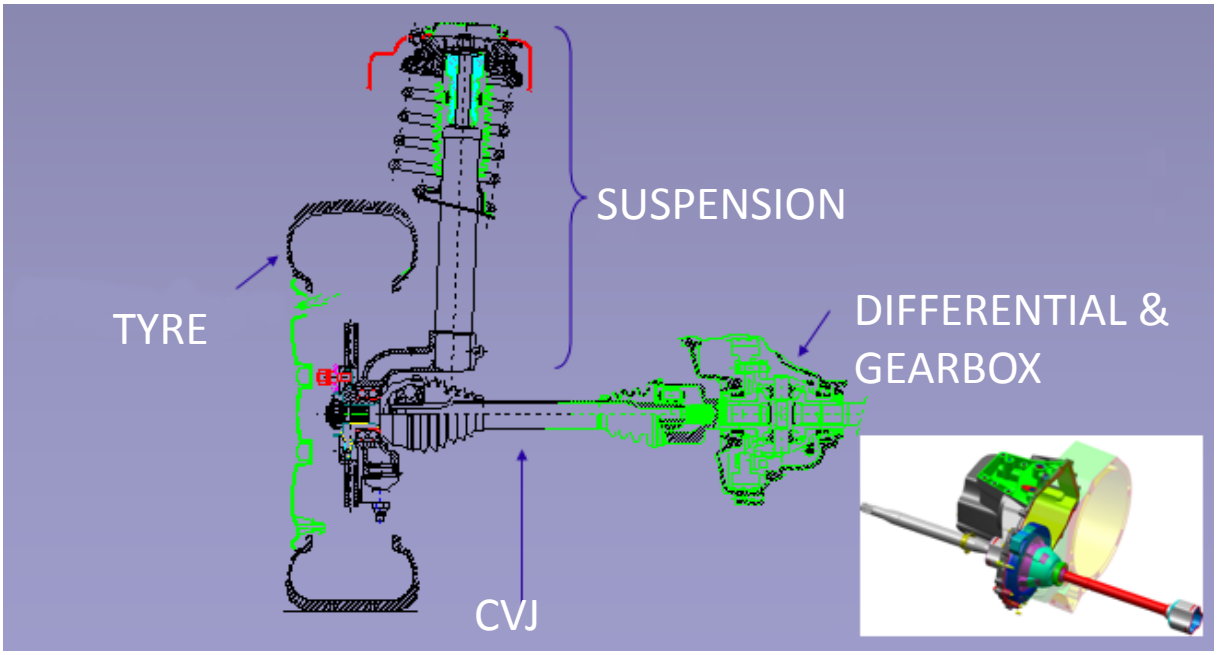


*Figure 1.2: CAD view of front transmission*

Two configurations are possible: with (figure 1.3) or without (figure 1.4) a steady rest bearing.

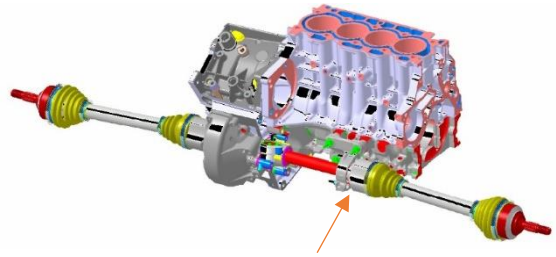

*Figure 1.3: with a steady rest bearing*

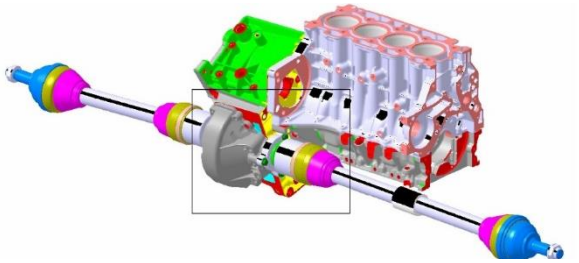

*Figure 1.4: without a steady rest bearing*

The steady rest bearing use is determined by the car design, and particularly by the engine implantation. However, the joint composition is exactly the same:

- An Rzeppa joint (ball joint) [1]
- A shaft
- A tripod joint [2] – *the focus of this thesis*

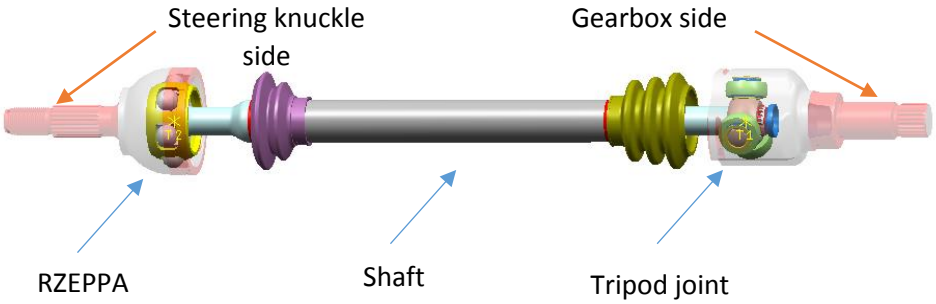


*Figure 1.5: transmission general view*

### 1.1.2.Environmental regulations

Nowadays, environmental regulations are the most important factors of a car design. The evolution of the most common pollutants due to transport are available in figure 1.6.

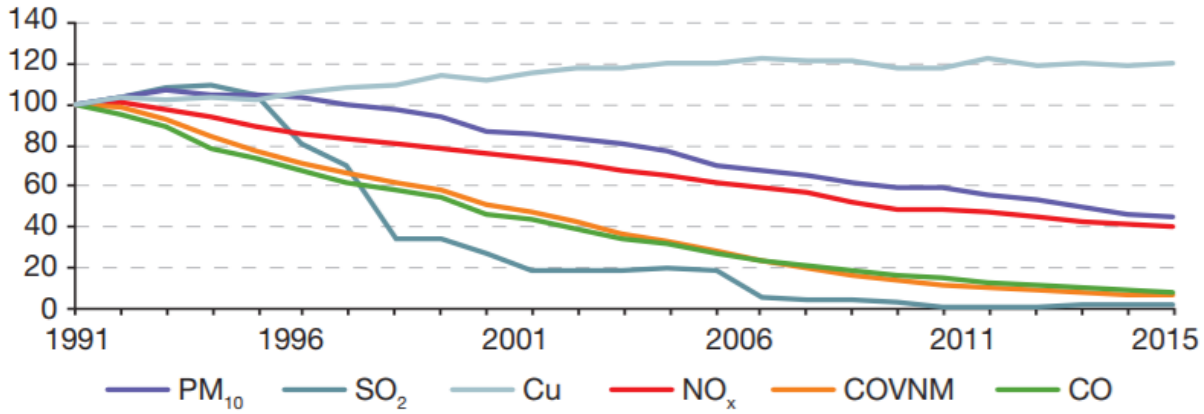


*Figure 1.6: from CCTN 2017 – Citepa april 2017 - Sceten*

The emission level in 1991 was set to 100 for all pollutants. Only copper increased since 1991. The use of brake pads and also the catenary multiplication caused this phenomena [3]. However, the other automotive pollutants like NOx (nitrogen oxides (NOx), PM (particulate matters) or CO (carbon monoxide) decreased significantly. It is due to European regulation which introduced the “EURO X” norm in 1992 [4].

With this and following standards, manufacturers have to homologate their cars using a certification driving cycle and not to exceed the respective specified thresholds. In figure 1.7, it is possible to observe this impressive reduction.

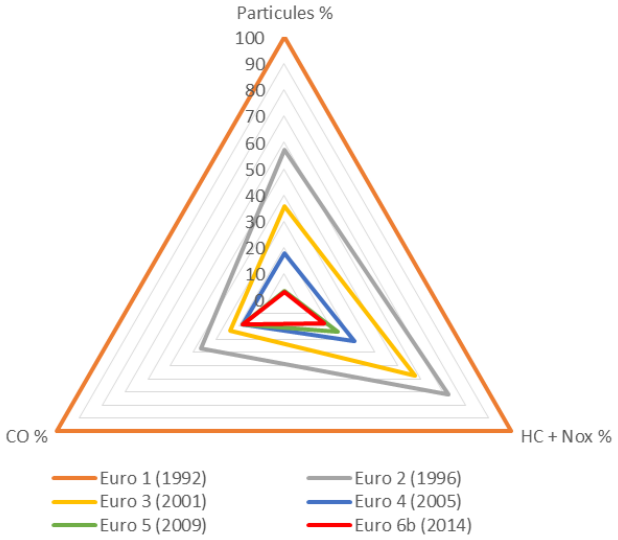


*Figure 1.7: Evolution of EURO norms in percentage [5]*

From 1992 till today the manufacturers were suggested to reduce their emissions by introducing for example on engine SCR (Selective Catalytic Reduction) or DPF (Diesel Particulate Filter) in order to respect the norms getting stricter and stricter. Moreover, in addition to the huge work done on engine technology, manufacturers had to reduce the power losses everywhere in vehicle to pass the norms. For the purpose of this thesis, it is noticeable that drivetrain losses represent 5 to 6% of total vehicle losses [5].

In addition, future regulations like EURO 6.D will use a new validation cycle named WLTP (Worldwide harmonized Light vehicles Test Procedures). This procedure takes into account more realistic cycle in order to approach the actual consumption and emissions of the vehicle on the road. In order to show the difference between the old validation test cycle NEDC (New European Driving Cycle) and a realistic test cycle done by a NGO (T&E), the first public comparison of fuel consumption have been done by Groupe PSA in 2016 [6] (Figure 1.8).

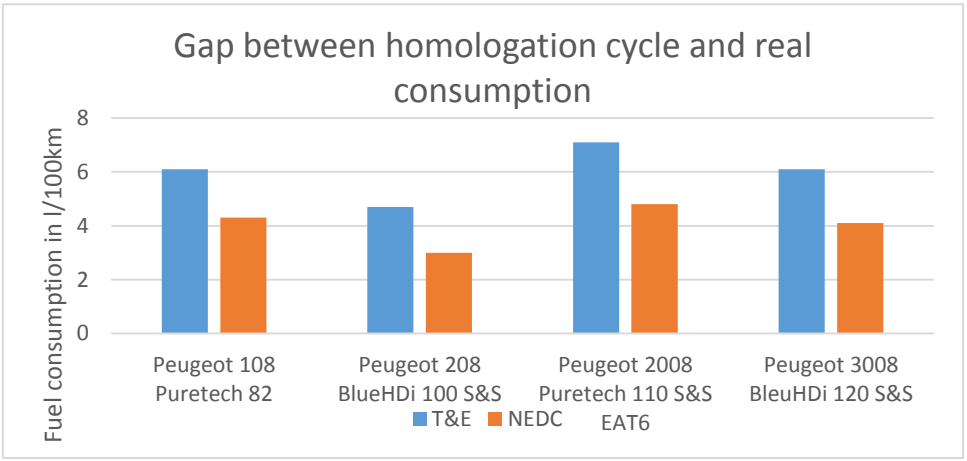


*Figure 1.8: Comparison of fuel consumption for different car models*

As expected, the fuel consumption increases with a realistic procedure. And as pollutant emissions are directly linked to the fuel consumption, passing the EURO norms with the new WLTP test cycle is likely to be more complicated. Some studies show that decreasing driveshaft losses by 20% will lead to a fuel economy of about 0.1% [7].

It is in this context that constant velocity joint manufacturers have studied the possible benefit of working on it. For example, a new constant velocity joint technology [8] has improved the $CO_2$ emission by 1 g/km. In addition, for SUV (Sport Utility Vehicle) which have higher articulation angle, the reduction goes to 3 g/km.

### 1.1.3.Focus on Tripod joint

Tripod joint is identified as a key point. Let's focus on it.

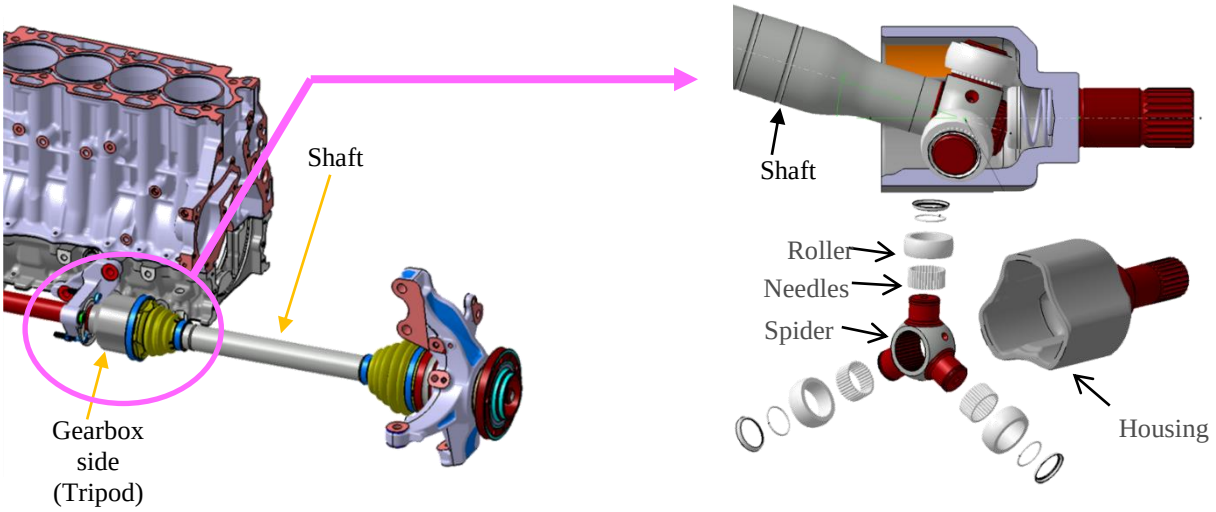


*Figure 1.9: Focus on tripod*

It can be noticed that two major contacts contribute to the energy transmission. The contact between the needles and the rollers and the contact between the roller and the track inside the housing. This second contact is the most complicated one to understand. In fact slipping, rolling and also a variation of orientation in operating condition take place.

One of the tripod singularity is that it could be considered as twice isostatic [9]:

- Globally, because there is not too much connection between the led and the leading shaft (Housing). It is always possible to have the 3 straight lines corresponding to the spider axis that are passing by a plan defined with 3 random points. It is a unique and stable system even if there are some coplanar issue, parallelism trouble between the track and the housing shaft or the 120° between the 3 main spider axes is not respected.
- Locally each roller is a combination of a sphere groove joint and a sliding pivot. Indeed, one of the rotations is blocked by the axial rotation of the sliding pivot. So, there are five degrees of freedom per roller.

In this way, the force calculation for the all tripod joint or for only one roller is always possible. In addition, the vibrations in the tripod joint are very important. In fact, the roller behaviour includes rotation and translation with friction inside the housing. This phenomena on each roller, induces different order of forces during the CVJ rotation generating the Generated Axial Force (GAF) [10]. This force increases with angularity due to the increase of:

- slipping between roller and housing track,
- friction between spider and roller,
- friction during roller tipping in the track due to the offset.

The force is directly felt by the car driver in the steering system.

Moreover, it can be noticed that the tripod has a perfect homokinetic rotation if the spider shaft stays parallel to itself, and if it does not, the homokinetic error stays very light [2]. To complete this part, main components of the CVJ tripod (Roller & Housing) are made of steel. However, they do not have the same material properties: the housing is made of C48P and the roller made of 100 Cr6.

## 1.2. Tribology Tools Box

### 1.2.1.Hertz Theory

In 1880, a 23 years old man named Hertz proposed the first satisfactory analysis of a contact between two elastics solids [11]. Hertz formulated equations in case of a single contact point. The Hertz' theory main goal is to study the contact constraints in order to choose among the different material or the maximal loads which could be supported by the mechanism.

Three different hypothesis are made to apply this theory:

- Geometric hypothesis

In general case, 2 solutions are possible as drawn in figure 1.10:

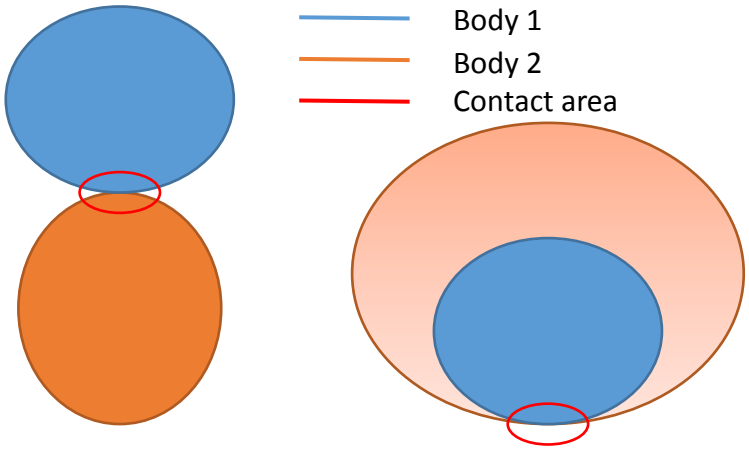


*Figure 1.10: geometry illustrations of conformal and non conformal contact*

To begin, two bodies are defined: body 1 and body 2. Also, the curve center is calculated using the stiff side. To the left, the surfaces are both convex and have positives radii. It corresponds to a non-conformal contact [12].

To the right, there are one convex surface and one concave surface. It corresponds to a conformal contact. However, a condition to apply Hertz' theory is that dimensions of the deformed contact has to be small compared to the radii of curvatures of the contacting bodies. So, for highly conformal contact, Hertz' theory may not be adapted because of this hypothesis. It is possible for the CVJ to evaluate the error for the contact pressure to 10% when using Hertz theory [13].

- Material hypothesis

The material behaviours in the contact zone are supposed elastic linear, homogeneous and isotropic. Moreover, the contacting surfaces have to be smooth and frictionless. To define the calculation parameters, two material young modulus $E_1$ and $E_2$ and also their Poisson ratios $v_1$ and $v_2$ are introduced. The result will be E*, the equivalent young modulus:

$$\frac{2}{E^*} = \frac{1-v_1^2}{E_1} + \frac{1-v_2^2}{E_2}$$

It can be noticed that the contact constraints would be highly non-linear during loading (direction variation or un-proportional principal constraint).

- Load hypothesis

The load will be considered as a center normal load. The calculation remain valid as long as the area remains small to assimilate the area as a plane area. To do this, the following equation need to be validated:

$$2a < \frac{1}{2} min_{i=1,2} R_i$$

With all these hypothesis, a general case of Hertz' theory is presented:

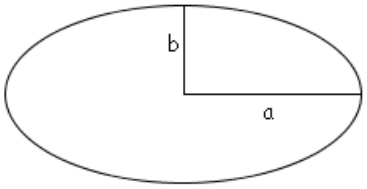


*Figure 1.11: ellipse axis*

The general contact area is represented by an ellipse with a (along x direction) and b (along y direction) the semi-axis. Different radii are introduced:

- Reduced radius of curvature in elliptical contacts $\frac{1}{R'} = \frac{1}{R_x} + \frac{1}{R_y}$
- Reduced radius of curvature in x direction $\frac{1}{R_x} = \frac{1}{R_{1x}} + \frac{1}{R_{2x}}$
- Reduced radius of curvature in y direction $\frac{1}{R_y} = \frac{1}{R_{1y}} + \frac{1}{R_{2y}}$

Introducing after the elliptical integrals $\boldsymbol{\mathcal{E}}$ and $\boldsymbol{\mathcal{F}}$:

$$\mathcal{E} = \int_0^{\frac{\pi}{2}} \left[1 - \left(1 - \frac{1}{k^2}\right)\sin^2\varphi\right]^{\frac{1}{2}} d\varphi$$

$$\mathcal{F} = \int_0^{\frac{\pi}{2}} \left[1 - \left(1 - \frac{1}{k^2}\right)\sin^2\varphi\right]^{-\frac{1}{2}} d\varphi$$

An approximate solutions of these elliptical integrals are given by [14]:

$$\mathcal{E} = 1 + \frac{\mathrm{s}}{\beta}\ ;\ \mathcal{F} = \frac{\pi}{2} + \mathrm{s}\ln\beta\ ;\mathrm{k} \approx \beta^{\frac{2}{\pi}}\ \text{with}\quad \mathrm{s} = \frac{\pi}{2} - 1\ \ ;\ \ \beta = \frac{R_y}{R_x}$$

So, *a* and *b* dimensions can be calculated:

$$a^3 = \frac{6\mathcal{E}wR'}{k\pi E^*} \qquad b^3 = \frac{6k^2\mathcal{E}\mathrm{w}R'}{\pi E^*} \qquad with\ k = \frac{b}{a}$$

And also the maximum deformation $\delta$ and maximum Hertzian pressure $p_h$:

$$\delta = \mathcal{F}\sqrt[3]{\frac{9}{2\mathcal{E}R'}\left(\frac{w}{k\pi E^*}\right)^2} \qquad and \qquad p_h = \frac{3w}{2\pi ab}\ with\ w\ the\ load$$

All these tools and notations offer a unique notation for all the manuscript in order to describe contact geometry and its characteristics.

### 1.2.2.The Lubrication theory

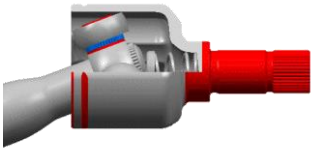

*Figure 1.12: Tripod's view*

Each study of friction in contact is different. Indeed, the speed, the roughness, the lubricant viscosity and formulation, the material have to be considered. The contact which will be studied here is between the roller and the housing track. To better understand the tribological system the lubrication regime and operating conditions have to be consider.

The lubrication regime is one of most important parameter in a tribological problem. It is Pr. Richard Stribeck who formalized first the existence of a friction coefficient in lubricated contacts in 1902 from journal bearings tests [15].

The friction coefficient is changing with the lubrication regime itself function of the velocities of the contacting surfaces, the lubricant viscosity, the temperature, the roughness, etc. This is described on the Stribeck curve (figure 1.13) [16].

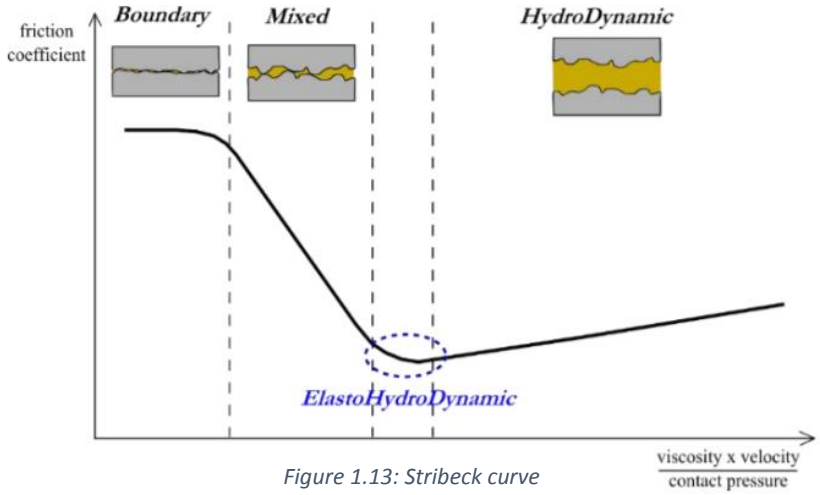


*Figure 1.13: Stribeck curve*

This curve shows different states of a lubricated contact. First of all (starting from abscissa zero), the friction coefficient is assumed constant and at its maximum. This friction coefficient is referred to as the boundary lubrication friction coefficient. Then, decreases with speed and stabilizes to increase to the end. So, film thickness increases with the speed but also with viscosity. It decreases when the load increase.

A simple parameter was created by T.E. Tallian in 1967 [17] to characterize the film thickness ratio. It allows to predict the lubrication regime of contacts. It is defined by the ratio of minimum film thickness and mean surface roughness. $\Lambda = \frac{h_{min}}{\sqrt{R_{q1}^2+R_{q2}^2}}$ $with$ $h_{min}$ minimum film thickness and $R_{q1}, R_{q2}$ root mean square roughness of contacting bodies. To resume, a table is avaible below.

| Film thickness parameters | | | |
|---|---|---|---|
| Regime | Conformal surfaces | Non-conformal Surfaces | Friction coefficient |
| Boundary | $\Lambda$<1 | $\Lambda$<1 | High |
| Mixed | 1<$\Lambda$<5 | 1<$\Lambda$<3 | Decrease |
| EHD | Does not exist | 3<$\Lambda$<10 | Minimum |
| Hydrodynamic | $\Lambda$>5 | $\Lambda$>10 | Viscous friction mainly |

*Table 1: Thickness parameters*

- Boundary regime

This regime corresponds to $\Lambda$<1. At the beginning of motion, the lubricant film is not thick enough to separate the surfaces. The friction coefficient is high and typically goes from 0.1 to 1 if the film does not exist. The load is only supported by rough patches. Two cases remain possible:

- A dry contact exist between the 2 surfaces, the wear is very important in that case
- A transfer film or tribofilm exists in order to dissipate heat and provide additives to the contact to reduce friction and wear.

This is the most severe regime. It exists for low lubricant viscosities or/and low entrainment speeds.

- Mixed regime

This regime is obtained when 1 < $\Lambda$<3 for conformal surfaces or 1< $\Lambda$<5 for non-conformal surfaces. It is a transition between Boundary and Hydrodynamic regimes. As the contact velocity increases, the film thickness increases and a separation between the 2 contacting surfaces begins to appear. However, the velocity is not high enough to assure a hydrodynamic pressure with the complete load-bearing capacity. So this load bearing-capacity is partially carried by the asperities and the film.

- Elastohydrodynamic regime (EHD)

This regime is only available for non-conformal surfaces (3< $\Lambda$<10). The separation between surfaces is perfect. The film thickness is very low and the elastic deformation on surfaces is important. It is in this regime that friction coefficient will be at its minimum value before going back up when the film thickness increases beyond a certain threshold. However, wear can be observed. For higher loads, the lubricant will behave like an elastic solid in the contact zone before leaving the contact and becoming again a liquid.

- Hydrodynamic regime

This regime is reached when $\Lambda$> 5 or 10 depending of geometry. With high velocity and low contact pressures, the film thickness increases and becomes thick. Indeed, the film fully separates the contacting surfaces. So pressure distribution becomes bigger and the elastic deformation disappears. The main friction becomes the viscous one and friction coefficient increases with velocity.

Most of these lubrication regimes can be found in automotive industry. Moreover, in our case, contacts are with conformal surfaces so the EHD regime for these applications into Constant Velocity joint is not reached.

To realize lubrication, a lubricant is needed. In the present work, only grease lubrication will be used.

### 1.2.3.Rheology

Rheology is used to qualify grease. It is the science of flow and deformation. It is the alliance of physics and chemistry. The word rheology takes it origins from Greek and means “to flow” [18]. Indeed, the grease acts like a visco-elastic material [19] so rheology is used to study the grease behaviour. During the different tests led in this manuscript, the temperature has to be set to have reliable measurement. In fact, the rheological study of some grease can be an extra thesis as show previously [20]. The rheological behaviour that will be studied will only be limited to the transition between solid and liquid behaviour of material. It is represented by the notation below:

- *G’* in Pa which is storage moduli. It represents the deformation energy stored by the sample. This deformation is completely reversible. It is the elastic behaviour of the material.
- *G’’* in Pa which is the loss moduli. It represents the deformation energy used by the sample during the shear process. This energy is lost from the sample.
- The damping factor $\tan\delta = \frac{G''}{G'}$ It is the ratio of the viscous and elastic portion of the viscoelastic deformation behaviour.

An example of oscillatory measurements is available in figure 1.14. The aim of these tests is to obtain 3 properties G’, G’’ and tan(δ) variating the shear stress τ. When G’>G’’, the grease acts like a solid. There is a linear Visco-Elastic region (LVE) where the grease acts really like a solid. When the stress increases G’’ & G’ start to decrease and G’’ & G’ cross at $\tan\delta = \frac{G''}{G'} = 1$. It is the cross over stress $\tau_{CO}$ also named “flow point”. After this point, the storage moduli becomes smaller than the loss moduli and G’’>G’. So, thickener is not able to recover elasticity: the grease acts like a liquid.

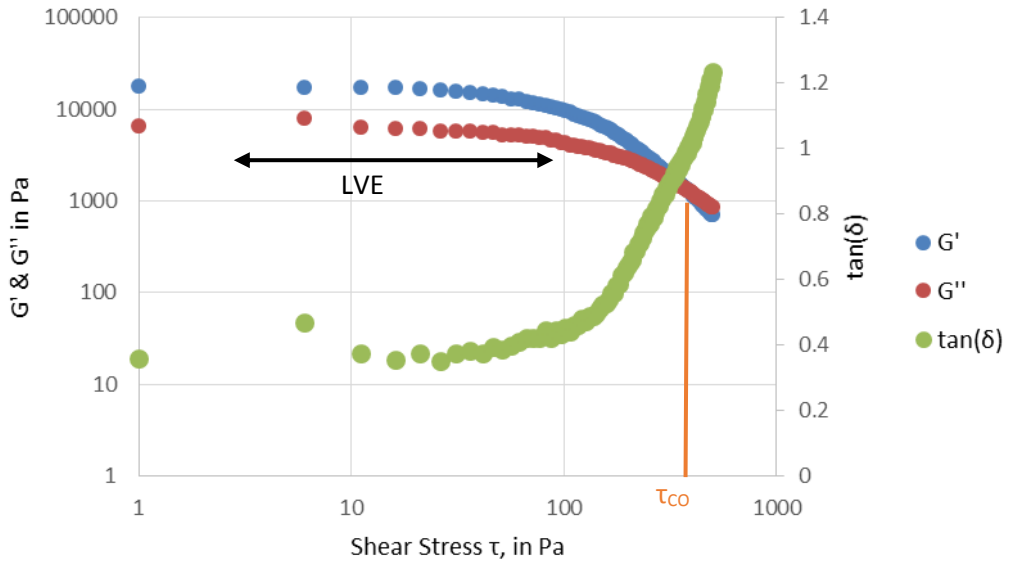


*Figure 1.14: Oscillatory test example*

In addition rotational tests on a rheometer can be performed to qualify the flow. They are referred to as flow curves. The test gives viscosity function of the shear rate from 0.01 to 5000 $s^{-1}$. An example is available for grease in figure 1.15.

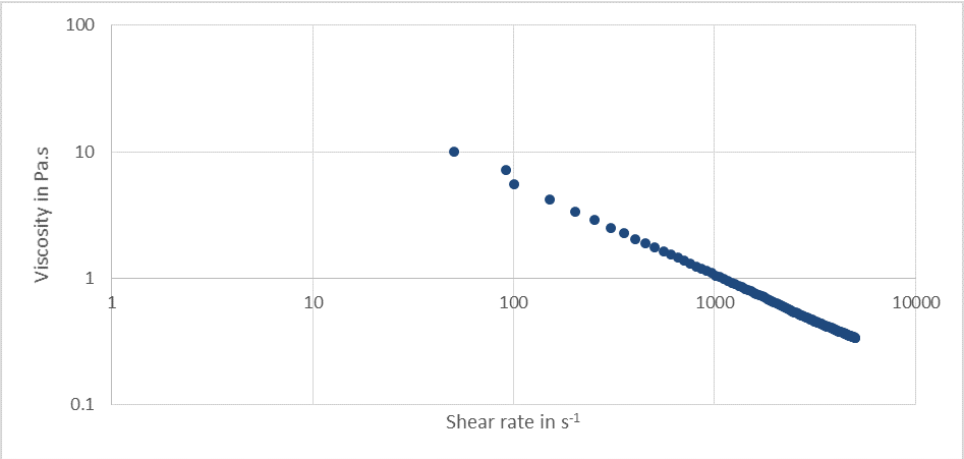


*Figure 1.15: Grease flow curves example*

The grease flow curves with a slope s<0, indicates a shear thinning (pseudoplastic) which will be always the case in the present study. In addition if, s is equal to zero, it is ideally viscous and if s greater than zero, it is shear thickening (dilatant) [18]. Moreover, this curves without a zero shear viscosity plateau indicates that there is a yield point. The yield point is the shear stress value at which the linear-elastic deformation is exceeded.

### 1.3. Grease lubrication: What is a grease?

First of all, when 2 parts are in contact, lubrication can be used for different functions like [21]:

- Allow to separate the surfaces
- Protect the surface and decrease wear (oxidation, corrosion, …)
- Evacuate wear debris and heat from the contact

The lubrication used for this study is grease. Greases have some disadvantages (no evacuation of contamination nor heat) but also many advantages:

- Their consistency is higher so it flows only under significant force,
- Lower friction coefficient most of the time,
- Better adherence to surfaces,
- Grease does not leak easily,
- Grease does not require a pump…

Greases are made from oil but contain also other components as can be seen in figure 1.16 [20].

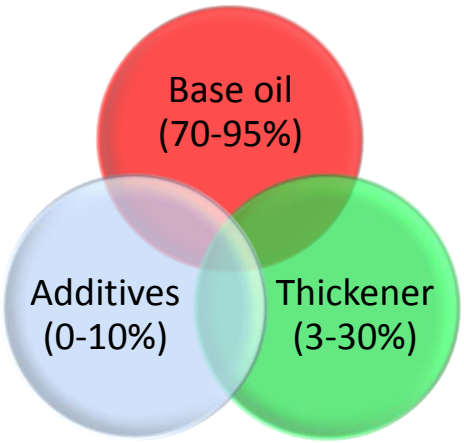


*Figure 1.16: Greases compositions*

This composition example could be considered very simple. However, it is very complex for manufacturer to find the right composition which will correspond to the right application. Manufacturers do not mix these components randomly. Different parameters have to be considered: the application, the cost, the environmental impact (pollution for example in case of leak) or the existing composition.

In addition, today greases are classified by NLGI numbers according to their consistencies with cone penetration method (figure 1.17) [22].

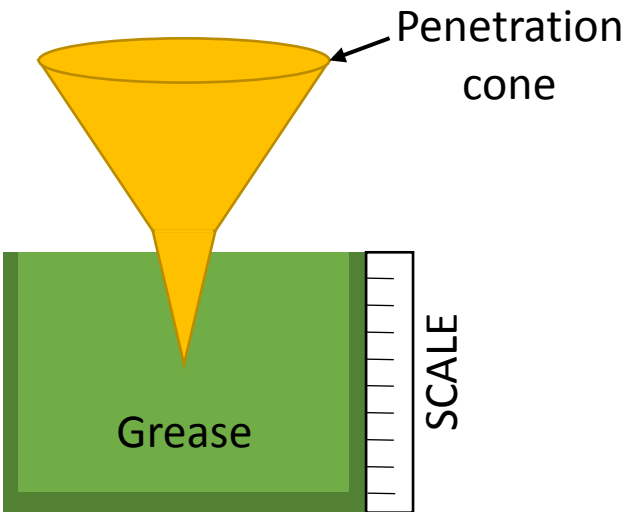


*Figure 1.17: Cone penetration method illustration*

| NLGI Number | Appearance | ASTM worked penetration (1/10 mm) | Application |
|---|---|---|---|
| 000 | Semifluid | 445-475 | Gear greases |
| 00 | | 400-430 | |
| 0 | | 355-385 | |
| 1 | Soft | 310-340 | |
| 2 | Creamy | 265-295 | Greases for bearings |
| 3 | | 220-250 | |
| 4 | | 175-205 | |
| 5 | | 130-160 | |
| 6 | Soap-like | 85-115 | Block greases |

*Table 2: NGLI numbers*

1.3.1.Base oil

Different types of base oil can be used:

- Vegetal oil

These oils are extracted from plants such as: sunflower, rapeseed or palm. Their advantage is their capacity to be biodegradable. Their uses could be when the application environment is open to reduce the risk of pollution (agricultural for example). They are not used in lubrication of automotive application due to their low stability (oxidations at high temperature).

- Mineral oil

It represents the grease majority. These oils are extracted from petroleum during the distillation of crude oils. The results of this distillation could be paraffinic, naphthenic or aromatic. This operation also influences the viscosity of final oil. This last one is mostly composed of carbon and hydrogen atoms. Thanks to their non-toxicity and cheaper price, the most common oil base in industry is paraffin with the high viscosity index (VIs) thanks to its viscosity stability across a wide temperature range. It is noticeable that the difference between the solubility parameters of the base oil and thickener will lead the thickening effect [23]. The grease properties must depend of the ratio between temperature and pressure viscosity coefficient of base oils. It is also important to know that a small change of base oil composition may not be underestimated [24][25].

- Synthetic oil

The origin of this kind of oil was a lack of mineral oils available on market. Usually, they are chosen under specific lubrication conditions (extreme temperature, high oxidation…) when mineral oils performances are not enough. These molecules (artificially synthetized) own specific chemical groups with other atoms than carbon or hydrogen. Organic ester base oils have the advantage of being non-toxic and biodegradable; polyalphaolefins (PAO) are non-toxic and have high oxidation resistance; and polyglycols (PG) are non-toxic and can be used for high temperatures. Both PAOs and PG are non biodegradable. However, base oil have to match with the thickener. Some compatibility problems between synthetic oil and thickener can occur. Also, using a synthetic oil if thickener limits the advantage, is useless. It is for this reason that most of the time it are used in order to make semi-synthetic oil in order to improve lifetime.

1.3.2.Thickener

The thickener is an essential part of grease. Indeed, without the thickener, greases would not exist. It is the mixture of thickener and base oil that creates the new consistency but also new properties. Grease final properties result from these interactions forces between the various molecules of the thickener and the base oil hydrocarbons.

There are two main families of thickeners:

- Soap grease and soap complex grease

Most of greases results of a reaction between a metallic hydroxide (as lithium, calcium or sodium) or in case of aluminum soap of an aluminum alkoxide, and a fatty acid which the most popular one is 12-hydroxystearic acid. The principal soaps are: Lithium (bearings, various automotive applications) or Calcium (Low load or damp application) [20].

Another technical solution is to mix a fatty acid with 2 bases. In most cases the calcium hydroxide and lithium hydroxide that are mixed together. It does not give the same result as a mix with a simple soap grease.

During the saponification the soaps crystallize and form a new structure. The soap nature (lithium, aluminum…) and the making conditions (temperature kinetic during the process) will influence the structure dimensions. As an example, it is possible to observe in figures 1.18 &1.19 the difference between a lithium soap structure and a sodium one. On one hand the lithium will produce big tangle fibers and on the other hand the sodium will have smaller and independent fibers.

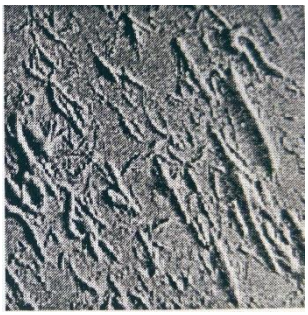

*Figure 1.18: Sodium soap (unknown scale)* [20]

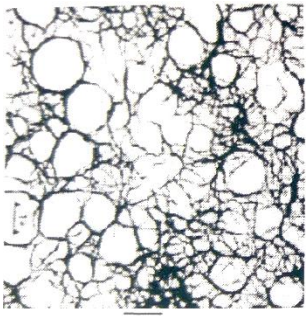


*Figure 1.19: lithium soap*

In this way, the oil and thickener system cannot be considered as a simple diphasic material. These two component systems are governed by two types of forces: chemical ones (Van Der Waals and hydrogen), physico-chimical ones (by capillarity).

Each lubricant manufacturer has their own process. However, the processing of soap greases have the same main steps. First of all, a saponification process is launched between the oil base and an acid. After this process additives are added to crush the grease. During all along this process, a temperature kinetic is followed to ensure the desired properties. Finally, the grease consistency is often checked to adjust, if necessary, the base oil to thickener ratio.

These processes allow manufacturers to reproduce the same grease compositions. However, it is very difficult to compare greases between manufacturers because their processes are not the same and in consequence, their greases differ too even if components are the same.

To finish, complex metallic soap can be used too. They are made with a metallic base mix with 2 organic acids (one with long and the other with short chain) in different proportion. The main advantage of this grease is a significant increase of the high dropping points (from 50 to 100°C) but also the reduction of oil separation. As a result, it gives a better using range in high temperature. Examples of these complex greases are: Lithium, Calcium, Aluminum or Barium. Nowadays, the complex soap accounts for 20% of all grease sold.

All of these will modify the viscosity of the mixture compared to base oil. Moreover, to create this new structure, a thermal activation around 200°C is necessary.

- Grease without soap: Nonionic Organic Thickeners

These greases are used when the temperature is very high. Generally, its high dropping points are over 260°C. It is possible to mention polyurea greases which have an excellent thermal stability and anti-oxidant capability. Moreover, they resist very well to vibrations. However, their manufacturing are much regulated due to the high toxicity of their main components. Typical applications for this kind of thickener is a precision ball bearing. Another example is polytetrafluorethylene or silicones which are also use as an organic thickener [26].

To finish, inorganic thickener can be used. It mainly concerns high temperature applications. Components which can deal with these roles are silica or bentonite. In contrast with a soap, the mixture does not create fibers but small grains or strips. This mixture does not need thermal activation.

### 1.3.3.Additives

In proportion, additives constitute a small part of grease. However, their role is one of the major ones. A distinction could be drawn between two subcategories: the functional one and the structural one. The functional additives allow enhance of grease properties (less wear, less oxidation). The structural additives govern thickener and as a consequence the global grease structure. The key additives are describe below:

- Boundary lubrication additives: as shown previously, boundary lubrication is the worst lubrication regime because the surface are not separated. Additives chemically react with the surfaces to create a tribofilm in order to avoid as much as possible wear or friction. To fulfil this function, there are particularly: Antiwear (AW), Friction Modifiers (FM) and Extreme Pressure (EP) additives. As an example, FM ensure a reduction of friction at the interface. Molybdenum dithiocarbamates (MoDTC) are often used in automotive industry for its capacity to form $MoS_2$ which is an excellent friction-reducer on steel. EP are releasing sulfur or chlorine under high temperature to form friction reducing metal sulfide or/and chloride films on substrate. EP is one of AW additives, which characterizes all surface-protecting components. In automotive industry, the most common AW remains ZnDTP which is also an oxidation inhibitor. These additives (AW, EP & FM) often fulfill multiple roles at once.

- Oxidation inhibitors: the main role of these additives is to capture oxygen in order to slow down oxidation of the lubricant. These elements need to be very reactive to $O_2$ so there are often phenolic compounds or aromatic amines. At high temperatures, phenol or amine are not efficient. So they have to be replaced by phosphor or sulfur molecules.

- Rust and corrosion inhibitors: the main role of this additive is to eliminate the corrosion between the lubricant and all other elements in contact. They need to have a good adherence to metal surface. The main goal is to attract polar groups at the metal surface in order to create, thanks to the non-polar groups, a hydrophobic film. These additives can be amines or carboxylic acids.

- VI improvers: these components decrease the viscosity fluctuation with temperature and increase the viscosity at high temperature. Between -5°C and 120°C, a mineral oil viscosity can typically decrease by 400. So to ensure a correct film thickness at high temperature, a VI improver is necessary. There are polymers or copolymers with high molecular weight. At low temperature, the molecules are hunched. At high temperature, these molecules expand and cause many interactions with hydrocarbons which increases viscosity.

- Others (detergent, dyes, tackiness agents…): other various types of additives can be found on greases. Indeed, for each tribological application, a special grease composition can be found in order to respect the contact constraints.

In table 3, the most common additives used are listed.

| Boundary Lubrication | Corrosion Inhibitors | Oxidation inhibitors | Demulsifiers | Dispersants |
|---|---|---|---|---|
| Metal dialkyl/diaryl dithiophosphates | Zinc and other dithiophosphates | Zinc dithiophosphates | High-molecular weight Ca and Mg sulfonates | Polyamine succinimides |
| Alkyl phosphates | Metal sulfonates | Metal dithiocarbamates | Alkylene oxide derivates | Hydroxy benzyl polamines |
| Phosphorized fats and olefins | Overbased metal sulfonates | Hindered phenols | Heavy metal soaps | Polyamine succinamides |
| Phospho-sulfurized fats and olefins | Metal phenate sulfides | Phenol sulfides | **Emulsifiers** | Polyhydroxy succinic esters |
| Sulfurized olefins/paraffins/fats/ fat derivatives/carboxylic acids | Overbased metal phenate sulfides | Metal phenol sulfides | Soaps of fats and fatty acids | Polyamine amide imidazolines |
| Fatty acids/other carboxylic acids and their metal salts | Fatty acids | Metal salicylates | Low-molecular weight Na and Ca sulfonates / naphtenates | **Detergents** |
| Esters of fatty acids | Acide phosphate esters | Aromatic amines | | Metal sulfonates |
| Oxidized paraffins and oils | Chlorinated was | Phospho-sulfurized fats and olefins | **VI Improvers** | Overbased metal sulfonates |
| Organic molybdenum compounds/ molybdenum disulfide | Amines | Sulfurized olefins/paraffins /fats/fat derivatives/ carboxylic acids | Ethylene-propylene copolymers | Metal phenate sulfides |
| Graphite | 2,4-Bis (alkyldithio)-1,3,4-thiadiazoles | Disalieylal-1,2-propane diamine | Polymethacrylates | Overbased metal phenate sulfides |
| Borate dispersions | | 2,4-Bis (alkyldithio)-1,3,4-thiadiazoles | Styrene isoprene / butadiene / maleic ester copolymers | Metal salicylates |
| Chlorinated fats/fat derivatives/ carboxylic acids | Alkyl succinic acids | Polyamine amide Borate dispersions D | | Metal thiophosphonates |

*Table 3: Review of the most common additives* [27]

With all these examples, infinite grease compositions are possible. Also, these possibilities create problems due to the difficulty to reproduce the exact grease compositions. For CVJ application, the most common additives used are organo-molybdenum complexes from 0.5% to 5% with other appropriate additives especially Sulphur donating ones. The effect on friction coefficient is estimated ranging from 0.12-0.15 down to 0.06 [28]. More precisely these ones:

- Molybdenum dithiophosphate which reduces wear

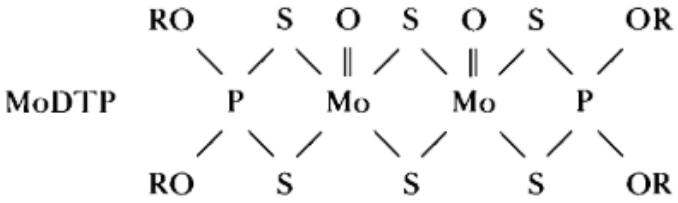


*Figure 1.20: MoDTP illustration* [54]

- Molybdenum dithiocarbamate which allows to increase load carrying capacity [29]

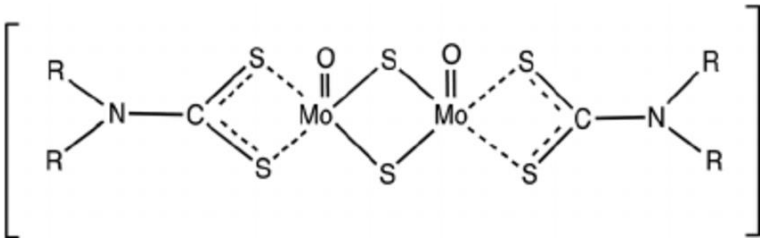


*Figure 1.21: MoDTC illustration* [55]

It is noticeable that a mix between MoDTC and MoDTP have to be preferred compared to a use of one of them alone [30].

- As said in introduction, molybdenum compounds work better with sulfur and in particular Zinc dithiophosphates can be used.

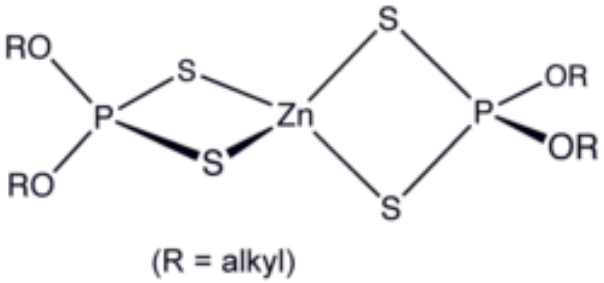


*Figure 1.22: ZnDTP illustration* [56]

These additives (among others) will be considered in the rest of this manuscript.

## 1.4. Objective and challenges of this thesis

In this thesis some scientific difficulties will have to be overcome:

- Characterize the CVJ tripod contact (loads, pressures…),
- Understand the CV joint kinematic and find a way to observe this in a confined volume,
- Determinate the CVJ lubrication characteristics. Also the lubricant quantity, its influence and the grease property are studied.

In this way, a lubrication grease mechanisms of the transmissions is done. It is based on tribological experiments. The influence of different parameters is established too. This allows to provide answers on the greased conformal contacts and establish design rules to choose greases.

Chapter two

# Experimental test rigs & methodologies

*The chapter two describes the experimental test rigs used for this work. To explore lubricants, 3 tribometers are used. They have wide range of operating conditions which enables to partially simulate real-life application conditions. In addition, one observation rig is created in order to qualify the slip inside constant velocity joint tripod tulip/roller contact.*

*To complete theses rigs, 2 analyses means & techniques are used during the following work. They help to understand wear mechanisms in the test rigs and in application.*

## 2.1. Tribological means

### 2.1.1.HFRR (High Frequency Reciprocating Rig)

A PCS instruments HFRR is used to study the different greases available for CVJ. This rig is available at the LaMCoS facilities. The tests principle is to study a ball on disc contact configuration in pure sliding conditions as shown on figure 2.1. The load is applied by 100 grams weights on upper shaft specimen (figure 2.2).

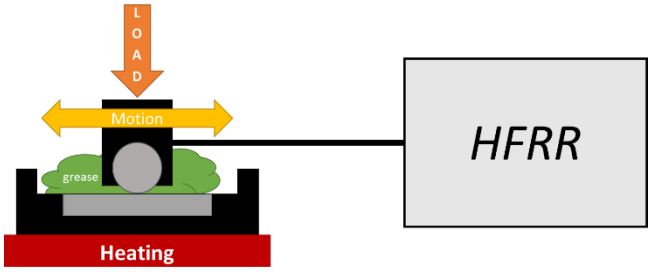


*Figure 2.1: Schematic of the HFRR*

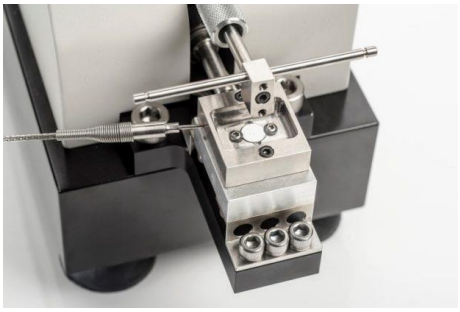

*Figure 2.2: picture of HFRR (PCS Instruments)*

The upper specimen is a 6 mm diameter ball and the bottom specimen a flat disc. They are made from polished 100Cr6 steel with surface roughness of Ra < 20 nm for the disc and Ra < 50 nm for the ball.

The rig can be configured in terms of frequency (from 10 Hz to 200 Hz) and stroke (from 20 µm to 2 mm). However, a rule between these 2 factors have to be respected in order to remain in operating rig conditions (figure 2.3).

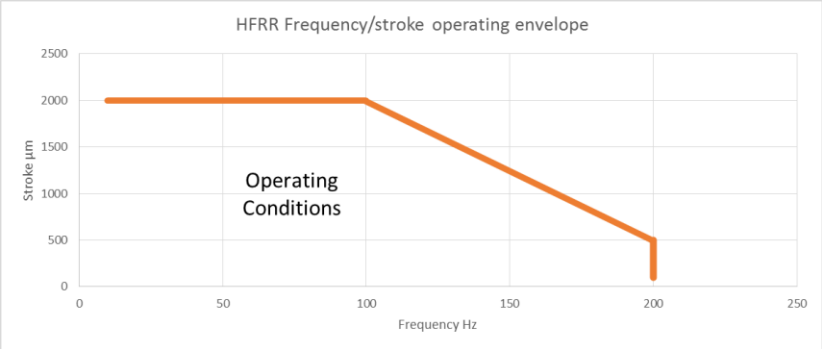


*Figure 2.3: HFRR operating conditions (PCS Instruments)*

Also, temperature can be set from ambient temperature to 150°C thanks to the heater block placed under the lower specimen (figure 2.1). Finally, the Hertz pressure range is available in Table 4.

| *Load in N* | *0.981* | *1.962* | *2.943* | *3.924* | *4.905* | *5.886* | *6.867* | *7.848* | *8.829* | *9.81* |
|---|---|---|---|---|---|---|---|---|---|---|
| *$P_h$ in GPa* | 0.652 | 0.821 | 0.940 | 1.035 | 1.114 | 1.184 | 1.247 | 1.304 | 1.356 | 1.404 |
| *Contact radius in mm* | 0.027 | 0.034 | 0.039 | 0.043 | 0.046 | 0.049 | 0.051 | 0.054 | 0.056 | 0.058 |

*Table 4: HFRR pressure and contact radius function of load*

Results provided by HFRR are (figure 2.4):

- Friction coefficient (deduced from the force applied and the force generated by friction, measured by piezoelectric force transducers)
- Electrical contact potential (can give qualitative information on film formation)


*Figure 2.4: HFRR results example*

In order to have repeatable test results, technical solutions corresponding to test parameters are given in table 5.

| | Parameter | Technical solution (operating range) |
|---|---|---|
| Applied | Stroke length / Frequency | electromagnetic vibrator (20 µm – 2.0 mm / 10 – 200 Hz) |
| | Normal load | hanging weights (0 - 1.0 kg) |
| | Temperature | two 24V, 15W cartridge heaters (ambient to 150°C) |
| Measured | Stroke length / Frequency | Linear Variable Differential Transformer (LVDT) |
| | Friction force | piezoelectric force transducer (Up to 10.0 N) |
| | Film variation | changes in electric contact potential |
| | Temperature | platinum RTD probe |

*Table 5: PCS Instruments, HFRR parameters*

A procedure test was created to insure repeatability. Each parts (Specimens, hex keys, screws, tweezers …) have been rinsed and cleaned in an ultrasonic bath during 3 minutes.

The solvents used (in order) are:

- Ethyl acetate (except for specimens)
- Ethanol
- Heptane

### 2.1.2.MTM (Mini Traction Machine)

Another PCS instruments MTM (Mini Traction Machine, figure 2.5) available also at the LaMCoS facilities consists of a ball on disc contact with rolling and sliding possibilities. The ball is mounted on a rotational shaft with speed control. The disc is also on a rotational shaft with speed control too. These speeds are independent and so the slide-to-roll ratio can be controlled inside the contact (figure 2.6). The load is applied controlling the ball height displacement on MTM (figure 2.7).

Figure 2.5: MTM picture (PCS Instruments)

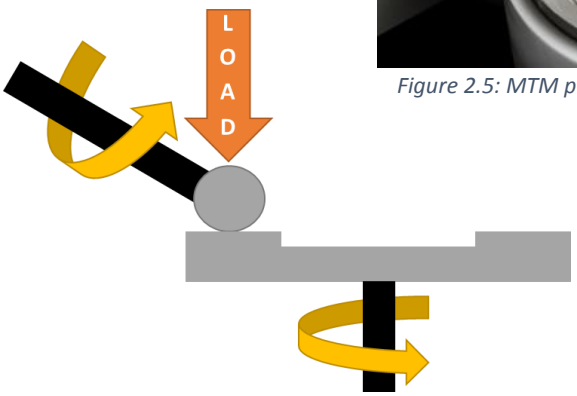


Figure 2.6: MTM principe

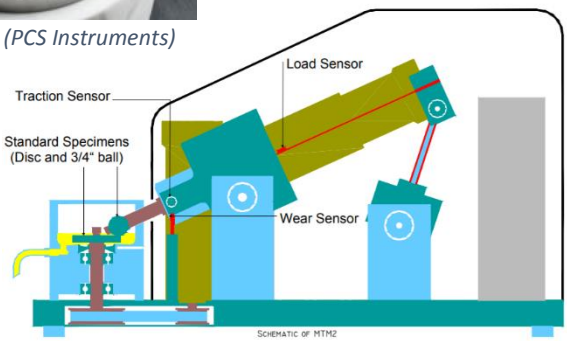


Figure 2.7: MTM load system (PCS Instruments)

The rig can supply various types of friction measurements. For example:

- Evolution the friction coefficient according time
- Stribeck curves (given SRR, velocity, load or temperature variation)
- Traction curves (given rolling speed, SRR variation)

The load can be set from 0 to 75 N. Standard specimens are made from 100Cr6 steel. The ball diameter used for this study is ¾" (19.05 mm). Two different finishing surfaces are available for discs: smooth (Ra < 0.01 µm) or rough (Ra > 0.1 µm). The ball is smooth (Ra < 0.01 µm). Contact pressure can be up to 1.28 GPa (Table 6).

| *Load in N* | *10* | *20* | *40* | *60* | *75* |
|---|---|---|---|---|---|
| *$P_h$ in GPa* | 0.654 | 0.825 | 1.039 | 1.189 | 1.281 |
| *Contact radius in mm* | 0.085 | 0.108 | 0.136 | 0.155 | 0.167 |

*Table 6: MTM pressure and contact radius function of load*

The other parameters are available in table 7.

| | Parameter | Technical solution (operating range) |
|---|---|---|
| Applied | Velocity / SRR | Direct current motor (-4 – 4 m.s-1 / 0 – 100%) |
| | Normal load | imposed displacement => Force (from 0 – 75 N) |
| | Temperature | electrical resistance (ambient to 150°C) |
| Measured | Velocity / SRR | tachymeter (+/- 2 mm.s-1 below 100 mm.s-1 +/- 2% above) |
| | Normal Load | load sensor (+/- 1 N) |
| | Friction force | piezoelectric force transducer (+/- 0.2 N) |
| | Temperature | thermocouples (+/- 0.5°C) |

*Table 7: MTM parameters (source PSC Instruments)*

An accessory is used in order to insure contact supply when lubricant is grease. As shown in figure 2.8, its role is to merge the 2 lines created by the grease pushed by the ball on rolling track sides to track center. So, contact lubrication is ensured.

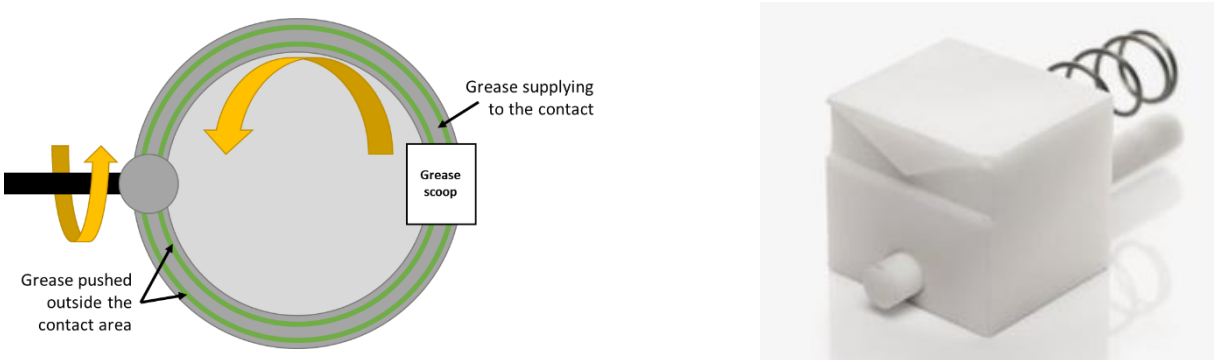


*Figure 2.8: MTM grease scoop schematic and picture (PCS Instruments)*

### 2.1.3.EHD2 (Ultra Thin Film Measurement System)

In addition to other PCS instruments Rig, EHD2 (Ultra Thin Film Measurement System, figure 2.9) consists of a ball or roller on disc contact with rolling and sliding possibility like MTM (figure 2.10). This rig is also available at the LaMCoS facilities or on Institute of Science and Innovation in Mechanical and Industrial Engineering from Porto University. The ball is mounted on a rotational shaft with speed control. The disc is also on a rotational shaft with speed control too. These speeds are independent and so a SRR can be introduced inside the contact. It can measure traction coefficient like on MTM.

*Figure 2.9: EHD2 from PCS Instruments (PCS Instruments)*

*Figure 2.10: Contact view (PCS Instruments)*

The main principle is exposed on figure 2.11. Knowing the lubricant optical properties, the lubricant film thickness can be calculated using interferometry by measuring the wavelength of light at a point [31].

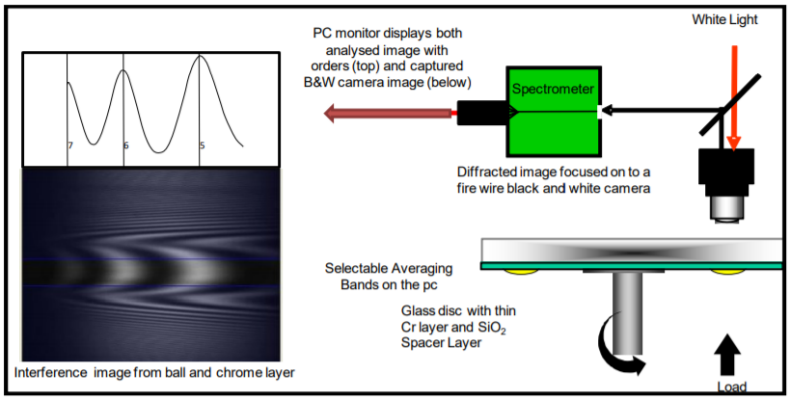


*Figure 2.11: Interferometry principle (PCS Instruments)*

Standard specimens are made from 100Cr6 steel. For disc, Glass or Sapphire can be used. The main parameters of the rig are available in table 8.

| Parameter | Operating range |
|---|---|
| Velocity | 0 to 4 m/s |
| Normal load | 0 to 50 N |
| Temperature | ambient to 150°C |
| Contact Pressure | 0 to 0.7 GPa (steel ball on glass Disc),<br>0 to 3 GPa (WC on sapphire) |
| Film thickness | load sensor (+/- 1 N) |
| Friction force | 1 to 1000 nm |

*Table 8: EHD parameters*

### 2.1.4.Observation Rig [32]

The main idea was based on the previous work by C. H. Lee [33]. This study is using a holed housing to observe the SRR in the contact between track and roller. To complete this work, an idea was to keep the geometry and find a solution to see the contact using a transparent tulip. Translucent resin allows to observe in real time the roller behaviour from outside. The rig was designed at the LaMCoS facilities using FDM 3D printing and some standard part like threaded rod, screws, nuts and stub. A lateral transmission from Groupe PSA was cut to have only the gearbox side without the housing. Moreover, an electric motor was put at the end of the transmission shaft.

*Figure 2.12: Translucent housing*

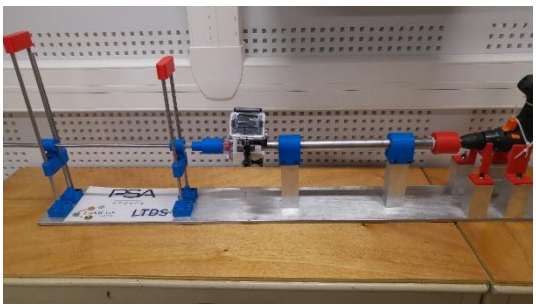


*Figure 2.13: Observation Rig*

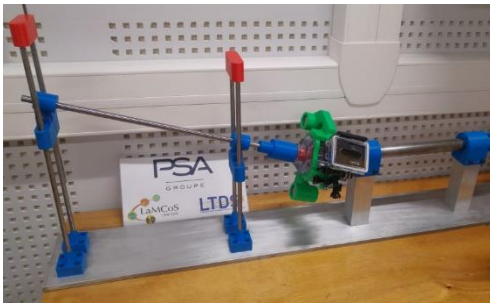


*Figure 2.14: Observation Rig*

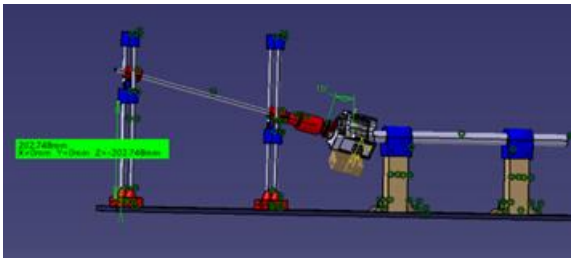

*Figure 2.15: CAD with articulation angle control*

In order to observe the contact, a sport camera was attached to the housing (Figure 2.13). The articulation angle is controlled by threaded rods (Figure 2.15). Polyurea grease was added before tests into housing and 2 displacement directions were defined. The first one goes from the gearbox to the shaft and the second one from the shaft to the gear box as shown in figure 2.16.

In addition, in order to post process the results from the camera different numerical tools were created:

- Rolling distance calculation

The first one used the model from F. ESNAULT [34] to calculate the rolling distance for each angle chosen. For example, with an articulation angle α of 10 degrees and a 20 mm distance between the roller axis and the track the ESNAULT's equations predicts a rolling distance of 3.53 mm.

- Scale calculation

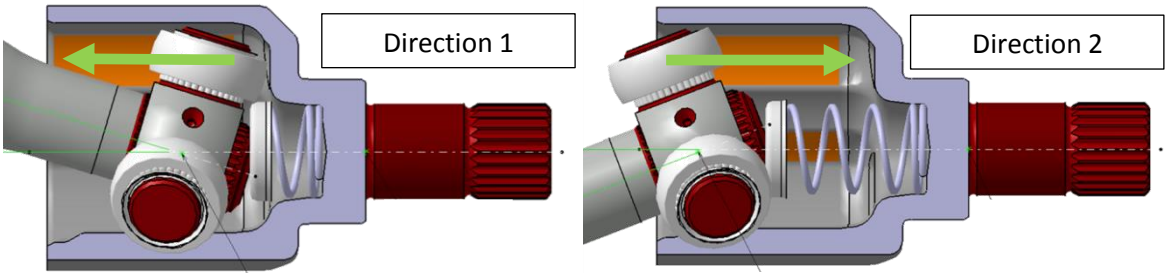


*Figure 2.16: Directions Definition*

Analyses of the video in order to have the same views at several rounds of intervals are conducted. A conversion step from pixels to millimeters is necessary, selecting 4 points to define the scale as shown on figure 2.18.

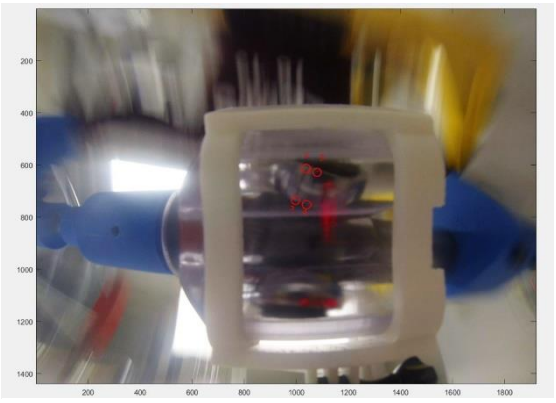

*Figure 2.17: scale selection*

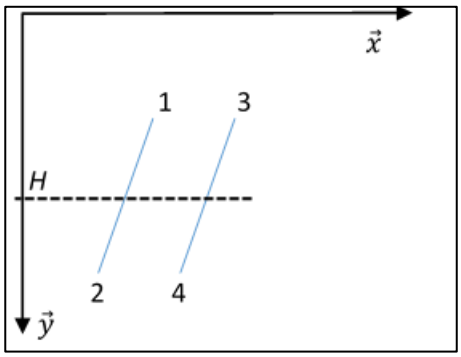


*Figure 2.18: scale explanation drawing*

The slope is calculated for the 2 straight lines using equation 1 and compared in order to check the parallelism.

$$slope_{12} = \frac{y_2 - y_1}{x_2 - x_1};\ slope_{34} = \frac{y_4 - y_3}{x_4 - x_3} \quad (1)$$

The constant part $D_{slipXX}$ from the strait line equation is given:

$$\begin{cases} D_{slip12} = y_2 - x_2 * slope_{12} \\ D_{slip34} = y_4 - x_4 * slope_{34} \end{cases} \quad (2)$$

The physical distance between 2 lines is known at the roller surface. It corresponds to a 10 degrees strut used to draw the line on rollers. Numerically, the distance is calculated thanks to equation (3)

$$D_{pixel} = \left| \frac{H - D_{slip34}}{slope_{34}} - \frac{H - D_{slip12}}{slope_{12}} \right| \quad (3)$$

With H the mean roller height, most of the time around 1000 pixels.

- Slipping difference during a complete joint rotation

Image correlation is used to study straight line displacement. Knowing the rolling distance, slip difference between direction 1 and direction 2 is calculated.

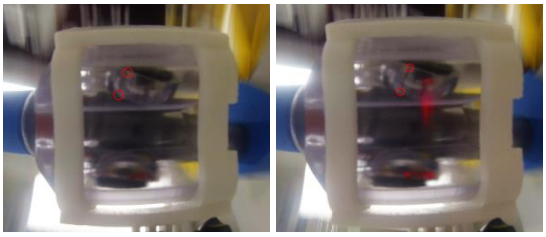

*Figure 2.19: slipping selection step*

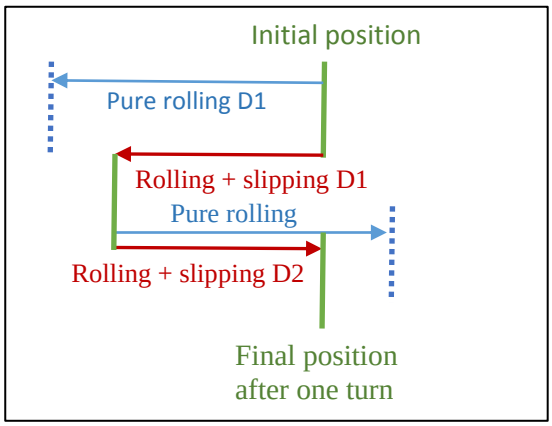


*Figure 2.20: Slipping drawing*

In this way, if slipping is symmetric in both directions, the distance between the initial position and the final one will be zero. In order to study this symmetry, parameter S is created (4).

$$S = \frac{sd}{rd * 2 * X} \quad (4)$$

With: - *sd* the slipping distance between initial and final position after X turns

- *rd* the theoretical rolling distance after X turns

- slipping distance

This post-processing studies only one CVJ turn. The main goal is to obtain the slip rate in the 2 directions. The maximal rolling distance (mrd) is used (5).

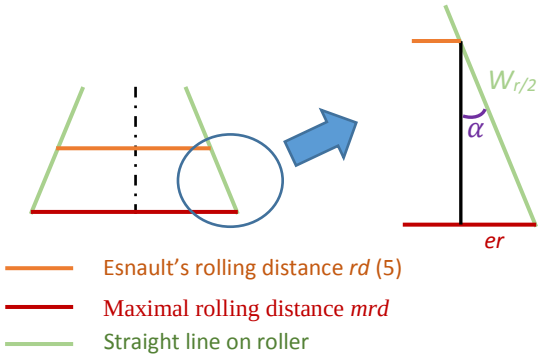


*Figure 2.21: slip rate drawing*

$$mrd = rd + 2 * er \quad (5)$$

$$er = W_{\frac{r}{2}} \sin \alpha \quad (6)$$

With $W_{r/2}$ being the roller half width

Slip ratio $\tau_s$ is calculated using equation 7 and the measured distance between the 2 straight line *md:*

$$\tau_s(\%) = \left( \frac{md}{mrd} - 1 \right) * 100 \quad (7)$$

## 2.2. Surface Analysis

### 2.2.1. Wear scar qualification

*Figure 2.22: Sensofar PLu neox picture (source sensofar)*

A Sensofar PLu neox optical profiler with Nikon objectives is used in order to qualify the wear scar (figure 2.22). It is available at the LaMCoS facilities. Its vertical resolution is less than 0.1 nm. It uses interferometry in order to determinate topography.

Interferometry is a measurement process using wave interference phenomena. Here, it is light waves that have been used. By using two light rays (generally dividing a ray into two), an interference pattern can be formed when these two rays are superposed. As the wavelength of visible light is very short, it is possible to detect small variations in the differences in the optical paths (distance traveled) of the two rays, since these differences will produce noticeable variations in the interference pattern.

The measures are post-processed using MoutainMap Topography software. The wear is characterized by the scar width [35] and the volume above and below the surface [36]. The different steps are:

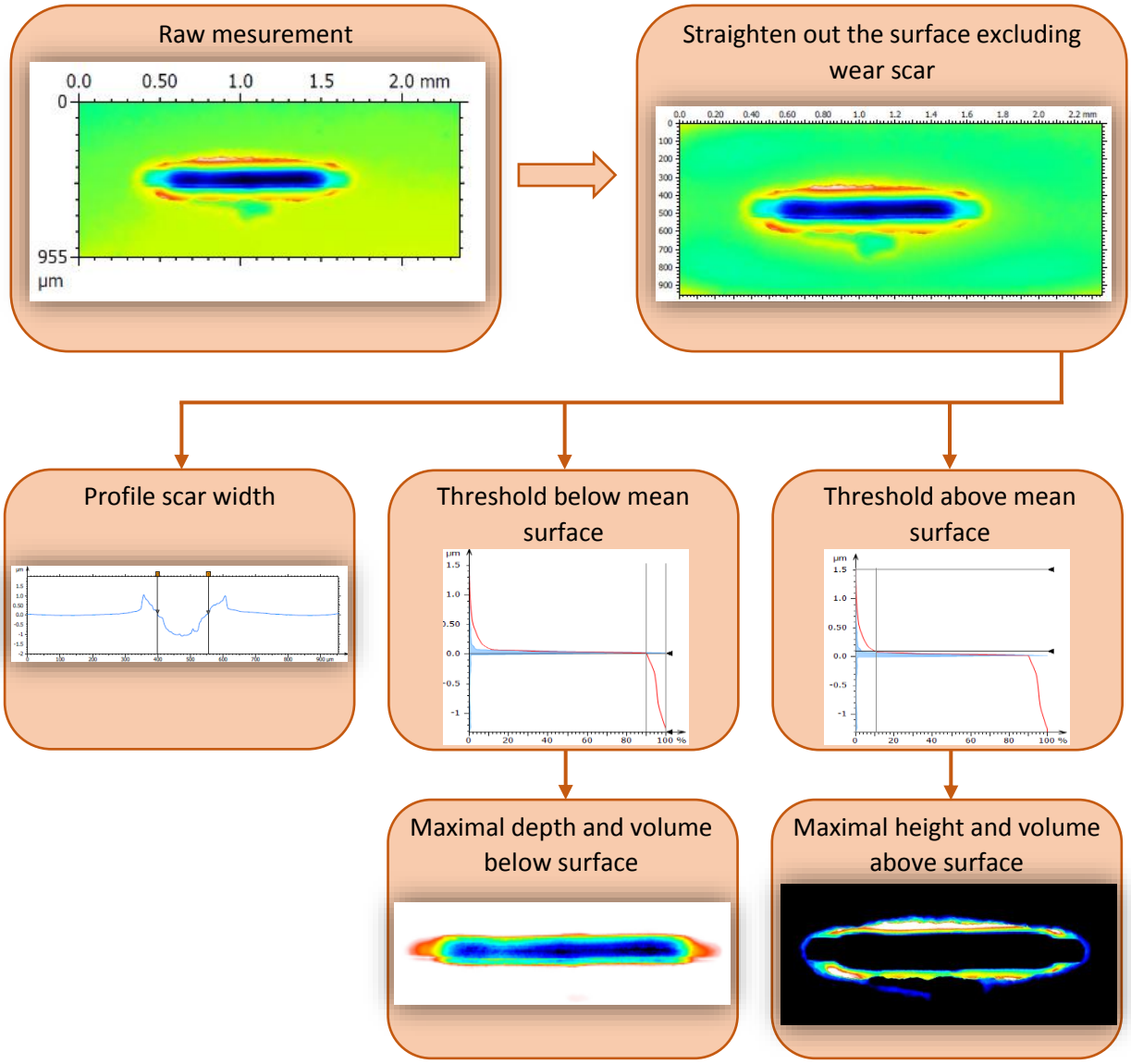

Topography of flat surfaces are carried out. Indeed, the measurement is easier than on ball and plastic deformation can be studied. The raw measurement gives a tilt surface that needs to be corrected. To do this step, the wear scar has to be excluded in order to have a perfectly horizontal mean surface. With these results, the surface can be post-processed exporting the chosen factors in order to qualify wear: wear scar width, volume below & above the mean surface with the maximal and minimal vertical dimensions of lower specimen.

### 2.2.2.X-Ray Photoelectron Spectroscopy (XPS)

The XPS is an analytical technics to analyze the chemical composition of extreme surface (few nanometers). It is available on LTDS facilities. In particular, it is used in order to determine the tribofilm composition as it can supply elemental composition of the sample. In addition their chemical environment are also available.

This analysis is based on the measurement of kinematic energy of electron ejected from the sample under impact of X-Ray (figure 2.23).

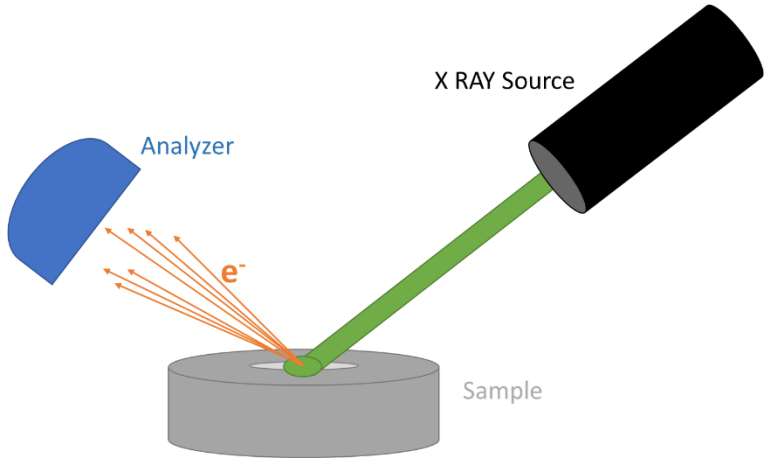


*Figure 2.23: Schematic of XPS principle*

Indeed, knowing the source energy (keV) and the kinematic energy, the blinding energy can be deducted (equation 8).

$$hv = E_b + E_k \quad (8)$$

where $E_b$ is the blinding energy, $E_k$ is the kinematic energy of emitted photon, $hv$ the energy of incident photon (with $h$ the Planck constant and $v$ the photon frequency)

The spectrum is obtained by an electron counting as a function of their binding energy.

The XPS energy resolution is 0.2 eV and carbon peak have been taken as reference at $C_{1s}$=284.88eV. The source can be set to 1486.6 eV using $AlK_\alpha$ or 1253.6 eV using $MgK_\alpha$. All the tests were done under a pressure of $10^{-9}$ Pa to prevent contamination. To clean the sample, heptane and isopropanol are used in an ultrasonic bath (10 minutes both).

A survey scan was first recorded in order to identify the chemical elements on the surface. High resolution spectra were then recorded to focus on these element energies. An XPS Handbook and Multipack software were used to match the energy peaks to chemical elements.

With all these tribometers presented in chapter two, experimental investigations are performed in following chapters dealing with work objectives. These devices helped to reproduce with repeatability the phenomena that could be found on vehicle in laboratory. After these steps; the analysis means supplied key information on constant velocity joint durability.

Chapter three

# Contact characterization

*The chapter three characterizes the contact of a constant velocity joint tripod which influences the component durability and power losses. It starts from Hertz' theory presented in chapter one to calculate the contact pressure. To complete, a dynamic simulation is performed to calculate the kinematic of each component which influences the contact velocities.*

*Then, the amount of slip which is a challenge to qualify in that type of high conformity contacts is investigated. The technique used is experimental: it gives slipping as a function of constant velocity joint angularity.*

## 3.1. Geometrical contribution

### 3.1.1.Contact Pressure for the roller – track contact

In order to qualify contact pressure, Hertz theory is used. The Young modulus is chosen E = 210 000 MPa and the Poisson's ratio is 0.29 which correspond to the steel of the roller (100Cr6) and the track (C48). To know the maximum load applied on a roller in CVJ, an equal load repartition between the 3 rollers is considered. The track radius is considered as the roller radius plus 0.5 mm to match with reality.

It should be noticed that in the present case it is not corresponding exactly to Hertz hypothesis. A range between the Hertz pressure and 110% of the Hertz pressure will be used for further application in the manuscript to compensate the hypothesis deviation thanks to the work of Lee et al [13]. However, Hertz calculation can be consider as a good approximation.

| Torque N.m | Force on track in N | $P_h$ in GPa | $P_h$ in Gpa +10% | Semi Axis b mm | Semi axis a mm | Contact area in mm² |
|---|---|---|---|---|---|---|
| 250 | 3516 | 1.30 | 1.43 | 3.49 | 0.37 | 4.05 |
| 300 | 4219 | 1.38 | 1.52 | 3.71 | 0.39 | 4.58 |
| 400 | 5626 | 1.52 | 1.67 | 4.08 | 0.43 | 5.55 |
| 500 | 7032 | 1.64 | 1.80 | 4.40 | 0.47 | 6.44 |
| 600 | 8439 | 1.74 | 1.92 | 4.67 | 0.50 | 7.27 |
| 700 | 9845 | 1.83 | 2.02 | 4.92 | 0.52 | 8.06 |

*Table 9: Contact characteristics as function of engine torque*

### 3.1.2.Roller kinematic inside the housing tracks

A numerical model using a dynamics simulation software is used in order to characterize kinematics between the track and the roller during one CVJ rotation. It is based on CAD geometry that has been imported on software. The used hypothesis is available in appendix A together with all results. The first important results are to identify the rolling distance of the rollers in the track (figure 3.1) and the instantaneous roller speed (figure 3.2) in the track or instantaneous rotational roller speed in the track (figure 3.3).

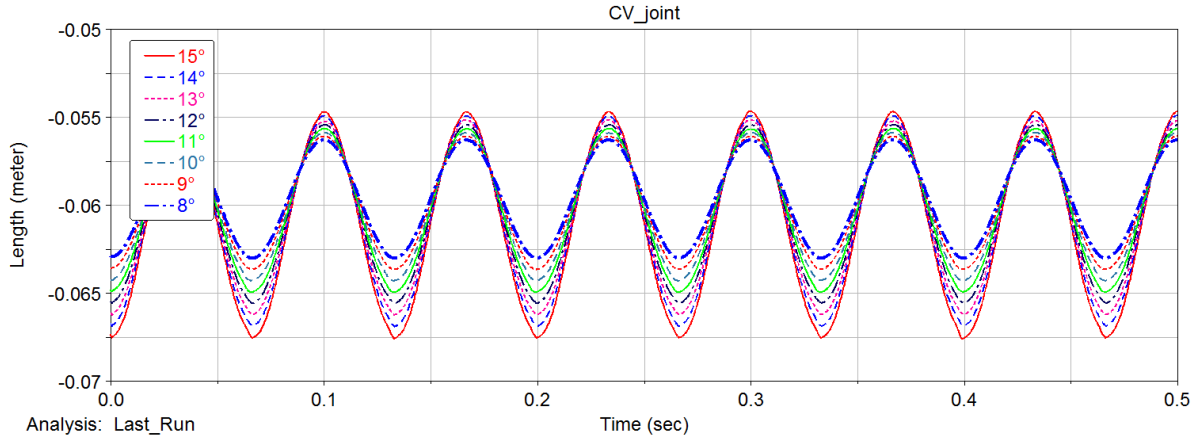


*Figure 3.1: Displacement distance example*

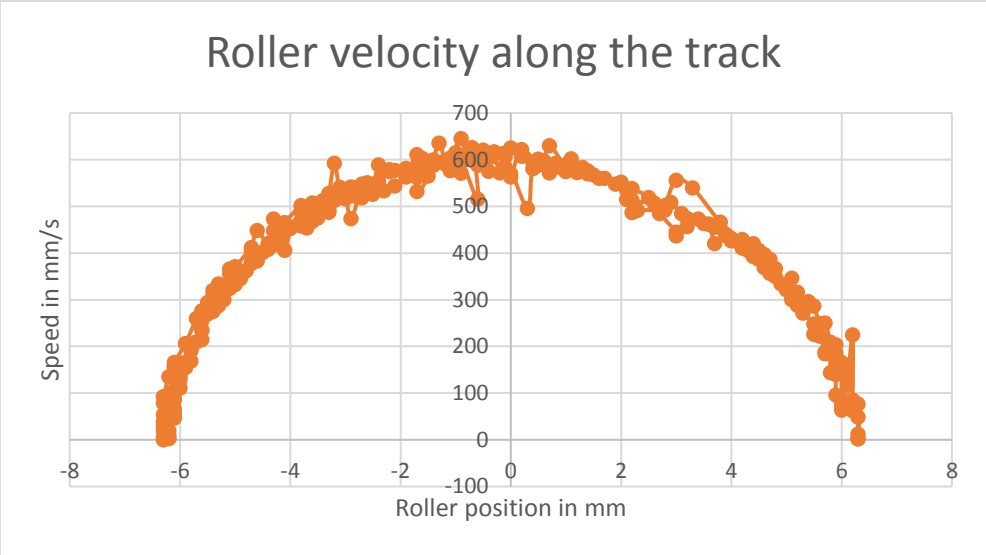


*Figure 3.2: 15° velocity example from dynamic simulation*

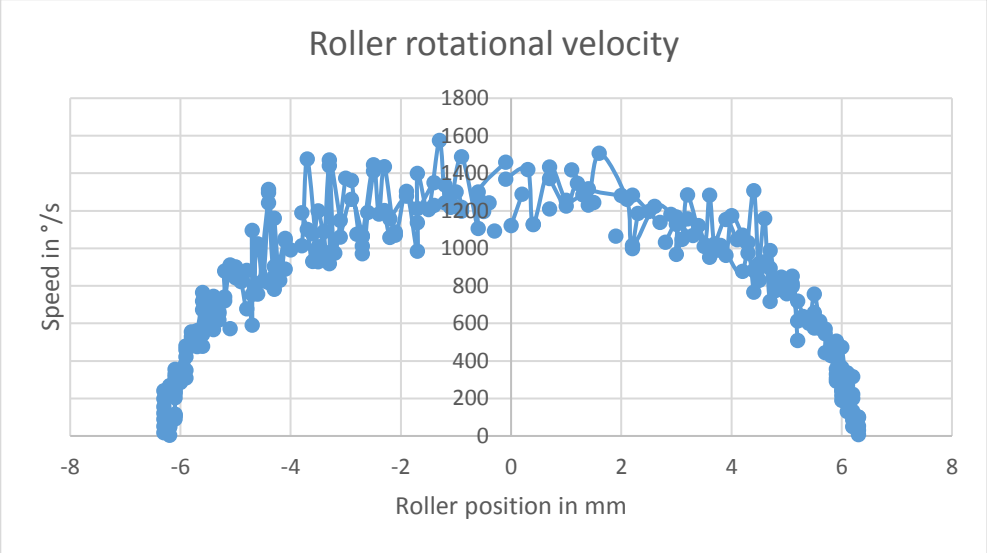


*Figure 3.3: 15° rotation velocity example from dynamic simulation*

However, even if this simulation works well with an example at 15°, an analytical calculation was chosen in order to decrease calculation CPU time. To deal with that objectives these equations were used [34]:

- The spider center S (figure 3.4) describe a circle with a radius R in the spider plan.

$$R = d\frac{1-\cos\alpha}{2\cos\alpha} \quad (9)$$

*With:* *- $\alpha$ articulation angle*

*- d distance between the rolling track and the rotational axis*

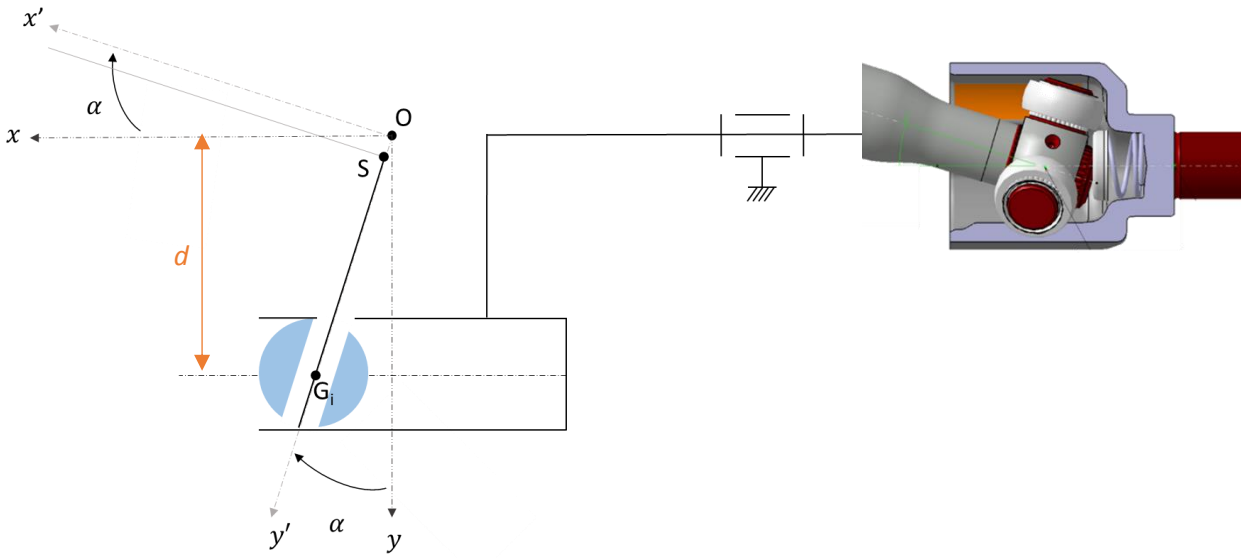


*Figure 3.4: Position schematic with view of CVJ*

Also, the spider variated its position along the spider from point E (minimum position) to F (maximal position) in this same plan (figure 3.5)

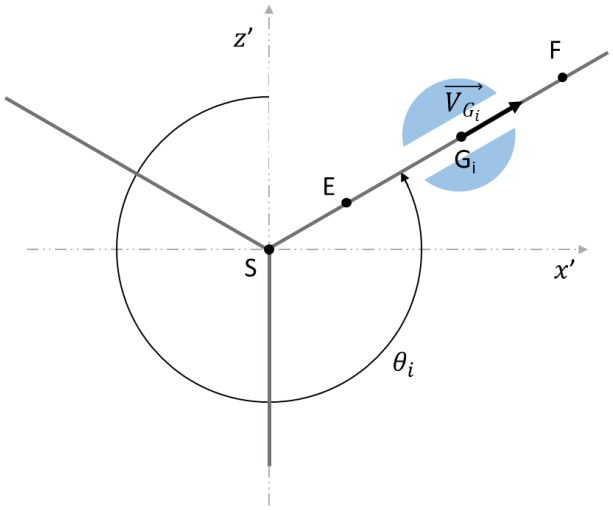


*Figure 3.5: Position schematic 2*

$$\left\|\overrightarrow{SE}\right\| = \frac{d(3\cos\alpha - 1)}{2\cos\alpha} \quad (10)$$

$$\left\|\overrightarrow{SF}\right\| = \frac{d(3 - \cos\alpha)}{2\cos\alpha} \quad (11)$$

*With α articulation angle, d distance between the rolling track and the rotational axis*

- In this plan, the roller velocity ($G_i$ roller center of inertia) between the roller and the spider is :

$$\overrightarrow{V_{G_i}} = 2d\omega\frac{1-\cos\alpha}{\cos\alpha}\sin 2\theta_i \quad (12)$$

*With α articulation angle, ω rotational speed, d distance between the rolling track and the rotational axis*

- The position $\overrightarrow{OG_i}$ in the system $(O, \overrightarrow{x'}, \overrightarrow{y'}, \overrightarrow{z'})$ is (figure 3.4):

$$\overrightarrow{OG_i}\left|\begin{matrix}0\\ \frac{d}{\cos\alpha}\sin\theta_i\\ d\cos\theta_i\end{matrix}\right.$$

*With $\theta_i$ the rotation angle of the CVJ, d distance between the rolling track and the rotational axis, $\alpha$ articulation angle*

A comparison between the dynamic simulation and the analytical model is performed. As it is possible to observe in figure 3.6, the analytical model corresponds to dynamic simulation.

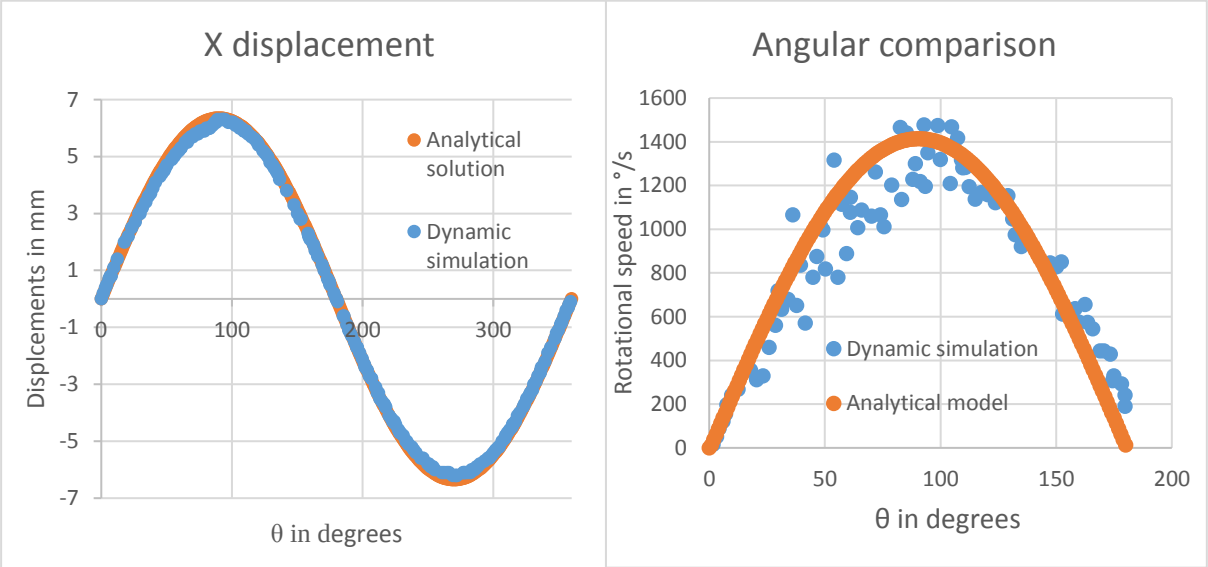


*Figure 3.6: Comparison between models for 15°*

To summarize the principle data from these models are available in table 10.

| Articulation angle α in degrees | 1 | 2 | 3 | 4 | 5 | 6 | 7 | 8 | 9 | 10 | 11 | 12 | 13 | 14 | 15 |
|---|---|---|---|---|---|---|---|---|---|---|---|---|---|---|---|
| Displacement in mm | 0.8 | 1.7 | 2.5 | 3.3 | 4.1 | 5.0 | 5.8 | 6.7 | 7.5 | 8.4 | 9.2 | 10.1 | 10.9 | 11.8 | 12.7 |
| Translation velocity in mm/s | 39.0 | 78.0 | 117.1 | 156.2 | 195.4 | 234.8 | 274.3 | 313.9 | 353.8 | 393.8 | 434.2 | 474.8 | 515.7 | 556.9 | 598.5 |
| Rotational velocity in °/s | 94.2 | 188.5 | 282.7 | 377.0 | 471.2 | 565.5 | 659.7 | 753.9 | 848.2 | 942.4 | 1036.7 | 1130.9 | 1225.2 | 1319.4 | 1413.6 |

*Table 10: Kinematics data for 15 Hz frequency*

## 3.2. Lubrication contribution: observation rig [32]

### 3.2.1.Technical choice of materials for Observation Rig & Dry tests

An investigation of traction coefficient has been lead using a Mini Traction Machine (MTM, 2.1.2) in order to compare the behaviour between steel (100Cr6)/steel contact and steel/plastic (disc) contact (figure 3.7) under greased lubrication. The plastic used is phenol-formaldehyde resin [37]. This preliminary study is done in order to validate material choices for the observation rig design.

*Figure 3.7: Steel and Plastic MTM discs*

Tests considering slide-to-roll ratio (SRR) and load can characterize the grease ability to separate surfaces and also evaluate traction coefficient. Plastic resin used for MTM disc will be the same as the one used for the housing 3D printing (2.1.4). In order to know exactly the disc roughness, it has been measured on an optical profilometer (2.2.1) (figure 3.8 & 3.9).

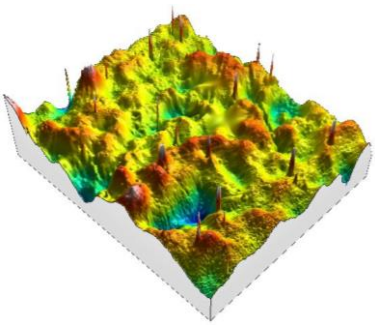

*Figure 3.8: 3D view of 3D print disc*

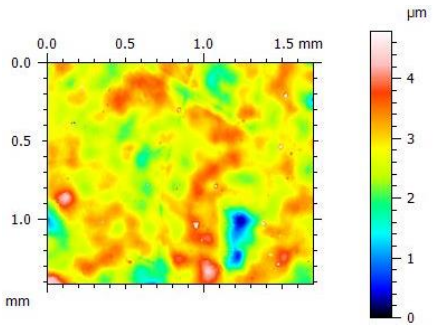


*Figure 3.9: Optical disc measurement*

These measurements give a $Ra \approx 0.2\ \mu m$ that corresponds to a MTM rough disc surface.

In order to validate the chosen conditions (a rotational speed of 150 rpm and ambient temperature), tests at 50°C and 80°C were conducted. Thus maximum speed was fixed to 200 mm/s in order to fit the rotational speed (150 rpm) to roller contact speed. The load was set to 20 N to fit the load from the observation rig to MTM rig.

Traction curves for plastic/steel contact and steel/steel contact almost fit at 50°C (figure 3.10).

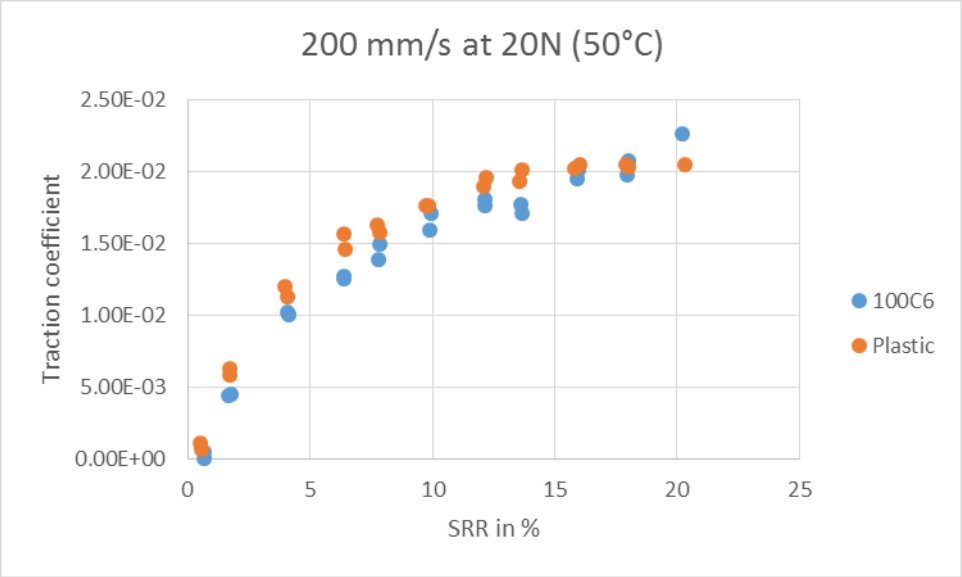


*Figure 3.10: Traction coefficient using different disc material at 50°C*

In addition, Stribeck curves were constructed at 80°C with an SRR of 10% for steel/steel contact and steel/plastic contact (figure 3.11)

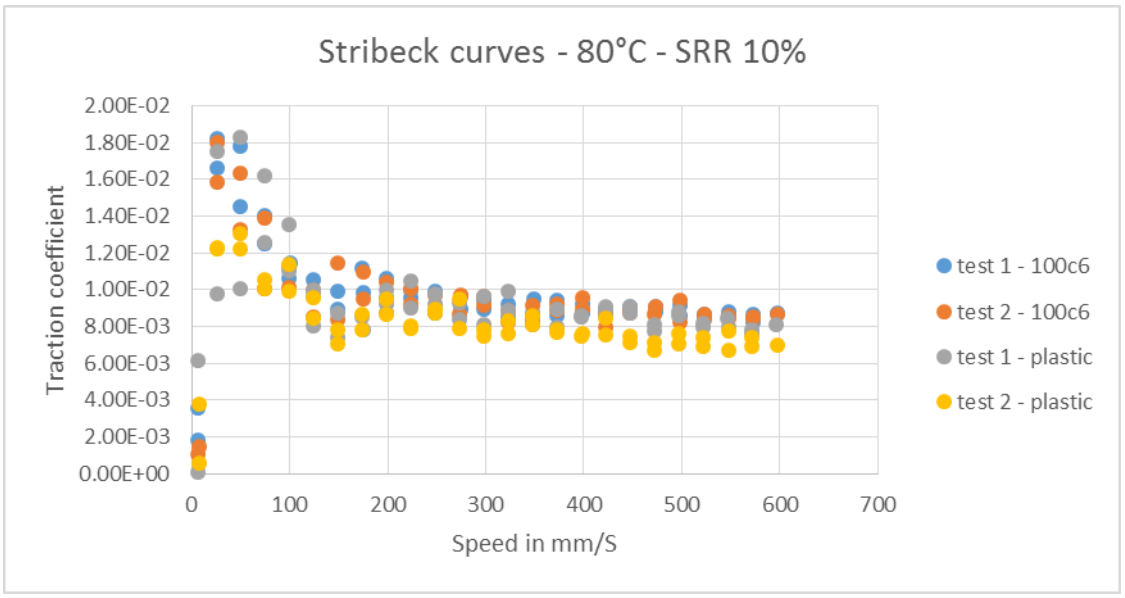


*Figure 3.11: Stribeck curves for different materials contact*

First of all, it is noticeable that experiments are repeatable. With these two different tests, the impact of plastic material versus steel one seems negligible under the tested contact conditions. So the use of plastic 3D printed housing seems relevant in our case.

In the following works, each experiment using the user-made rig was conducted twice. A reference corresponding to the work of C.H. Lee [38] gives the slide to roll ratio as a function of the articulation angle: with the articulation angle α.

$$SRR\ (\%) = 0.585 * \alpha\ (°)\ \ (13)\ \ with\ the\ articulation\ angle\ \alpha\ [38].$$

### 3.2.2.Slip difference

Different tests are conducted:

a. Dry Test
b. Full of grease, 100% lubricated (standard vehicle quantity)
c. With 55% of grease doing an acquisition with the articulation angle α varying from 18° to 0°
   With 55 % of grease doing an acquisition with the articulation angle α varying from 0° to 18° and 18° to 0°

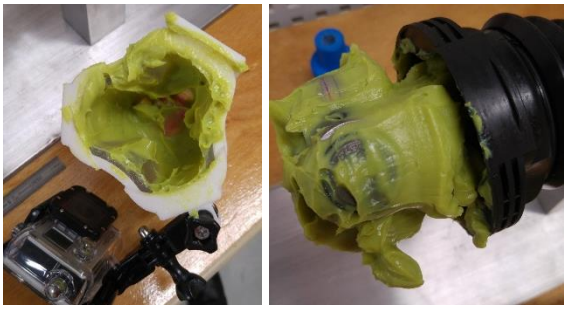

*Figure 3.12: greasing*

a. Dry test

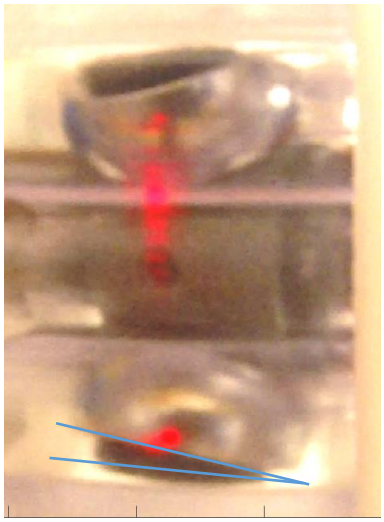

*Figure 3.13: roller misalignment*

In this study it is difficult to keep all grease volume inside the housing because the joint is partially opened (no seal).

Initially, dry tests have been led. The first observation is that a roller misalignment is noticed as shown in figure 3.13. This minor misalignment should be the result of functional clearance between needles, rollers and spider or due to the roller inertia. However, it delays the roller angular position and could be the cause of some dysfunction like wear or shudders.

b. Full of grease

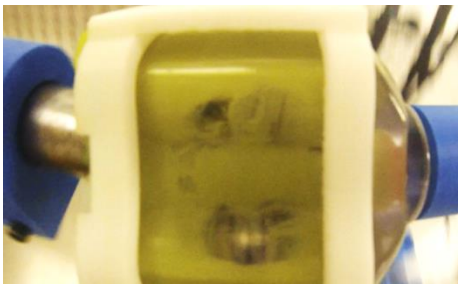

*Figure 3.14: cavities*

In order to study the greased tripod CVJ, the housing is filled with polyurea grease volume and then put together. Tests were conducted at ambient temperature and at 150 rpm. In these tests which were repeated twice, some cavities are observable in the grease at the end of the test (figure 3.14) suggesting that the grease is pushed out of contact zone and not able to replenish the contact. Thus, it was noted that, as the operation progressed, the grease migrated as if being "pushed" by the large roller displacement (figure 3.15).

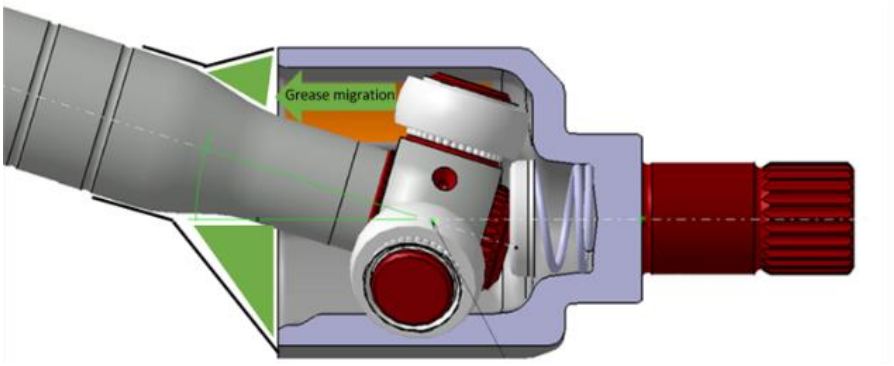


*Figure 3.15: grease migration illustration*

A higher articulation angle leads to a quicker grease migration. This phenomenon therefore allows more freedom to rollers and thus allows more sliding and slipping difference between the 2 directions (figure 3.15). It seems, that the base oil in the grease has an impact on the unsymmetrical slippage and lubrication conditions. In addition, when the housing is full of grease, with a large volume occupied, the grease will not be able to migrate out of the contact zone and will ensure a continuous lubrication and vibration damping. The final result is a symmetrical sliding behaviour so a slip difference near to 0% (figure 3.16).

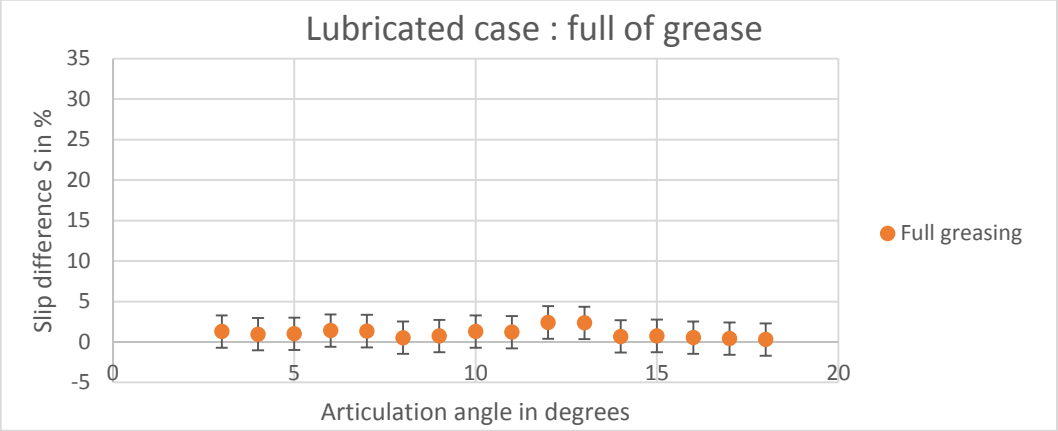


*Figure 3.16: lubrication with all grease volume available*

c. Incompletely greased

*Figure 3.17: grease distribution*

In order to study the grease quantity influence, an experiment was lead, called incompletely greased. First of all, 30 % of grease is distributed along the tracks (figure 3.17). Then the joint is assembled on the rig and re-lubricated with the remaining quantity of grease to provide lubrication on both sides of the rollers.

The methodology was not modified for other acquisitions and repeatability is observed (figure 3.18). Moreover, the 3rd test (figure 3.19) was conducted increasing the articulation angle from to 18° and then reducing it from 18° to 0°.

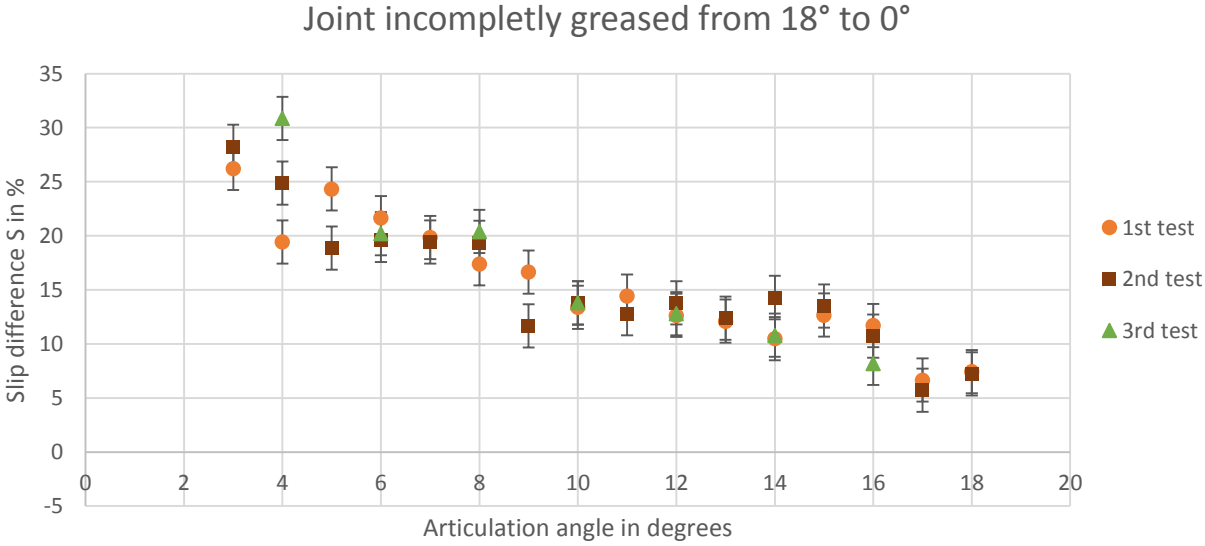


*Figure 3.18: housing incompletely greased, decreasing angle (55% of grease mass; from 18° to 0°of articulation angle)*

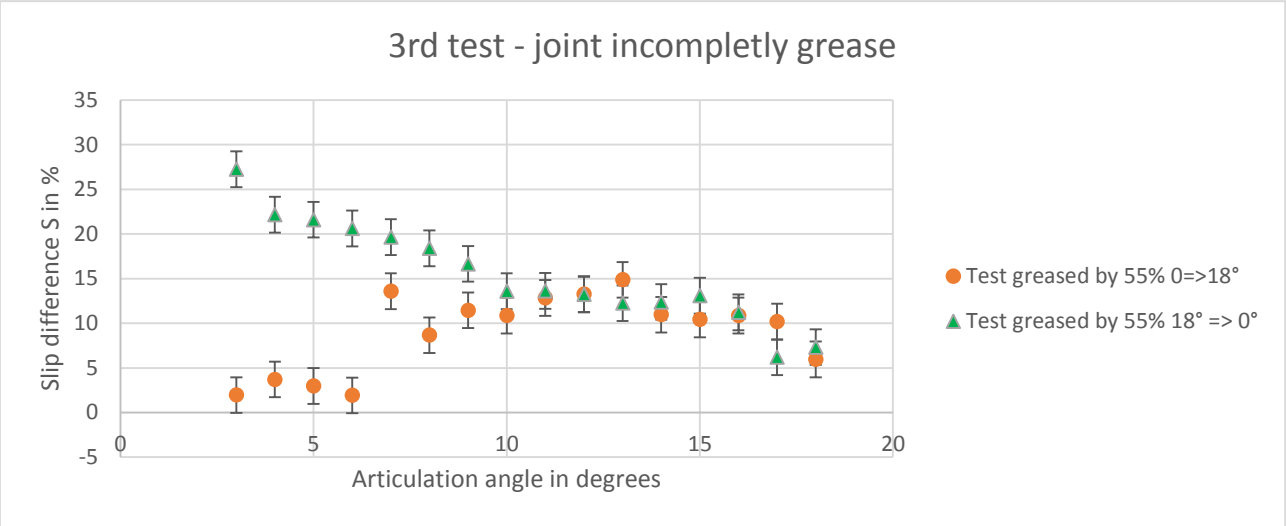


*Figure 3.19: housing incompletely greased, increasing angle*

When starting acquisition at 18°, cavities are created. Contact conditions are subject to degradation resulting in an increase in the slip difference. Thus, with a reduced grease volume the roller will tend to not have the same slip conditions in both directions. On one hand, some points match with the full lubricated case, and, on the other hand some points present a higher slip difference.

It can be explained by lubrication defects. When the acquisition starts at 18°, roller displacement is very large. If articulation angle decreases, cavities are formed and the lubrication only depends on the grease ability to come back to contact area. At the opposite, if the acquisition starts at 3°, the roller displacement will increase finding always grease to push outside the track. Indeed, it is possible to observe this phenomenon on figure 3.20.

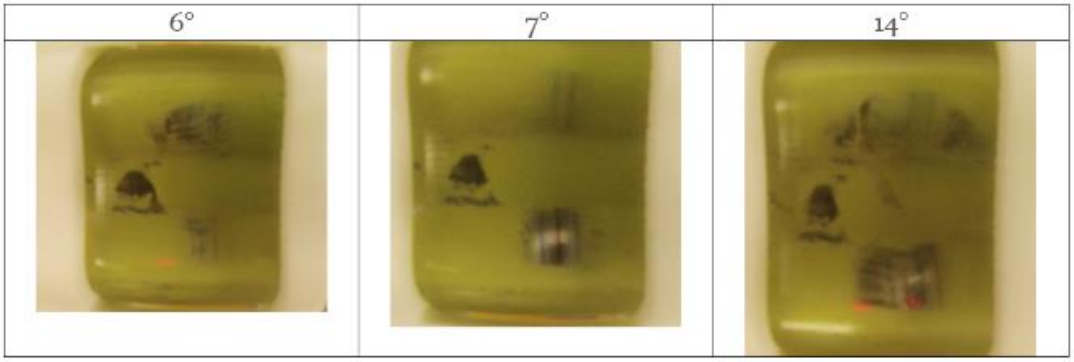


*Figure 3.20: lubrication defaults*

At 6°, grease can be observed between the track and the roller. Then, at 7°, there is no grease in the contact. To finish, it is possible to observe above, at 14° that the grease conditions are almost the same than at 7°. It is possible to notice the same thing in figure 3.19, where the points are converging from 8 degrees to 18 degrees.

### 3.2.3.Slip ratio

To explain the slip difference between the 2 directions (as defined on 2.1.4), another slip ratio experiment was done on 100% greased conditions. Also, another test was lead under gearbox oil lubrication condition.

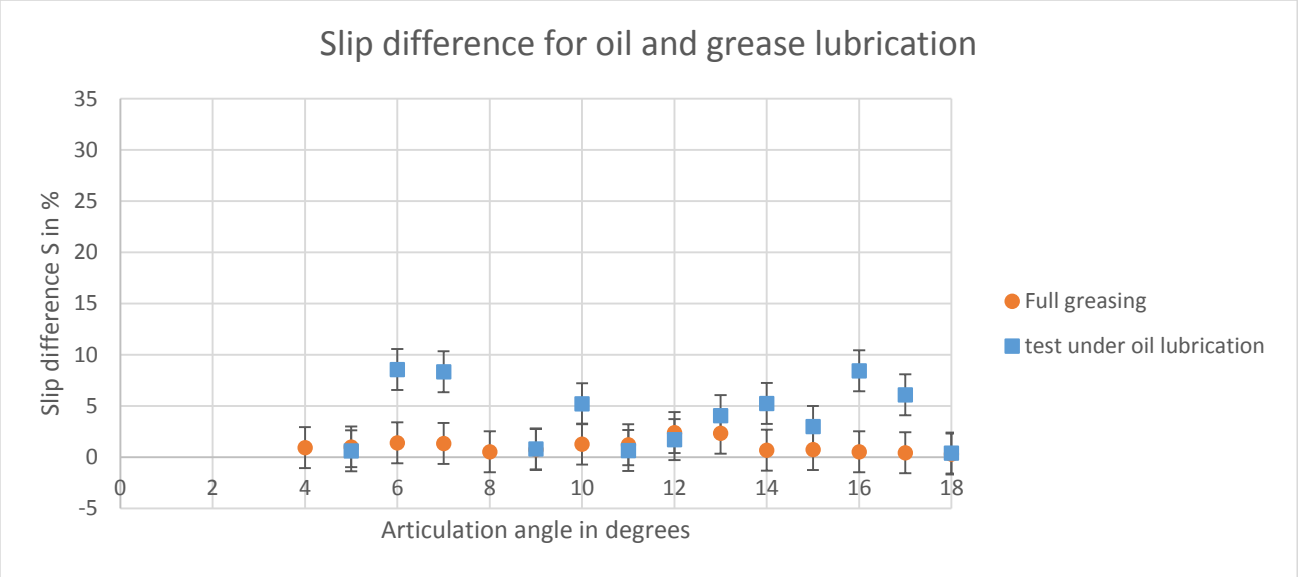


*Figure 3.21: comparison of slip in function of the rolling direction*

As it can be seen in figure 3.21, oil and grease have almost the same behaviour in terms of symmetrical slip. So, it is possible to compare their behaviours in the 2 directions.

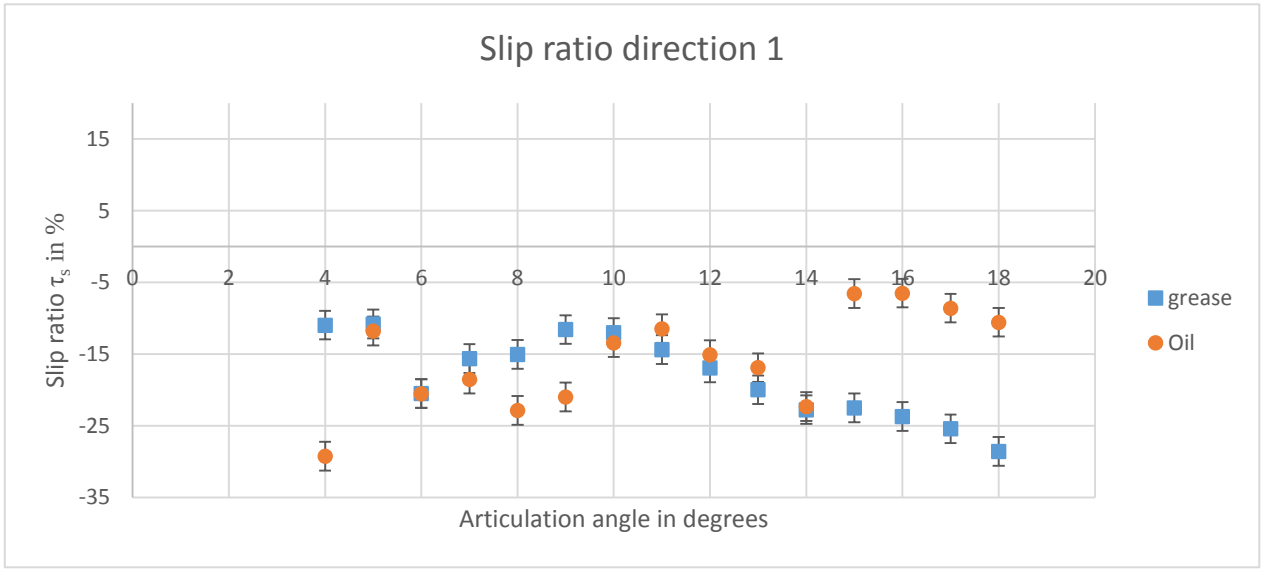


*Figure 3.22: slip into direction 1*

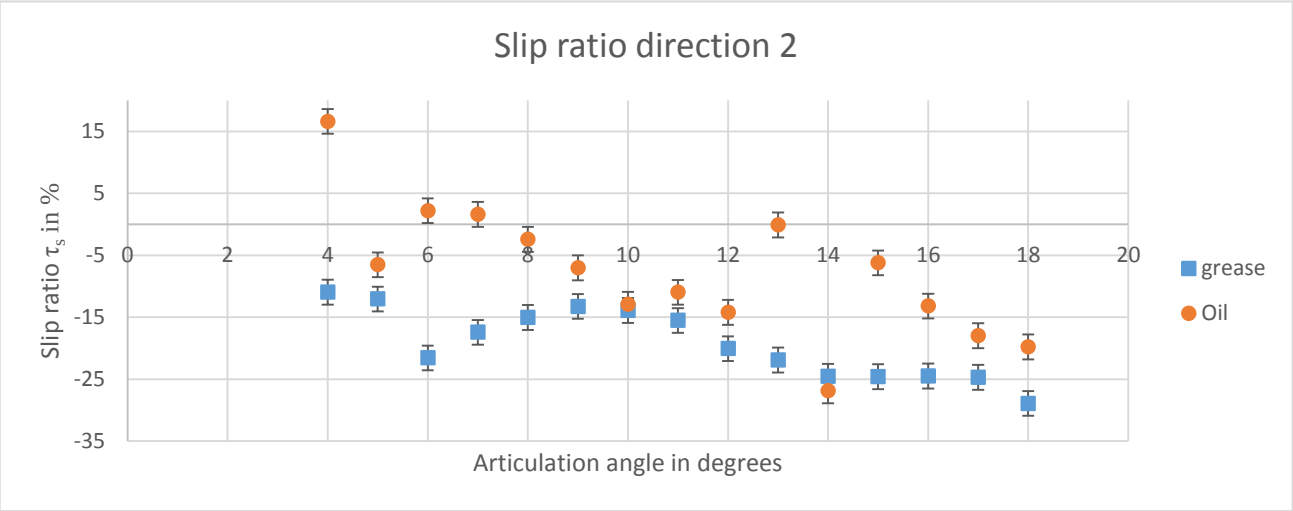


*Figure 3.23: slip into direction 2*

On figures 3.22 and 3.23, the oil and the grease tend to have a similar behaviour in the 2 directions (define in figure 2.16). Moreover, the grease increase the negative sliding probably due to its apparent viscosity higher than the oil one. Comparing the 2 directions with grease, it is possible to notice that they give almost the same result with a little tendency to have more negative sliding. It is also underlines the viscosity role in CVJ lubrication system.

Moreover, a comparison between the 2 directions in the case “full of grease” has been done in order to characterize the slip rate (figure 3.24).

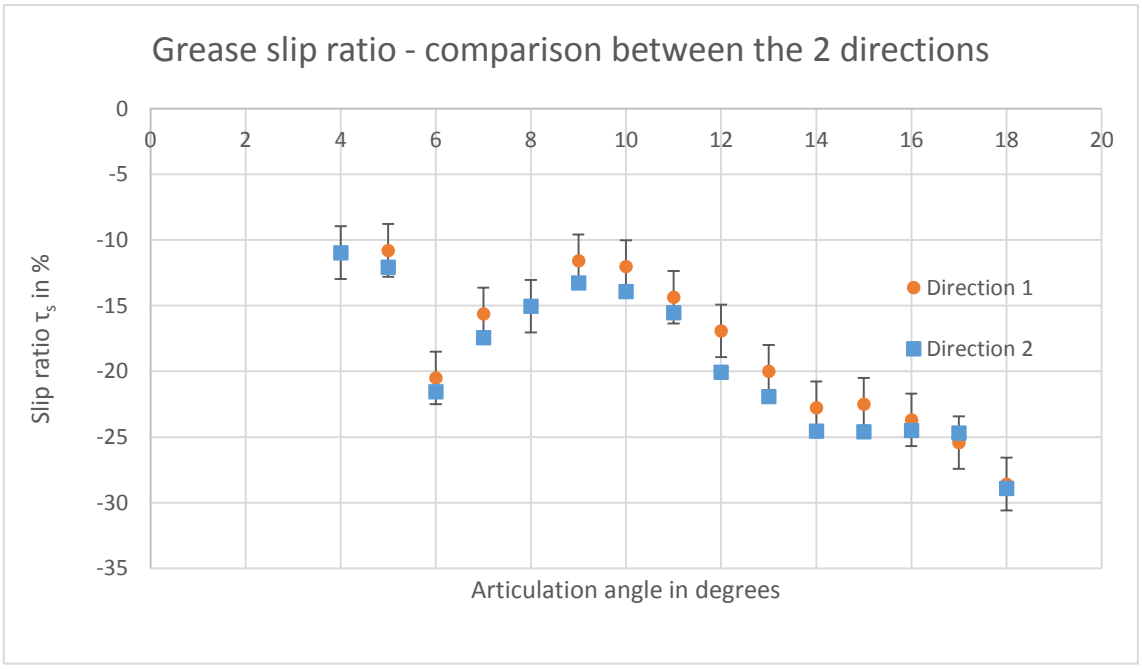


*Figure 3.24: comparison between direction 1 & 2 in case of grease lubrication*

As observable, with standard vehicle quantity, the slip ratio is equivalent in both directions.

3.2.4.Conclusion on Observation Rig

Referring to the figure 3.24 & 3.25, a slip ratio equation (14) can be determinated for the geometry used in the present study:

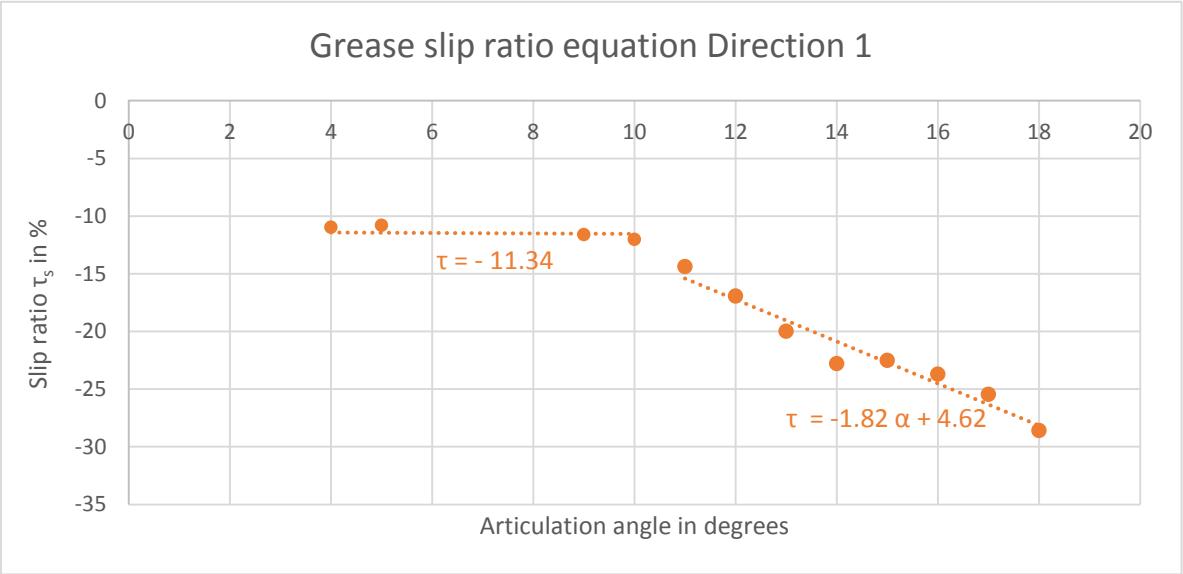


*Figure 3.25: slip ratio interpolation*

$$|\alpha| \leq 10°, \tau_s = -11.34\ \%\ (14)$$

$$|\alpha| \geq 10°, \tau_s = -1.82 * \alpha + 4.62\ \%\ (15)$$

In addition, between 6 and 9 degrees, a particular roller behaviour can be noticed (figures 3.24 & 3.25). Indeed, in each oil or grease tests, the slip ratio takes higher value than for 5 or 10 degrees. It can be due to a particular CV joint design or to a particular lubricant repartition in the contact for this angularity. This hypothesis will be investigated in the following chapter.

Finally, it is important to note that the grease quantity has an important role on the lubrication process. These tests highlights the importance of having the good quantity of grease in transmission, here called “full of grease” case.

Chapter four

# Grease Lubrication

*Knowing the operating conditions of the contact inside the CVJ tripod, the chapter four will focus on lubricants used inside. To begin, an overview of the greases studied during this work is done (grease constraints, composition, wear induced on vehicle). After this, the vehicle conditions known thanks to previous chapter are applied to the lubricant characterization in the laboratory.*

*Then, greases are tested on tribometers to explain how they are performing at low temperature and operating temperature. After the tests, topography measurements and surface analyses are made to obtain the amount of wear induced and the chemical composition of the tribofilm formed for each grease.*

## 4.1. Greases overview

### 4.1.1. Industrial Issues and greases presentation

From an industrial point of view a grease has to fulfill several functions:

- As seen in chapter 1, the friction coefficient is directly linked to the generated axial force of the tripod. So, a car manufacturer will have to choose a grease that will involve a reasonable axial force, thus a limited grease friction coefficient.
  For a regular car (sedan for example) the CVJ has a low articulation angle and does not need a particularly low friction coefficient. To the opposite, for Sport Utility Vehicle, the CVJ has a higher articulation angle due to the engine position compared to wheel position. So it will require a lower friction coefficient at higher angularity than for regular cars in order to maintain reasonable axial forces.

- Generally, the CVJ is maintenance-free during vehicle life. So the grease cannot be replaced. But yet, it does need to protect as far as possible the parts from wear.

During this work, only 4 greases are tested. As seen in section 1.3, to make a grease oil, thickener and additives are necessary.

- 2 Oils have been used. The first one is a mix between PAO and a mineral oil. The second one is a synthetic oil. It is not possible to disclose these oils due to confidentiality issue.
- 2 different thickener technologies are used in order to transform the oil in grease. The first one is a complex soap using Lithium and Calcium. The second one is a polyurea thickener.
- Conventional CVJ additives are used. They are MoDTC and MoDTP. Due to confidentiality issue, the respective concentrations have been normalized to 1 as the maximum concentration of MoDTC.

| | C1 | C2 | P1 | P2 |
|---|---|---|---|---|
| Oil | Mineral + PAO | Mineral + PAO | Synthetic ester + PAO | Synthetic ester + PAO |
| Thickener | Lithium / Calcium Complex | Lithium / Calcium Complex | Polyurea | Polyurea |
| Additives | MoDTC 0.28 | MoDTC 1 | MoDTC 1 | MoDTC 1 |
| | | MoDTP 0.4 | MoDTP 0.4 | MoDTP 0.4 |
| NLGI number [22] | 2 | 2 | 1-2 | 1-2 |

*Table 11: grease composition*

In addition, C1, P1, P2 are industrial grease production and C2 is a prototype of C1 with the additive quantity of P1&P2. C2 cannot be used for each test in the following section for available quantity reasons. P1 and P2 own the same components however the oil and thickener concentration could variate.

### 4.1.2.Grease properties

Several studies are done to differentiate the greases C1, P1 & P2 in terms of wear under contact conditions relevant to the application. To do that, a complete transmission has been mounted on an endurance rig at Groupe PSA facilities. The articulation angle and the torque are set to values that correspond to real operating vehicle conditions which remain confidential. The rig is launched for pre-defined duration with these operating conditions. After a desired duration, the rig is stopped, the transmission is disassembled and the wear scar depth measured on the 3 different tripod tracks. These tests are done at least 6 times and the values averaged.

In table 12, the values have been normalized to the maximum wear depth measured. A color code is associated in order to help to understand the critical values for operating conditions.

| Track damaging in percent | | | | | |
|---|---|---|---|---|---|
| Duration | C1 (%) | Duration | P1 (%) | Duration | P2 (%) |
| 200h | 14 | 200h | 17 | | |
| 400h | 23 | 400h | 35 | | |
| 600h | 32 | 600h | 53 | | |
| 800h | 31 | 800h | 100 | 730h | 5 |
| | | | | 1130h | 8 |

*Table 12: Endurance wear*

As observable in table 12, grease P2 gave the best wear results far and away with real components. The grease C1 gave acceptable results in terms of wear. Grease P1 induced critical wear on tracks that could cause a critical failure in the field.

*Figure 4.1: used cups*

To explain the difference in terms of wear two tests are led to better differentiate the 4 greases. First of all, oil separation is determined on the three industrial greases using IP121 method which is equivalent to NF T60-191 and DIN 51817 methods [39]. It measures the oil that is bled from grease under conditions described in the method. The cups used in this study are available in figure 4.1. In table 13, differences appear. Even if P1 & P2 have the same oil type, thickener technology and additive packages, the grease P1 does not have the same ability to bleed oil than P2. In terms of oil bleed again, C1 is in the middle of P1 & P2.

| **C1** | | | **P1** | | | **P2** | | |
|---|---|---|---|---|---|---|---|---|
| S_Oil (%) | 3.4 | 3.6 | S_Oil (%) | 0.4 | 0.7 | S_Oil (%) | 5.9 | 6.1 |
| Average | | 3.5 | Average | | 0.6 | Average | | 6 |
| Standard deviation | | 0.12 | Standard deviation | | 0.15 | Standard deviation | | 0.14 |

*Table 13: Oil bleed results*

In order to know the difference between the different greases, methodologies from the literature are used [40]. An Angilent Cary 630 infrared spectrometry (with attenuated total reflectance accessory) is used on the greases and respective bled oils to have additional data.

This technic was only used in order to know the difference between the supplied greases. As it is possible to observe in figure 4.2, the bled oil from P1 and P2 are exactly the same. The bled oil from C1 is different which corresponds to Table 11.

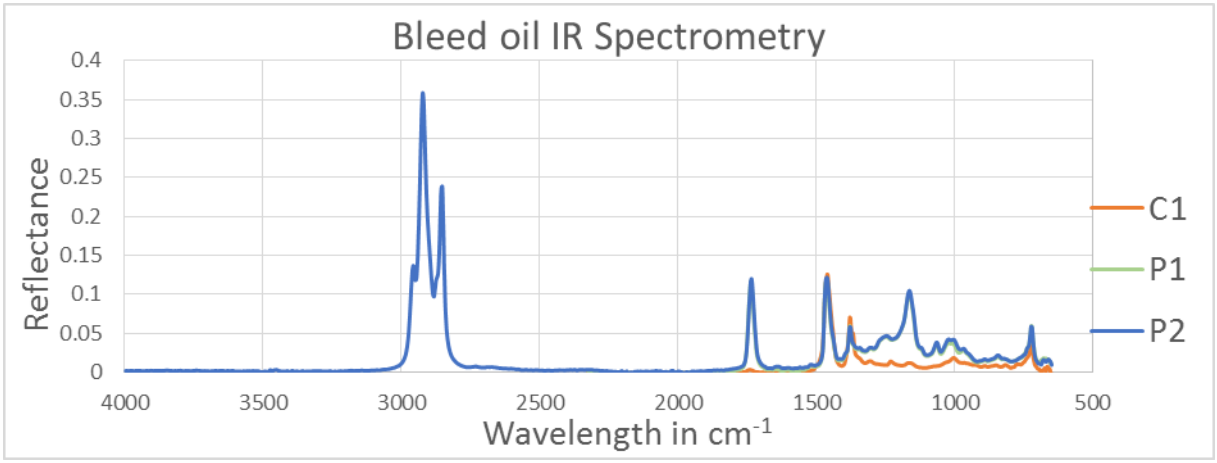


*Figure 4.2: Oil bleed IR spectrometry*

In figure 4.3 the same methodology is performed on greases for comparison purpose.

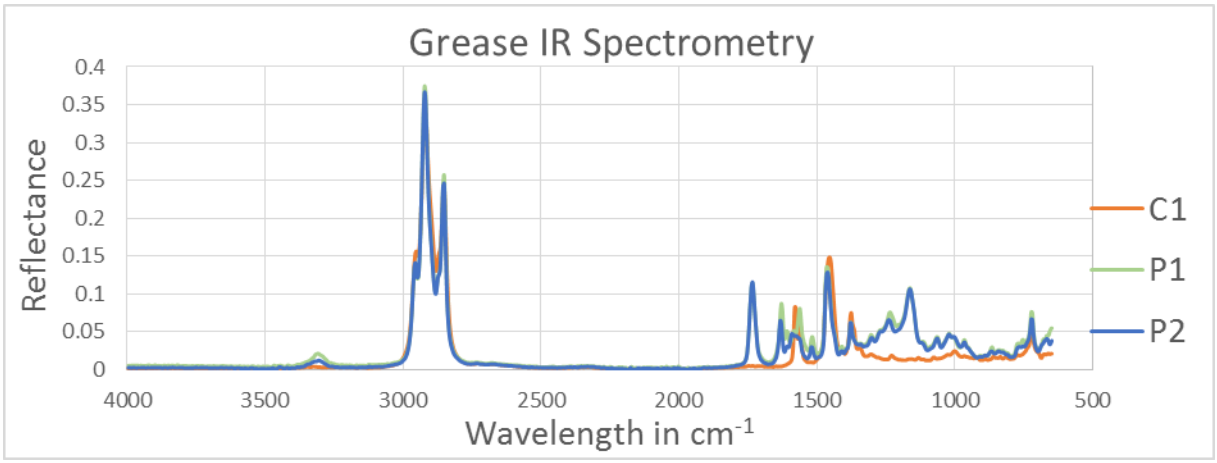


*Figure 4.3: Grease IR spectrometry*

It is possible to observe that P1&P2 differ (especially at 1561 cm-1). This wavelength corresponds to the thickener contribution (figure 4.4). Indeed, it means that the additive package and the base oil are the same. But even if the thickener corresponds to the same family, it differs. As expected, C1 is significantly different from P1 and P2.

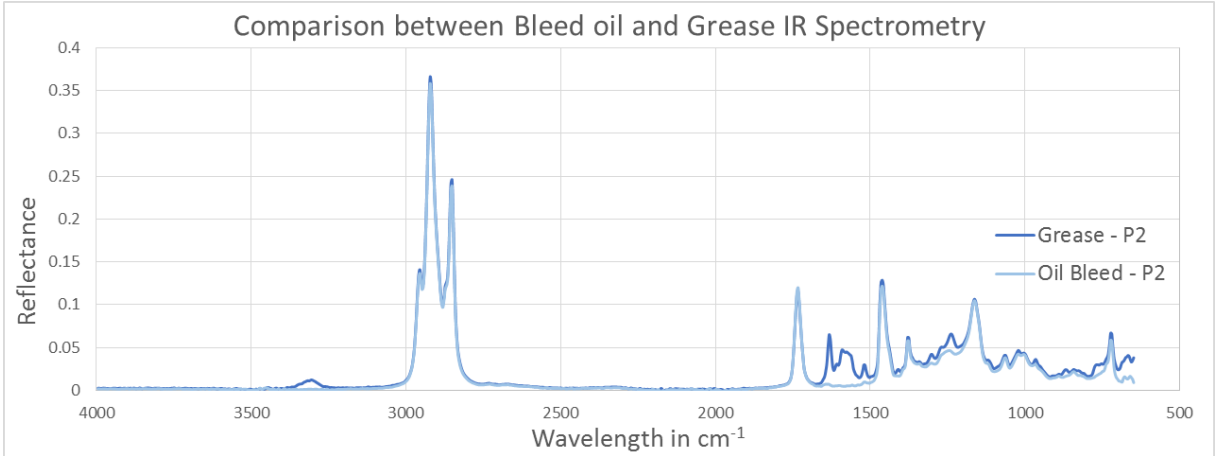


*Figure 4.4: contribution identification between grease and bleed oil*

4.1.3.Transferring contact conditions from vehicles to laboratory rigs

As mentioned in chapter 3, it is possible to evaluate the Contact Hertz pressure at about 1.3 to 1.4 GPa for 250 Nm, which is the most common torque during a vehicle life duration (example of 90km/h on a flat road, no winds). At 90km/h, the contact frequency can be estimated to 15 Hz. Also, a common articulation angle can be set to 10° for some vehicle segment. It gives a rolling displacement of 8.5 mm. Referring to section 4.2.4, if 10% slipping is to be considered, the slipping distance will be 0.85 mm. In that case, only the slipping contribution is considered.

In this way these conditions are used for the following HFRR tests:

$$f_{HFRR} = 15\ Hz\ ; d_{HFRR} = 1\ mm\ ;\ P_{h-HFRR} = 1.32\ GPa$$

Under these conditions relevant for the applications, different duration and temperature are associated in order to conduct the study. There are summarized in Table 14.

| Test number | $f_{HFRR}$ | $d_{HFRR}$ | $P_{h-HFRR}$ | Duration | Temperature |
|---|---|---|---|---|---|
| 1 | $15\ Hz$ | $1\ mm$ | $1.32\ GPa$ | 3 h | 40°C |
| 2 | $15\ Hz$ | $1\ mm$ | $1.32\ GPa$ | 18 h | 40°C |
| 3 | $15\ Hz$ | $1\ mm$ | $1.32\ GPa$ | 3 h | 80°C |
| 4 | $15\ Hz$ | $1\ mm$ | $1.32\ GPa$ | 18 h | 80°C |

*Table 14: HFRR conditions for section 5.2*

## 4.2. Grease behaviour

### 4.2.1.Low temperature

The first idea was to study the grease at 40°C. This temperature has 2 advantages:

- It corresponds to the lower end of the operating temperatures in application,
- It could be reproduce on a test rig independently of the room temperature (summer or winter) in order to reproduce easily the results.

The first step is to use HFRR (section 2.1.1) in order to qualify grease in terms of friction coefficient and surface separation. As shown previously, the friction coefficient is directly linked to transmission shudders. These shudders lead to a CVJ degradation and also an unpleasant feeling for drivers. In figure 4.5, the friction coefficient evolution is represented. For each grease, 2 different durations are done: 3h (10800s) and 18h (64800s). The tests were done twice and the curves are superposed on figure 4.5. All the different tests are available in appendix B. The repeatability is also available in appendix B and gives a measurement uncertainty of 2.5%.

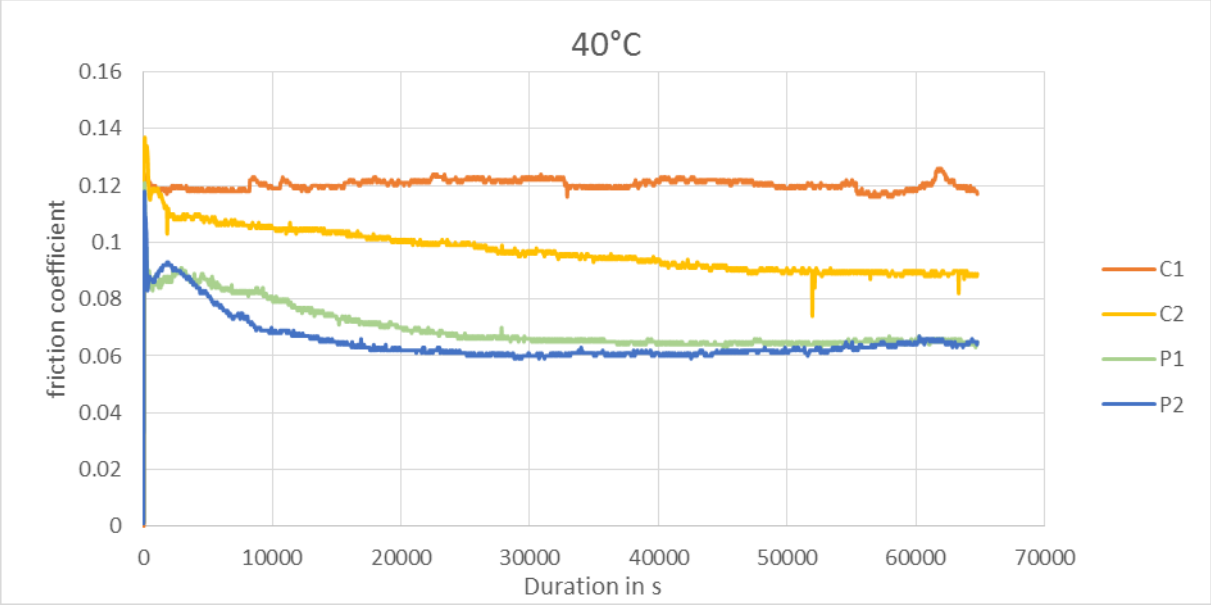


*Figure 4.5: Grease friction coefficient results at 40°C*

At 40°C, the first observation is the role of the additives percentage in the grease. Indeed, the modification of MoDTC percentage and/or also the addition of MoDTP allow to decrease the friction coefficient by 25% between C1 and C2. Moreover, the replacement of thickener and base oil allow again to decrease the friction coefficient by 30% in order to give a low friction grease comparing C1, C2 to P1, P2. Theses 2 major modifications give two kind of grease for CVJ application: a low friction grease at 0.06 (P1, P2) and a regular grease at 0.12 (C1).

The figure 4.6 gives an indication of the film thickness during these tests. It is noticeable that C1 is probably not very good in terms of wear due to film variation (near to 10%). Moreover, the film for polyurea grease P1&P2 variates a little bit until its friction coefficient stabilizes at around 8h. For Complex grease, the friction needs 14h to stabilize. In order, to go deeply in wear study, interferometry was used (figure 4.7).

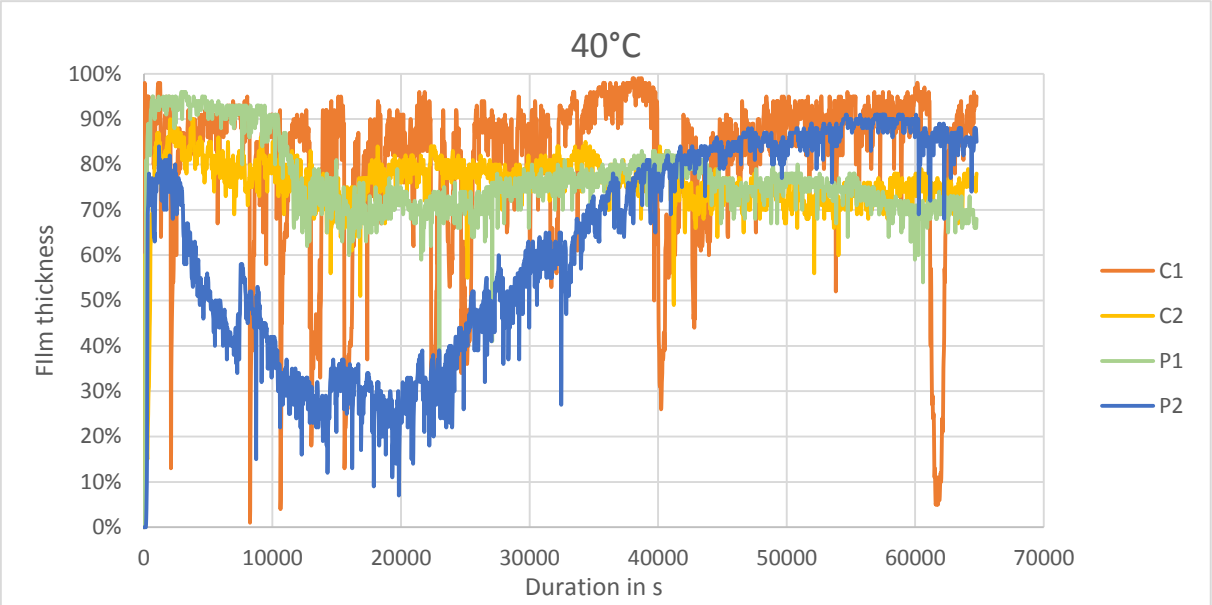


*Figure 4.6: greases film thickness at 40°C for 18h*

The method describes in section 2.2.1 in order to evaluate wear gives good information about the quantity (volume & scar width) and type of wear (figure 4.7). The width measurements are available in appendix C. Qualitatively for example, the grease C1 has no plastic deformation as P1 (no material above the mean surface).The results for 40°C are summarized (figure 4.8 for 3h duration and figure 4.9 for 18h duration).

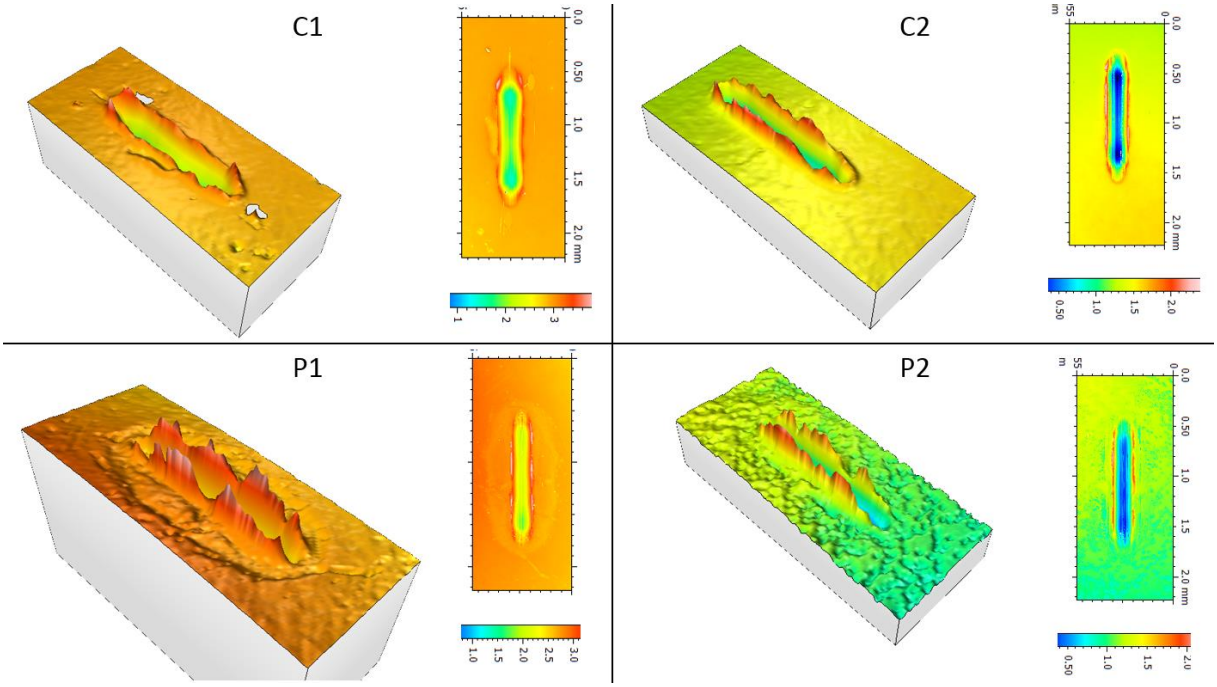


*Figure 4.7: Interferometry example for 18h at 40°C (test condition 2)*

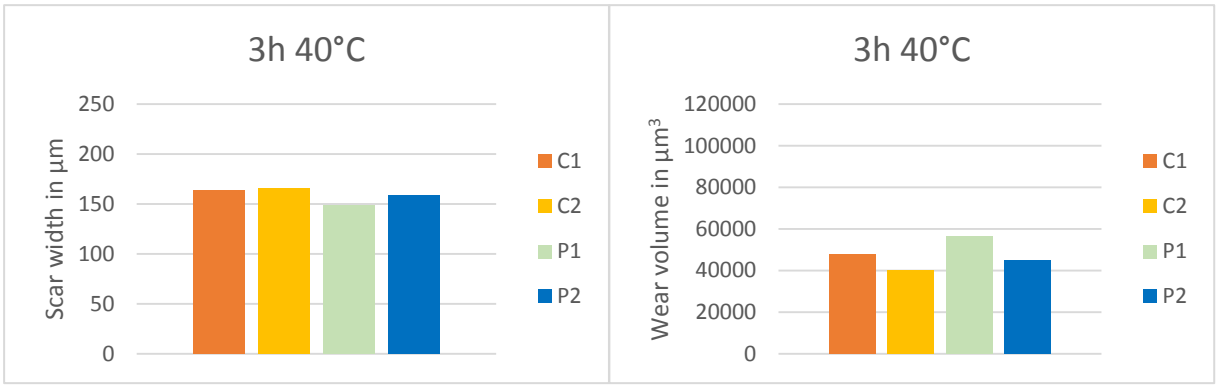


*Figure 4.8: Wear characteristics for 3h at 40°C*

Even if friction coefficient is not stabilized yet after 3h, it is possible to observe that the wear rate could be consider as equal. Indeed, the volumes are almost similar and width too.

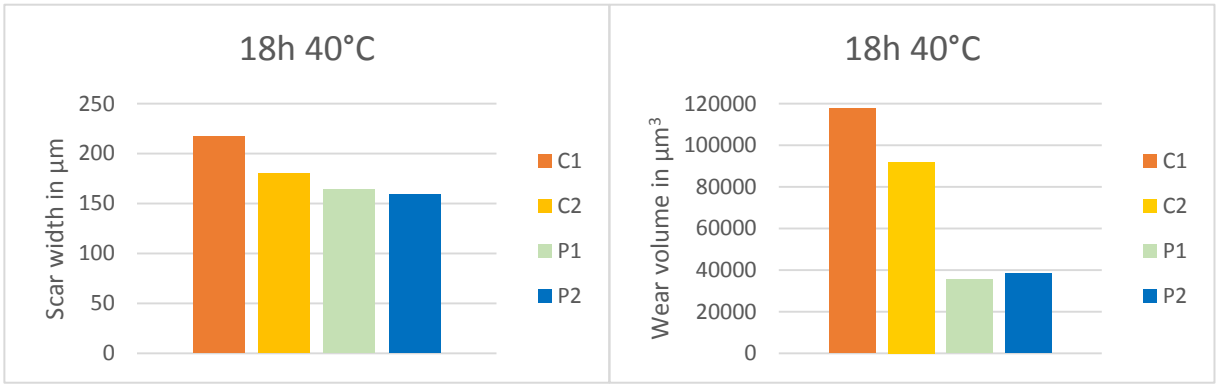


*Figure 4.9: Wear characteristics for 18h at 40°C*

After friction coefficient stabilization, a distinction can be done between the grease with the full additives and the grease C1 without the same MoDTC concentration and MoDTP. In addition, the polyurea grease seems to better protect the surface. So, the oil and the thickener at 40°C also have a role to play in terms of wear. However, in comparison with the CVJ wear, in that case, wear does not seem to match with industrial case (section 4.1.2).

In order to explain these results, XPS analysis (section 2.2.2) is done (all data available in appendix D). To begin, the first general spectrum is realized on each greases to identify the chemical species (figure 4.10). Without any surprise, C, O Fe, Zn, Mo, S, P were found in the wear scar. These elements are found in steel and most common AW and FM additives. It is then possible to focus on energy peaks in order to identify the chemical forms of species.

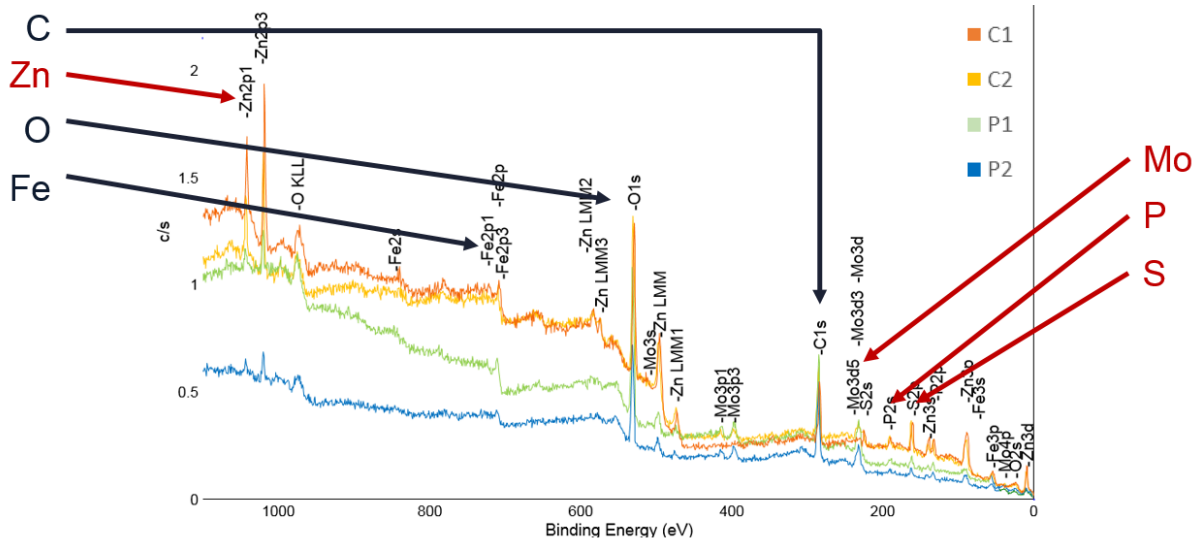


*Figure 4.10: Spectra of C1, C2, P1 & P2 at 40°C for 18h*

In order to explain the different friction coefficient, a focus is made on Mo (Molybdenum) peaks at around 230eV. The different fits are available on figure 4.11 &4.12.

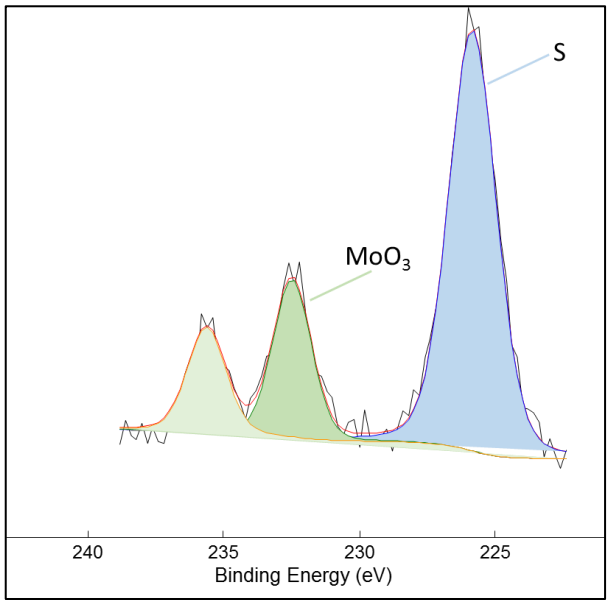


*Figure 4.11: Molybdenum peaks: example for grease C1 at 40°C 3h*

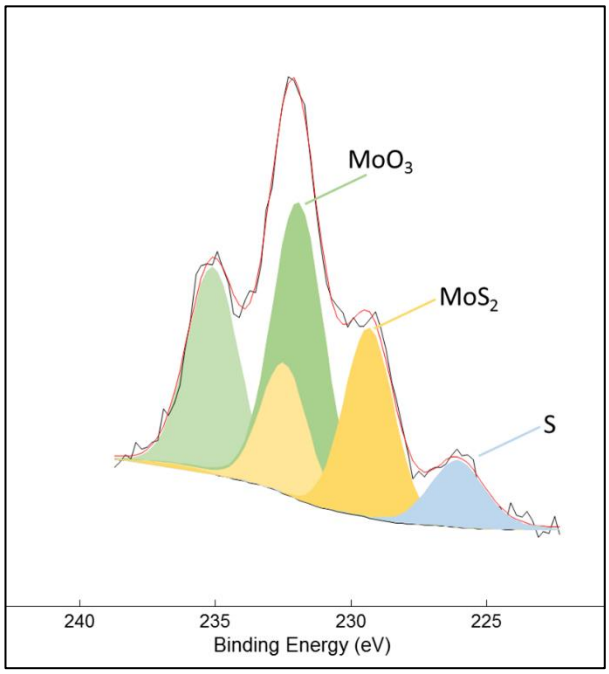


*Figure 4.12: Molybdenum peaks: example for grease P2 at 40°C 3h*

It is possible to notice the difference between the figures 4.11 and 4.12. Indeed, the grease P2 has additional peaks corresponding to $MoS_2$. These differences can be observed during friction too. Due to the lack of $MoS_2$, the grease C1 has a higher friction coefficient (figure 4.5). As a first approach, all the XPS analysis are fitted with these hypotheses (only $MoS_2$, $MoO_3$ and S available around 230eV).

In order to sum up the results, the relative concentration are illustrated in figure 4.13.

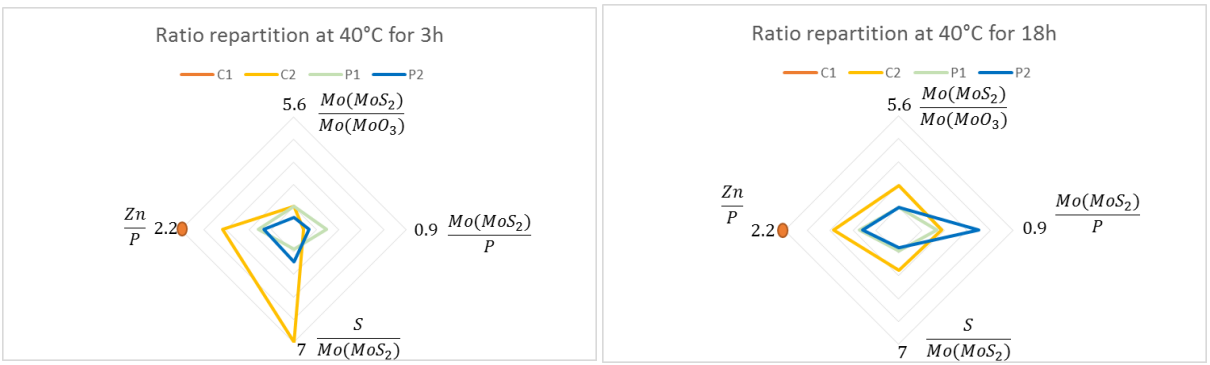


*Figure 4.13: Chemical ratio repartition for 40°C*

The grease C1 is not enough concentrated in additives to form $MoS_2$ in tribofilm. Also, $MoO_3$ is only on tribofilm in small quantity for C1. Greases P1 & P2 react exactly in the same way for 3h and 18h. Based on those XPS measurements, it is difficult to conclude more things about the grease. As it is possible to notice in appendix, the variations between compound ratios are very small. And this variation can be explain with a linescan. The goal of this measurement is to characterize the chemical repartition of the different elements present in the tribofilm all along a line as in figure 4.14.

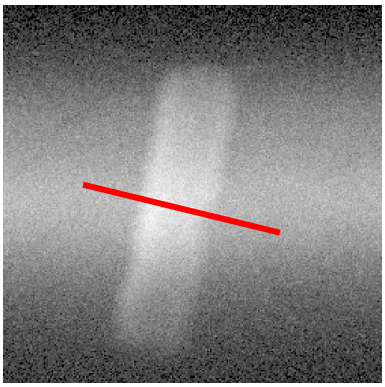

*Figure 4.14: SXI image use to draw the line*

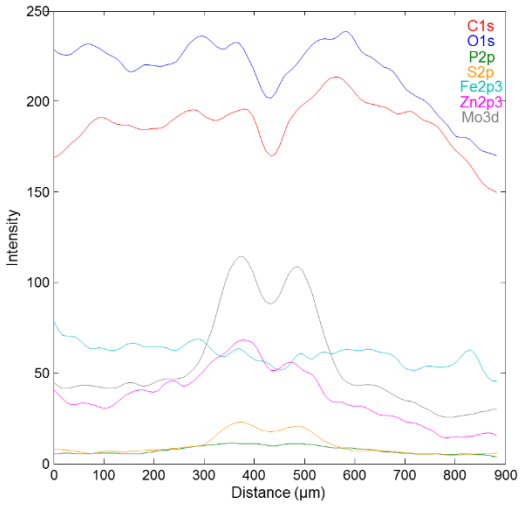


*Figure 4.15: Grease P2 linescan at 40°C for 18h*

In figure 4.15, the Mo intensity varies all along the scar width. So, if the selected area for XPS analysis is taken on the top or in the lower part of the peaks that will change ratio results. The only way to consider this is to use the ratio between the all Mo available compare to S. It gives an important information to explain the friction coefficient (figure 4.16).

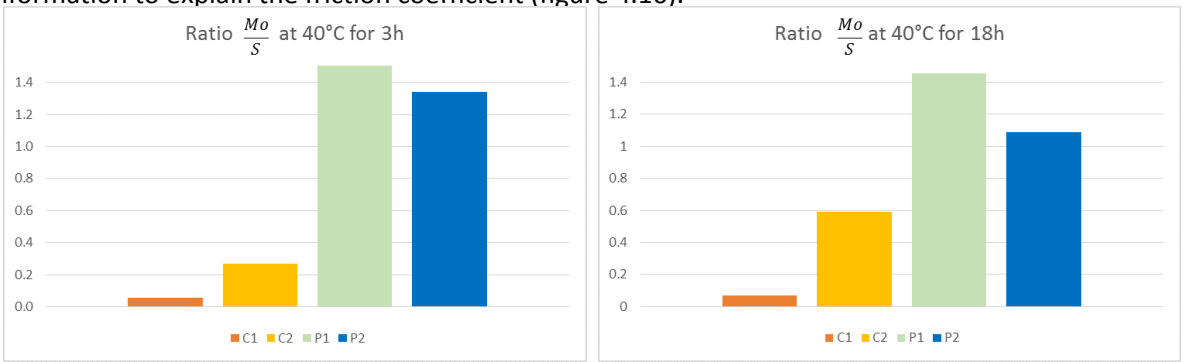


*Figure 4.16: Mo/S ratio at 40°C*

The greases P1&P2 with polyurea thickener and ester-PAO oils give a $\frac{Mo}{S}$ ratio higher than C1&C2. This information explains why the friction coefficient is smaller with these 2 greases than with C1 &C2 and decreases of 25% compared to C2. Also, there is only a small amount of Mo in C1 tribofilm. These ratios can be directly linked to figure 4.5 and gives almost the same classification than friction coefficient. Leaning on the friction coefficient and the grease composition it is possible to make the hypothesis that the molybdenum additives are active enough when the total ratio is closed to 0.5. Indeed, the additives quantities of P1, P2 & C2 are equal. Also the friction coefficient difference is explained by the thickener and oil changes.

In addition, the fitting realized for each grease can be discussed. Indeed, for grease P1, the ratio between S and $MoS_2$ is inferior to 2 (figure 4.13). In order to explore this problem, another fit was tried. It consists in considering that MoDTC remains in the scar. The 2 different fits are available in figure 4.17 & 4.18.

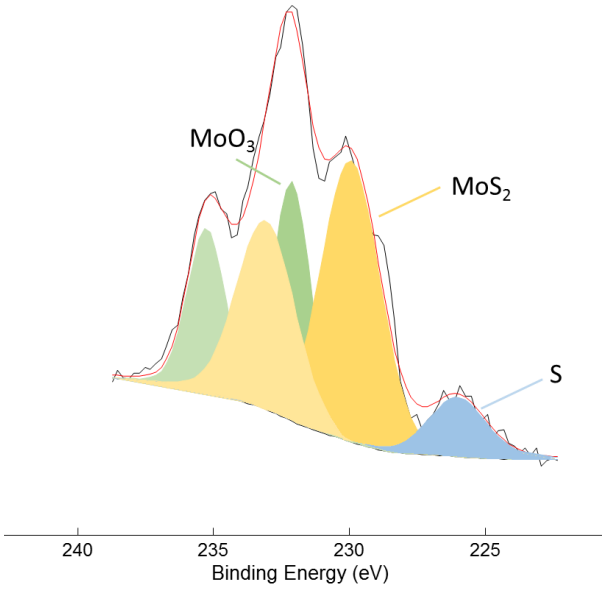


*Figure 4.17: Grease P1 at 40°C for 3h fitted with 2 peaks*

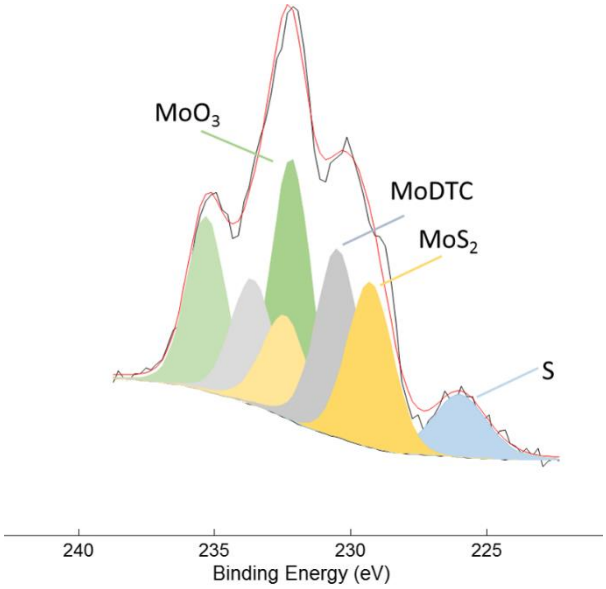


*Figure 4.18: Grease P1 at 40°C for 3h fitted with 3 peaks*

With this new fit, the ratio between S and $MoS_2$ increases to 2.2 which is more realistic. However, in order to compare results and to have almost the same peaks width, a fit with 2 peaks is used in all radar drawings presented. The fits with 3 peaks are available in appendix. Furthermore, the greases P1&P2 present the same ability to form $MoS_2$ and $MoO_3$ that confirm why the friction coefficient decrease of about 25%.

An abrasive method is used in order to evaluate the tribofilm thickness. The method is based on tribofilm abrasion [41]. A first abrasion is made outside the wear scar (figure 4.19).

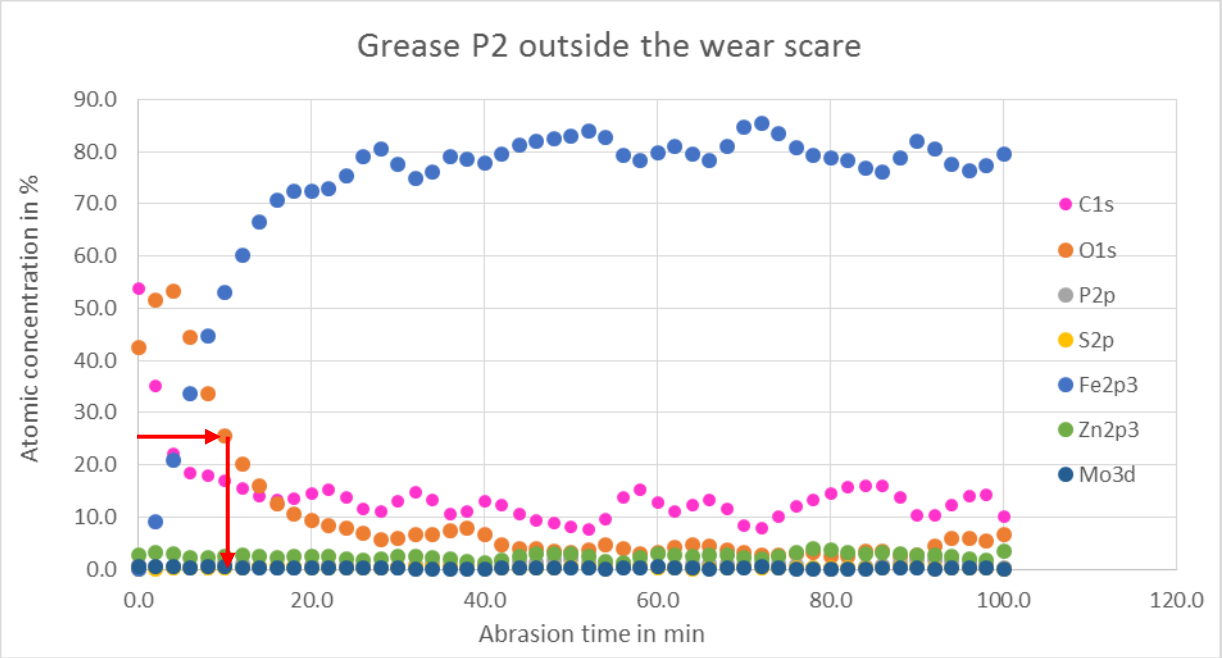


*Figure 4.19: XPS Profile for grease P2 at 40°C outside the wear scar.*

Figure 4.19 gives an information about the duration which is necessary in order to go over the native iron oxide layer (about 50% of the initial oxygen concentration). This time gives an approximate time which correspond to about 3 nm. Taking the hypothesis that the abrasion speed of native oxygen is equivalent to tribofilm, the tribofilm thickness can be estimate. In figure 4.19, this 3 nm layer corresponds to 8 min. After this step, the analysis inside the wear scar can be done.

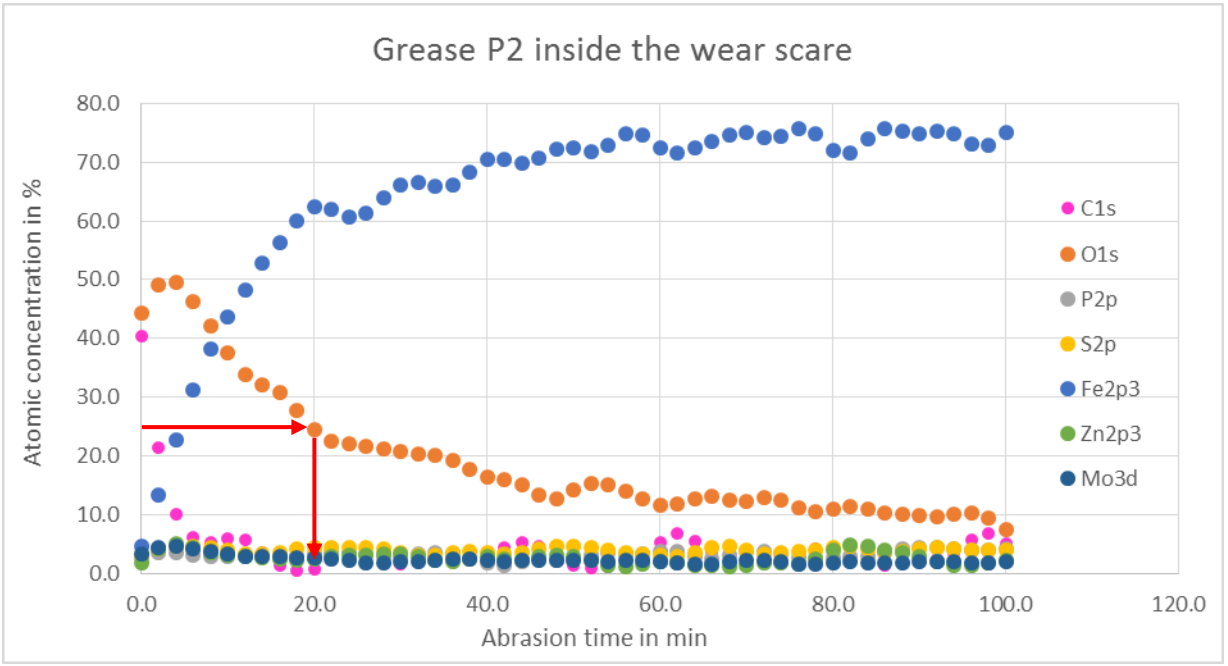


*Figure 4.20: XPS Profile for grease P2 at 40°C inside the wear scar.*

Based on figure 4.20 with the grease P2, a tribofilm thickness estimation of 8 nm can be done. The results for all greases are available in figure 4.21.

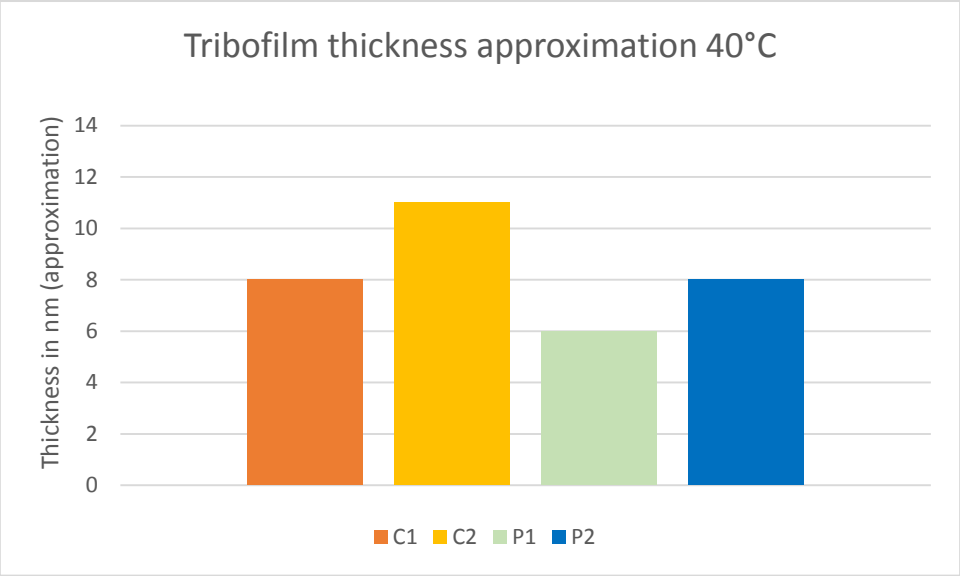


*Figure 4.21: Tribofilm thickness estimation at 40°c after 3h determined from XPS profile*

With figure 4.21, it is not possible to discriminate greases. Indeed, the variations are very small compare to the method reliability. So at 40°C, greases have the same ability to form tribofilm. The next step is to investigate greases behaviour at 80°C which is a most common operating temperature for CVJ.

4.2.2.Most common operating temperature: 80°C

A most common temperature is estimated at about 80°C. As at 40°C, HFRR (section 2.1.1) is used in order to qualify the grease in terms of friction coefficient and also surface separation. In figure 4.22, the friction coefficient evolution is represented. For each grease, 2 different durations were done: 3h (10800s) and 18h (64800s). The tests were done twice and the curves are superposed on figure 4.22. All the different tests are available in appendix B.

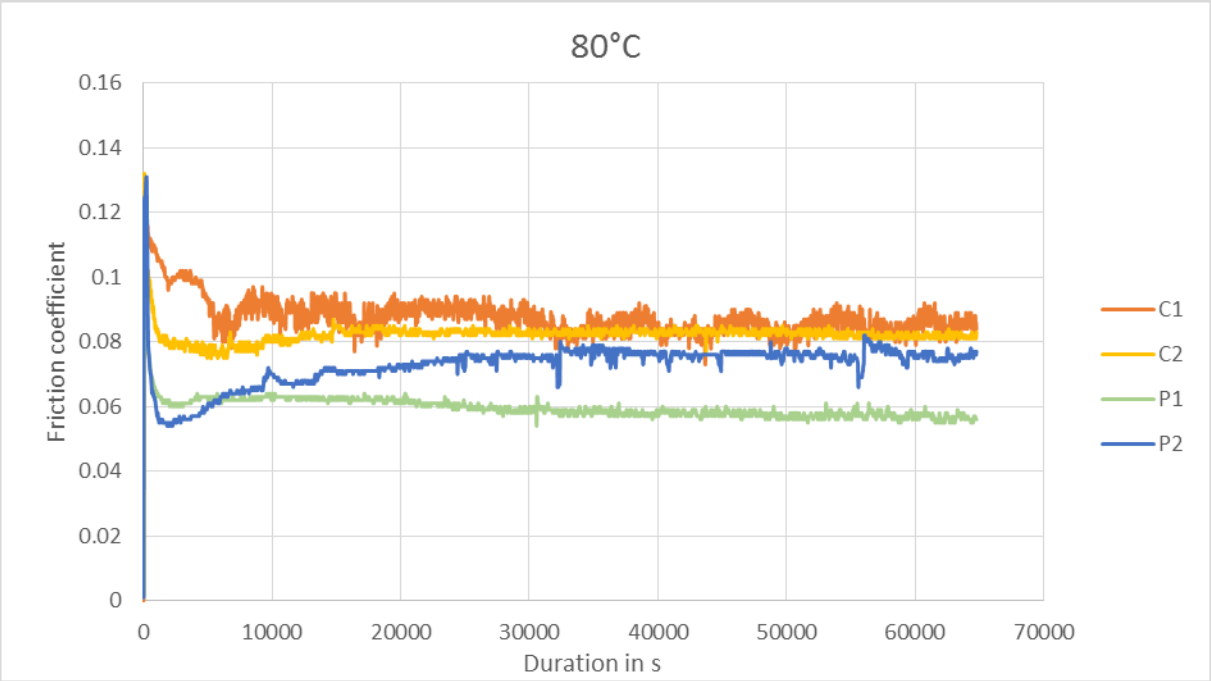


*Figure 4.22: Grease friction coefficient results at 80°C*

The first observation is that the friction coefficient of grease C1 & C2 converge at around 0.08 to 0.09. However, the C1 friction coefficient seems unstable. An explication can be that the tribofilm is heterogeneous due to low additive concentrations in grease. The additive percentage in grease composition at 80°C seems not to influence a lot the friction coefficient (between grease C1 & C2). The low friction greases P1 & P2 have a friction coefficient under 0.08 that is interesting for CVJ applications. In addition, a friction coefficient increase is present at around 3h. It will be interesting to investigate this behaviour which is reproducible.

On figure 4.23, the lubricant film thickness for each grease at 80°C is available. These films can be qualify as correct. Indeed, there are all along the tests a good surface separation.

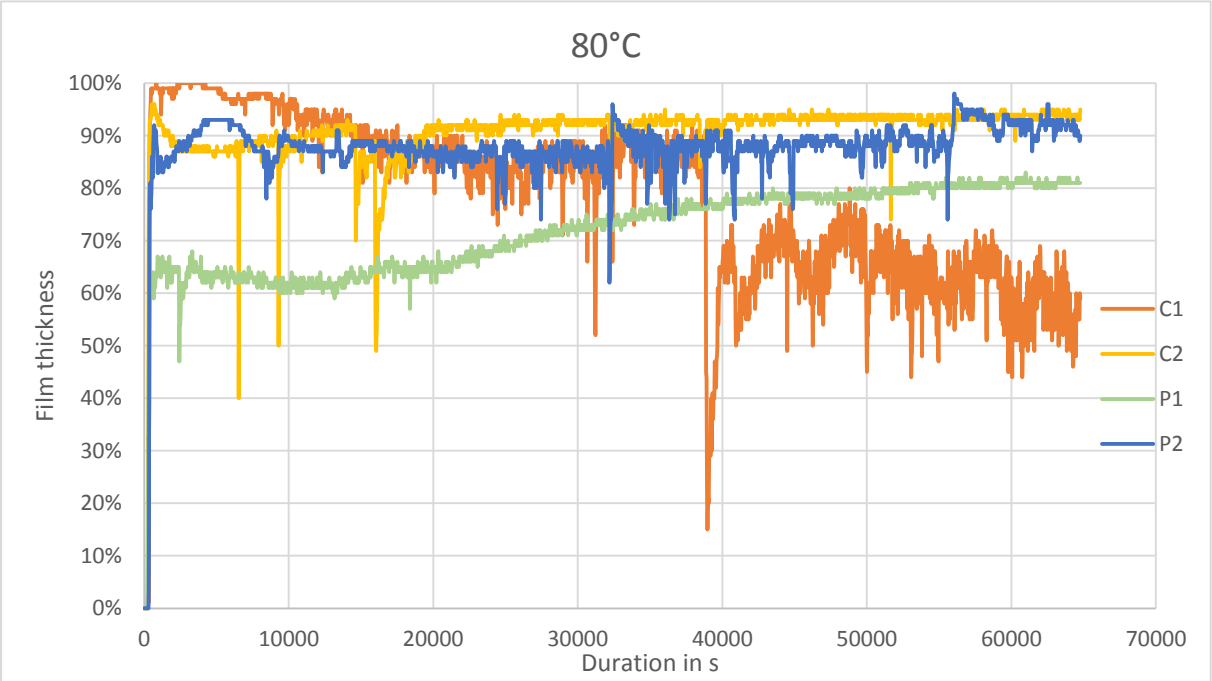


*Figure 4.23: greases film thickness at 80°C for 18h*

As at 40°C the same method is used to evaluate wear (volume & scar width) and the type of wear (section 2.2.1). The width measurements are available in appendix C.

Qualitatively for example on figure 4.24, there is a lot of plastic deformation (rabbit ear shown in appendix C). The results for 80°C are summed in figure 4.25 for 3h duration and in figure 4.26 for 18h duration.

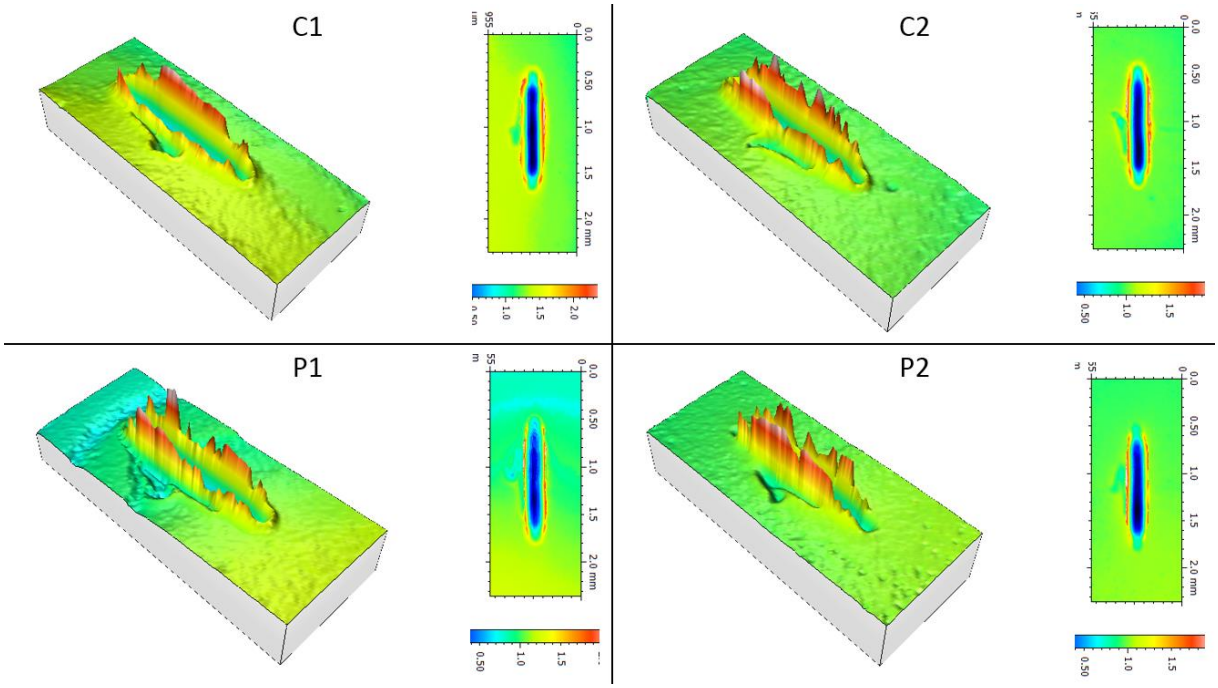


*Figure 4.24: Interferometry example for 18h at 80°C*

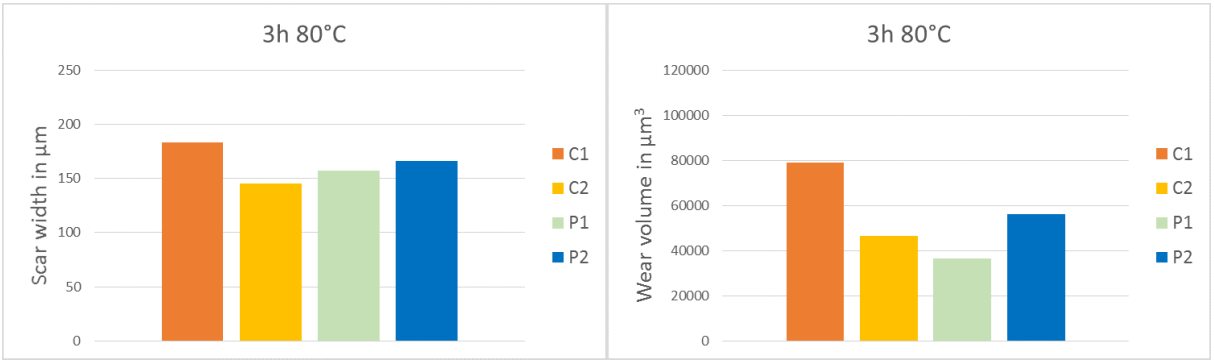


*Figure 4.25: Wear characteristics for 3h at 80°C*

Even if the friction coefficient is not stabilized yet for 3h (in particular for P2), it is possible to compare wear. Grease C1 involves more wear which is logical due to its composition and its friction coefficient behaviour. This is also present in volume. The other greases are almost similar due to measurement approximations.

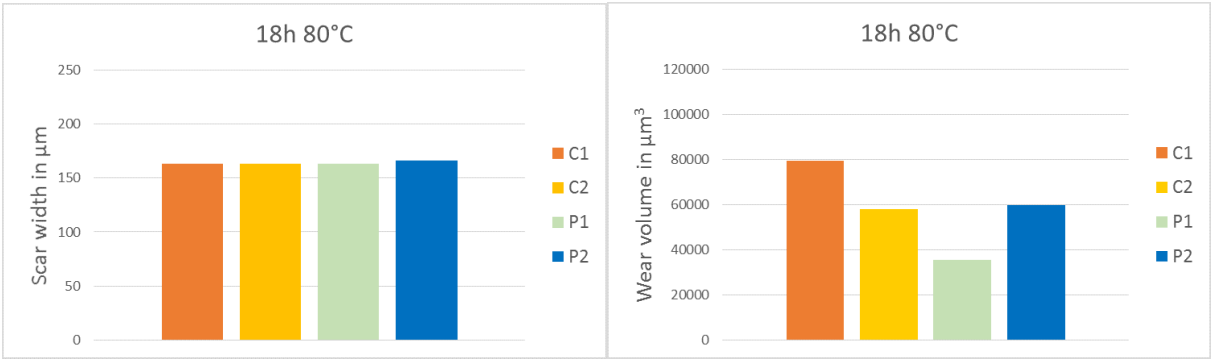


*Figure 4.26: Wear characteristics for 18h at 80°C*

After 18h, the wear is stabilized and the widths are equal. In addition, wear volumes are very low. The grease C1 involves once again more wear than the others. It is difficult to conclude more things due to the small difference between the values.

To study the tribofilm as at 40°C, XPS analysis is done. In the same way as at section 4.2.1, general spectra is recorded. After, energy peaks are fitted to obtain the different ratios (figure 4.27).

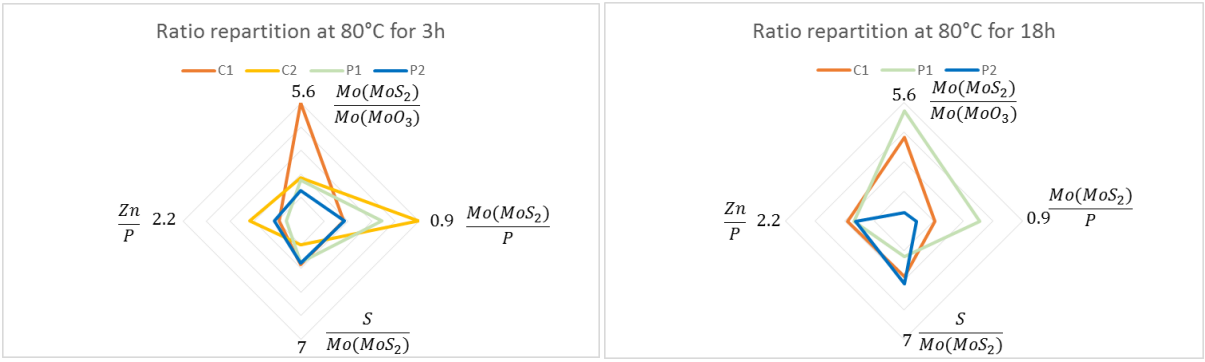


*Figure 4.27: Chemical ratio repartition for 80°C*

As at 40°C, (and possible to observe in appendix D - linescan) the chemical species have a particular repartition all along the width scar. So, it is difficult to have a correct interpretation of this ratio. However, thanks to the friction coefficient curves (figure 4.22) it is possible to explain the difference between P1 & P2. After 3h, there is a jump on the friction coefficient curve for P2. It corresponds to a degradation of the tribofilm. Indeed, after 18h, there is only $MoO_3$ on tribofilm and it is confirmed by figures 4.27 & 4.28.

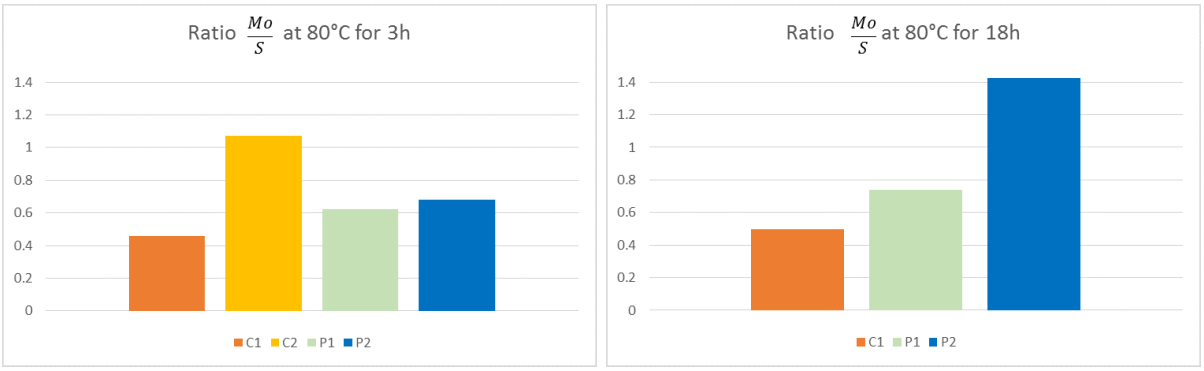


*Figure 4.28: Mo/S ratio at 80°C*

In figure 4.28, the ratios between Molybdenum and Sulfur have been reported. It is interesting to notice the difference between 40°C (figure 4.16) and 80°C. At 40°C, the C1 $\frac{Mo}{S}$ ratio was very low. Here, at 80°C, the ratio increases and so the friction coefficient decreases. For other greases C2, P1 &P2 are over 0.5. So it respect the hypothesis made in section 4.2.1 that this ratio needs to be closed to 0.5 ($MoS_2$) to show that the grease works well. In addition, the figure 4.27 shows the thickener role in terms of tribofilm formation and protection. Abrasion profiles have been done and summarize in figure 4.29.

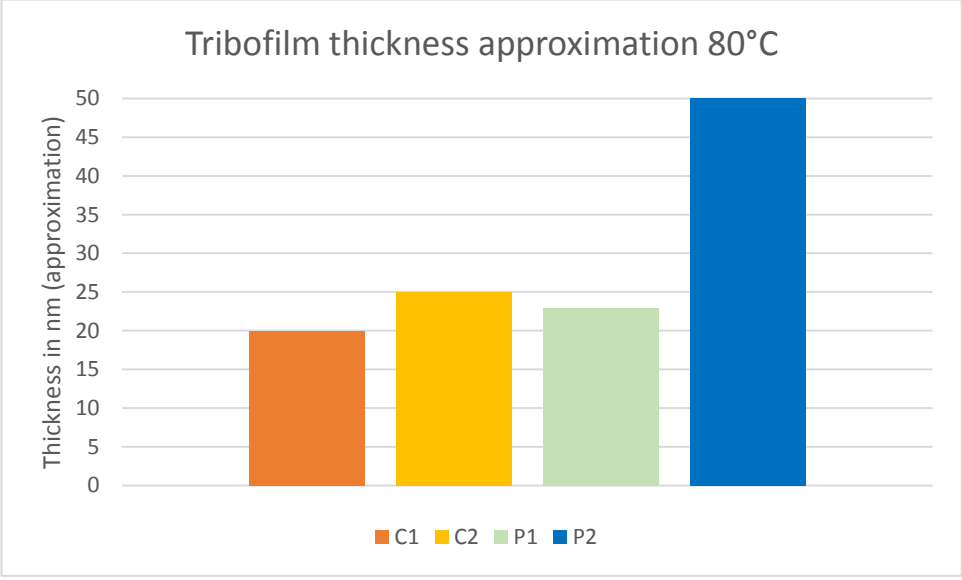


*Figure 4.29: Abrasion profiles at 80°C for 3h*

It confirms that thickeners play an important role during the tribofilm formation. In opposition to the 40°C case (fig 4.21), here grease P2 stands out. Its thickener is able to form a tribofilm twice thicker compared to the other greases.

### 4.2.3.Discussion

A first approach is proposed to explain the different wear performance of the tested greases from the experimental study. The friction coefficients at 40°C and 80°C on HFRR with conditions as close as possible to the reality allow to explain the shudder experienced on Constant Velocity Joint. Also, the different grease compositions were studied. It shows the important role of additives in the evolution of the friction coefficient but also that of the combination thickener - oil. This role is amplified at 40°C. Also, the combination oil - thickener has an influence on the time the friction coefficient takes to stabilize.

XPS analysis allowed to explain the friction coefficient difference in terms of chemistry. It shows the importance of having a ratio between Molybdenum and Sulfur closed to 0.5. The thickener plays a role in tribofilm thickness and also Molybdenum forms between sulfurized and oxide. The working temperatures change also the Molybdenum formation especially for grease C1 at 80°C.

However, compared to the results obtained with the full CVJ tests, the results of the HFRR tests do not match. During industrial component test on real Constant velocity joint, there was a critical wear with grease P1 that was not reproduced on the HFRR test.

So with the test conditions used in section 4.2 (table 14), a critical parameter seems to be missing to be able to differentiate the grease performance relevant to the CVJ application. In order to create this phenomena, a more critical test can be conducted (section 5.1). The first idea is to consider the real velocity and not only the sliding velocity. The second is to increase the contact pressure. This new conditions are available in table 15.

| Test number | $f_{HFRR}$ | $d_{HFRR}$ | $P_{h-HFRR}$ | Duration | Temperature |
|---|---|---|---|---|---|
| 5 | $100\ Hz$ | $2\ mm$ | $1.37\ GPa$ | 5h48 | 40°C |
| 6 | $100\ Hz$ | $2\ mm$ | $1.37\ GPa$ | 4h30 | 80°C |

*Table 15: New HFRR conditions to discriminate the greases in term of wear*

The results are presented in the following chapter.

Chapter five

# Wear investigation

*Durability of components remains the first objective of this work. To deal with that objective, chapter five focuses on wear investigations proposing new operating conditions. These conditions allow to reproduce wear from component vehicle to laboratory rigs. It reveals the phenomena which involves the constant velocity joint failure.*

*To complete this investigation, lubricant ability to supply oil inside the contact is studied thanks to a combination of a tribometer and a rheometer. It leads to an overall comprehension of the failure mechanism.*

## 5.1. Grease behaviour under extreme behaviour

### 5.1.1.Friction

In order to reproduce the wear of the component notably for grease P1 at 40°C, the test conditions given in table 15 are used on HFRR. The first step was to study the greases at 40°C. The friction coefficient (figure 5.1) and film thickness are available (figure 5.2).

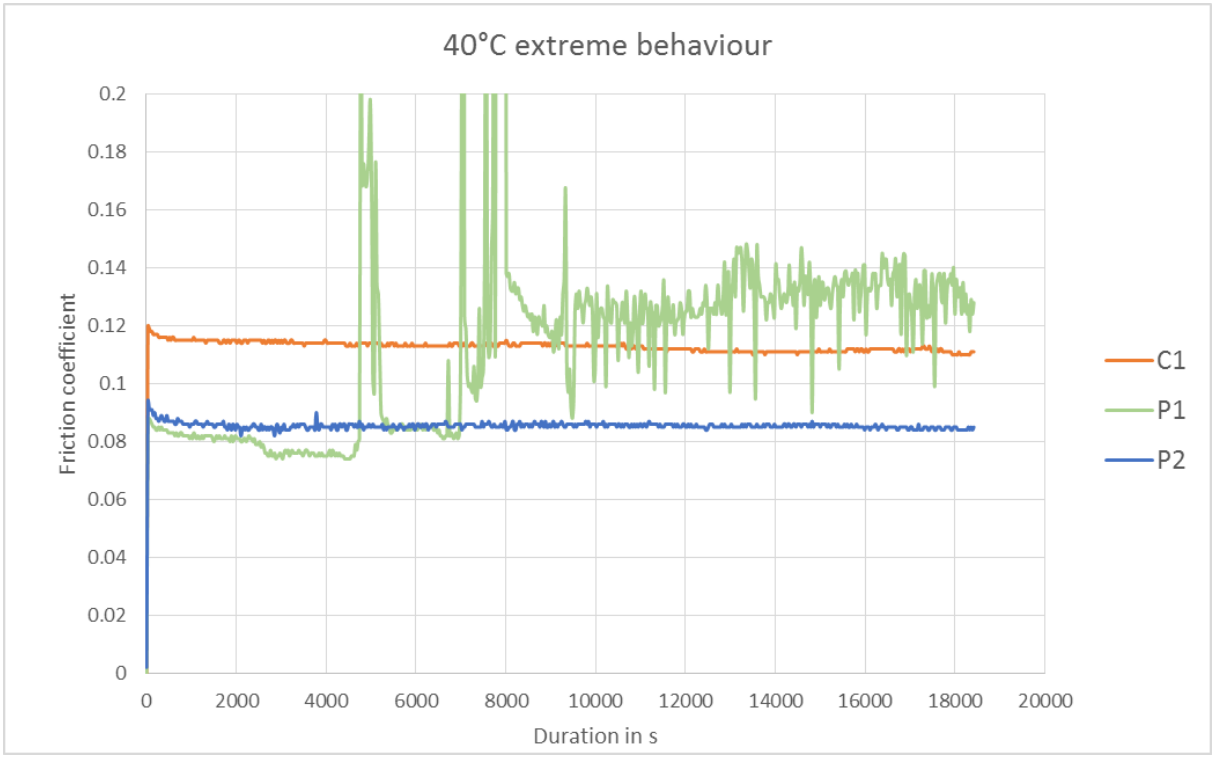


*Figure 5.1: Friction coefficient using test condition 5*

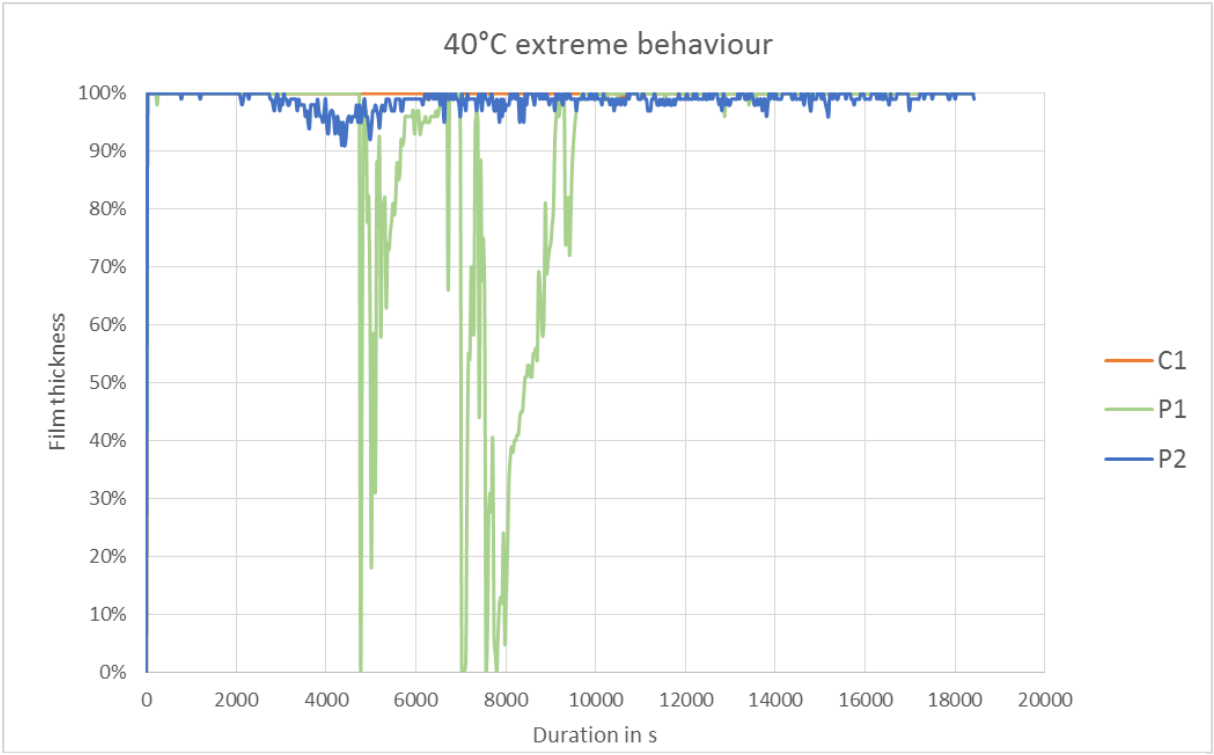


*Figure 5.2: Surface separation using test condition 5*

The first observation is that grease P2 & C1 have exactly the same reaction than with the previous conditions (table 14). Only a small variation of friction coefficient is noticed due to the velocity and pressure change. In addition, the surface separation is satisfying. However, for grease P1 a major friction coefficient instability occurs. Moreover, when this friction coefficient jump occurs, the film thickness collapses down to 0% as if the contact is suddenly starved. In order to go further the test is repeated (figure 5.3).

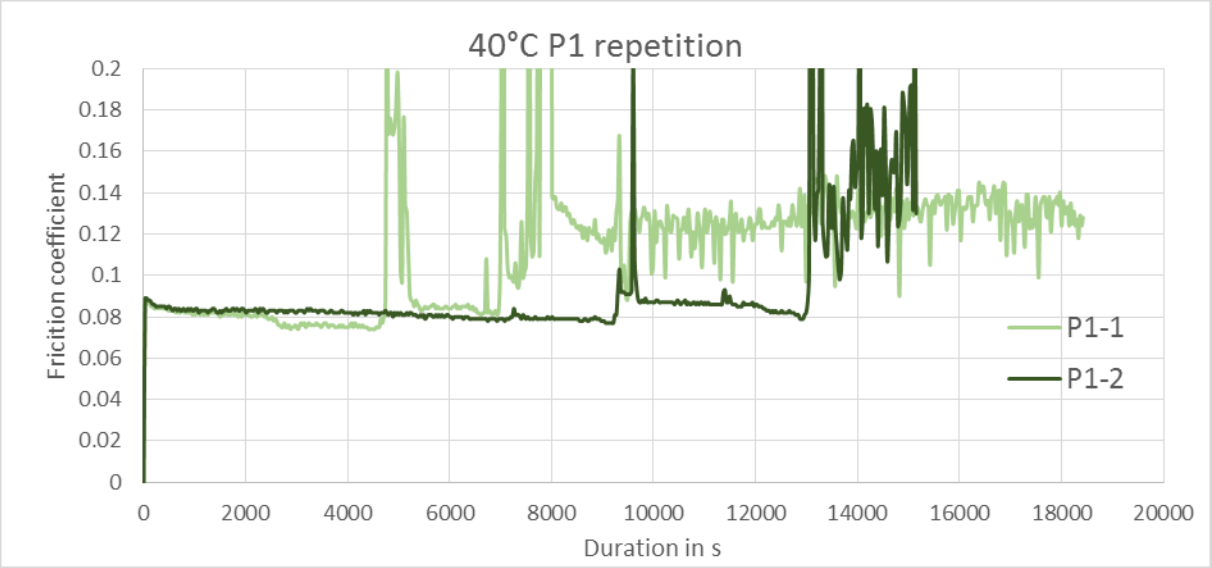


*Figure 5.3: Grease P1 at 40°C (condition 5)*

This friction instability correlated to the lubricant film collapsing is clearly repeatable. The first failure appears, after the lubrication recovers and second failure occurs. After these failures, probably induced by scuffing and surface degradation, the grease P1 is now the equivalent of a standard grease (not low friction) like C1. This implies a lot of shudders in vehicle and will spread the surface degradation eventually leading to irreversible failure of the CVJ.

Now, at 80°C the same tests are done and are available in figure 5.4 & 5.5.

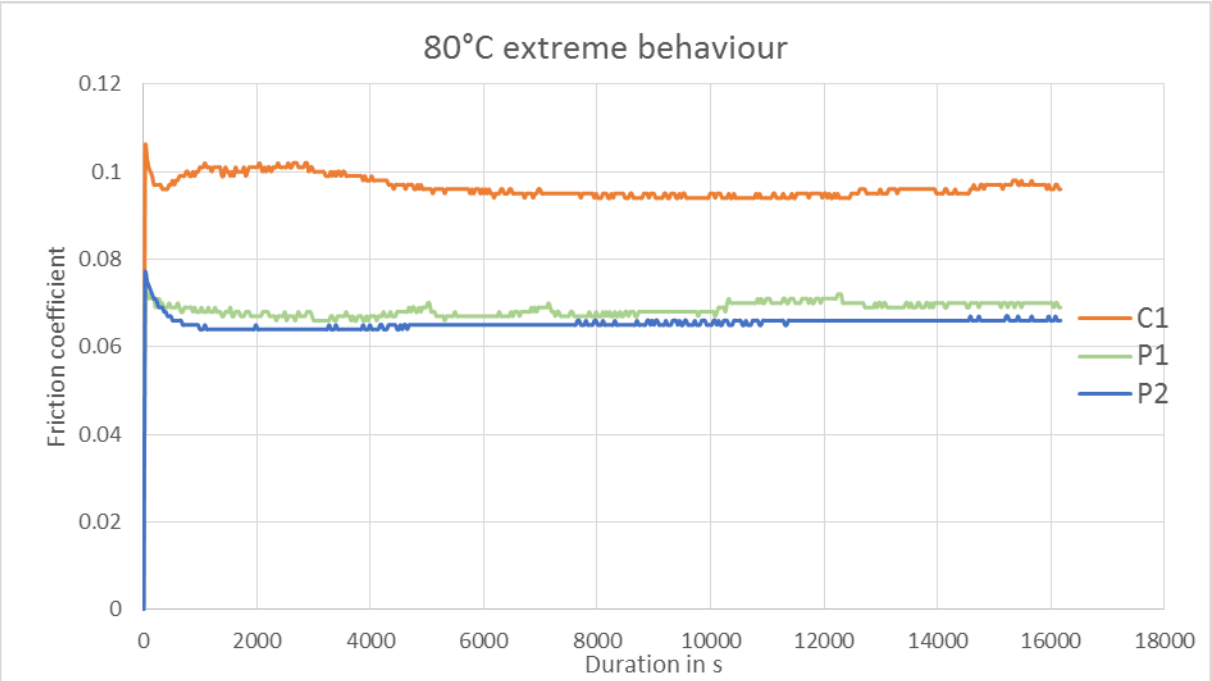


*Figure 5.4: Friction coefficient using test condition 6*

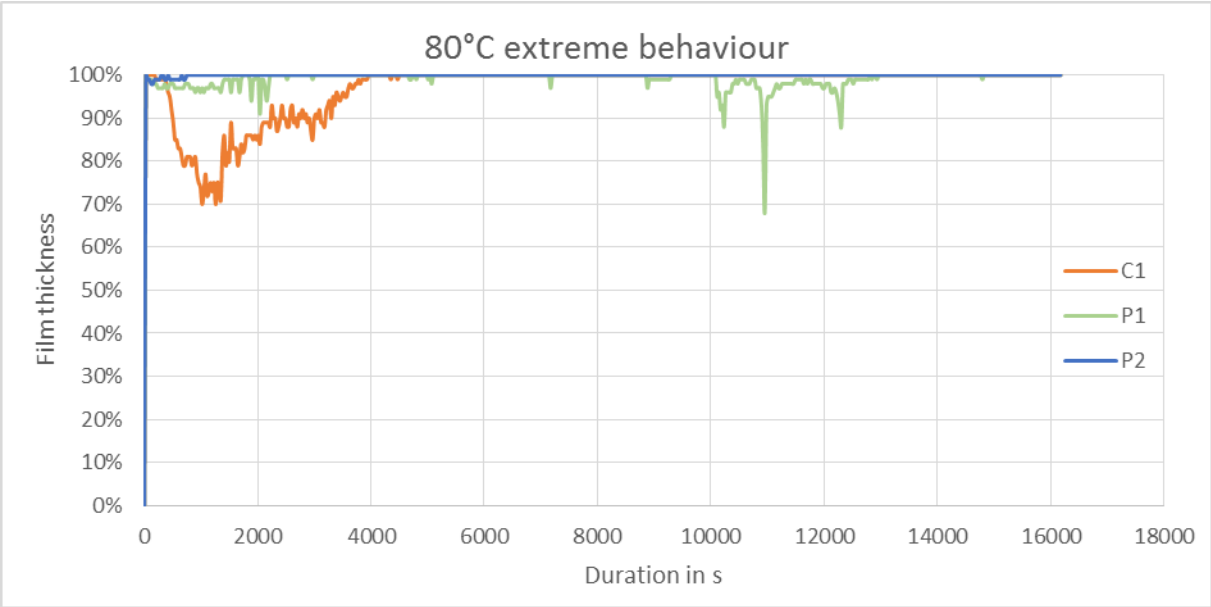


*Figure 5.5: Surface separation using test condition 6*

In figures 5.4 & 5.5 there is not any failure compared to 5.1 & 5.2. Indeed, here the friction coefficients are stable and the film thicknesses are always over 60%. It seems that failure occurs only at 40°C with grease P1. Wear needs to be investigated in order to compare it to component tests on real transmission rig.

5.1.2.Wear

Wear obtained by test conditions 5&6 gives clear results. Indeed, as observable in table 16, the results are visible to the naked eye at the end of the test. A comparison between unfailed sample and failed sample is available in figure 5.6.

| C1 | P1 | | P2 |
|---|---|---|---|
|  |  | 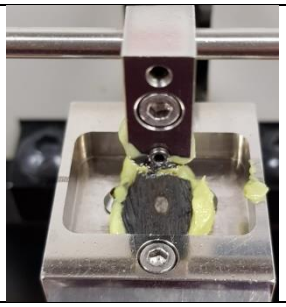 |  |

*Table 16: End of HFRR tests for condition 5*

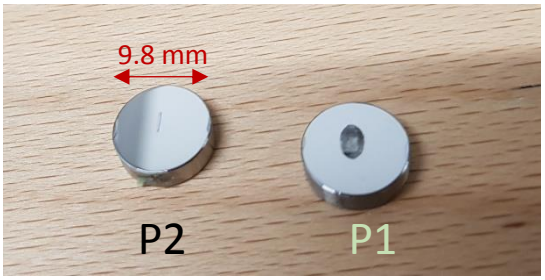


*Figure 5.6: comparison between sample after HFRR test condition 5*

In order to compare greases, the same methodology than in section 4.2 is used. As predictable, the figure 5.7 shows that the grease P1 stands out from the others. The surface is completely damaged.

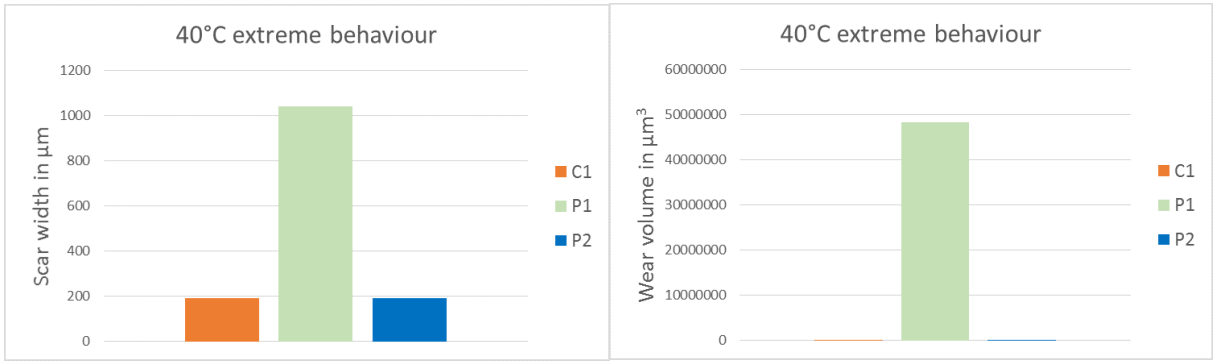


*Figure 5.7: Wear of HFRR test condition 5*

However, at 80°C, the wear shows in figure 5.8 indicate no failure.

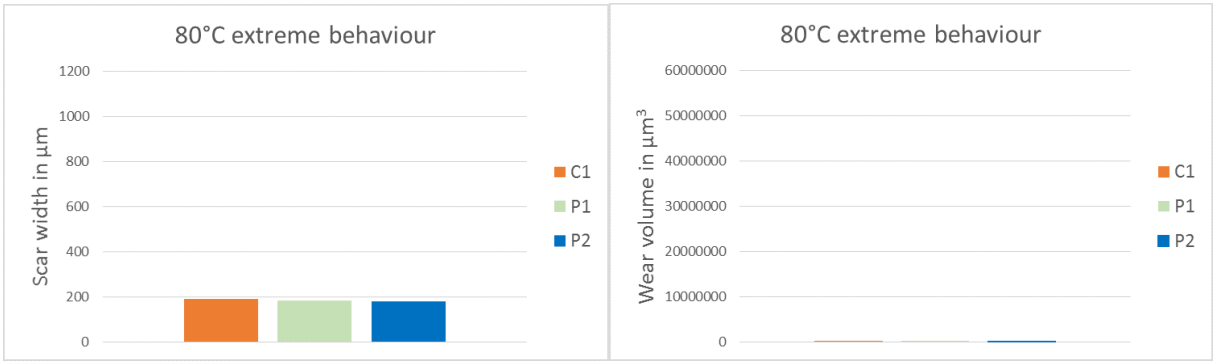


*Figure 5.8: Wear of HFRR test condition 6*

Indeed, wear measurements at 80°C correspond to previous test in section 4.2. The width and volume increase slightly probably due to the velocity and pressure increasing. However, it is a normal phenomenon which is not critical for CVJ reliability.

To complete this methodology, a test under operating condition 5 is stopped to investigate wear phenomena (figure 5.9).

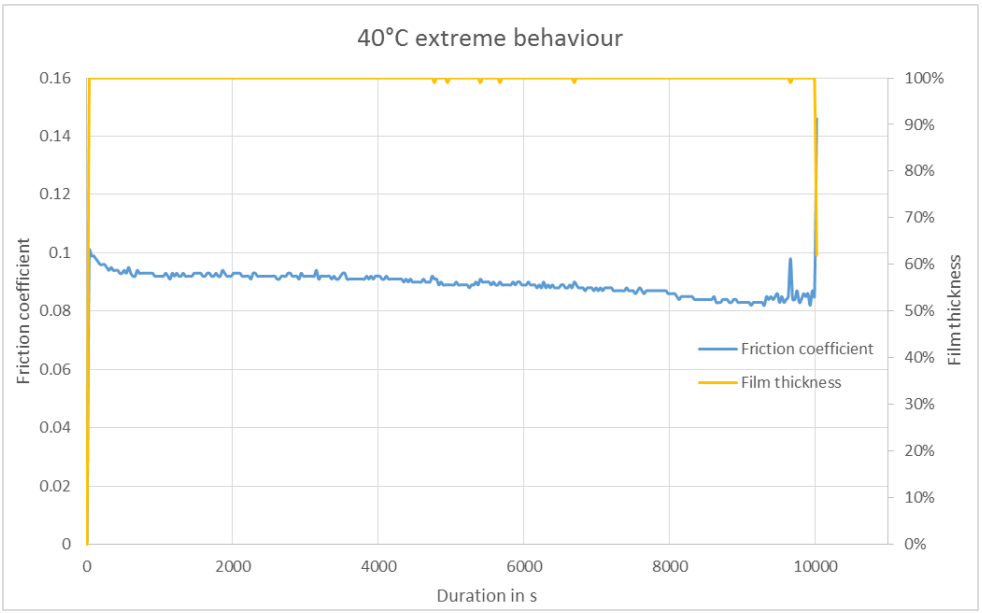


*Figure 5.9: HFRR test under condition 5 – grease P1*

Thanks to a profilometer, topographies are measured on the ball (figures 5.10 & 5.11) and on the disc (figures 5.12 & 5.13). In addition, profil from the disc surface is measured (figure 5.14)

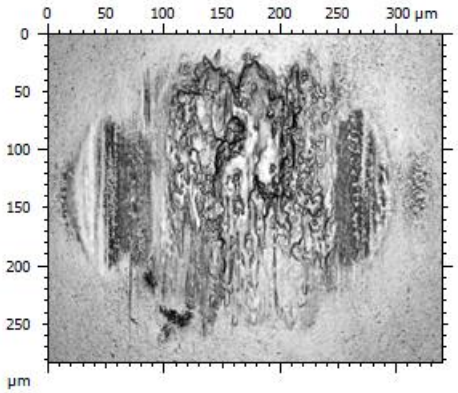


*Figure 5.10: image of the ball*

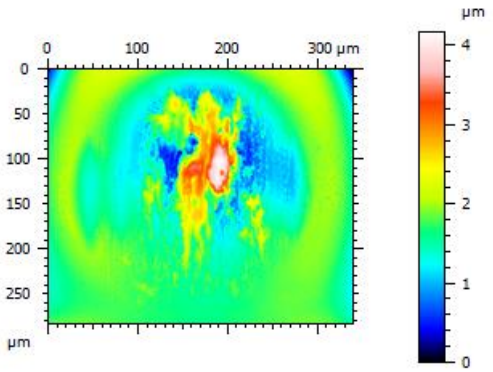


*Figure 5.11: surface of the ball using interferometry*

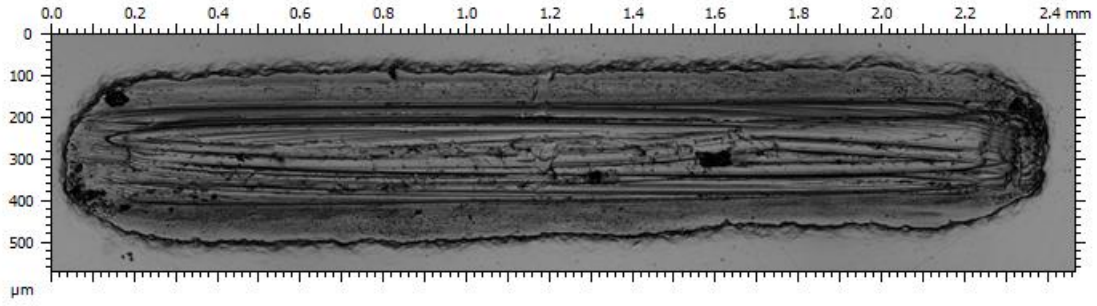


*Figure 5.12: image of the disc*

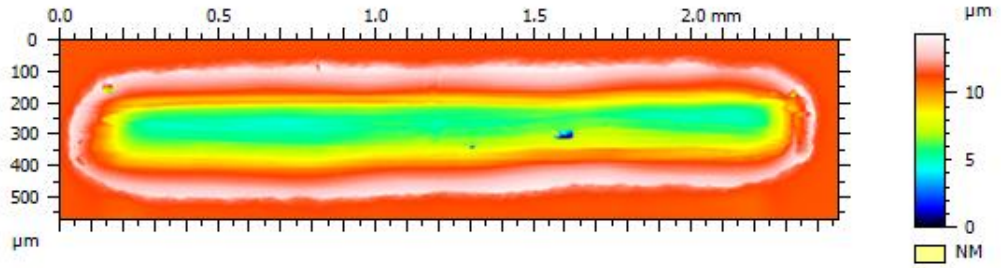


*Figure 5.13: surface of the ball using interferometry*

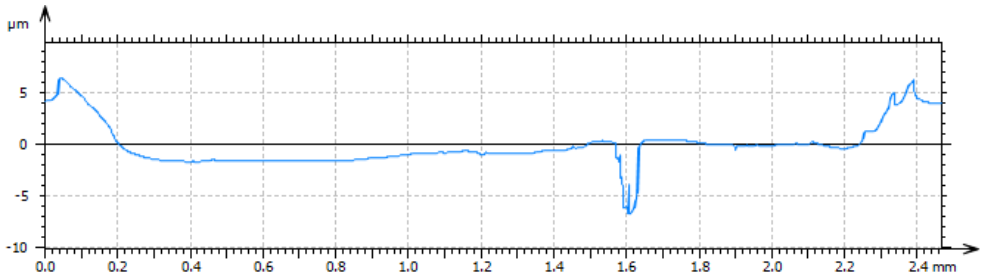


*Figure 5.14: profil of the disc*

As suggested in previous section, it is possible to observe some matter in relief on the ball surface. In addition, this matter is lost from the disc. The scuffing suggested is confirmed by these measurements.

5.1.3.Discussion

The industrial wear phenomenon described in section 4.1.2 is reproduced on a laboratory rig when using the updated test conditions taking into account the actual velocities rather than the sliding speed. The failure does not occur at 80°C but at 40°C and only with the grease P1. The wear obtained with P1 at 40°C reproduces exactly the CVJ wear on component.

The temperature of 40°C could match with some temperatures during the life of constant velocity joint. So, it seems that an explanation must be found on mechanical properties rather than on chemical compositions. As the scuffing does not appear at 80°C, it is not a contact thermal issue. Assumption is made that at 40°C, the grease supplies less oil than at 80°C in the case of P1 (not in the case of P2). A hypothesis of wear phenomena is available in figure 5.15.

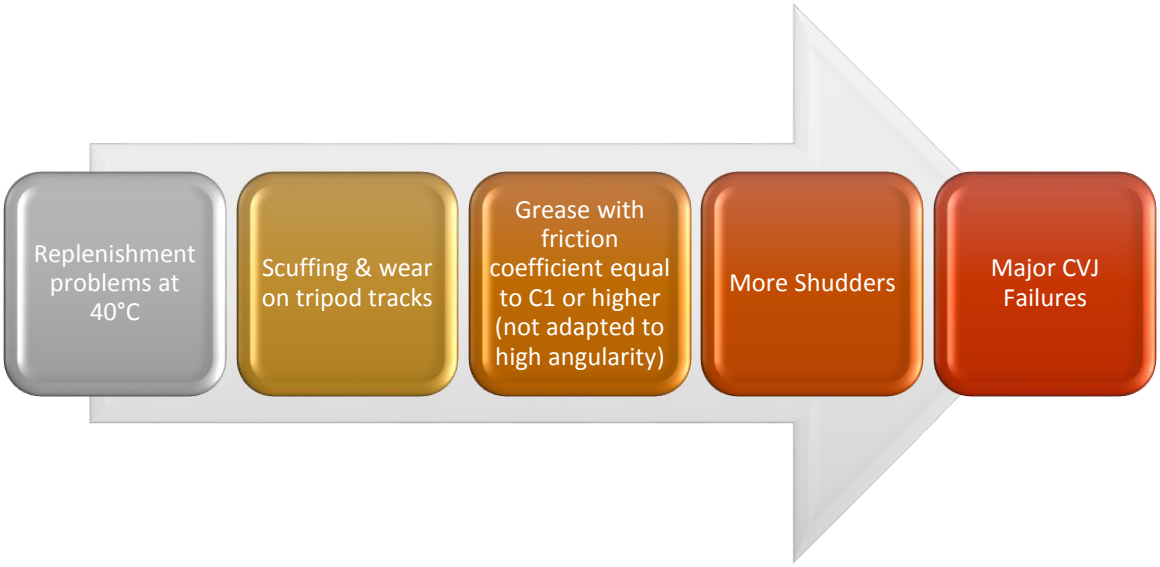


*Figure 5.15: wear phenomena hypothesis*

Furthermore, it seems to be a rheological and/or grease bleeding problem. In addition, between greases P1 & P2 only the thickener changes. It is investigated in the next sections.

## 5.2. Grease physical behaviour

### 5.2.1.Rheology

To explain results from HFRR tests, rheological measurements are performed to characterize the industrial grease samples C1, P1 and P2. Tests were performed at 40°C and 80°C on a HAAKE RheoStress 1, a stress-controlled rheometer using a plate-plate geometry PP20 (φ=20 mm) .
Two tests were conducted:

A. Oscillatory, with a gap of 1 mm, $\omega_R = 1\text{Hz}$ and $\tau$ from 1 Pa to 500 Pa;
B. Rotational, with a gap of 0.2 mm, measuring viscosity and controlling the shear rate from 0.01 to 5000 $s^{-1}$.

These operating conditions are chosen to have no influence of the geometry and surface roughness on results [42]. A satisfying repeatability was achieved with this rheometer and procedures.

#### A. Oscillatory tests

The aim of these tests is to obtain 3 properties as described in section 1.2.3 [42] :

- G' which is storage moduli. It represents the deformation energy stored by the sample. This deformation is completely reversible. It corresponds to the elastic behaviour of the material.
- G'' which is the loss moduli. It represents the deformation energy consumed by the sample during the shear process. This energy is irreversibly lost.
- The damping factor $\tan(\delta) = \frac{G''}{G'}$. It is the ratio of the viscous and elastic part of the viscoelastic deformation behaviour.

From the grease point of view [19],[43], the material behaviour is viscoelastic [44]. When G'>G'', the grease acts like a solid. When the stress increases, both G'' and G' start to decrease and G' & G'' cross at $\tan(\delta) = 1$. It is the cross over stress $\tau_{CO}$ also named "flow point". The storage moduli becomes smaller than the loss moduli. Then, when G''>G', thickener is not able to recover elasticity. The grease acts like a liquid. The results are summarized in table 17 and available in figures 5.16, 5.17 and 5.18. Values obtained for LVE (linear viscosity) area is calculated using 10 points for C1 (40°C and 80°C), P1 (40°C) & P2(40°C) and 5 points for P1 (80°C) & P2(80°C).

| Grease | Temperature in °C | G' in Pa | G'' in Pa | tan(δ) | $\tau_{C0}$ in Pa |
|---|---|---|---|---|---|
| C1 | 40 | 23966 | 6944 | 0.29 | 409 |
| | 80 | 13933 | 6167 | 0.40 | 127 |
| P1 | 40 | 23329 | 6547 | 0.28 | 192 |
| | 80 | 13096 | 4518 | 0.29 | 56 |
| P2 | 40 | 16246 | 6194 | 0.38 | 384 |
| | 80 | 7851 | 4860 | 0.5 | 106 |

*Table 17: Visco elastic properties*

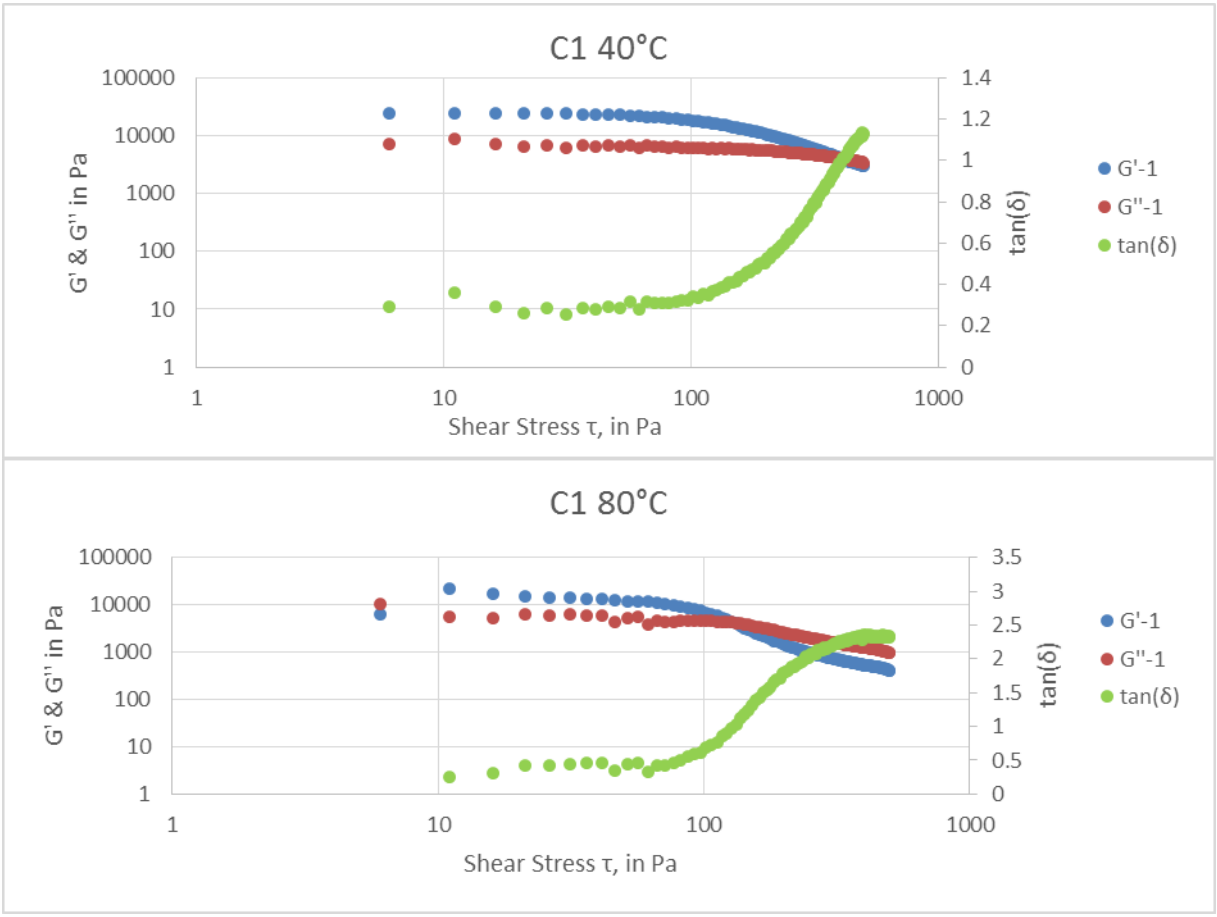


*Figure 5.16: Visco-elastic properties for C1*

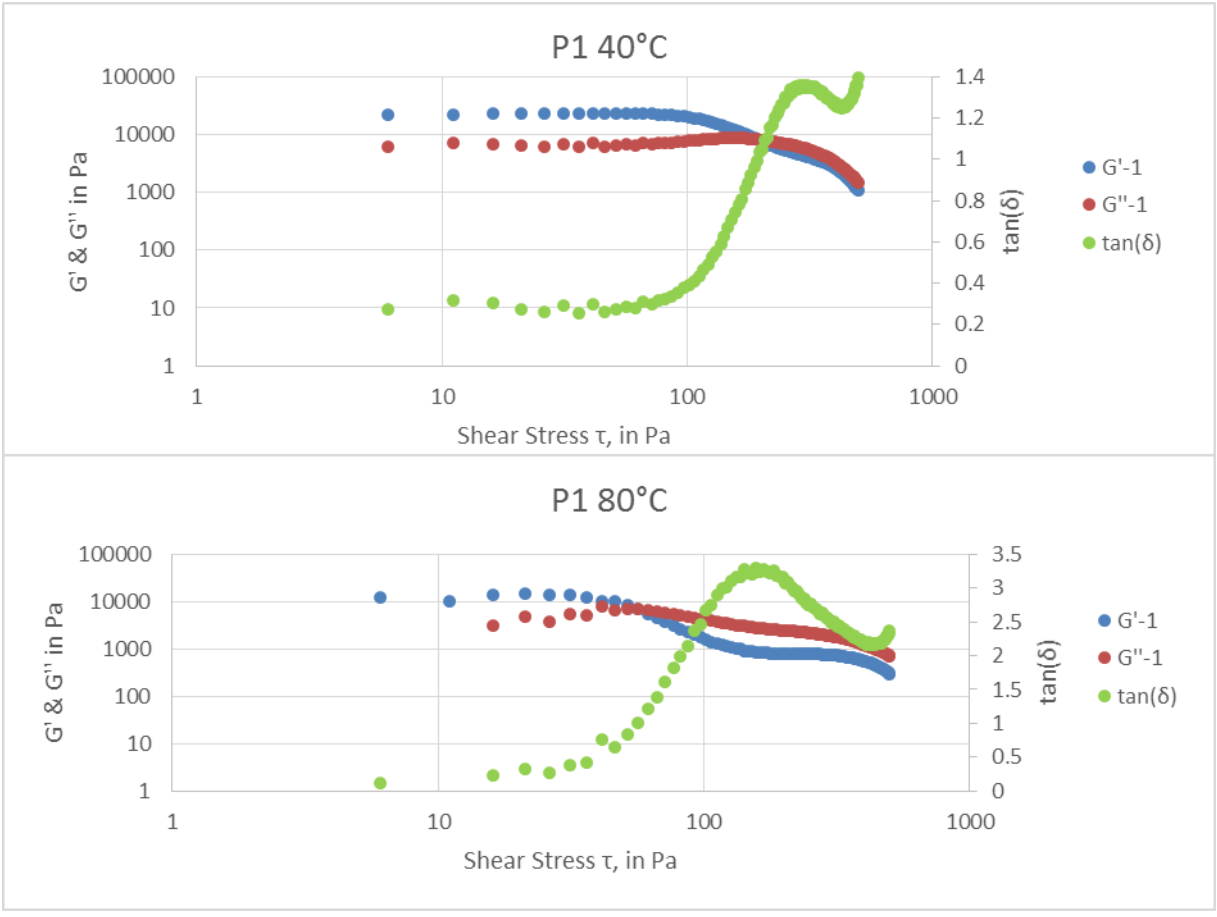


*Figure 5.17: Visco-elastic properties for P1*

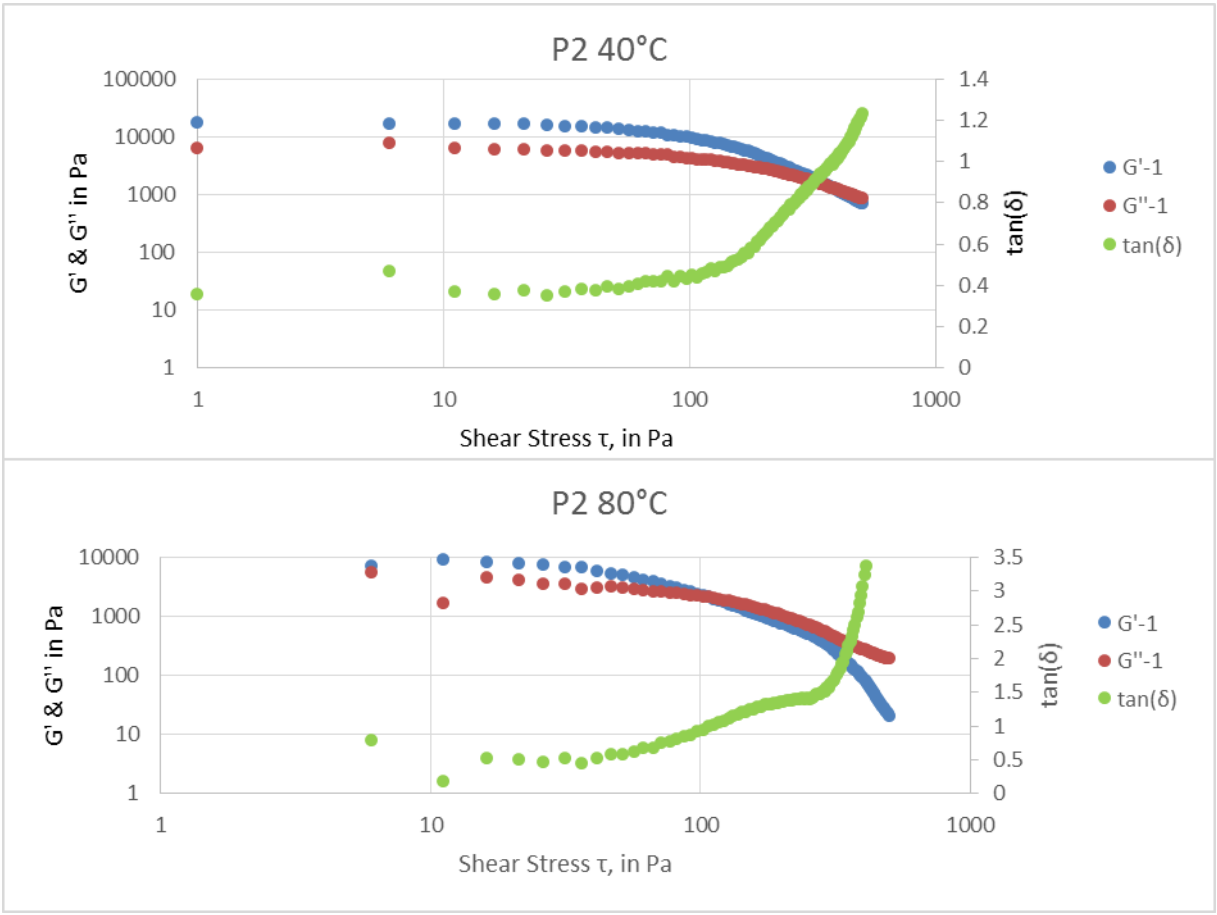


*Figure 5.18: Visco-elastic properties for P2*

The first observation is that general behaviour at 40°C and 80°C seems to indicate the validity of measurements. Indeed, according to the literature it is possible to observe that the flow point and G' decreases as temperature increases [45].

Secondly, C1 and P2 have a comparable behaviour. In fact, their flow points are around the same value at 40°C or 80°C. In addition, G' for P2 is lower than G' for P1 which has the same base oil. It indicates that P2 is less concentrated in thickener than the other greases [44]. Moreover, P1 has a lower flow point than the other greases at 40 °C and 80 °C respectively. It indicates that the grease stop working sooner as a solid and begin to have a liquid behaviour. However, the damping factors at 40°C and 80°C oscillate. This phenomena is not observable for the other greases. At 40°C, the values of G' and G'' after the crossover keep very close. So, it is difficult to know if the grease goes to a liquid behaviour or stays in some solid/liquid transitions state compared to its behaviour at 80°C.

Indeed, the comparable behaviour gives the same results in term of wear. In addition, when at 80°C, P1 does not have this "transition state", the HFRR test does not fail (as in figure 5.4).

Finally, the flow point, G' and consistency affect the mobility of the bled oil within the grease and therefore the ability of the grease to replenish the contact after being pushed out. However, the flow point and G' tend to the same behaviour in case of C1 and P2. At the opposite for NLGI number which gives information on consistency, P1 and P2 are closer. Even if the NLGI numbers are quite similar between C1, P1 and P2, this only mechanical property is not enough to qualify grease behaviour in the present study.

B. Flow properties

In addition to oscillatory tests, flow curves have been performed in order to validate the viscoelastic structure of the grease [18] and thickener content [44]. They are shown in figure 5.19 and 5.20.

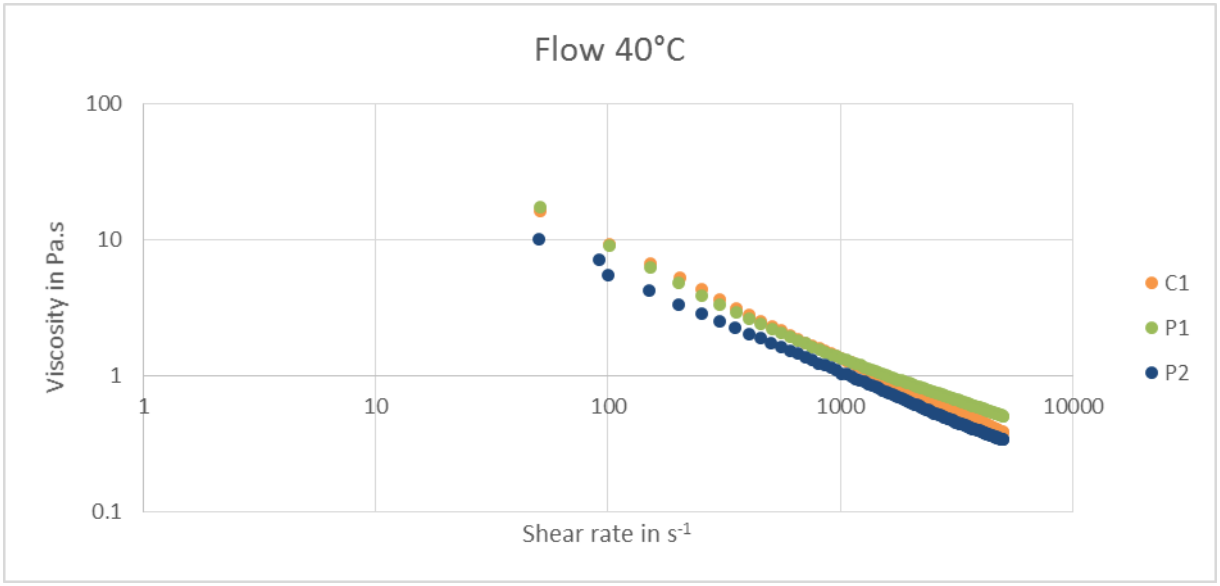


*Figure 5.19: Flow curves at 40°C*

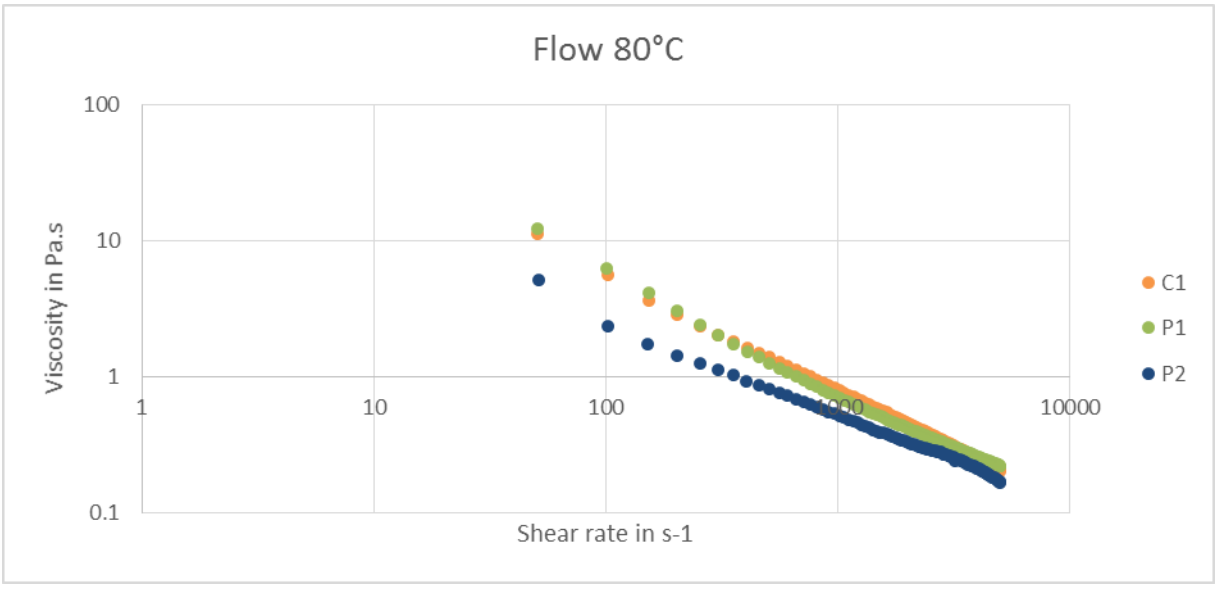


*Figure 5.20: Flow curves at 40°C*

As expected, the visco-elastic behaviour is confirmed. The thickener content hypothesis made with the value of G' for P2 thanks to the oscillatory measurements is confirmed. Indeed, the P2 curves are lower than P1 and C1 at 40° C and 80°C. To complete the rheology study, a film thickness study is performed. Indeed it helps to analyze the grease behaviour and its ability to form a film thickness to protect surfaces and prevent wear.

5.2.2.Film thickness measurement

In order to explain the different behaviour of the grease in terms of wear and to complete the rheological study, an investigation is done using EHD2 describe in section 2.1.3. The main goal is to measure the grease film thickness. The tests conditions are available in table 18.

Tests are conducted without grease scoop so that the contact is not artificially replenished in grease throughout the test duration. To insure repeatability, a 3D printed stencil is used (figure 5.21). When the stencil is filled, it allows to have 6.2 grams of grease on the disc (figure 5.21b) and ensuring the same volume of grease is used for all the tests.

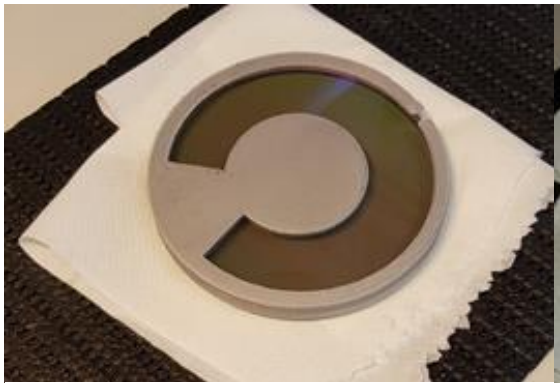

*Figure 5.21a: EHD stencil*

*Figure 5.21b: Stencil filled*

| Test number | $S_{EHD}$ | $SRR_{EHD}$ | $P_{h-HERR}$ | Duration | Temperature |
|---|---|---|---|---|---|
| 7 | 100 mm/s to 600 mm/s | 10% | 0.38 $GPa$ | | 40°C |
| 8 | 100 mm/s to 600 mm/s | 10% | 0.38 $GPa$ | | 80°C |
| 9 | 400 mm/s | 10% | 0.38 $GPa$ | 2100 s | 40°C |
| 10 | 400 mm/s | 10% | 0.38 $GPa$ | 2100 s | 80°C |

*Table 18: EHD tests conditions*

It must be noticed that grease test repeatability is very difficult to obtain due to the chaotic behaviour of the grease [46],[47],[48] even for exactly the same operating conditions and grease volumes. For conditions 7&8, the results are repeated twice. For conditions 9 & 10, tests are repeated more than twice to obtain meaningful results. Indeed, a lot of scatter was encountered due to the SRR and the geometrical configuration. Repetition curves are available in appendix F.

A. Study of the grease behaviour as function of speed

The main goal is to characterize the grease film thickness as a function of speed. It gives precious information in order to study grease characteristics. Results at 40°C are available in figure 5.22 and at 80°C in figure 5.23. Is it possible to notice that, like in section 5.2.1, at 40°C, grease P1 has a different behaviour than the other two. In addition, linear tendency curves have been added to underline this difference. However, at 80°C, the 3 greases have almost a similar behaviour. That confirms the results from sections 5.1.1 & 5.2.1. In addition, the film thickness for the 3 greases is smaller when the temperature increases from 40°C to 80°C.

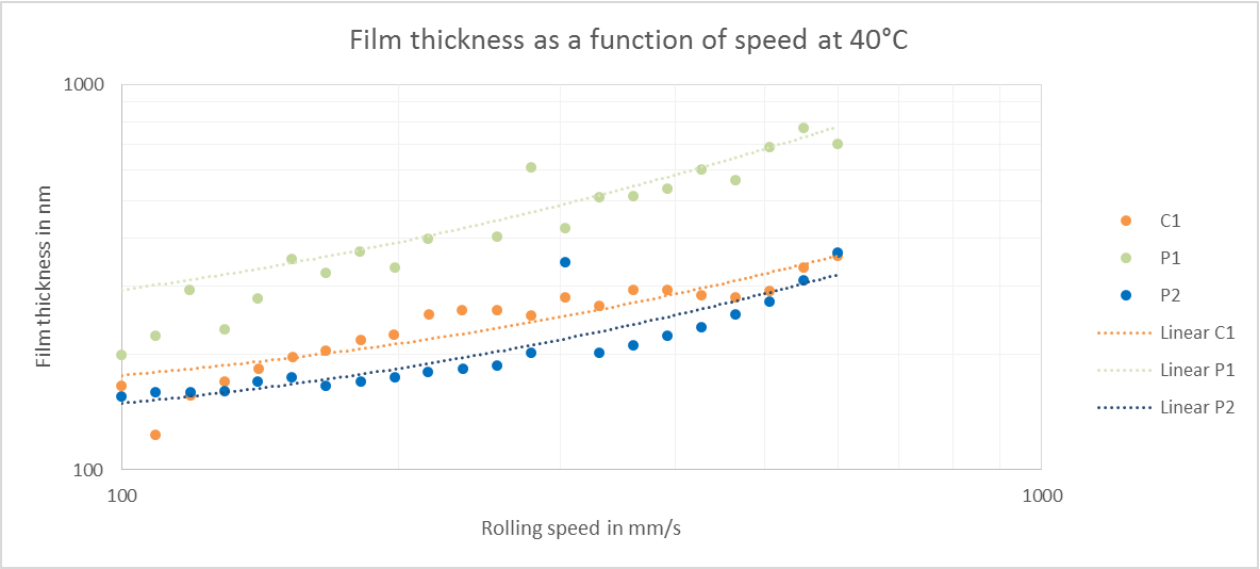


*Figure 5.22: Film thickness for test condition 7*

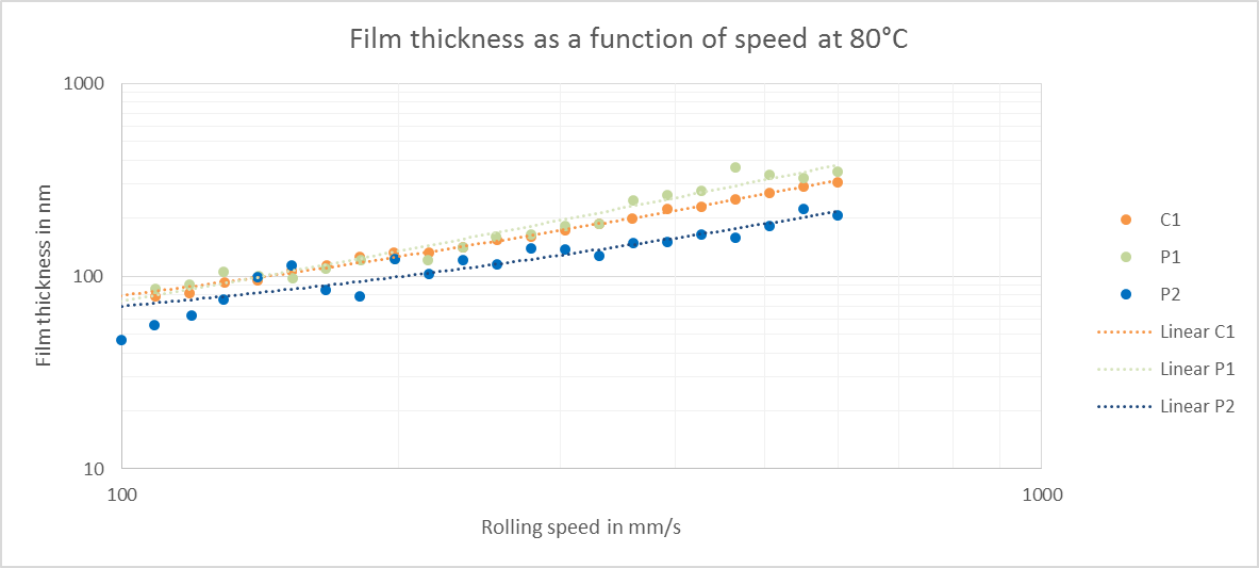


*Figure 5.23: Film thickness for test condition 8*

B. Study of the grease film thickness in time

In order to explain wear, the film thickness is measured as function of time. The operating conditions (9&10) seem relevant compared to the real application. It can be compared to conditions 5&6 from table 15 of the section 4.2.3. Results for C1, P1 and P2 are available respectively in figure 5.24, 5.25 & 5.26.

First of all, it is interesting to note that for the same test a grease can have different but repeatable results. For example grease C1 at 40°C has 3 distinct behaviours (figure 5.24). The first one separates correctly the surface around 250 nm. The second one is the opposite. The film thickness becomes smaller and goes near zero damaging the space layer coating of the test track on the disc. And another one which oscillate between the 2 curves. This behaviour is really interesting. In fact, it proves the grease ability to replenish the contact. The same ability is observable for P2 both at 40°C and 80°C.

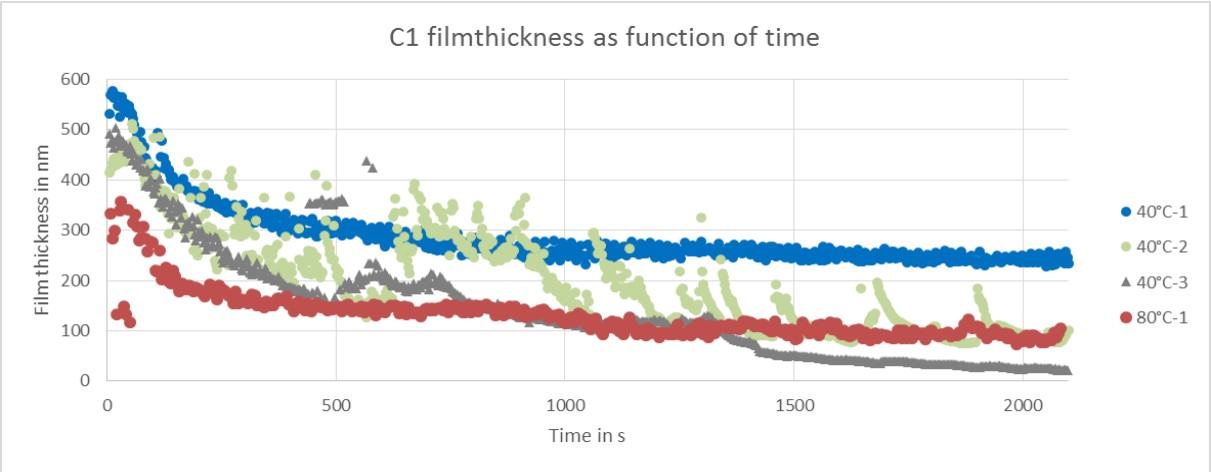


*Figure 5.24: C1 results for conditions 9 &10*

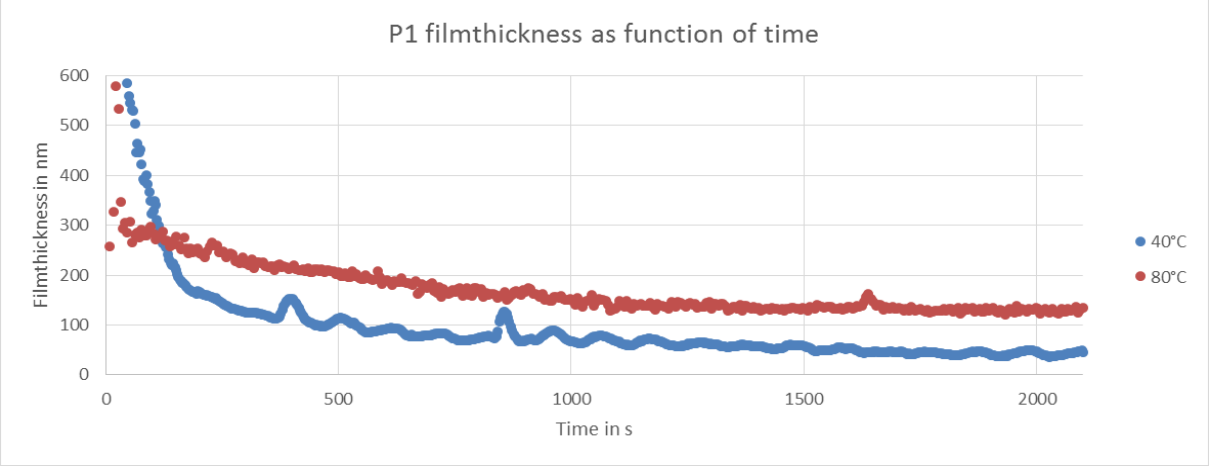


*Figure 5.25: P1 results for conditions 9 & 10*

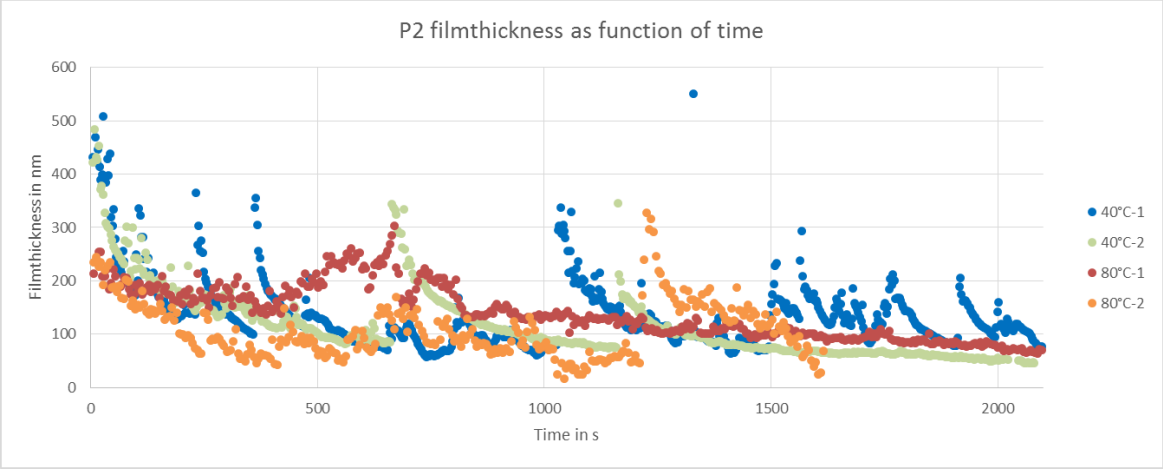


*Figure 5.26: P2 results for conditions 9 & 10*

In figure 5.27, images from EHD illustrate the contact state before and after the replenishment.

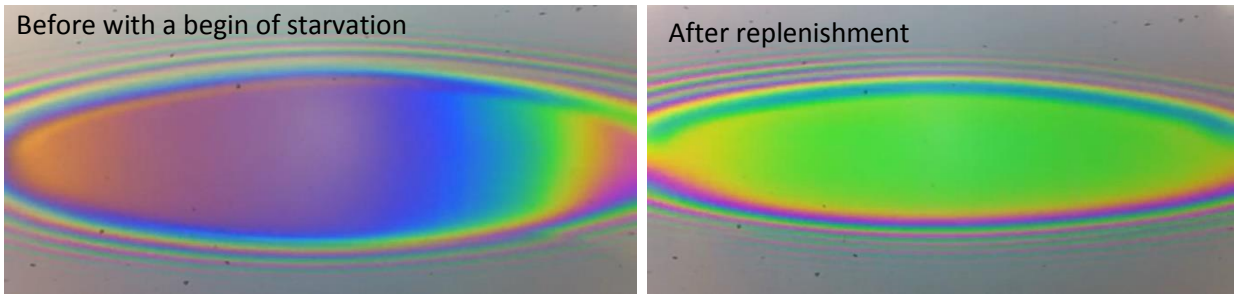


*Figure 5.27: contact replenishment with P2 at 40°C (same test with no external event)*

This lubricating ability of the grease prevents wear. When the contact film thickness is low, the grease can replenish the contact thanks to its bleeding ability even if it is against the centrifugal forces. For C1 at 80°C, the grease does not show the same ability. Nevertheless, the film thickness is lower than previous value due to the increase of temperature but it is more stable during the test and the surface separation is improved protecting the surfaces too.

There are sporadic replenishments at certain points in time during tests. It is possible to explain by the following explanations:

- Starvation induces vibrations due to the lack of lubricant.

These vibrations will allow to the grease to come back again inside the contact area.

- Centrifugal forces

As the grease is overrolled and pushed out of the contact, oil is stored at both sides of the contact. Due to centrifugal forces, the grease lump closer to the rotational shaft bleed oil in the direction of the contact area.

- Mechanical degradation of thickener matrix

Degraded grease thickener insures a residual film on the rolling track.

All these phenomena improve re-flow until the next starvation event occurs [49],[50].

However, this behaviour is not available with P1. At 40°C, the film thickness decreases quickly and never recover contrary to P2 &C1. Finally, after some time, it goes to zero and damage occurs on the track. This is illustrated in figure 5.28. It is possible to observe the beginning of the starvation on the right and the left sides of the contact. However, the grease never replenishes the contact and tends to zero. It is similar to the behaviour found by other authors [51]. At the opposite as it was expected, with P1 at 80°C, the film thickness is higher than at 40°C.

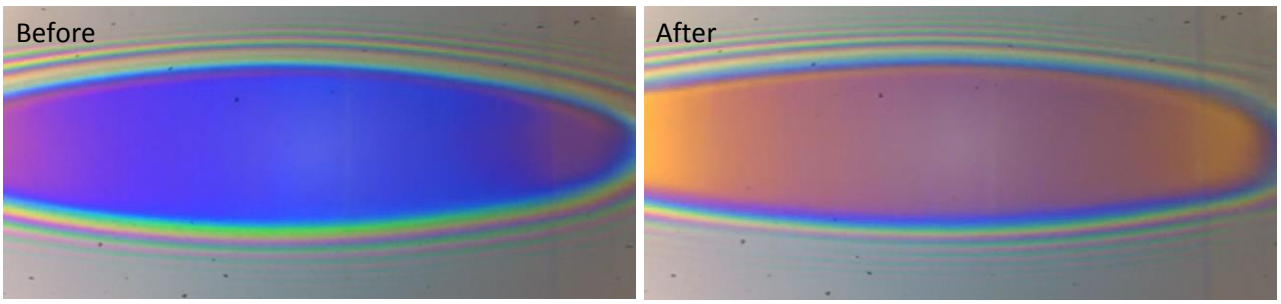


*Figure 5.28: Contact starvation with P1 at 40°C*

### 5.2.3.Discussion

The industrial wear phenomenon described in table 12 is reproduced on a laboratory test rig (HFRR). The failure does not occur at 80°C but at 40°C and only with the grease P1. The wear obtained with P1 at 40°C reproduces exactly the CVJ wear found on the actual components from full component tests mimicking the field application.

The temperature of 40°C matches the temperatures found for certain periods of time in a life duration of a CVJ. The wear investigation with the HFRR test rig confirms that the wear is due to some problems at 40°C. The rheological section (5.2.1) gives key information. P2 and C1 have the same behaviour. The crossover stress is almost equivalent at 40°C and 80°C. However, with P1, there is some problem when the grease begins to act like fluid material at 40°C. In addition, the flow test confirms that even if the greases P1 & P2 have the same bled oil and thickener, the thickener content is not the same. P2 has less thickener than P1 which explains different tribological and rheological behaviours.

Section 5.2.2 with EHD measurements confirms the findings of sections 5.1.1 & 5.2.1 (HFRR and Rheology). At 40°C, the grease P1 is not able to replenish the contact which can be linked to the “fluid behaviour “of P1 at 40°C. In addition, the film thickness is very low and damage occurs. At the opposite, P2 & C1 have this lubricating ability which guaranties sufficient surface separation during the test and prevents wear. It can be noticed that P2 has better lubricating ability than C1. It can be linked directly to the bled oil results (table 13).

To come back to CVJ wear, as the grease supplies less oil, the contact is under starved conditions. This behaviour does not occur at 80°C because the grease provides more oil due to temperature increase affecting its rheological properties. The complete wear process is available in figure 5.29.

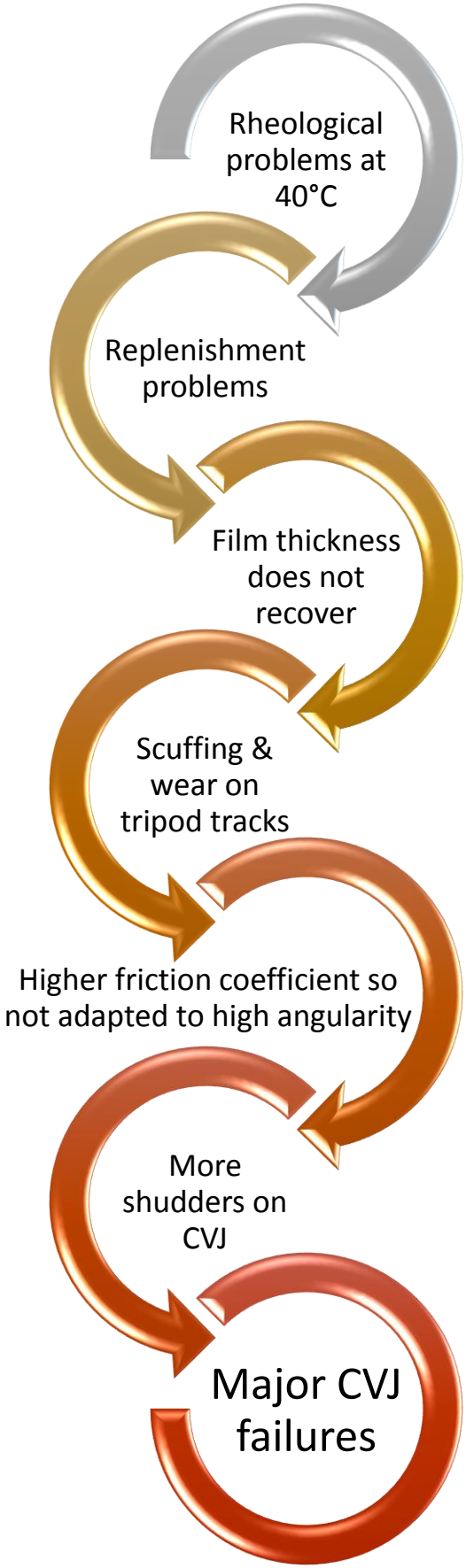


*Figure 5.29: Wear phenomena for P1 at 40°C*

# Conclusions & prospects

**Conclusions**

A Constant Velocity Joint remains an important component of actual vehicle transmissions. Its design has been used for decades and does not progress a lot. However, the challenges of a car manufacturer have progressed. Indeed, the fashion of SUV in Europe in particular has pushed the car manufacturers to consider new mechanical disposition for the transmission under the hood. It implies a higher articulation angle.

In addition, the technical specifications of the component have changed. First of all, satisfying durability to insure no failure during the vehicle life duration remains the primary objective. Secondly, the increase of articulation angle implies a low friction grease to avoid shudder to satisfy the customer and the durability. In addition, mechanical efficiency optimization remain a major requirement when designing automotive products. So, it reveals the importance of the friction coefficient. Finally, with technical specifications, the cost constraints push car manufacturer to find innovative solutions to solve technical challenges. In that case, the manufacturer has decided to work on grease to deal with this constraint.

The first chapter presents the technical needs to solve that challenge. Indeed, the tripod transmission joints on the gearbox side are known to produce wear and reliability problems for the customers in some known cases. As explained sooner, it has to deal with complicated technical specifications that implies knowledge on automotive transmission, tribology and grease. The automotive transmission is explained in 3 steps, a general one which gives key information on its function which implies a complex kinematics. Secondly, a focus on environmental regulations is necessary to understand the work on friction and its perspective. To finish a focus on Tripod joint has been done.

The tribology which is a technological niche for car manufacturer is popularized. It is decomposed to 3 parts. The first one gives information on the lubrication theory in particular its relation to the wear process. The second one helps to understand the rheology which deals with the deformation and flow of materials. The last one deals with the well-known Hertz theory used to calculate the contact pressure. In addition, greases are presented. Actually, it is a really interesting lubricant which is a savant mixture of oil, thickener and additives.

To deal with this work objectives, experimental approach was used to understand the wear phenomena. The major experimental means are described in chapter 2. It allows to provide reliable data thanks to proven tribological rigs and analysis technics. Furthermore, an observation rig created specifically for this study is also presented with the numerical tools.

The chapter 3 characterizes the contact using this new observation rig and chapter 1 theory. The contact pressure is calculated in order to have good operating conditions in further experiments. After this step, a complete analysis of the roller kinematics inside the tripod joint has been done. It helps to understand the contact area and it specific operating conditions. It has been noted that the ellipse described by the contact always changes during the rotation of orientation compare to the velocity vector. That specificity implies difficult lubrication. The material choices of the observation rig are also validated thanks to an investigation of the tribo sytem 3D printed plastic/steed and steel/steel. After this validation, an investigation led on the observation rig shows the importance of having the optimum lubricant quantity inside the housing in order to avoid lubrication defects. To study the wear on steel/steel contact, a quantification of sliding inside the tripod is realized on the observation rig thanks to camera and numerical tools developed for this rig. So, it provides sliding inside the component as a function of the CVJ angularity which is a first step toward the mechanical efficiency.

The chapter 4 focuses on greases used by Groupe PSA to lubricate its own transmission. These greases have different properties thanks to their composition. The major interest to use these greases is to have industrial basic composition and real results on component wear. These results are obtained by tests done by Groupe PSA on their own component reliability rigs (which are not described due to confidentiality aspect). In addition to these results, standard tests are used to give first clues on replenishment with oil bleed test. To validate the basic composition, IR Spectrometry is used. It was necessary to validate hypothesis on bleed oil and to have meaningful analysis with XPS analysis. In chapter 3, rig operating conditions have been set in order to reproduce on laboratory rig the contact condition as close as possible. Furthermore, the greases have been studied at low temperature (40°C) and 80°C. These results were essential to remain in the specification conditions set by Groupe PSA and also permit to see the importance of the grease composition on the CVJ behaviour (shudder). It is also shown that wear was not explained by these conditions even though grease chemical composition are different. This inconsistency between wear from laboratory rigs and components rigs will be a subject of a more complete study of wear in chapter 4.

The inconsistency shown in chapter 4 is investigated in chapter 5. First of all, hypothesis have been changed on rig conditions to try to reproduce this wear. The minor modification (rig velocity) lead to a major wear change. Indeed, at low temperature for one grease a repeatable surface degradation appears. This failure does not occur at 40°C with the other grease and at 80°C with any grease. More important, it correlates exactly the wear from laboratory with the wear from components rigs of Groupe PSA. It is possible to conclude to a physical failure of the grease. The following sections explain the material behaviour difference between the 3 industrial greases using rheology. It shows again a particularity for the same grease at 40°C than for the first test on HFRR. This grease with a lower flow point than the others indicates that the grease stops working sooner as a solid and begins to have a liquid behaviour. At 40°C, the values of G’ and G’’ after the crossover keep very close. So, it is difficult to know if this grease goes to a liquid behaviour or stays in some solid/liquid transition state compared to its behaviour at 80°C. This phenomena is not observable in the case of the other greases. This particular material behaviour at 40°C implies certainly a particular behaviour of the film thickness which is investigated with another rig (EHD). These tests show the ability of some greases to replenish the contact and so prevent the film to go to zero and damages the surfaces. However, the ability is not shared with again the same grease at 40°C. It is this phenomena of starvation which could cause CVJ failure on vehicle.

**Prospects on Constant Velocity Joint**

As mentioned in the conclusion due to cost constraint, the perspective of CVJ evolution in automotive industry is very low. Indeed this cost constraint is really present and actual CVJ fills perfectly their functions. However, as seen through the manuscript an improvement is possible on lubricant. To facilitate the work on lubricant and avoid a lot of expensive test made previously, an idea of a dedicated test rig emerged during this work. This rig was designed at the LaMCoS facilities.

The main idea of this rig is to reproduce the kinematics from the tripod joint seen in chapter 3 to a laboratory rig. The aim is to observe the contact lubrication thanks to interferometry and calculate the generated axial force of a CVJ to obtain the friction coefficient as function of grease [10]. So, it is necessary to decompose the kinematics to have a fix contact point to adapt the microscope. This rig have been patented in 2019.

The main movement is represented on figure P.1.

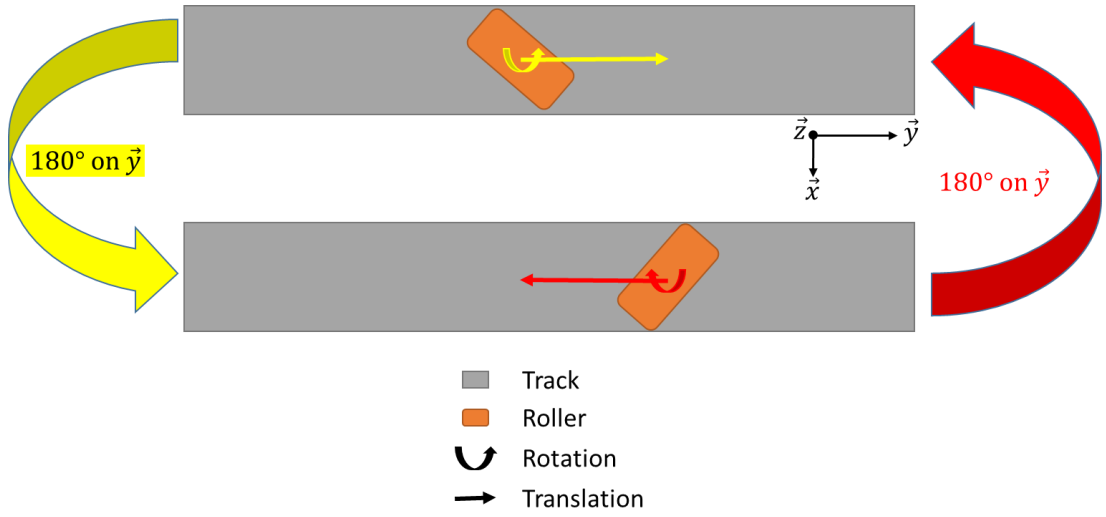


*Figure P.1: Movement decomposition inside a tripod's track*

The roller during one rotation (360°) goes from one position to another one and comes back to the first one with 2 main motions: a rotation and a translation. This principle is used to design the XEHD rig.

To deal with this objectives the design represented in figures P.2 & P.3 was created.

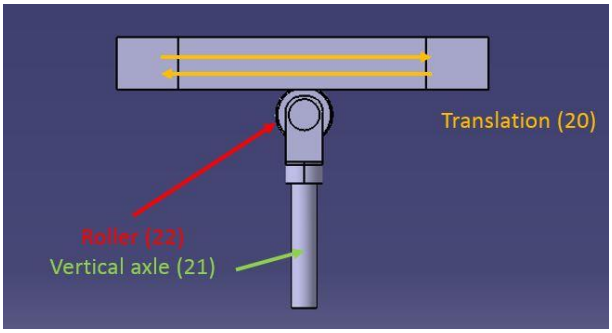


*Figure P.2: XEHD Design, side view*

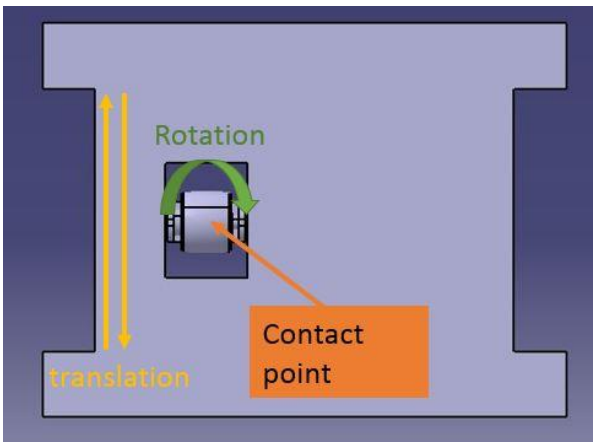


*Figure P.3: XEHD Design, top view*

The CVJ kinematics is respected with a mobile tray (20) which reproduces the translation movement and a roller (22) on an axle (21) which reproduces the rotational movement. On the mobile tray, a sample can be changed in order to use the interferometry mode or the friction coefficient mode.

To finish, in order to have the same velocity that in real CVJ, a crankshaft arrangement was chosen. That will lead the translation movement. The comparison between the kinematics model and the crankshaft chosen system is available in figure P.4 for an articulation angle of 5°.

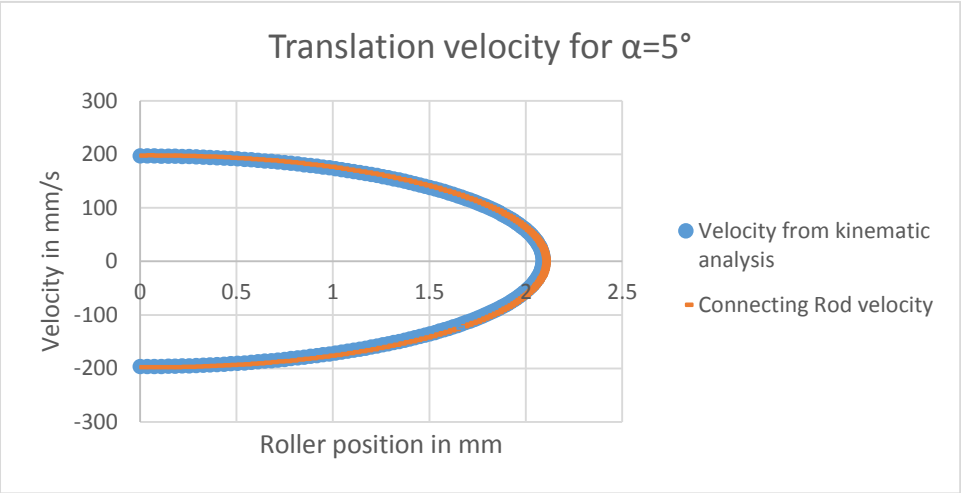


*Figure P.4: comparison for 5° between model and scotch yoke kinematic*

With this new tool (figure P.5), a new windows of dedicated transmission lubricant can be opened.

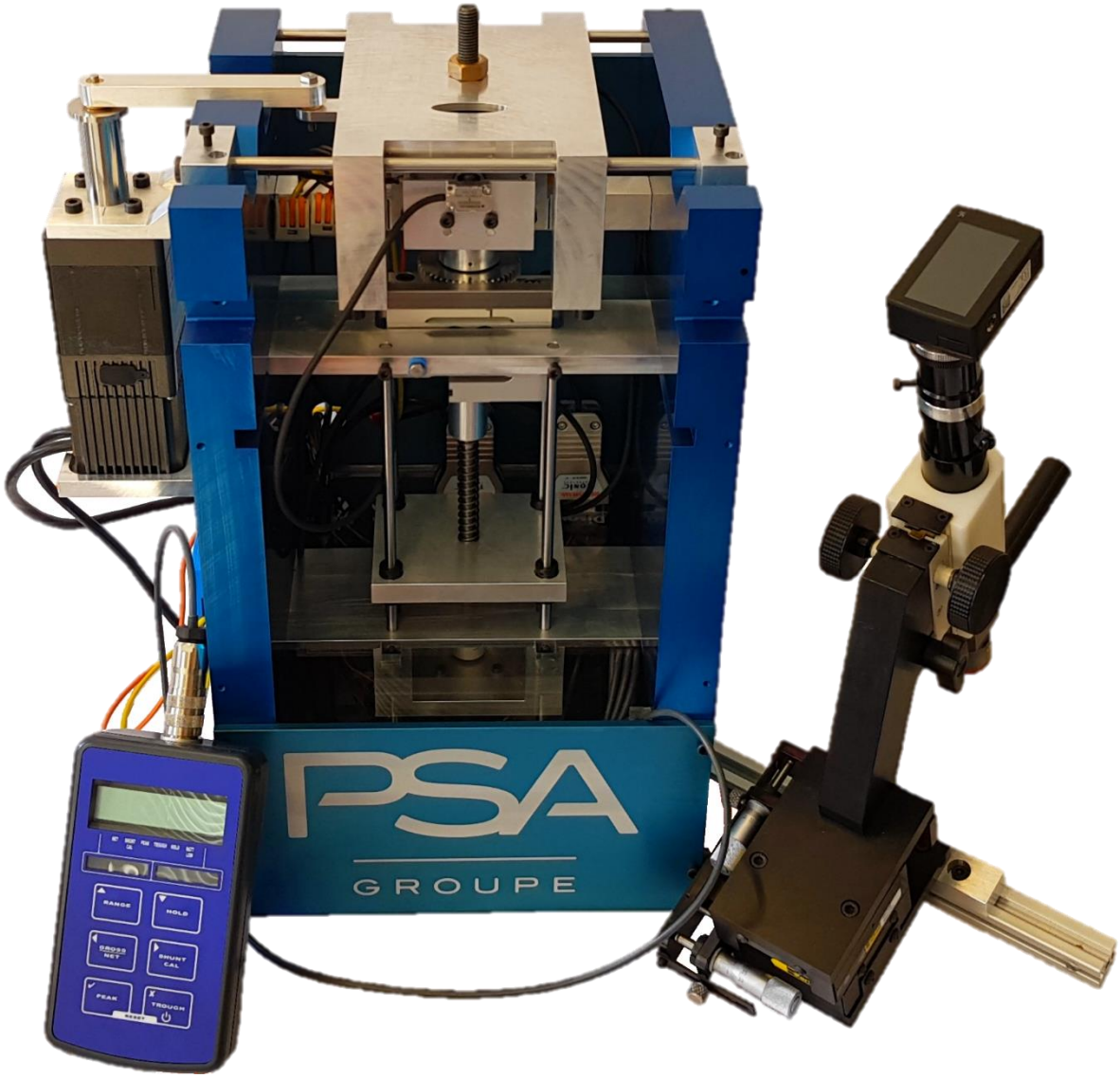


*Figure P.5: XEHD Rig*

Indeed, with that rig 2 operating modes can be set:

- Wear mode : using interferometry it is possible to detect lubrication failure during one test by watching qualitatively the video from a test as function of the articulation angle
- Grease properties mode: it is possible to obtain the friction coefficient as function of grease and angularity to help car designer to improve the transmission by increasing the efficiency.

The XEHD rig will provide to lubricant manufacturer and automotive manufacturer a precious tool to design the car of tomorrow.

# Appendix A – Dynamic Model under

A numerical model using a dynamics simulation software is used in order to characterize the kinematics between track and rollers during one CVJ rotation. It is based on CAD geometry that has been imported into the software. Different hypothesis were made in order to build the model:

- Geometrical simplification

To accelerate time calculations and to facilitate the sliding revolute joint between rollers and spider, the circlips size was increased.

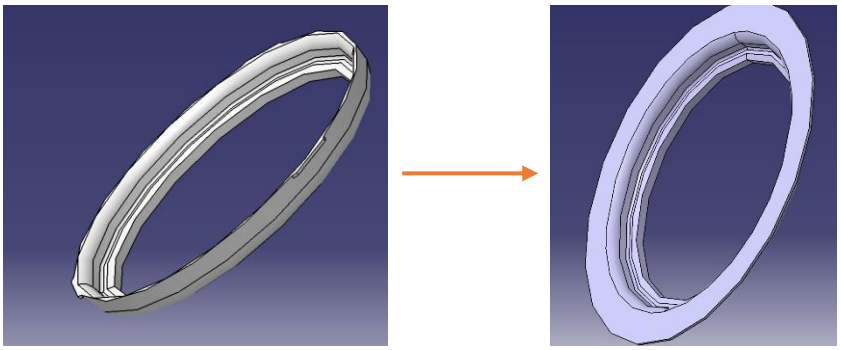

*Figure A.1: Circlips evolution*

- Initial conditions

Thanks to Groupe PSA data a revolution frequency of 15Hz will be consider. That means an angular velocity of 5400°/s. To check this velocity, the contact frequency has been exported (figure A.2).

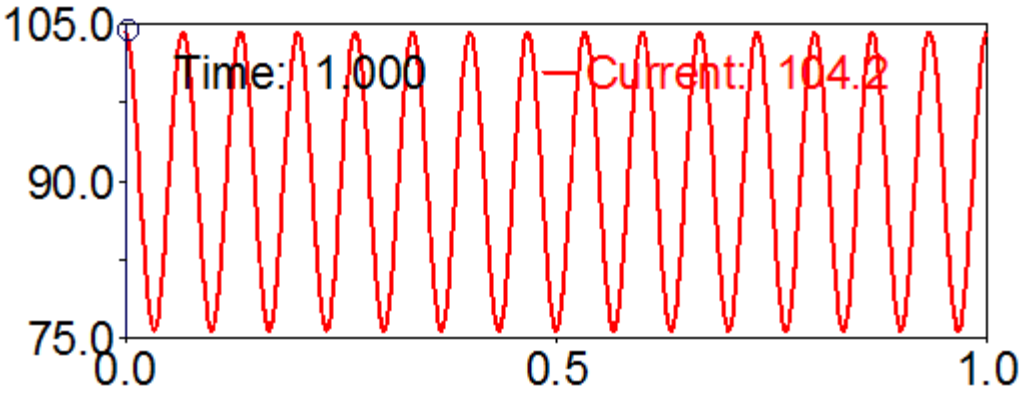


*Figure A.2: Contact frequency in the simulation software*

- Link

The links used are presented in table 19.

| Link | Illustration | Comments |
|---|---|---|
| Ground / Housing | 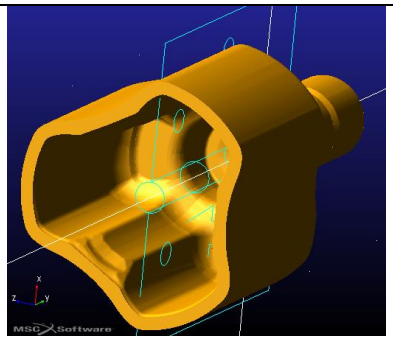 | The housing is linked to the gearbox. So a revolute joint is used |
| Spider / Circlips | 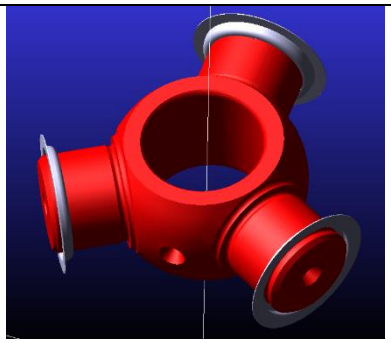 | The circlips were embedded into the spider to simplify the numerical calculation |
| Roller / Spider | 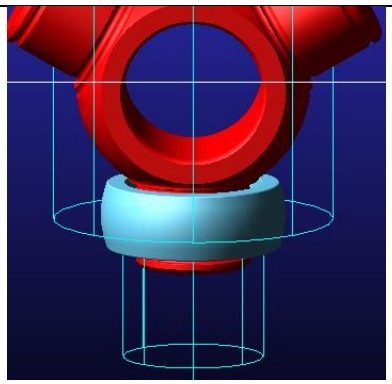 | The Rollers and spider are linked by a cylindrical joint. The translation are stopped by contacts with spider and circlips. |
| Ground / Spider : articulation angle | 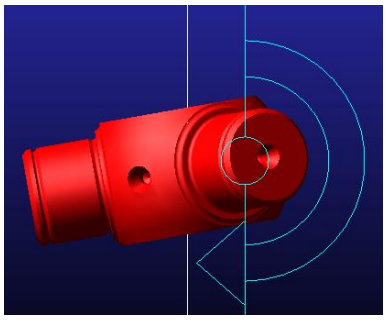 | Thanks to CVJ an articulation is possible between gearbox shaft and the transmission shaft. The rotation center is not in the inertia center. It is on the segment middle from roller inertia center to another roller inertia center as described in literature [52]. |

| | | |
|---|---|---|
| Ground / Spider : rotational angle | 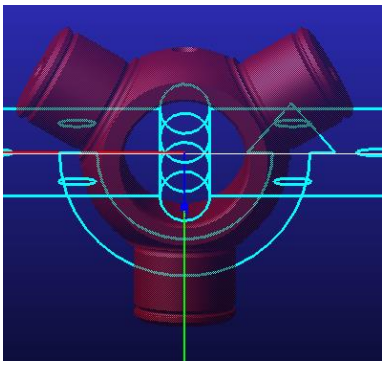 | A revolute joint is created in order to allow the transmission shaft rotation. |
| Rollers / Tracks | 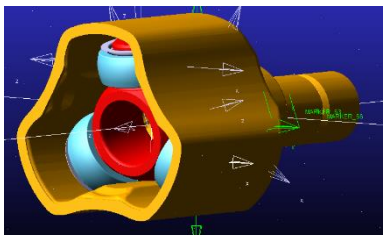 | Contacts are created in order to free the rollers behaviour. Inspired by bibliography [53], the chosen parameters are :<br>• k=10 $10^{11}$N/m<br>• e=2.2<br>• f=0.12 |

*Table 19: links list*

The main results from the dynamic simulation software are:

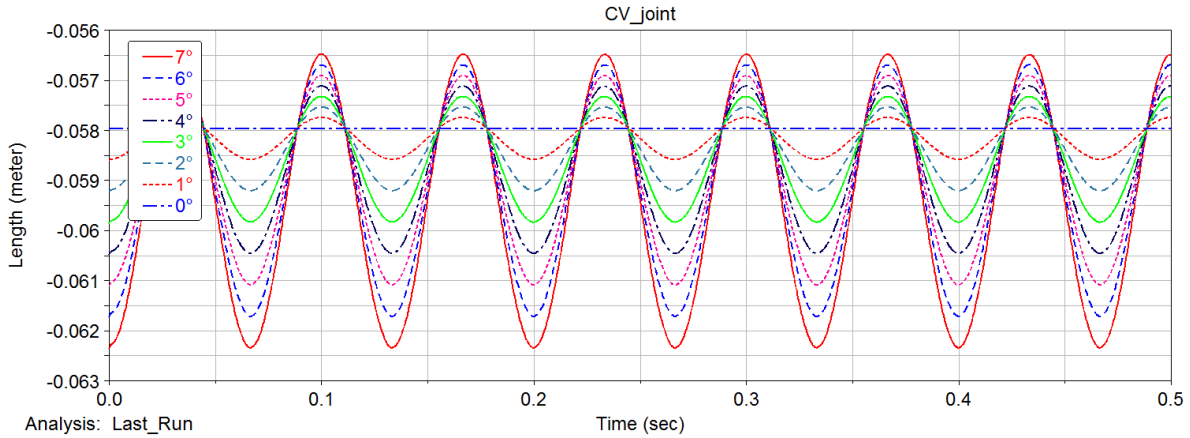


*Figure A.3: Displacement results from 0° to 7°*

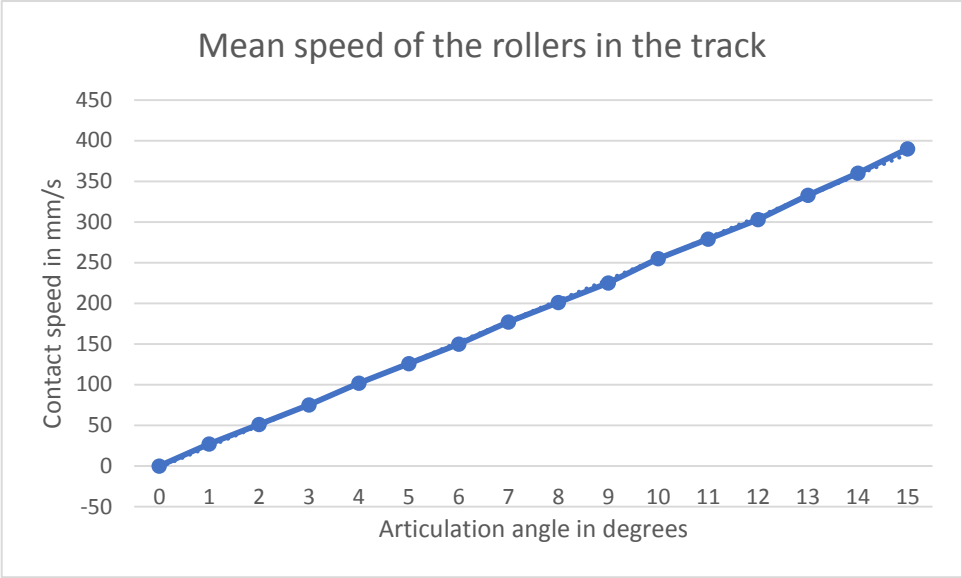


*Figure A.4: Mean velocities example for PSA CVJ*

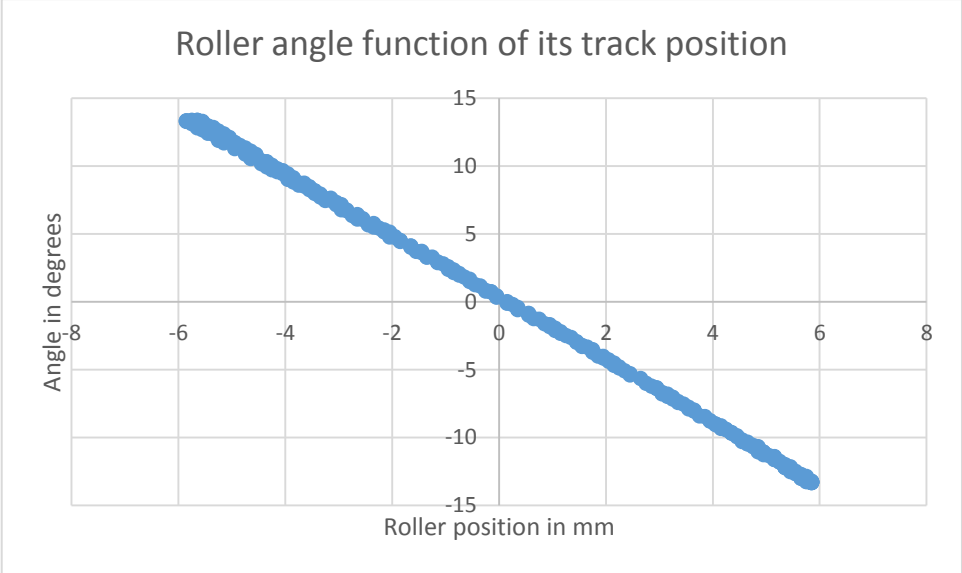


*Figure A.5: Roller angle evolution for 15° articulation angle*

# Appendix B – HFRR tests

- 40°C for 3h, $f_{HFRR} = 15\ Hz$ ; $d_{HFRR} = 1\ mm$ ; $P_{h-HFRR} = 1.32\ GPa$

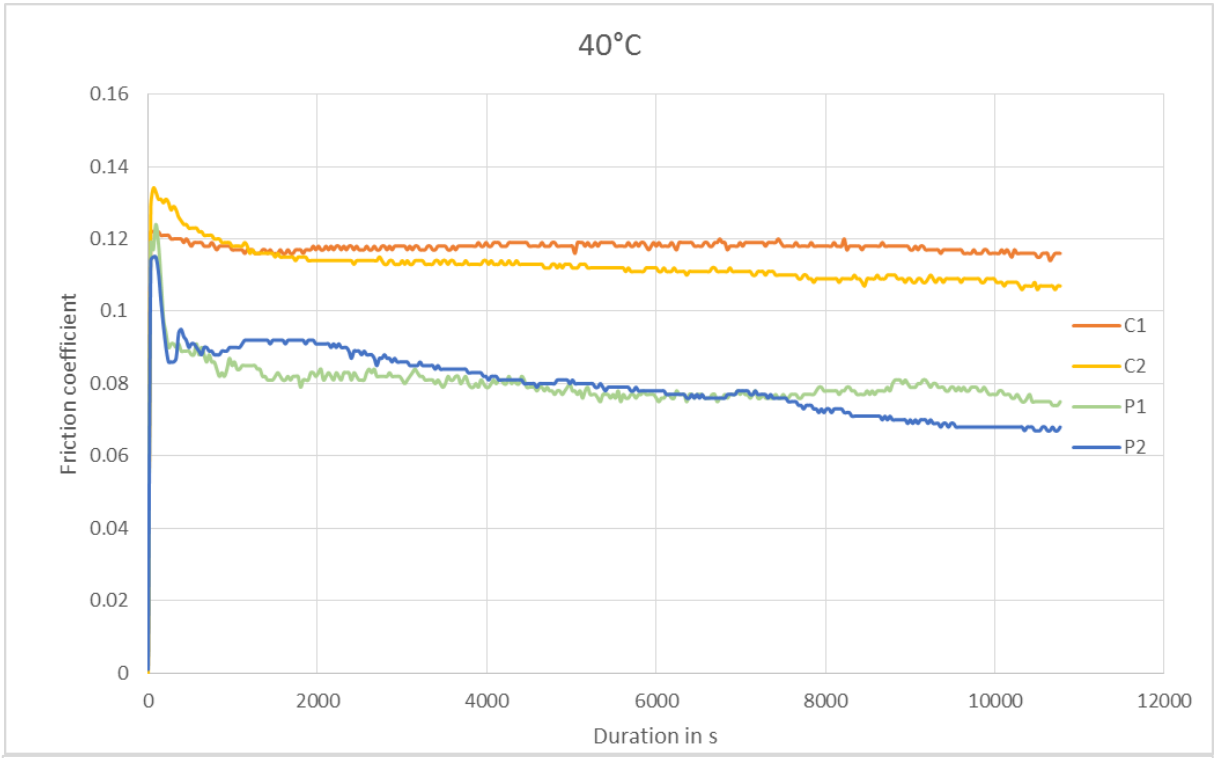


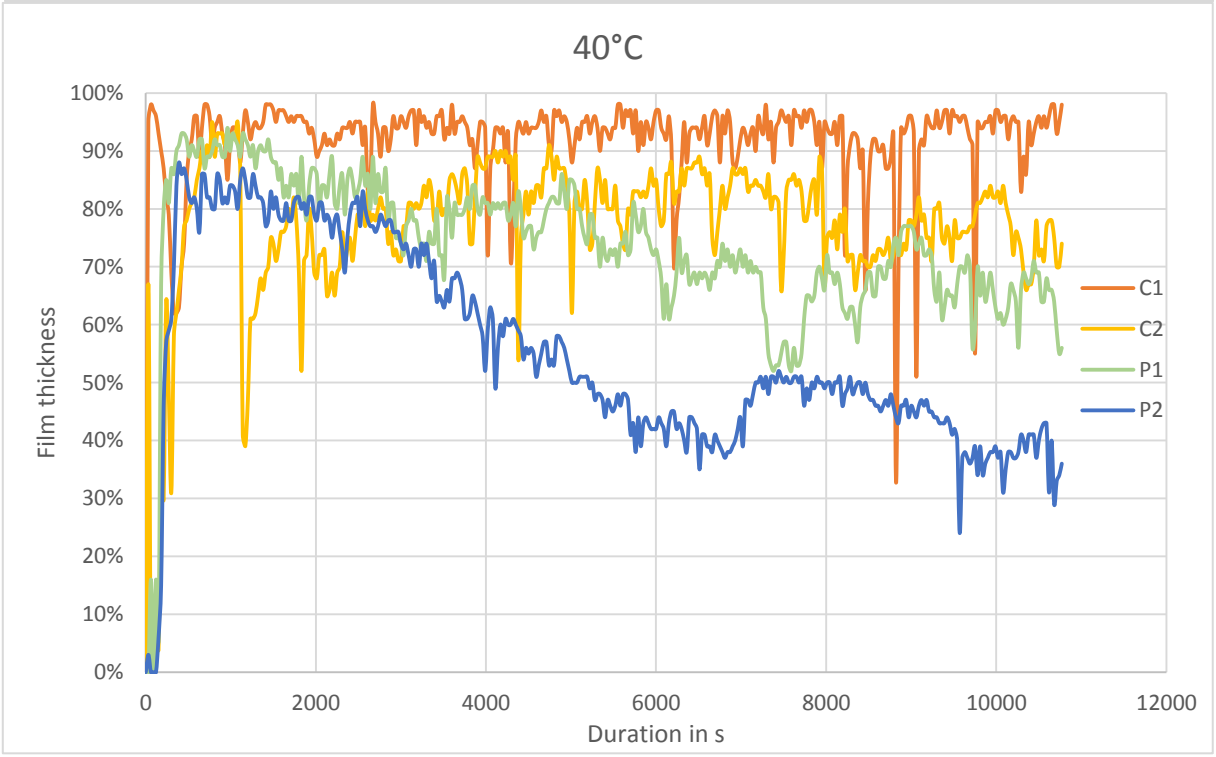

- 80°C for 3h, $f_{HFRR} = 15\ Hz$ ; $d_{HFRR} = 1\ mm$ ; $P_{h-HFRR} = 1.32\ GPa$

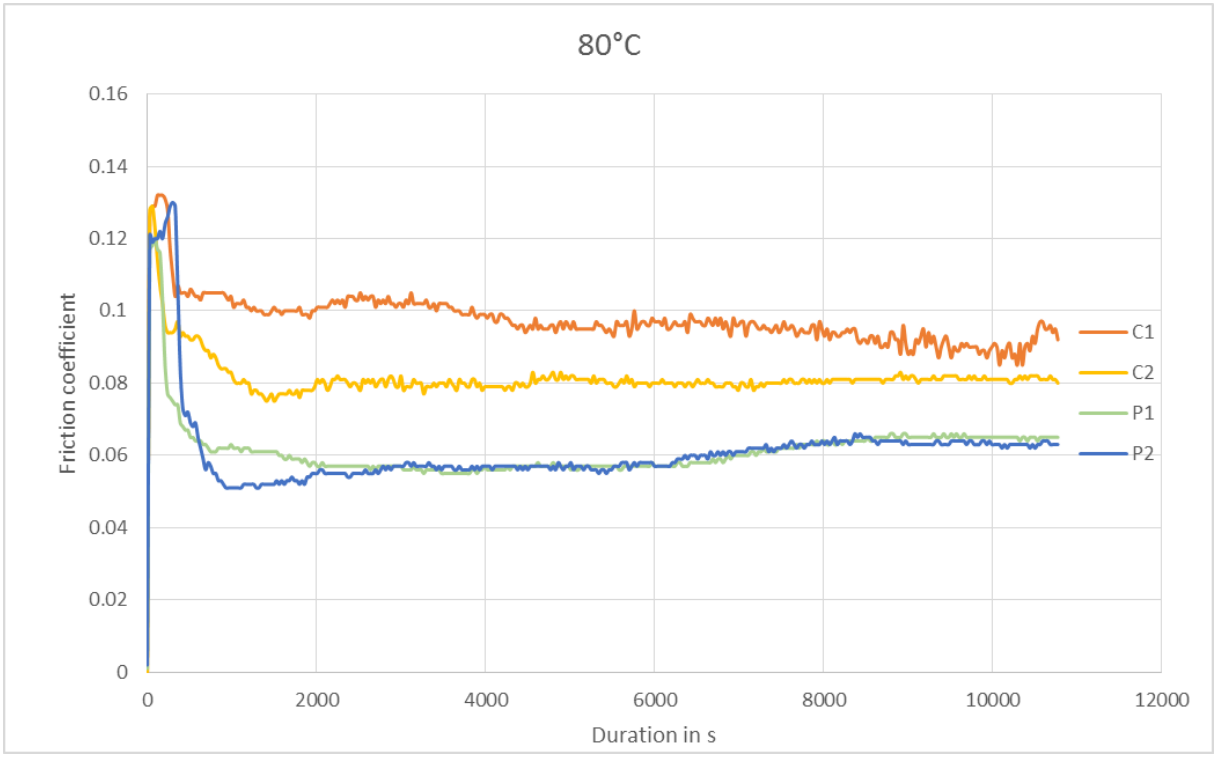


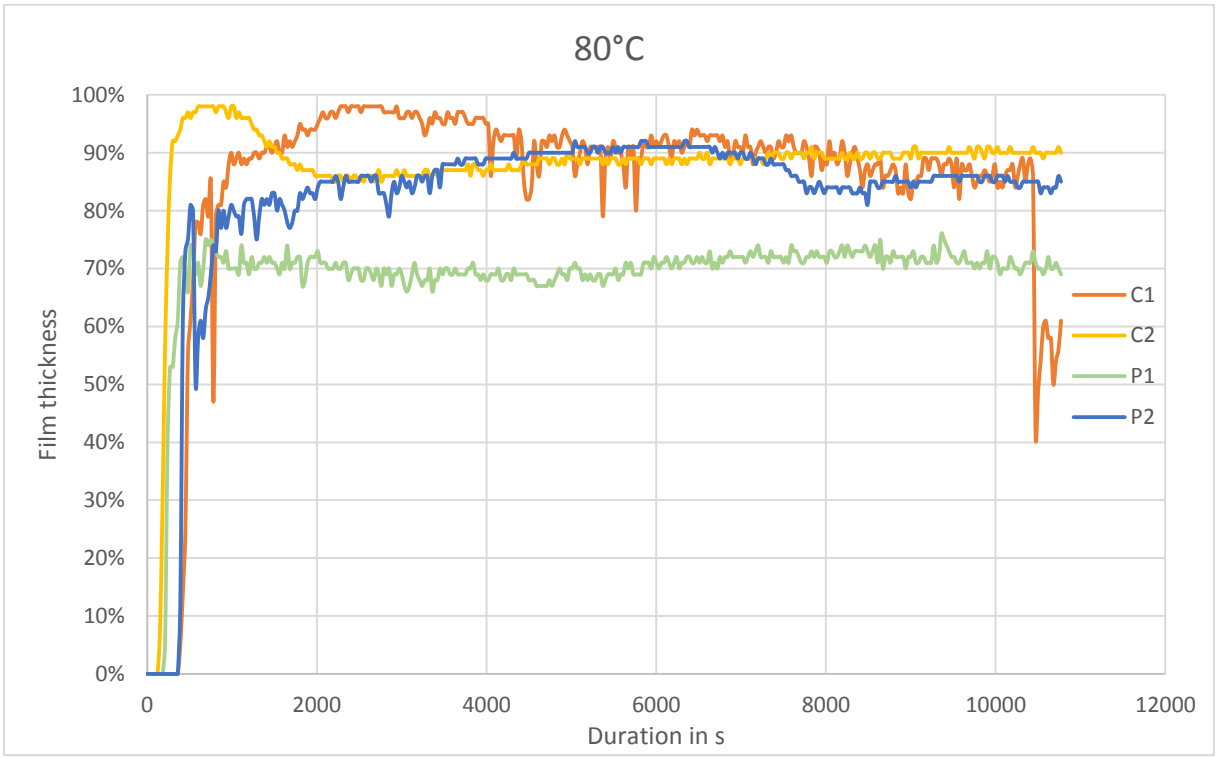

- Repeatability of the HFRR tests

The simple ball-on-flat configuration of the HFRR set-up provides the test results with great repeatability for short tests. In order to show this repeatability, the repeatability of the grease P2 is available at 40°C. In addition, a superposition between tests at 80°C for different duration is available.

- 40°C for 18h, $f_{HFRR} = 15\ Hz$ ; $d_{HFRR} = 1\ mm$ ; $P_{h-HFRR} = 1.32\ GPa$

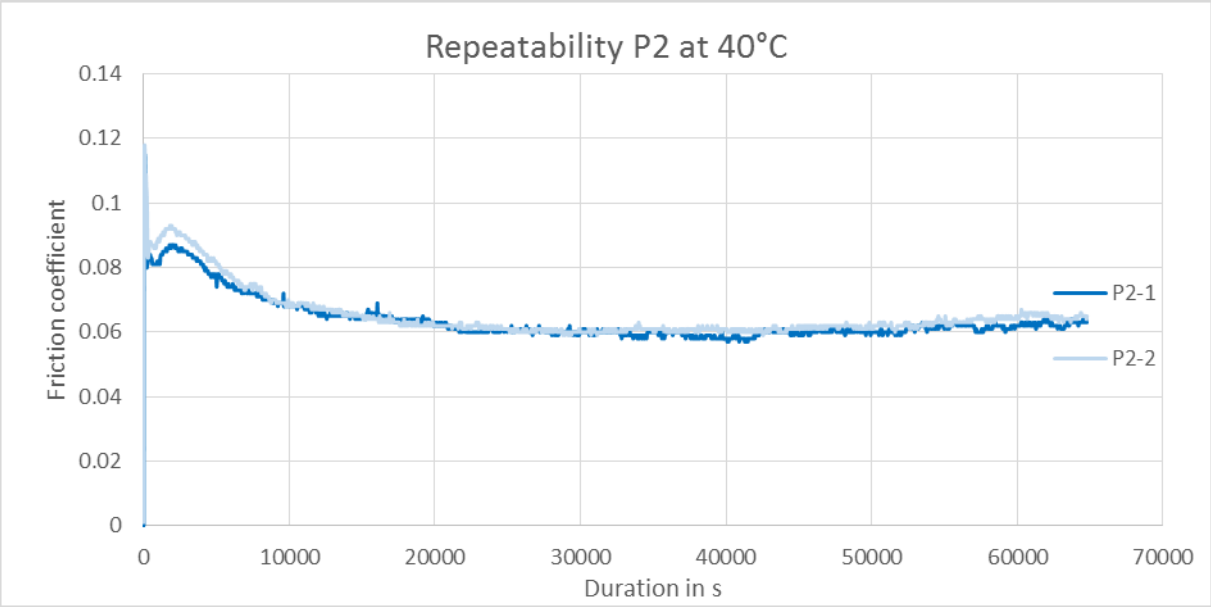


- 80°C for 3h & 18h, $f_{HFRR} = 15\ Hz$ ; $d_{HFRR} = 1\ mm$ ; $P_{h-HFRR} = 1.32\ GPa$
  Comparison for the first 3h

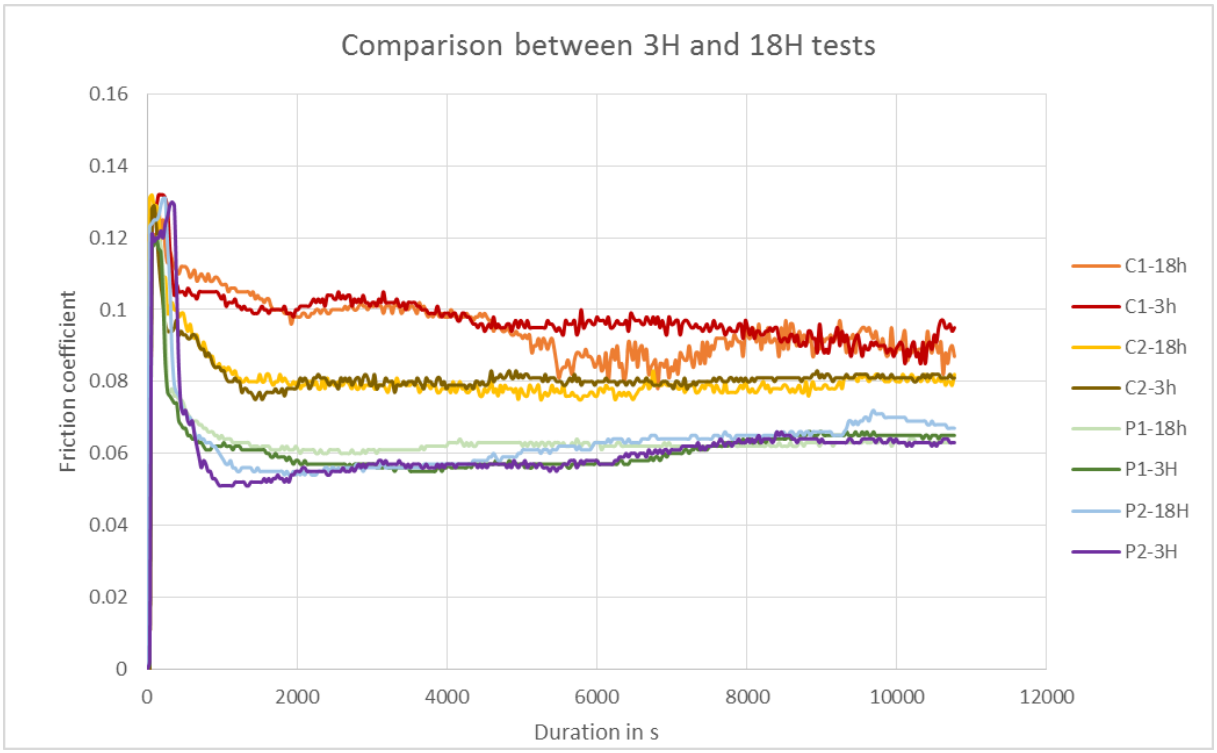

# Appendix C – Wear measurements for HFRR Tests

- 40°C for 3h, $f_{HFRR} = 15\ Hz$ ; $d_{HFRR} = 1\ mm$ ; $P_{h-HFRR} = 1.32\ GPa$

C1

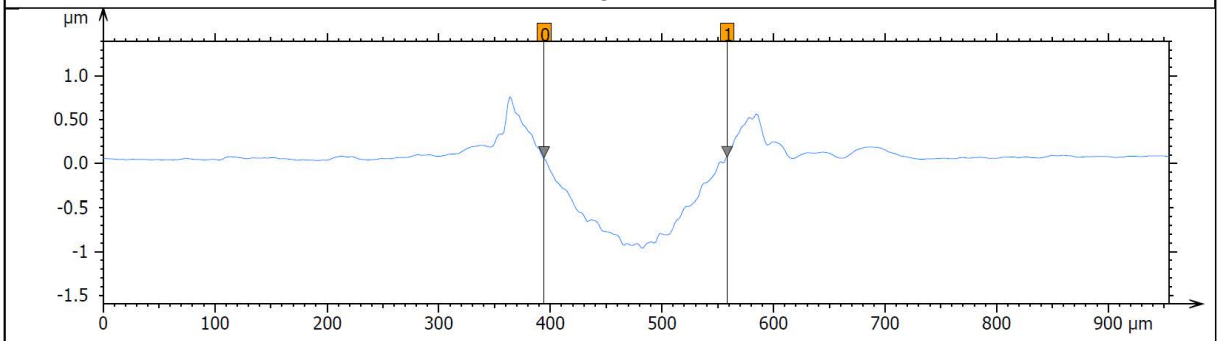


| Paramètres | 0-1 | Unité |
|---|---|---|
| Distance horizontale | 164 | µm |

C2

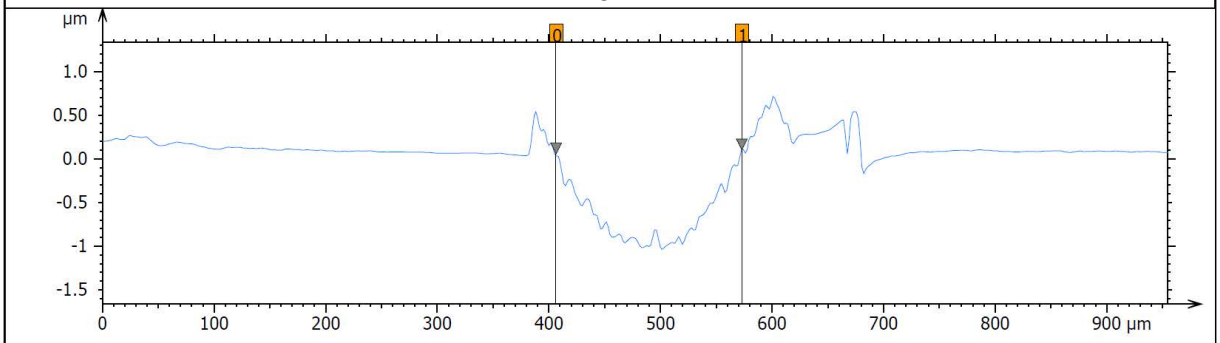


| Paramètres | 0-1 | Unité |
|---|---|---|
| Distance horizontale | 166 | µm |

P1

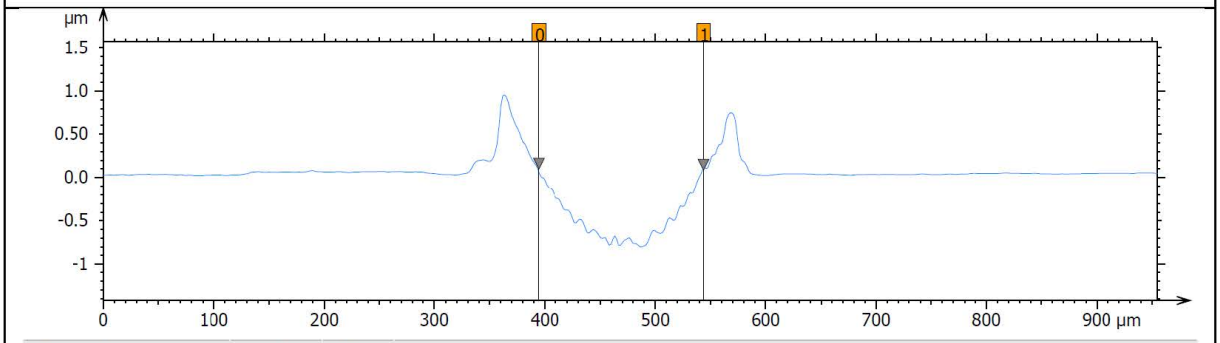


| Paramètres | 0-1 | Unité |
|---|---|---|
| Distance horizontale | 149 | µm |

P2

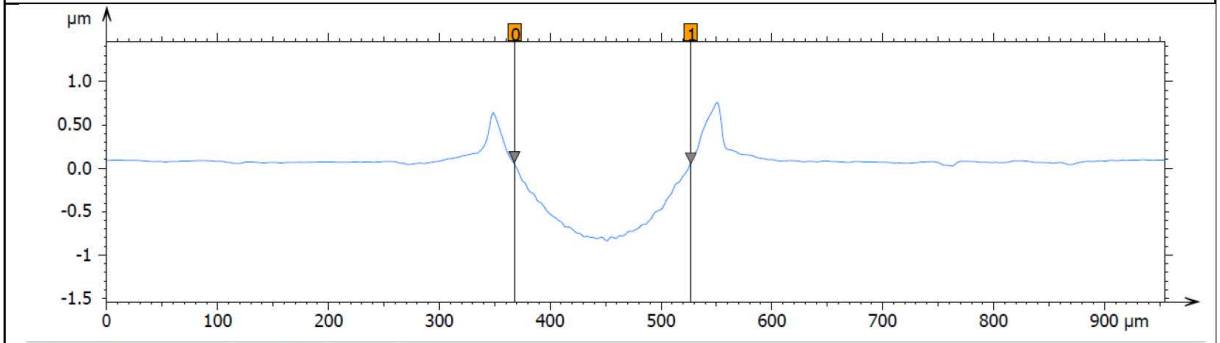


| Paramètres | 0-1 | Unité |
|---|---|---|
| Distance horizontale | 159 | µm |

- 40°C for 18h, $f_{HFRR} = 15\ Hz$ ; $d_{HFRR} = 1\ mm$ ; $P_{h-HFRR} = 1.32\ GPa$

C1

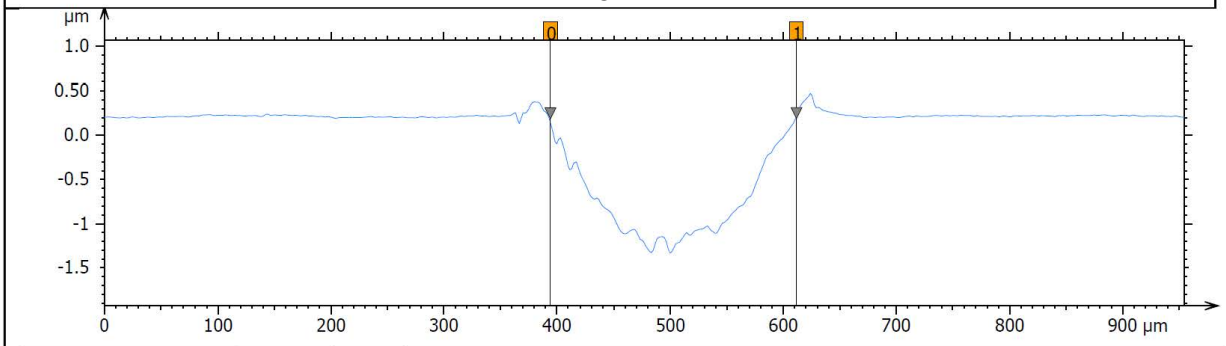


| Paramètres | 0-1 | Unité |
|---|---|---|
| Distance horizontale | 217 | µm |

C2

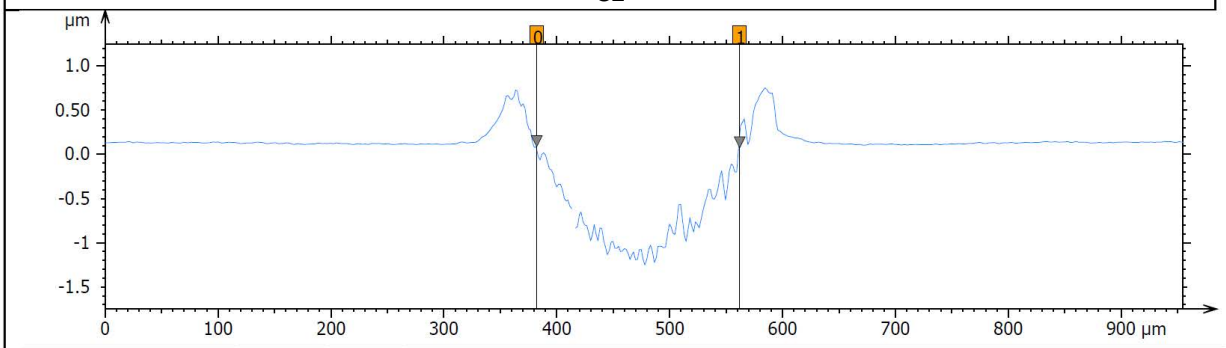


| Paramètres | 0-1 | Unité |
|---|---|---|
| Distance horizontale | 180 | µm |

P1

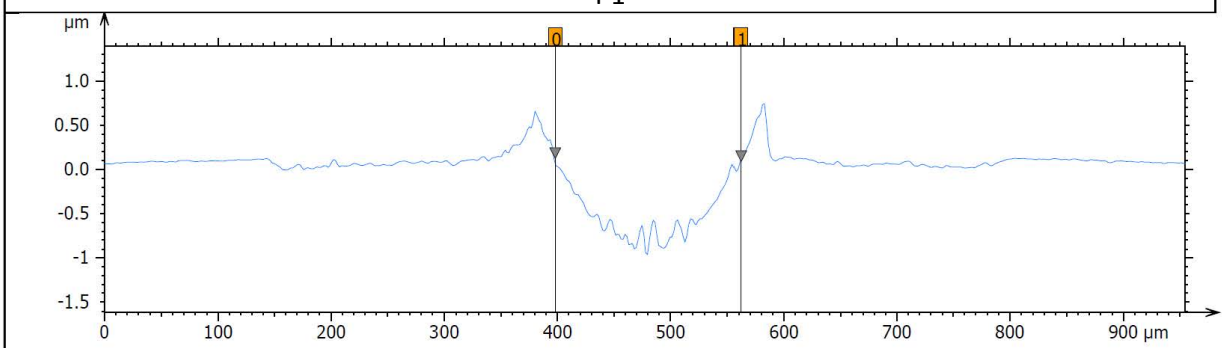


| Paramètres | 0-1 | Unité |
|---|---|---|
| Distance horizontale | 164 | µm |

P2

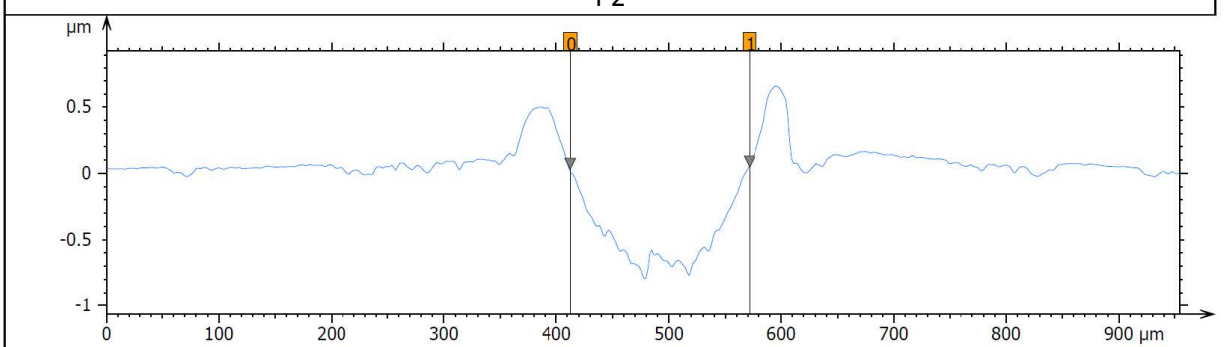


| Paramètres | 0-1 | Unité |
|---|---|---|
| Distance horizontale | 159 | µm |

- 80°C for 3h, $f_{HFRR} = 15\ Hz$ ; $d_{HFRR} = 1\ mm$ ; $P_{h-HFRR} = 1.32\ GPa$

C1

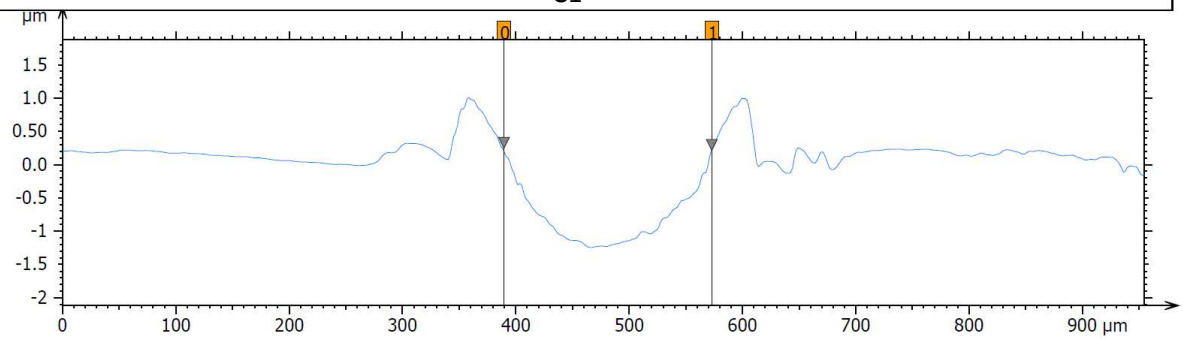


| Paramètres | 0-1 | Unité |
|---|---|---|
| Distance horizontale | 183 | µm |

C2

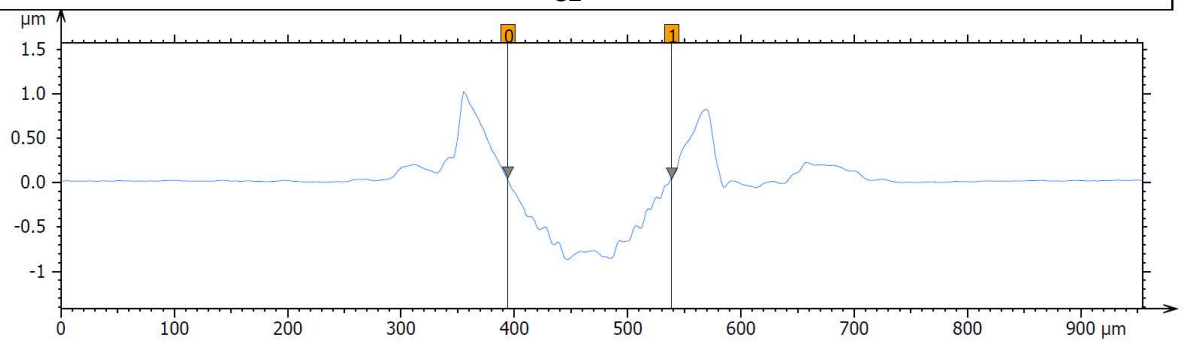


| Paramètres | 0-1 | Unité |
|---|---|---|
| Distance horizontale | 145 | µm |

P1

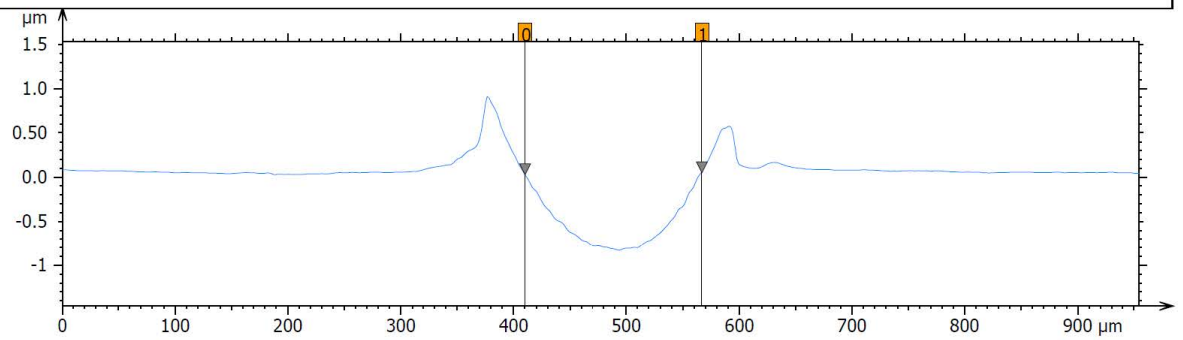


| Paramètres | 0-1 | Unité |
|---|---|---|
| Distance horizontale | 157 | µm |

P2

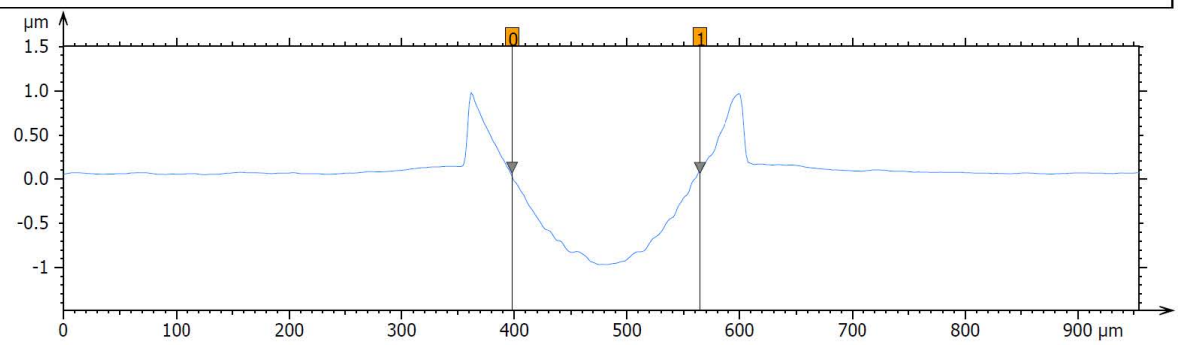


| Paramètres | 0-1 | Unité |
|---|---|---|
| Distance horizontale | 166 | µm |

- 80°C for 18h, $f_{HFRR} = 15\ Hz$ ; $d_{HFRR} = 1\ mm$ ; $P_{h-HFRR} = 1.32\ GPa$

C1

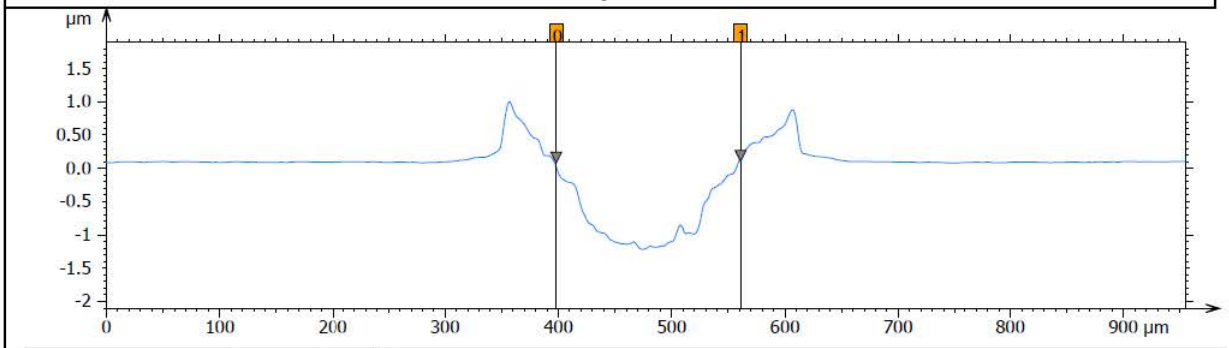


| Paramètres | 0-1 | Unité |
|---|---|---|
| Distance horizontale | 163 | µm |

C2

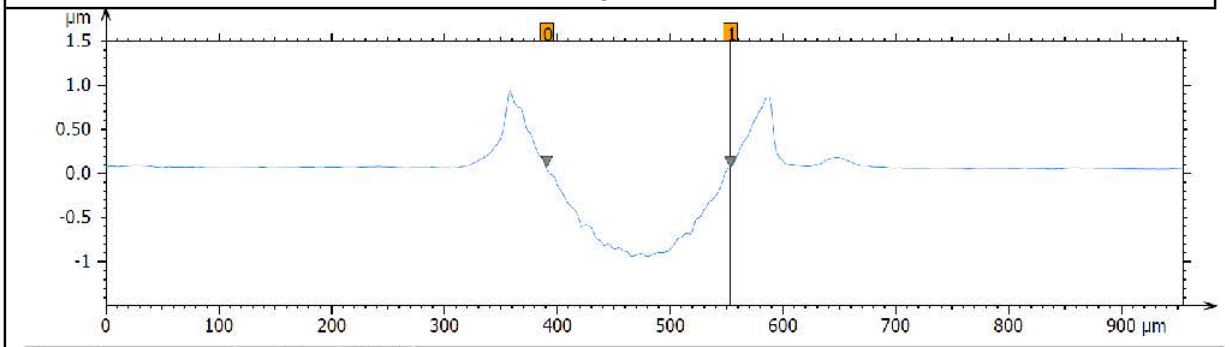


| Paramètres | 0-1 | Unité |
|---|---|---|
| Distance horizontale | 163 | µm |

P1

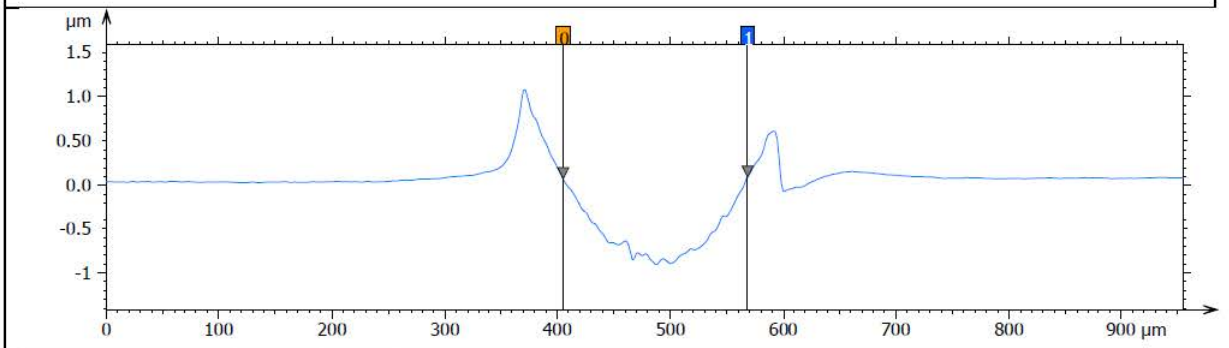


| Paramètres | 0-1 | Unité |
|---|---|---|
| Distance horizontale | 163 | µm |

P2

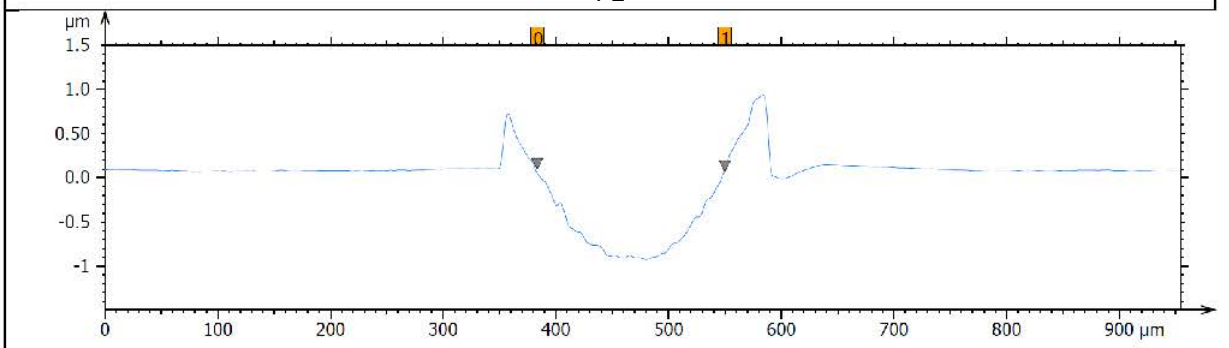


| Paramètres | 0-1 | Unité |
|---|---|---|
| Distance horizontale | 166 | µm |

- 40°C for 5h48, $f_{HFRR} = 100\ Hz$ ; $d_{HFRR} = 2\ mm$ ; $P_{h-HFRR} = 1.37\ GPa$

C1

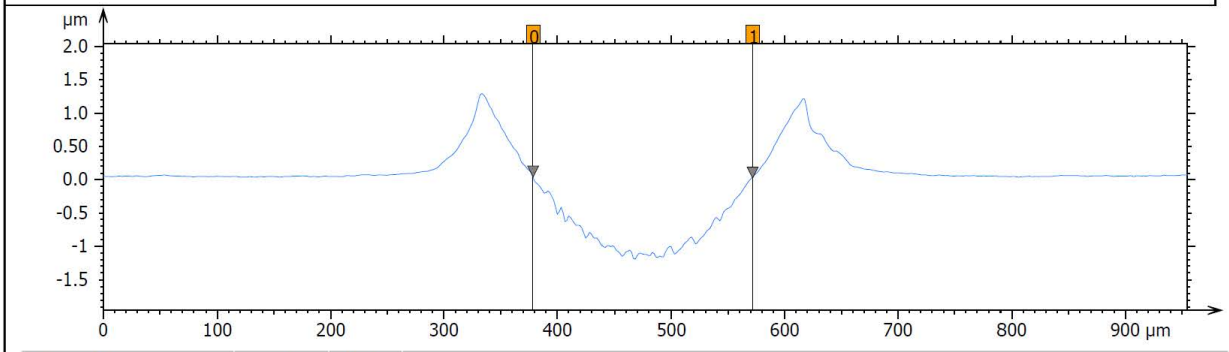


| Paramètres | 0-1 | Unité |
|---|---|---|
| Distance horizontale | 193 | µm |

P1

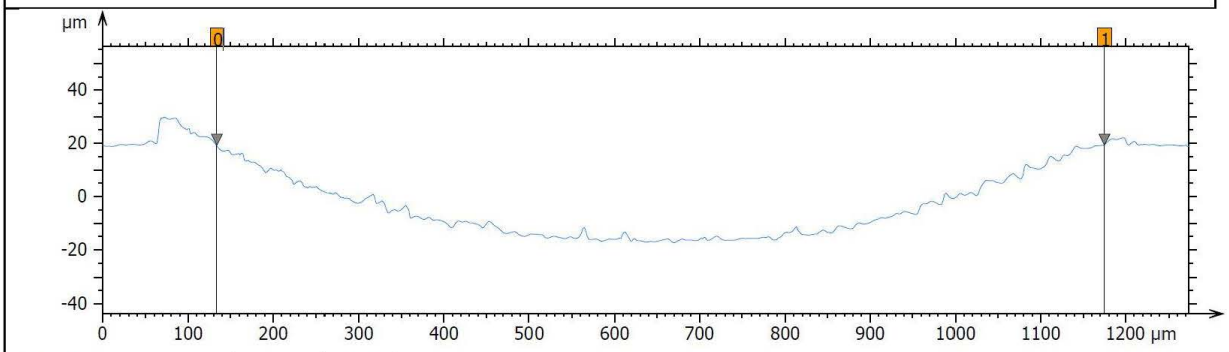


| Paramètres | 0-1 | Unité |
|---|---|---|
| Distance horizontale | 1041 | µm |

P2

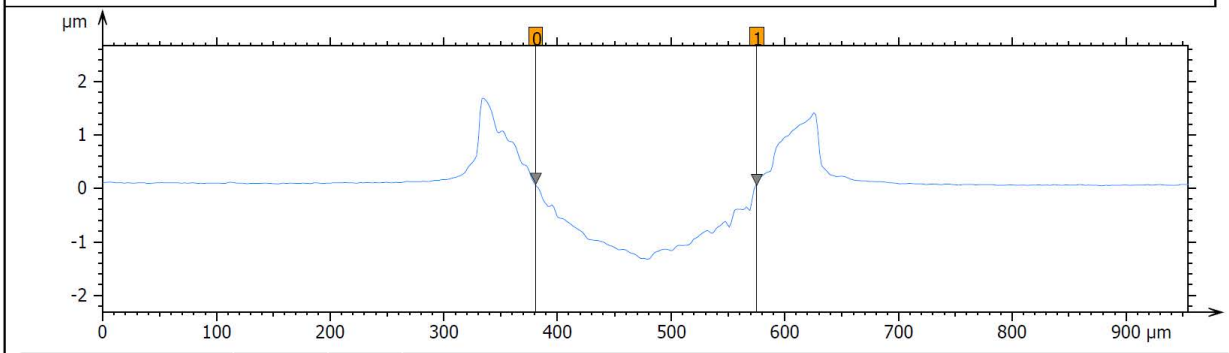


| Paramètres | 0-1 | Unité |
|---|---|---|
| Distance horizontale | 194 | µm |

- 80°C for 4h30, $f_{HFRR} = 100\ Hz$ ; $d_{HFRR} = 2\ mm$ ; $P_{h-HFRR} = 1.37\ GPa$

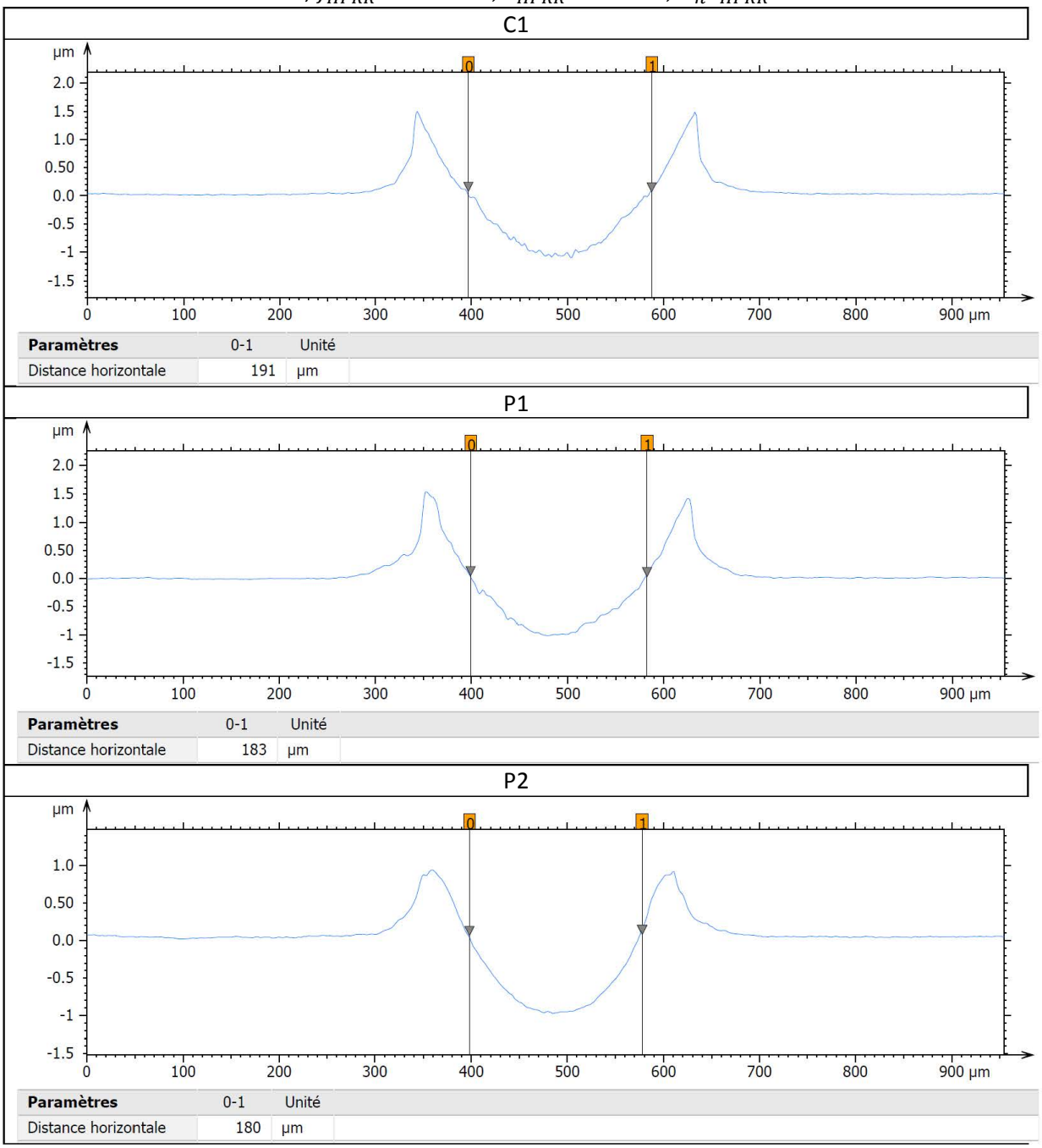

# Appendix D – XPS analysis:

- General Spectra 40°C 3h

C1

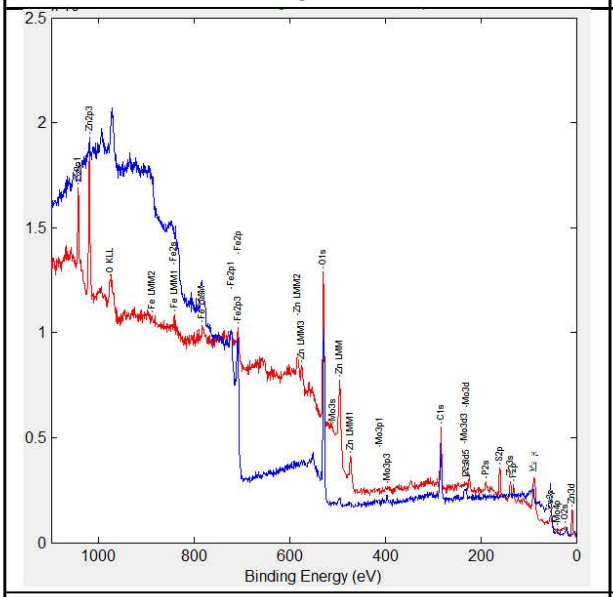


C2

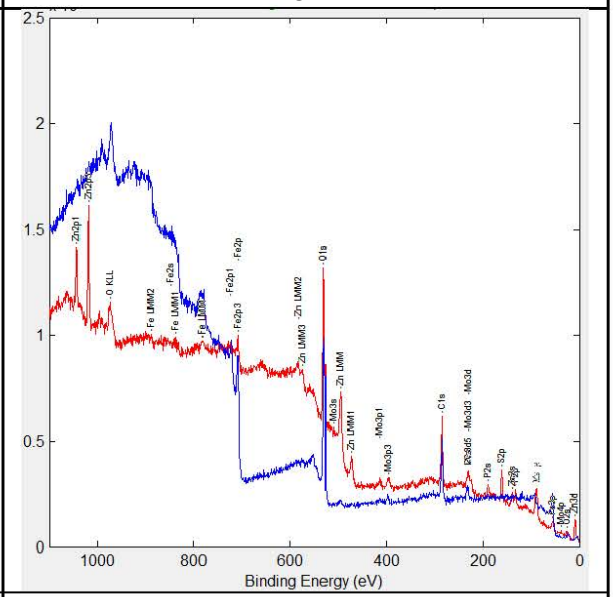


P1

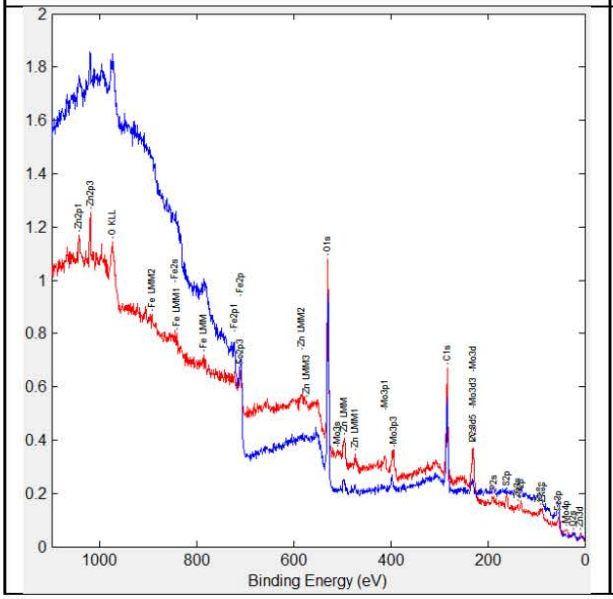


P2

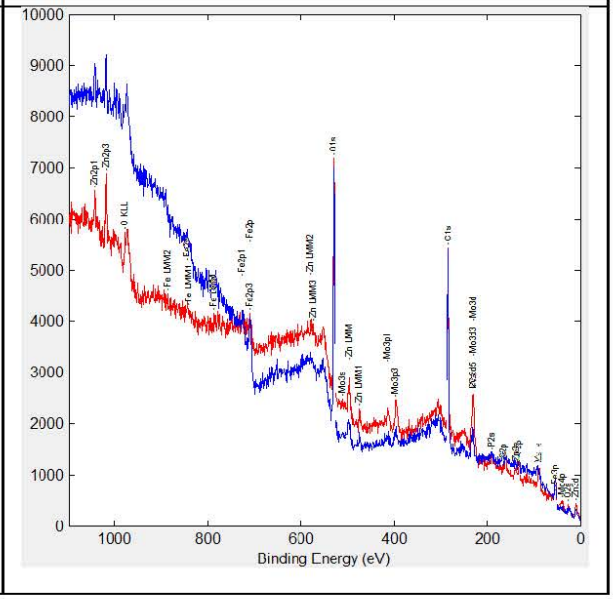

- General Spectra 40°C 18h

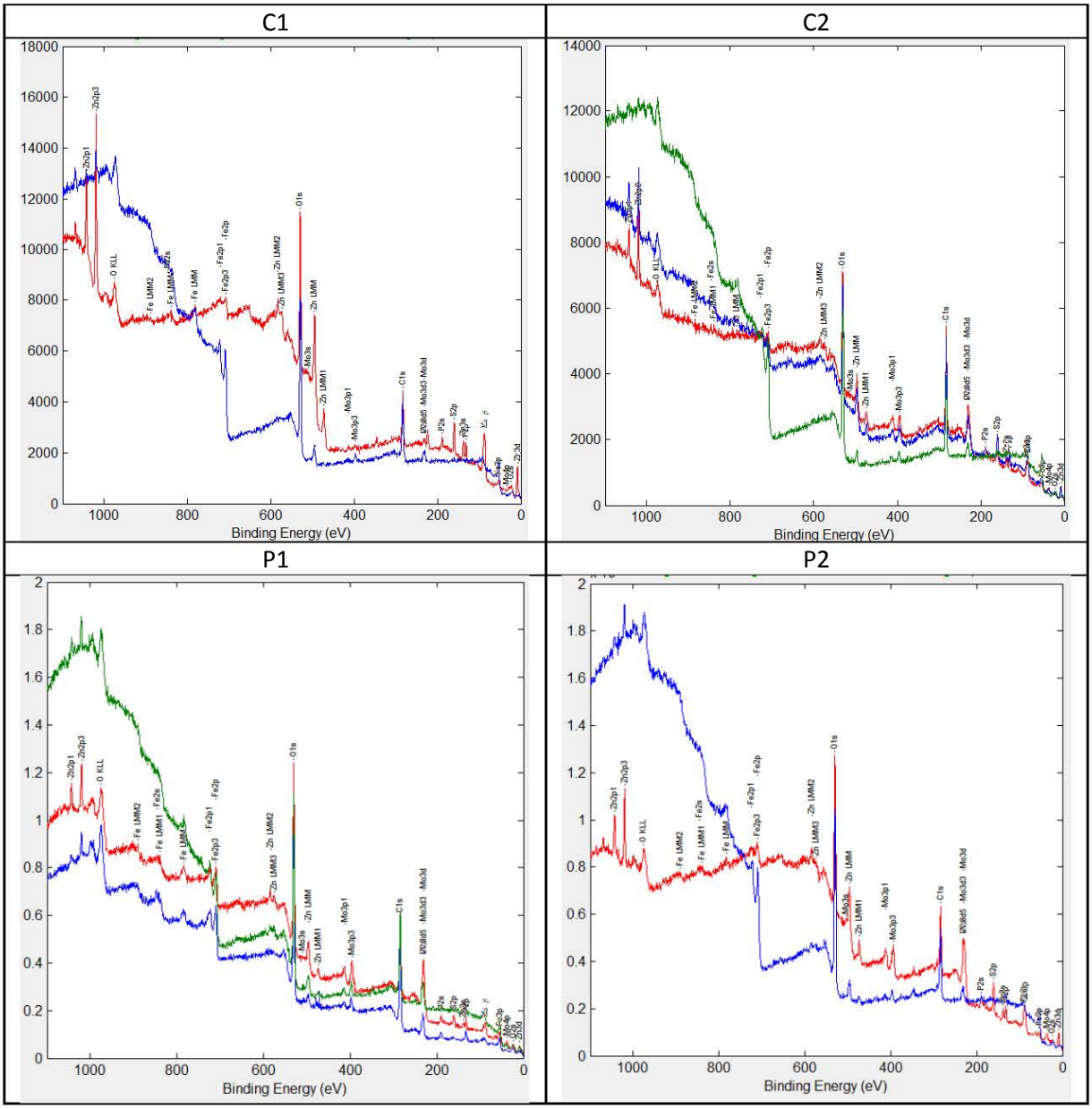

- General Spectra 80° 3h

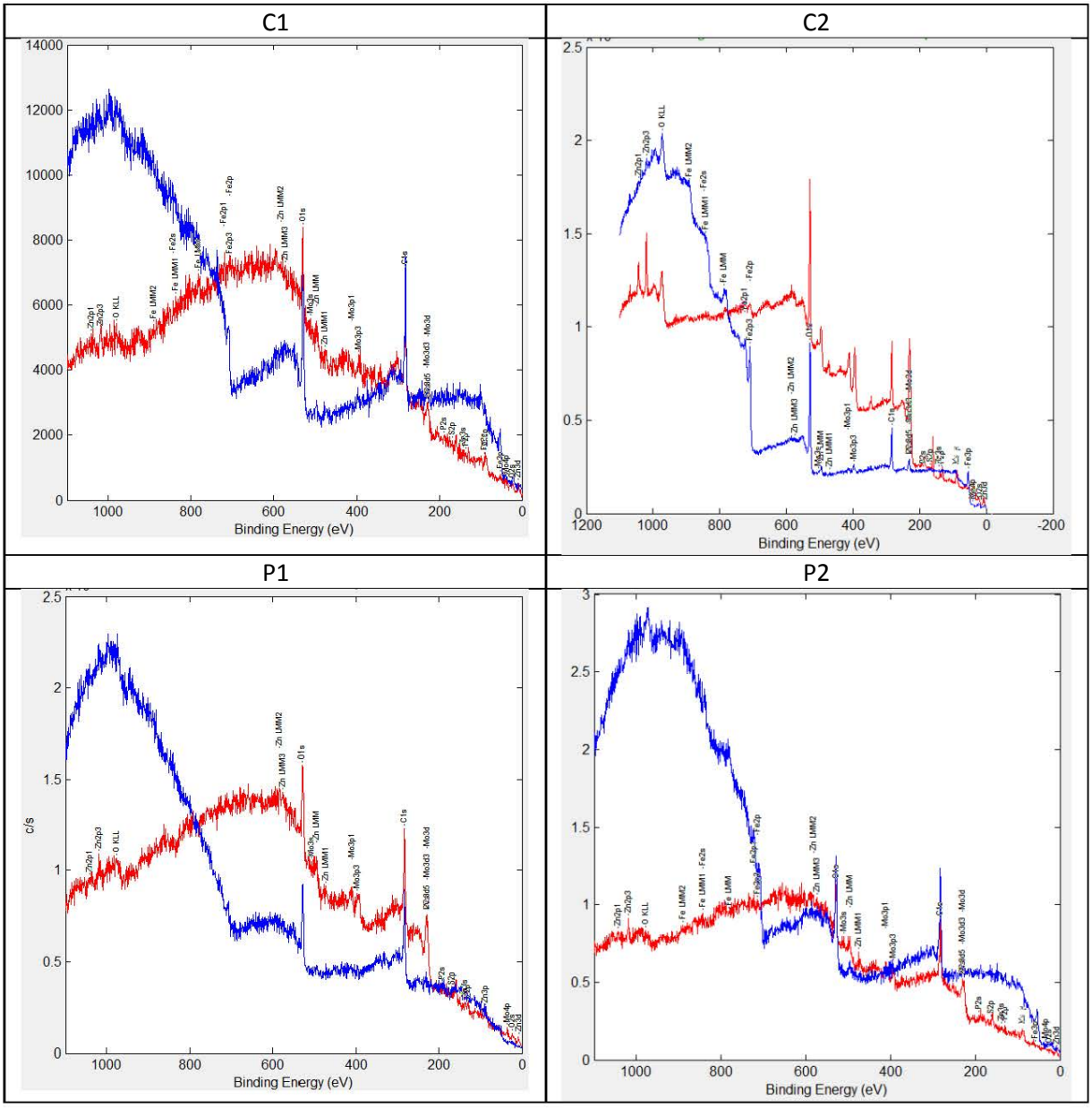

- General Spectra 80° 18h

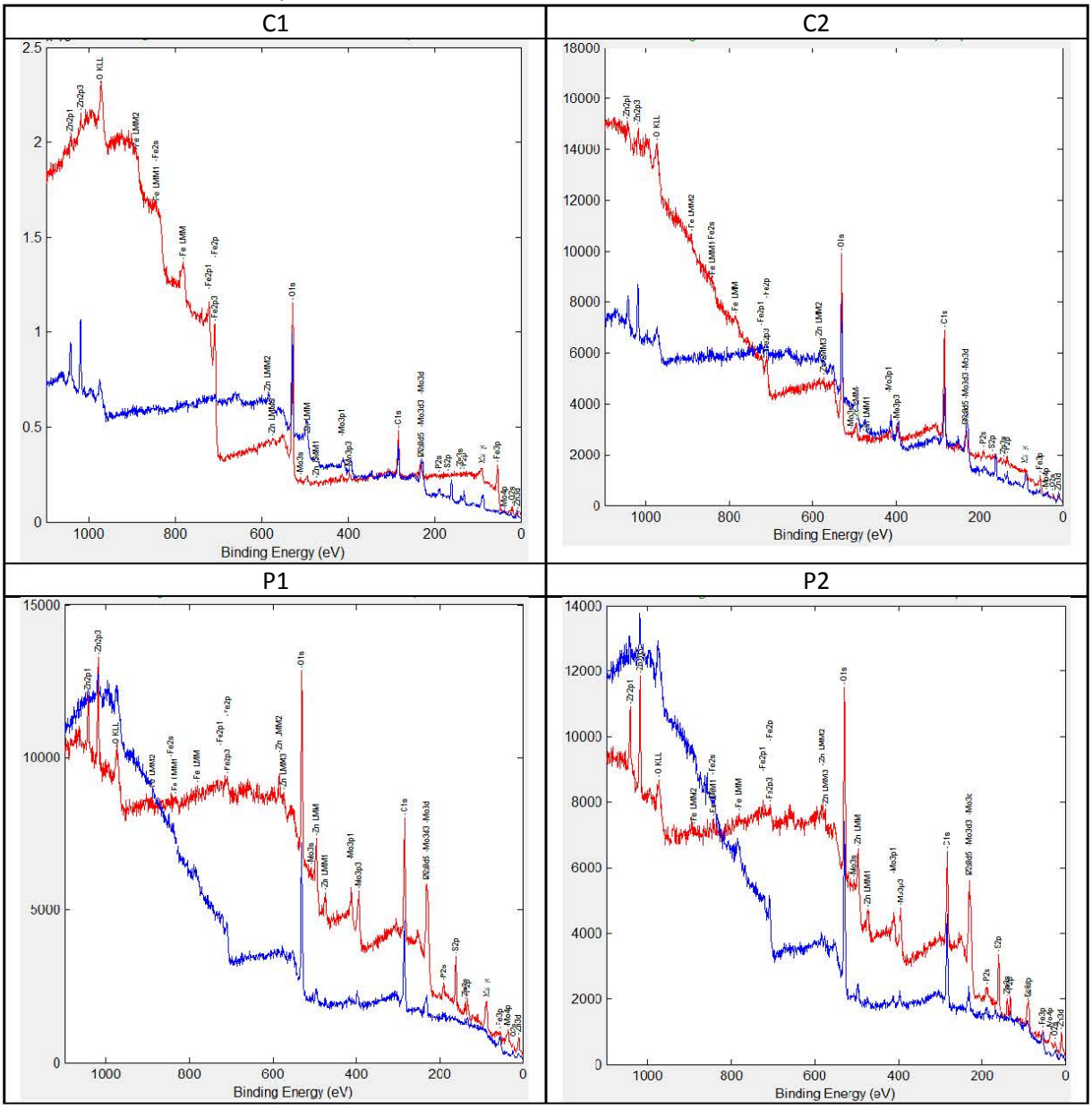

- Molybdenum peaks: grease C1

C1 at 40°C for 3h

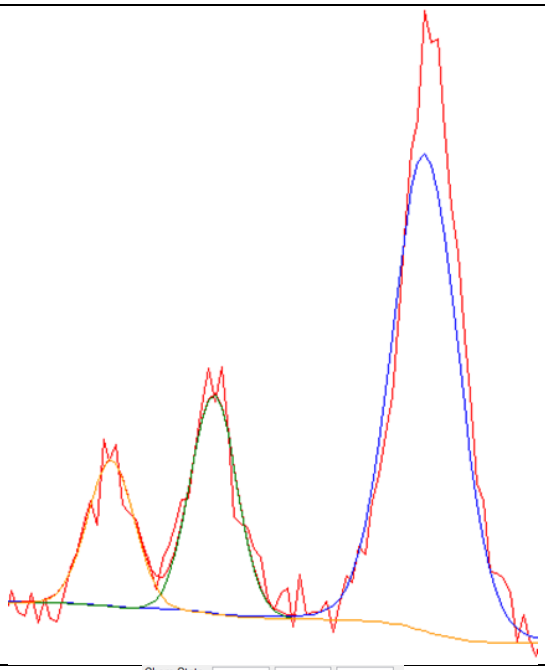

| Chem State | S2s | MoO3 | |
|---|---|---|---|
| Area | 171 | 133 | 89 |
| Position | 225.55 | 232.34 | 235.47 |
| Height | 66 | 75 | 50 |
| FWHM | 2.37 | 1.55 | 1.55 |
| % Gauss | 93 | 83 | 83 |

C1 at 40°C for 18h

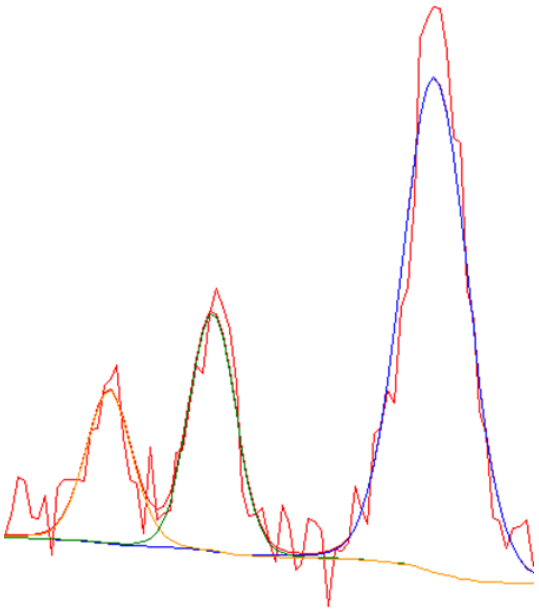

| Chem State | S2s | MoO3 | |
|---|---|---|---|
| Area | 171 | 133 | 89 |
| Position | 225.55 | 232.34 | 235.47 |
| Height | 66 | 75 | 50 |
| FWHM | 2.37 | 1.55 | 1.55 |
| % Gauss | 93 | 83 | 83 |

C1 at 80°C for 3h

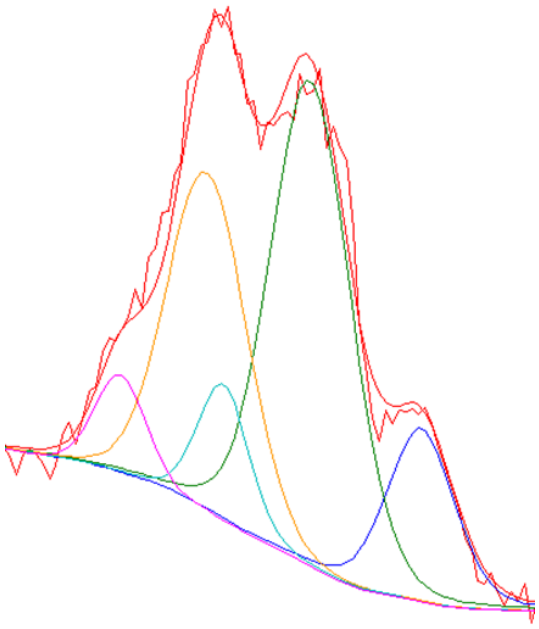

| Chem State | S2s | MoS2 | | MoO3 | |
|---|---|---|---|---|---|
| Area | 242 | 734 | 492 | 161 | 108 |
| Position | 225.95 | 229.31 | 232.44 | 232.05 | 235.18 |
| Height | 93 | 228 | 153 | 81 | 58 |
| FWHM | 2.37 | 2.91 | 2.91 | 1.73 | 1.73 |
| % Gauss | 93 | 93 | 93 | 83 | 100 |

C1 at 80°C for 18h

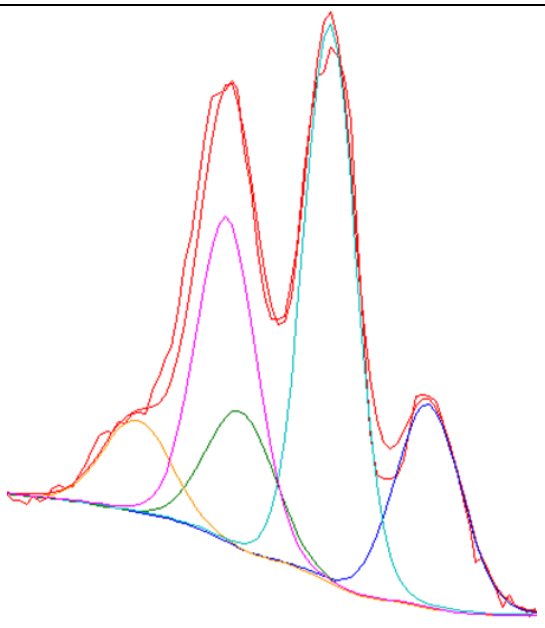

| Chem State | S2s | MoO3 | | MoS2 | |
|---|---|---|---|---|---|
| Area | 366 | 245 | 164 | 788 | 528 |
| Position | 225.84 | 231.51 | 234.64 | 228.80 | 231.93 |
| Height | 140 | 95 | 63 | 384 | 223 |
| FWHM | 2.37 | 2.43 | 2.43 | 1.86 | 2.15 |
| % Gauss | 92 | 100 | 100 | 92 | 93 |

- Molybdenum peaks: grease C2

C2 at 40°C for 3h

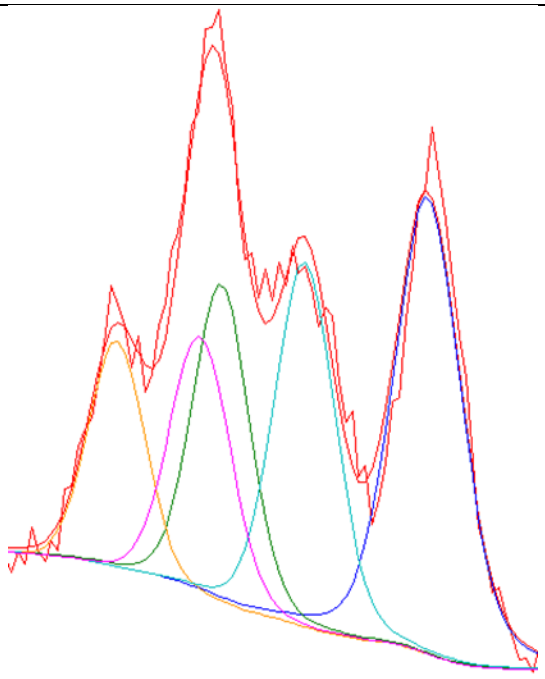

| | S2s | MoO3 | | MoS2 | |
|---|---|---|---|---|---|
| | 188 | 202 | 135 | 132 | 89 |
| | 226.00 | 232.20 | 235.33 | 229.70 | 232.83 |
| | 66 | 105 | 71 | 54 | 37 |
| | 2.37 | 1.67 | 1.67 | 2.15 | 2.15 |
| | 73 | 83 | 86 | 85 | 93 |

C2 at 40°C for 18h

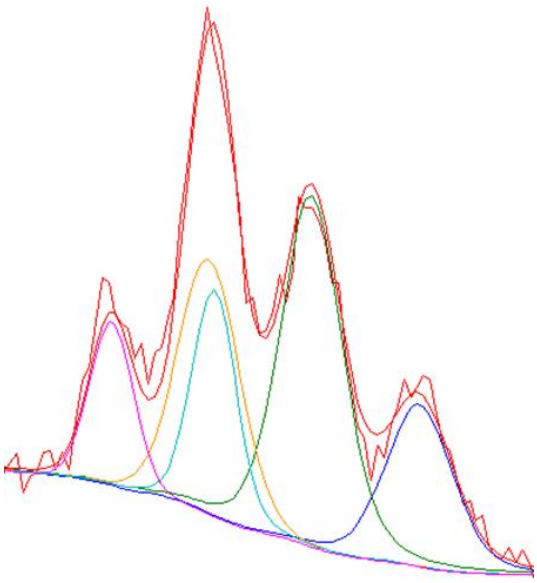

| Chem State | S2s | MoS2 | | MoO3 | |
|---|---|---|---|---|---|
| Area | 142 | 215 | 144 | 167 | 112 |
| Position | 226.00 | 229.28 | 232.41 | 232.24 | 235.37 |
| Height | 48 | 83 | 56 | 97 | 66 |
| FWHM | 2.44 | 2.33 | 2.33 | 1.48 | 1.48 |
| % Gauss | 73 | 90 | 93 | 83 | 84 |

C2 at 80°C for 3h

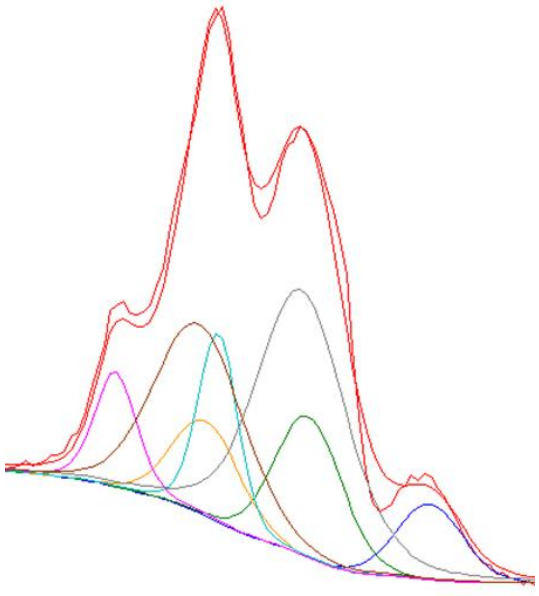

| Chem State | S2s | MoS2 | | MoO3 | | MoO2 |
|---|---|---|---|---|---|---|
| Area | 216 | 613 | 411 | 424 | 284 | 479 |
| Position | 225.73 | 229.43 | 232.56 | 232.19 | 235.32 | 229.65 |
| Height | 76 | 218 | 146 | 257 | 150 | 140 |
| FWHM | 2.37 | 2.56 | 2.56 | 1.43 | 1.71 | 2.99 |
| % Gauss | 74 | 93 | 93 | 83 | 92 | 84 |

C2 at 80°C for 18h

- Molybdenum peaks: Grease P1

P1 at 40°C for 3h

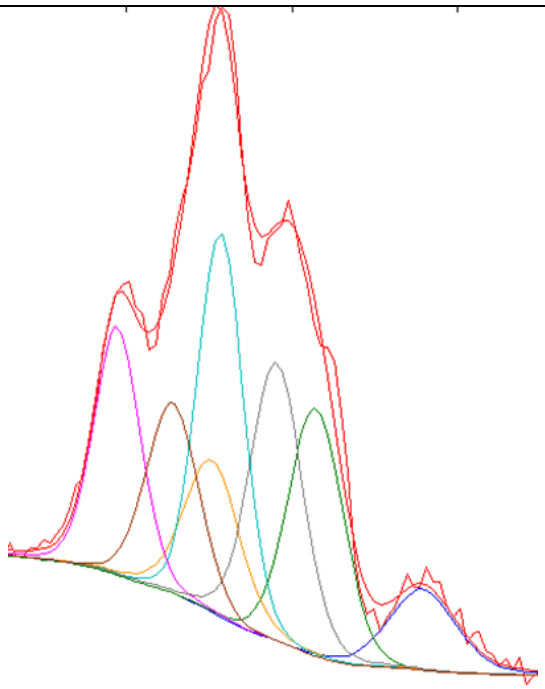

| Chem State | MoS2 | | MoO3 | | MoO2 | |
|---|---|---|---|---|---|---|
| Area | 123 | 82 | 239 | 160 | 158 | 106 |
| Position | 229.29 | 232.42 | 232.18 | 235.31 | 230.48 | 233.61 |
| Height | 57 | 35 | 133 | 85 | 73 | 51 |
| FWHM | 1.97 | 1.97 | 1.64 | 1.64 | 1.87 | 1.96 |
| % Gauss | 93 | 77 | 93 | 83 | 83 | 100 |

P1 at 40°C for 18h

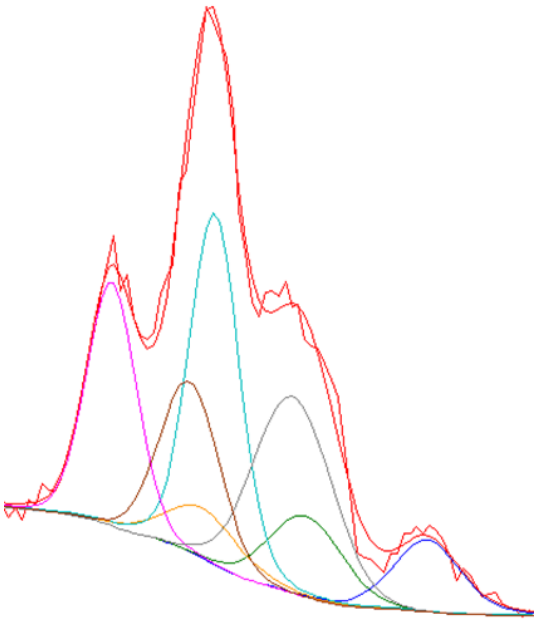

| Chem State | S2s | MoS2 | | MoO3 | | MoO2 |
|---|---|---|---|---|---|---|
| Area | 130 | 147 | 99 | 449 | 301 | 371 |
| Position | 225.71 | 229.40 | 232.53 | 232.17 | 235.30 | 229.80 |
| Height | 45 | 51 | 31 | 219 | 152 | 122 |
| FWHM | 2.39 | 2.63 | 2.63 | 1.78 | 1.78 | 2.82 |
| % Gauss | 73 | 93 | 73 | 83 | 91 | 99 |

P1 at 80°C for 3h

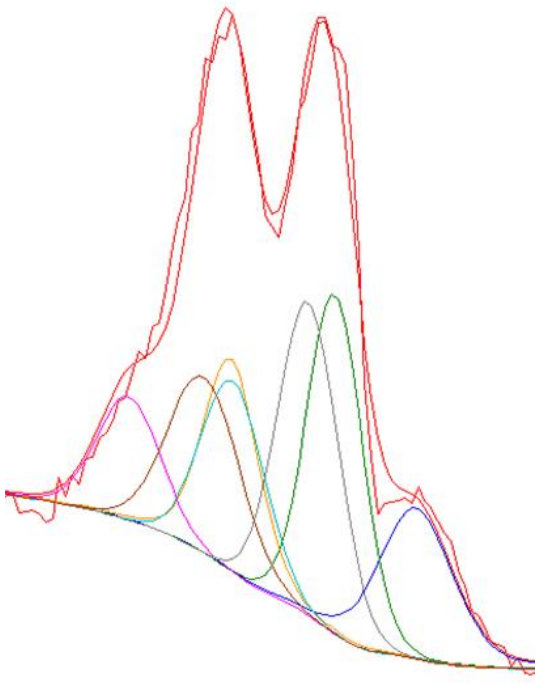

| Chem State | S2s | MoS2 | | MoO3 | | MoO2 |
|---|---|---|---|---|---|---|
| Area | 455 | 705 | 473 | 442 | 296 | 697 |
| Position | 226.25 | 228.70 | 231.83 | 231.76 | 234.89 | 229.50 |
| Height | 145 | 326 | 205 | 185 | 119 | 301 |
| FWHM | 2.60 | 1.97 | 1.97 | 2.25 | 2.25 | 2.15 |
| % Gauss | 73 | 93 | 79 | 100 | 92 | 97 |

P1 at 80°C for 18h

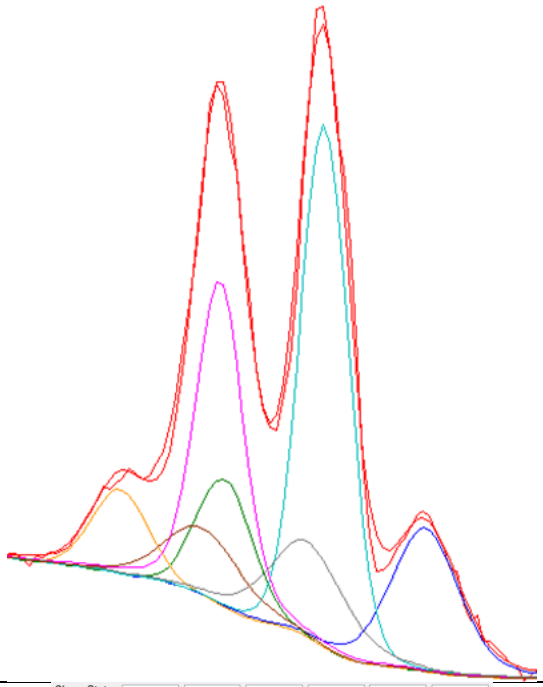

| Chem State | S2s | MoO3 | | MoS2 | | |
|---|---|---|---|---|---|---|
| Area | 392 | 256 | 172 | 919 | 616 | 301 |
| Position | 226.10 | 232.09 | 235.22 | 229.11 | 232.24 | 229.62 |
| Height | 137 | 122 | 80 | 496 | 309 | 91 |
| FWHM | 2.39 | 1.98 | 1.98 | 1.68 | 1.66 | 2.64 |
| % Gauss | 73 | 100 | 97 | 93 | 73 | 63 |

- Molybdenum peaks: Grease P2

P2 at 40°C for 3h

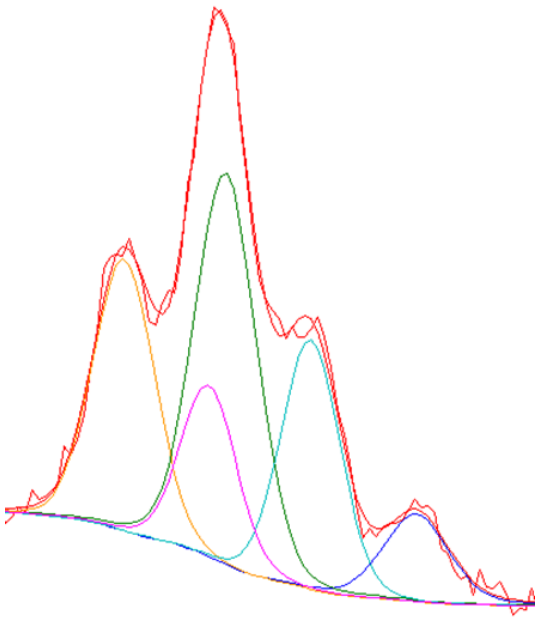

| Chem State | S2s | MoO3 | | MoS2 | |
|---|---|---|---|---|---|
| Area | 46 | 305 | 204 | 102 | 68 |
| Position | 226.10 | 232.11 | 235.24 | 229.39 | 232.52 |
| Height | 18 | 127 | 84 | 43 | 27 |
| FWHM | 2.37 | 2.11 | 2.11 | 2.15 | 2.10 |
| % Gauss | 93 | 86 | 83 | 93 | 73 |

P2 at 40°C for 18h

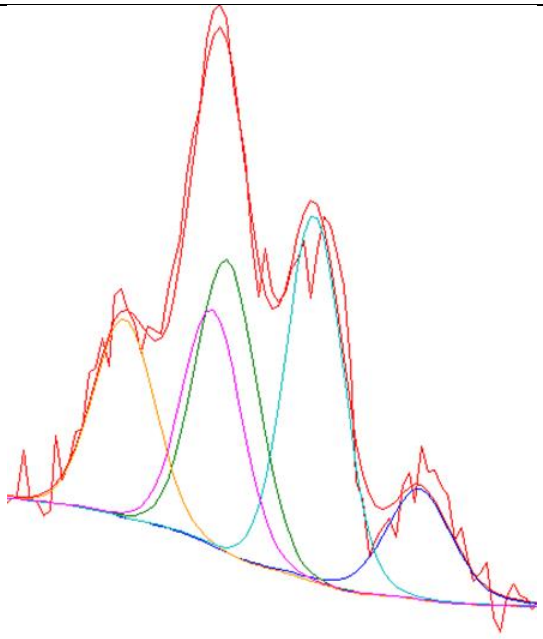

| | Band1 | Band2 | Band3 | Band4 | Band5 |
|---|---|---|---|---|---|
| Chem State | S2s | MoO3 | | MoS2 | |
| Area | 79 | 179 | 120 | 210 | 140 |
| Position | 226.10 | 232.00 | 235.13 | 229.31 | 232.44 |
| Height | 28 | 74 | 50 | 92 | 59 |
| FWHM | 2.37 | 2.22 | 2.22 | 2.07 | 2.15 |
| % Gauss | 73 | 94 | 97 | 93 | 93 |

P2 at 80°C for 3h

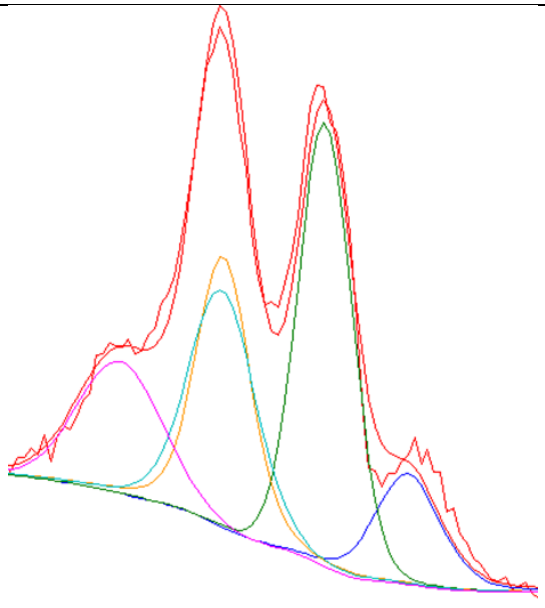

| Chem State | S2s | MoS2 | | MoO3 | |
|---|---|---|---|---|---|
| Area | 353 | 1115 | 747 | 753 | 504 |
| Position | 226.40 | 228.96 | 232.09 | 231.87 | 235.00 |
| Height | 135 | 515 | 316 | 279 | 158 |
| FWHM | 2.37 | 1.97 | 1.97 | 2.34 | 3.00 |
| % Gauss | 93 | 93 | 73 | 83 | 100 |

P2 at 80°C for 18h

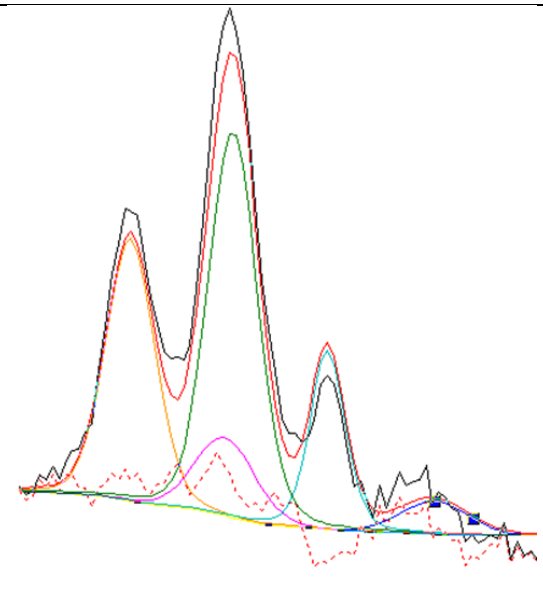

| Chem State | S2s | MoO3 | | MoS2 | |
|---|---|---|---|---|---|
| Area | 29 | 267 | 179 | 93 | 63 |
| Position | 226.10 | 232.26 | 235.39 | 229.36 | 232.49 |
| Height | 11 | 132 | 89 | 61 | 27 |
| FWHM | 2.37 | 1.76 | 1.76 | 1.27 | 2.15 |
| % Gauss | 93 | 83 | 86 | 73 | 93 |

- Tribofilm Profile: 40°: 3h

C1 inside

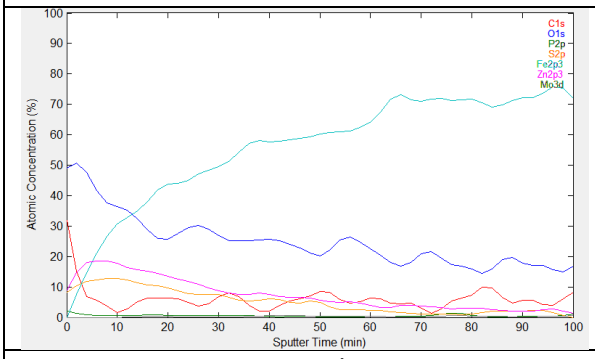


C1 outside

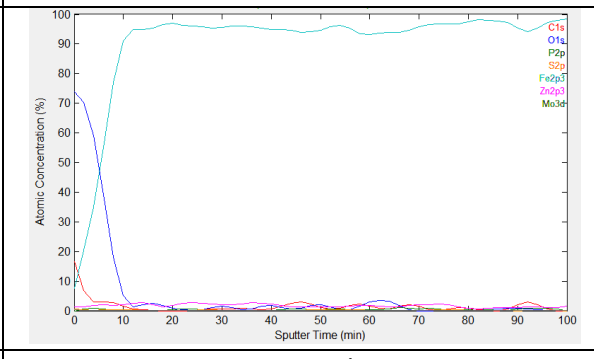


C2 inside

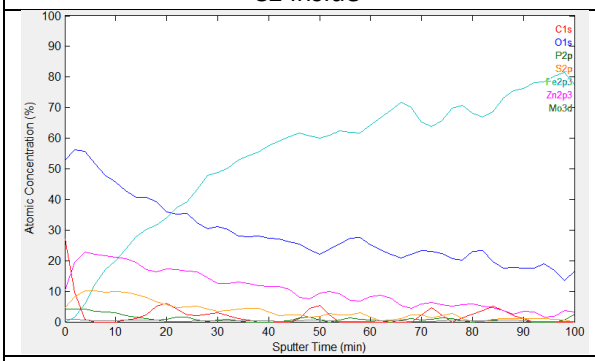


C2 outside

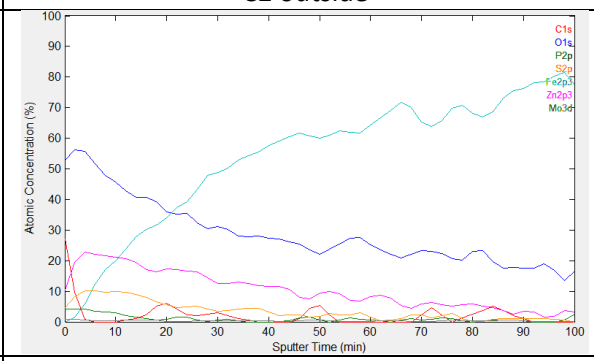


P1 inside

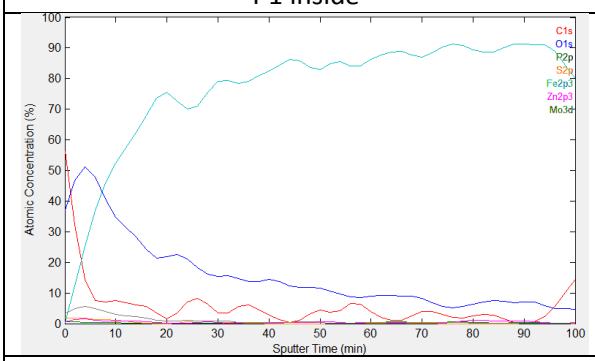


P1 outside

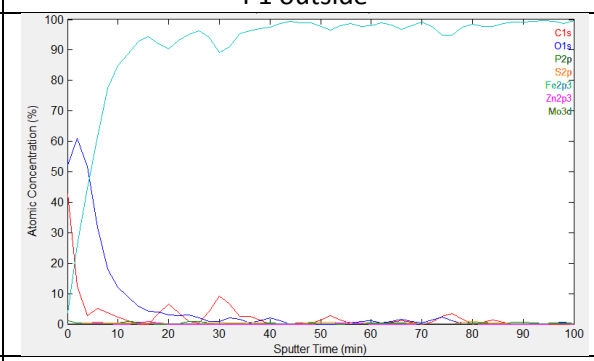


P2 inside

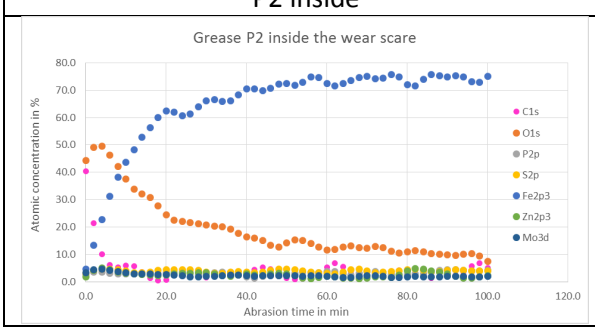


P2 outside

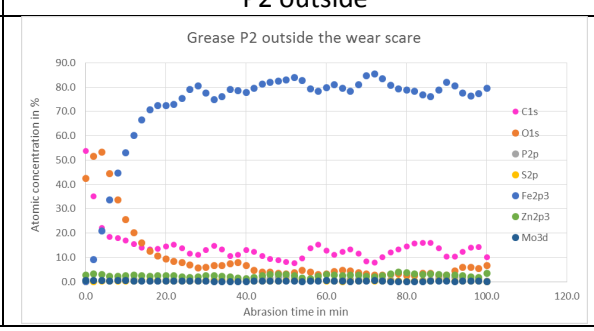

- Tribofilm Profile: 80°: 3h

| C1 inside | C1 outside |
|---|---|
| 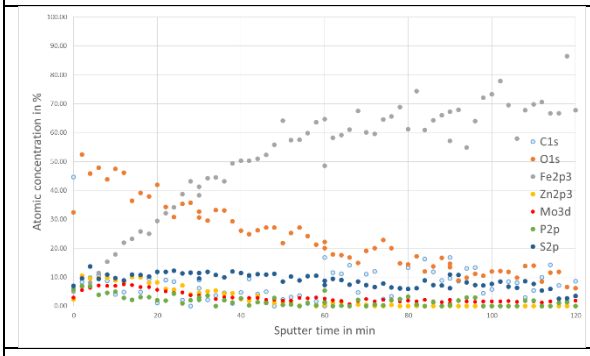 | 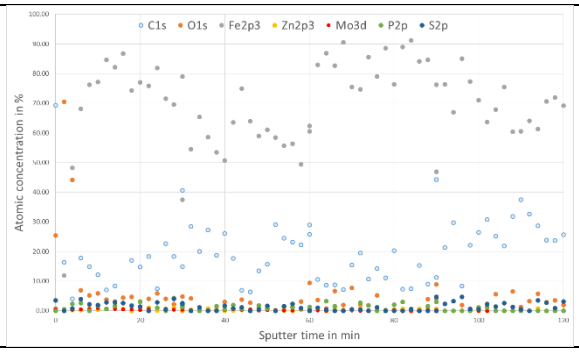 |
| C2 inside | C2 outside |
| 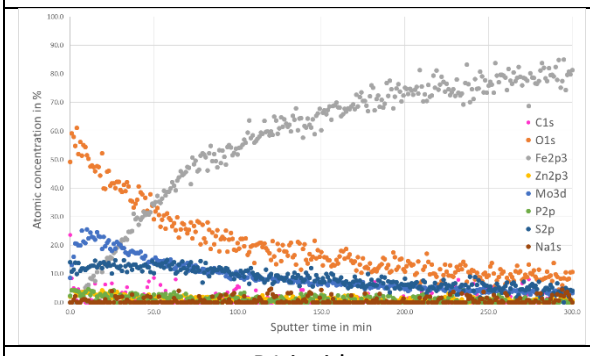 | 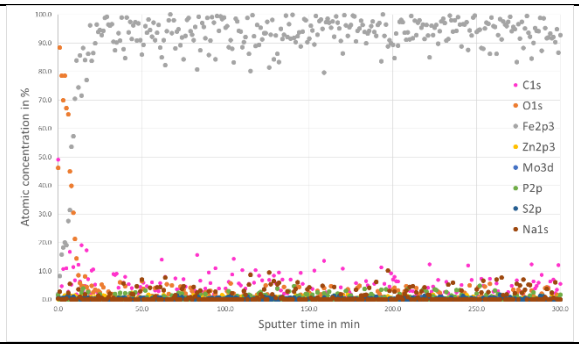 |
| P1 inside | P1 outside |
| 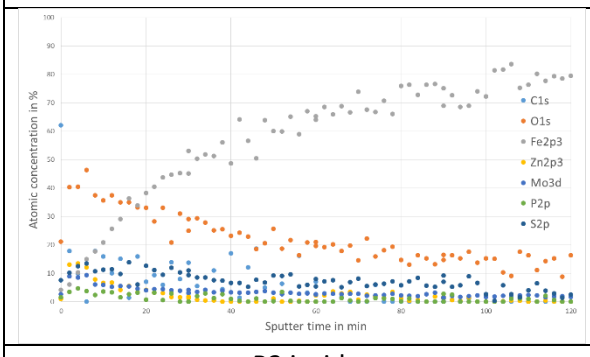 | 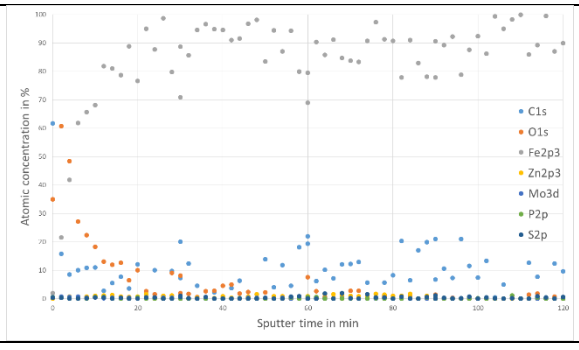 |
| P2 inside | P2 outside |
| 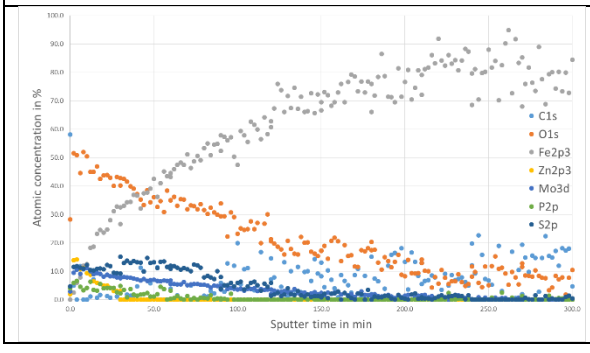 | 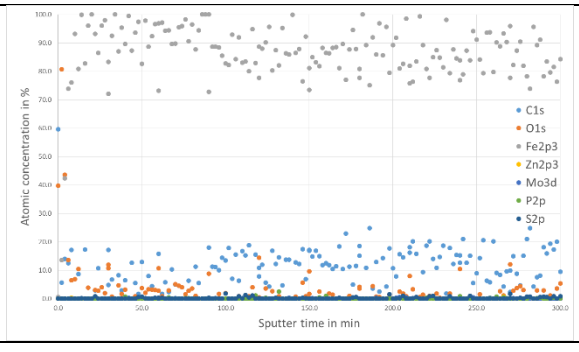 |

- Line Scan 40°C

| 40°C 3h | 40°C 18h |
|---|---|
| C1 | C1 |
| 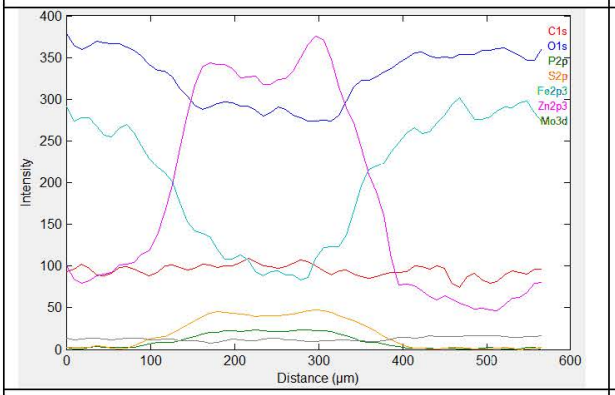 | 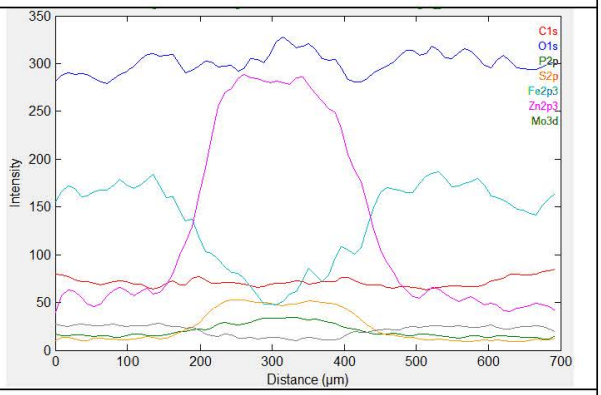 |
| C2 | C2 |
| 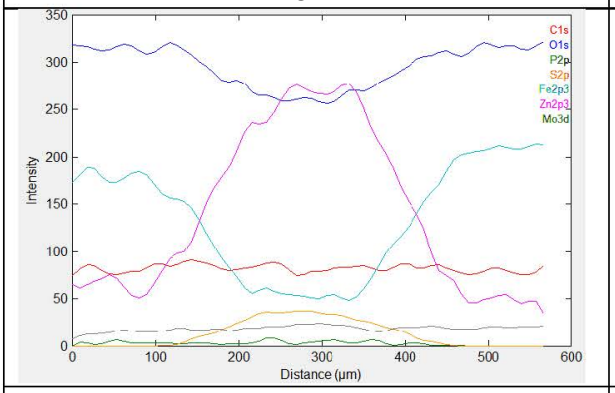 | 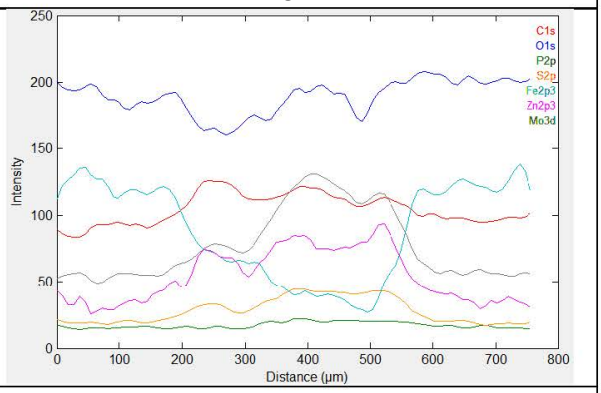 |
| P1 | P1 |
| 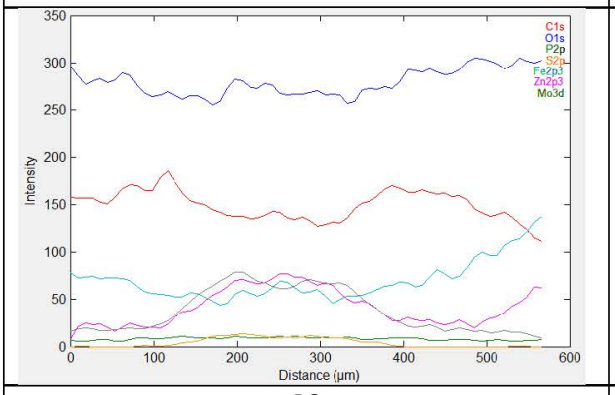 | 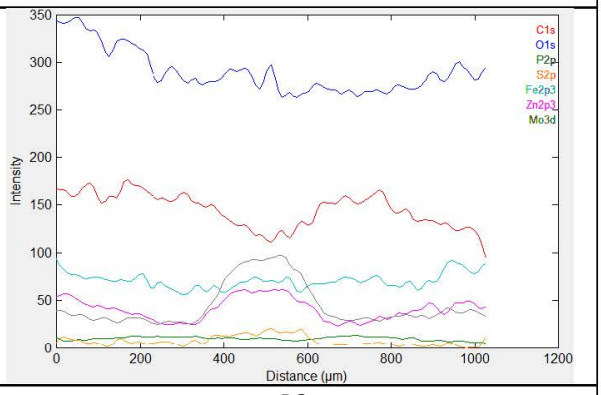 |
| P2 | P2 |
| 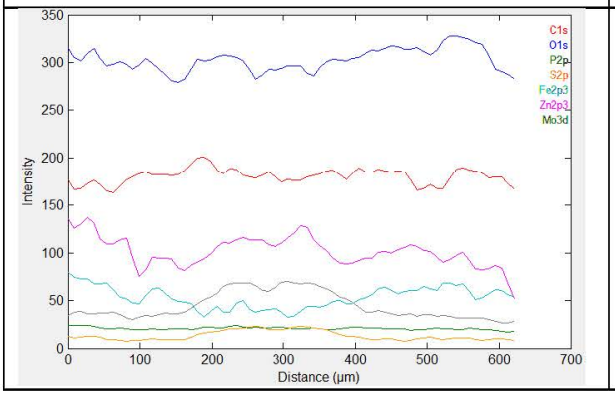 | 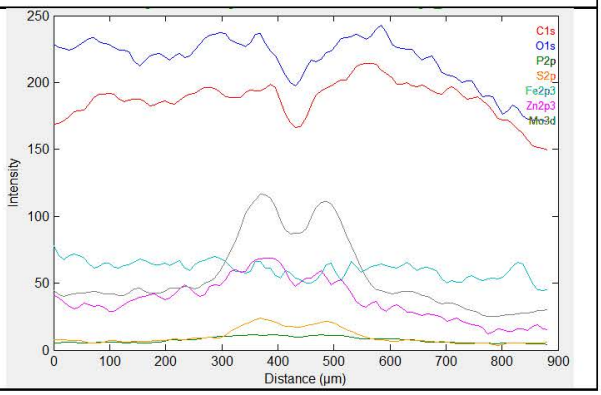 |

- Line Scan 80°C

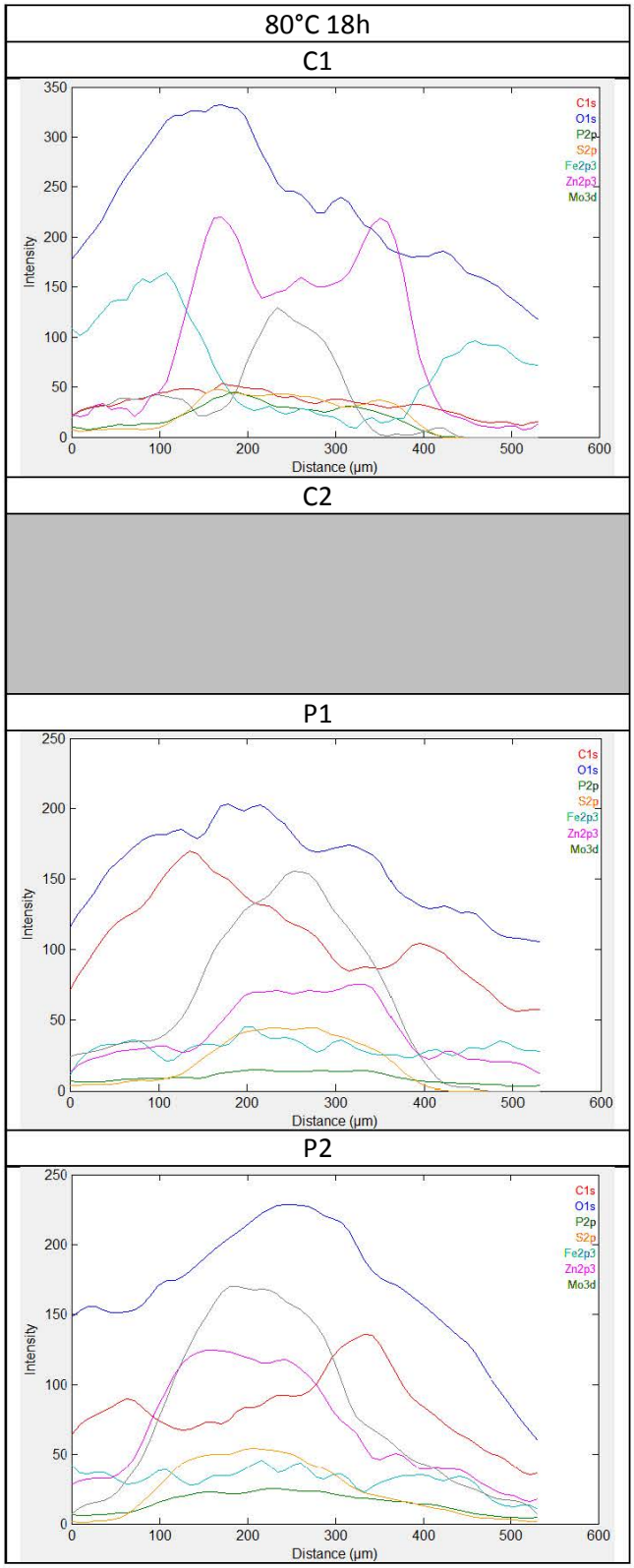

# Appendix E – Rheology repetition

- 40°C

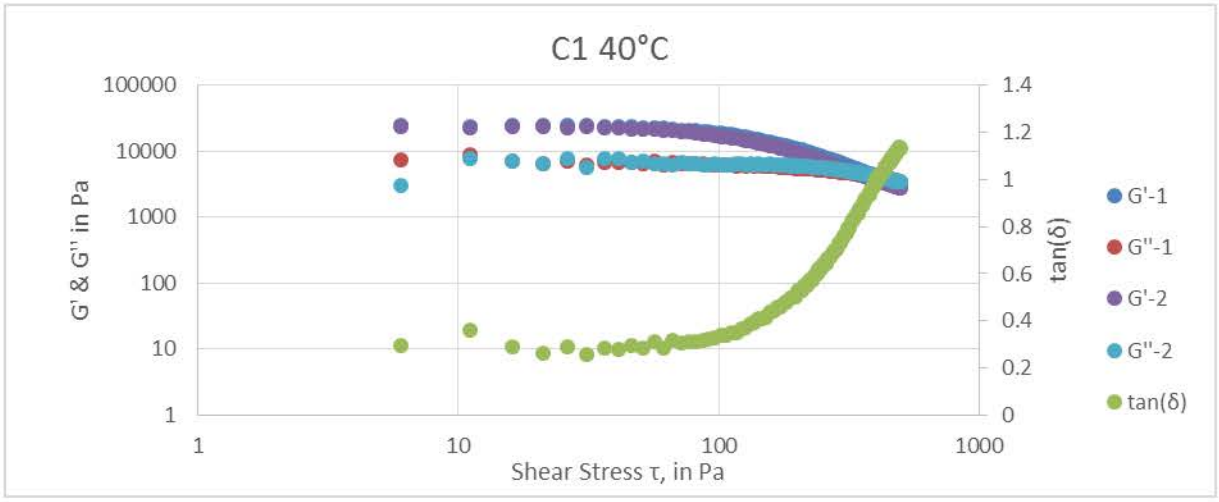


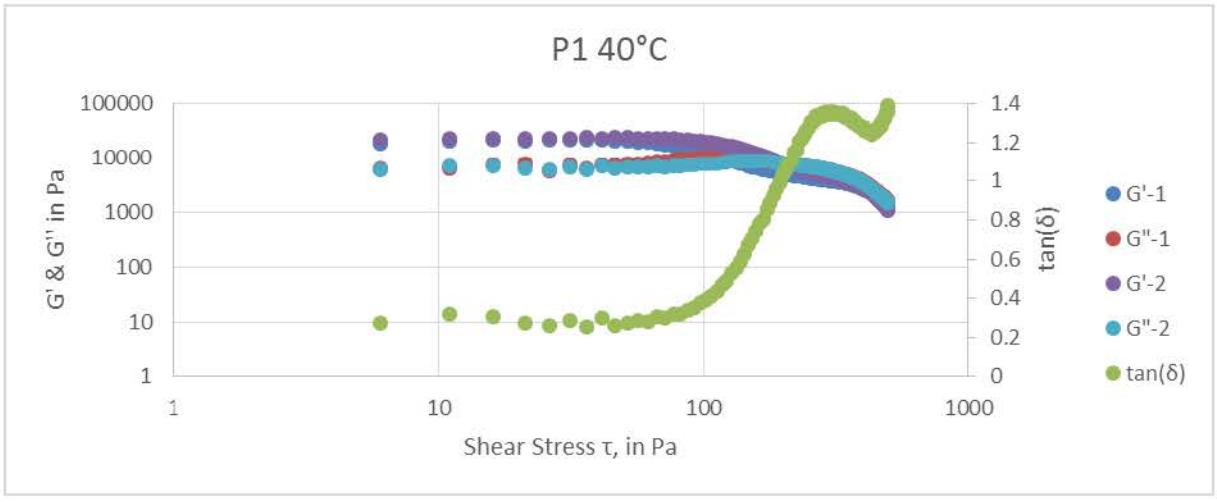


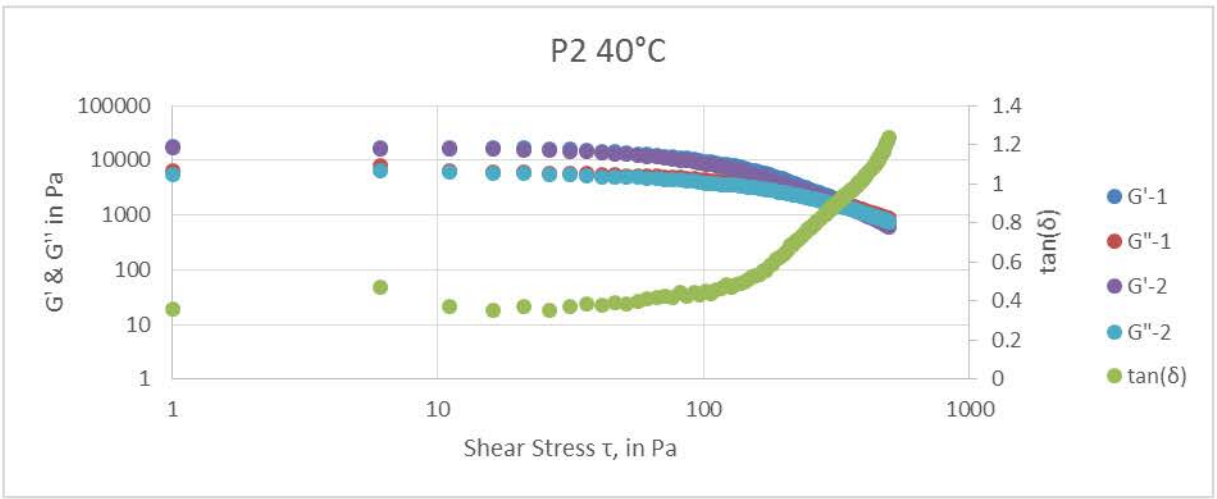

- 80°C

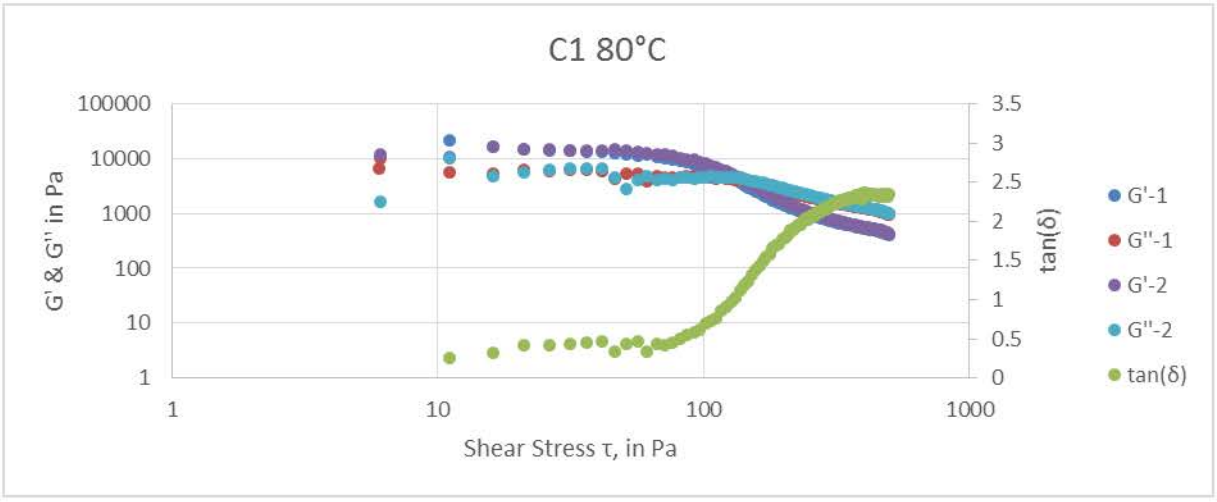


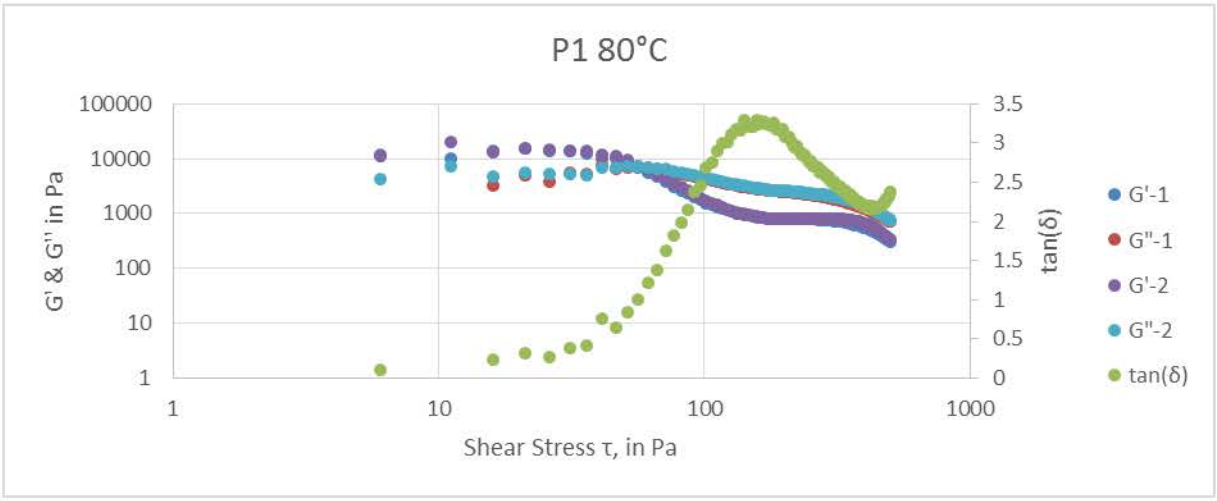


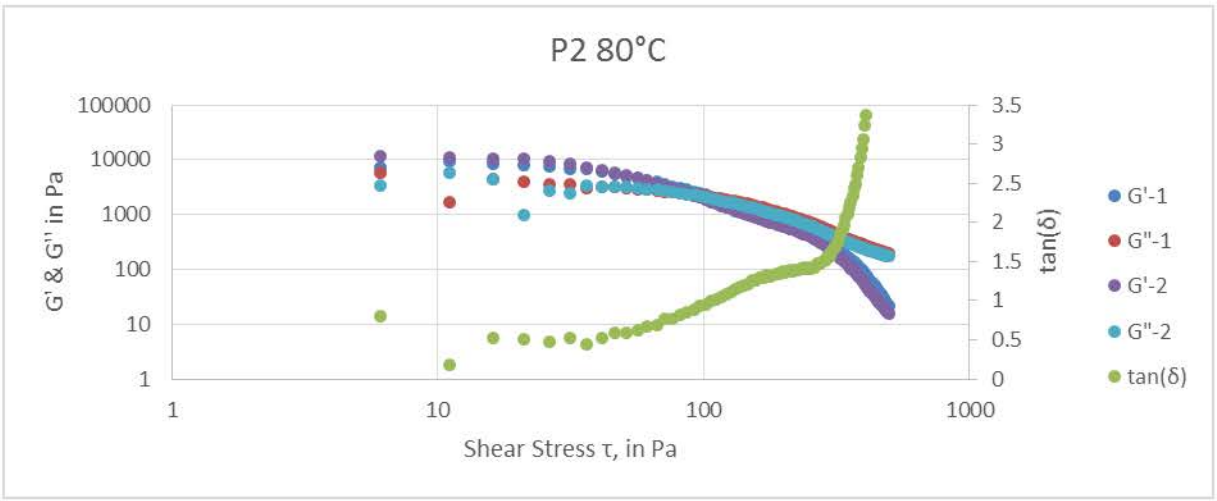

# Appendix F – EHD

- Test under operating condition 7 - Speed variation from 100 to 600 mm/s – 40°C

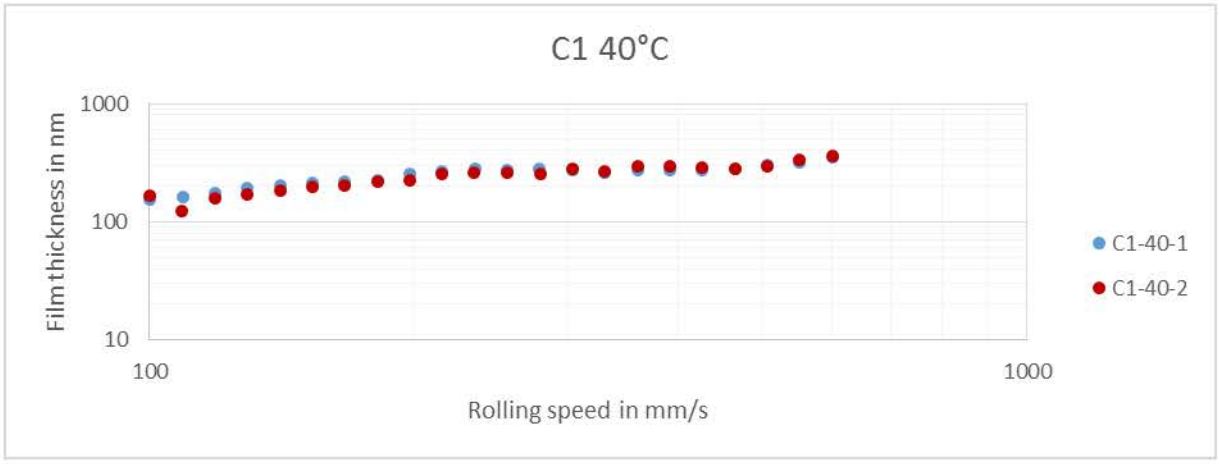


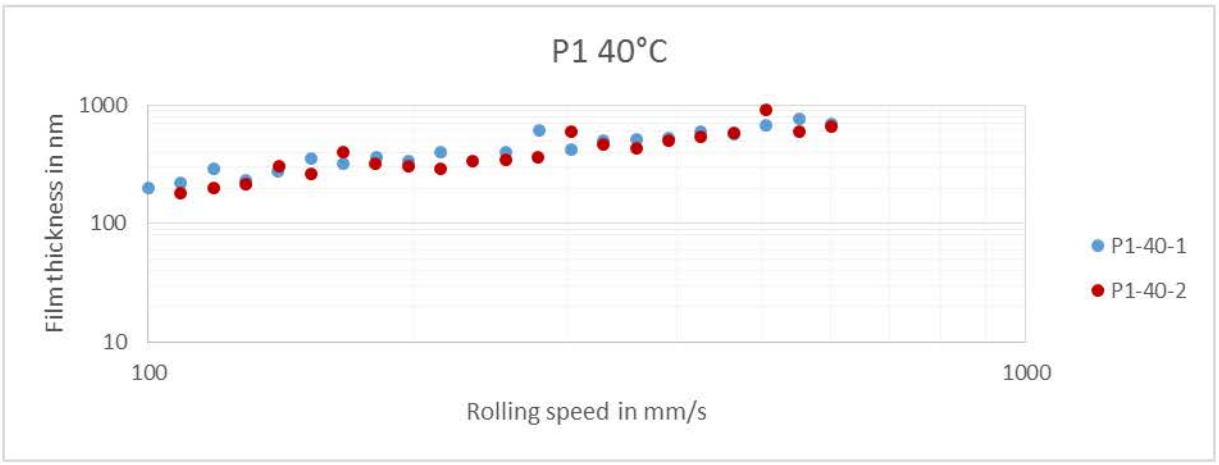


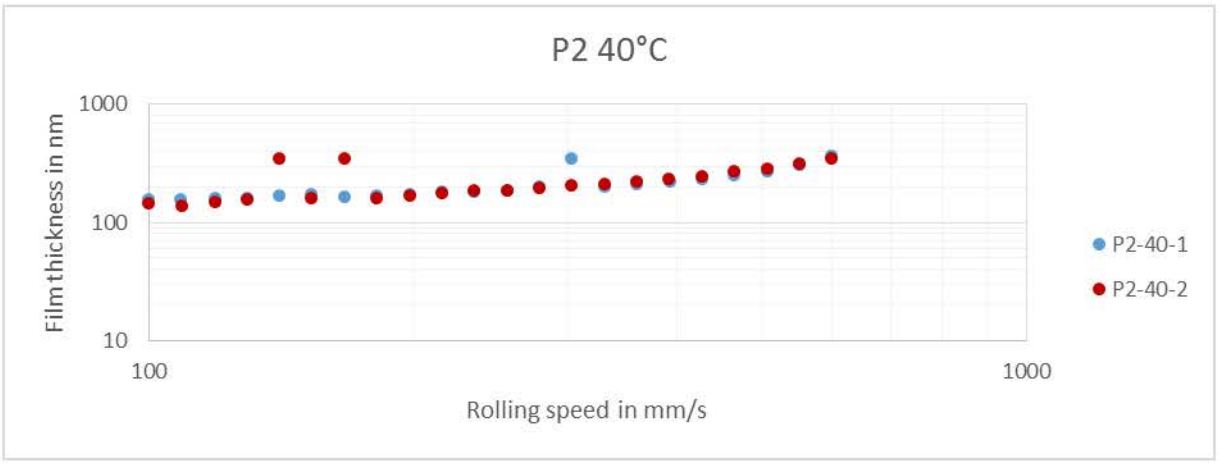

- Test under operating condition 8 - Speed variation from 100 to 600 mm/s – 40°C

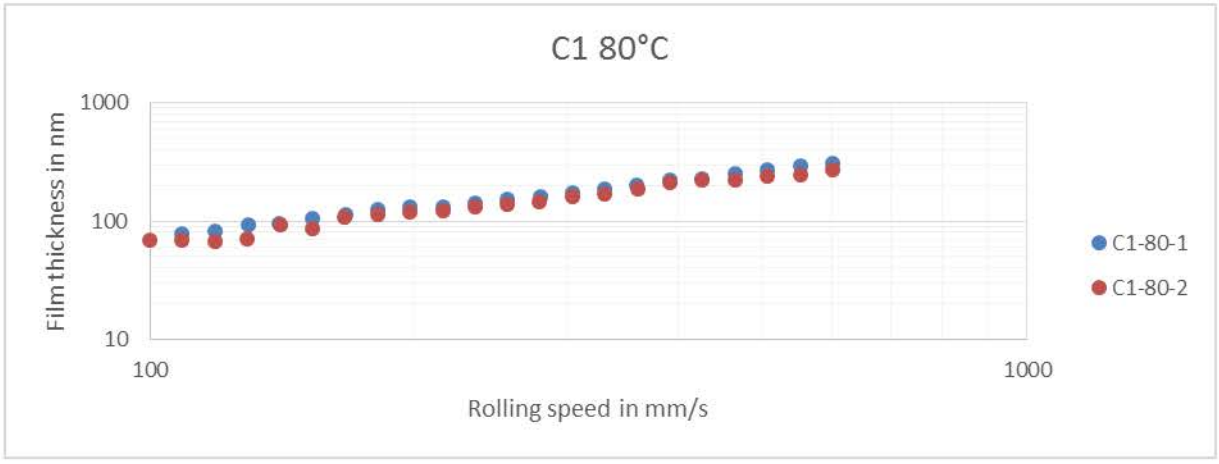


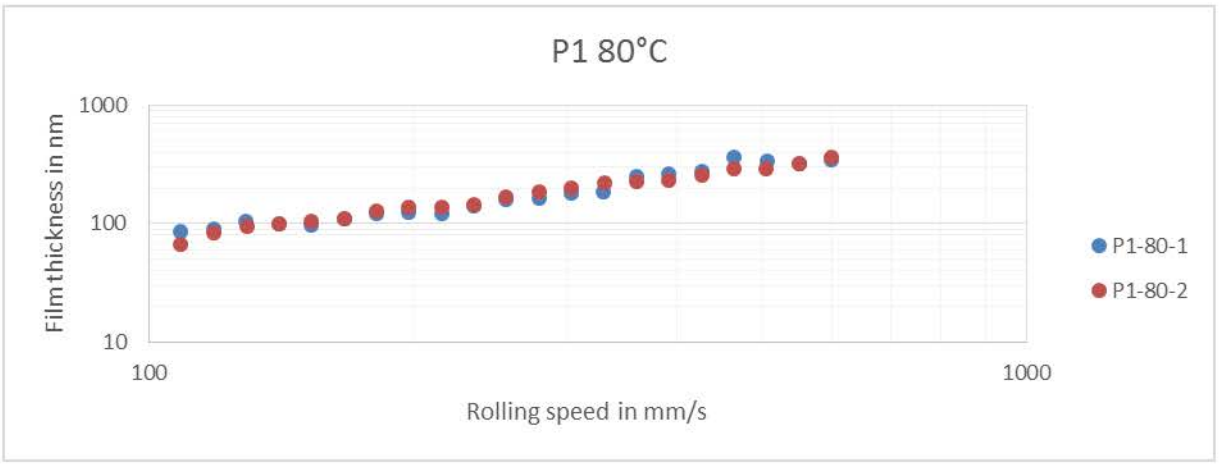


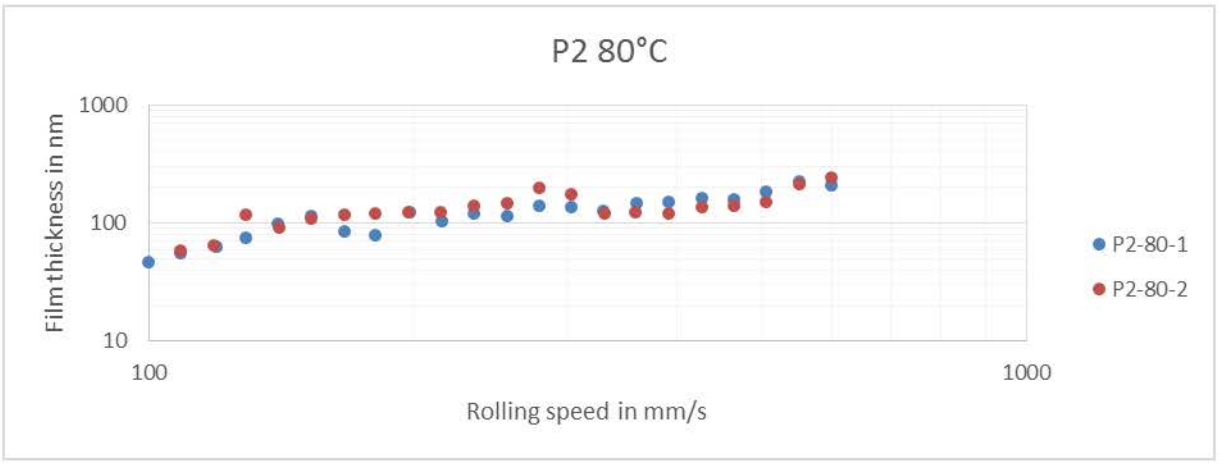

- Test under operating condition 9: grease behaviour along time – 40°C

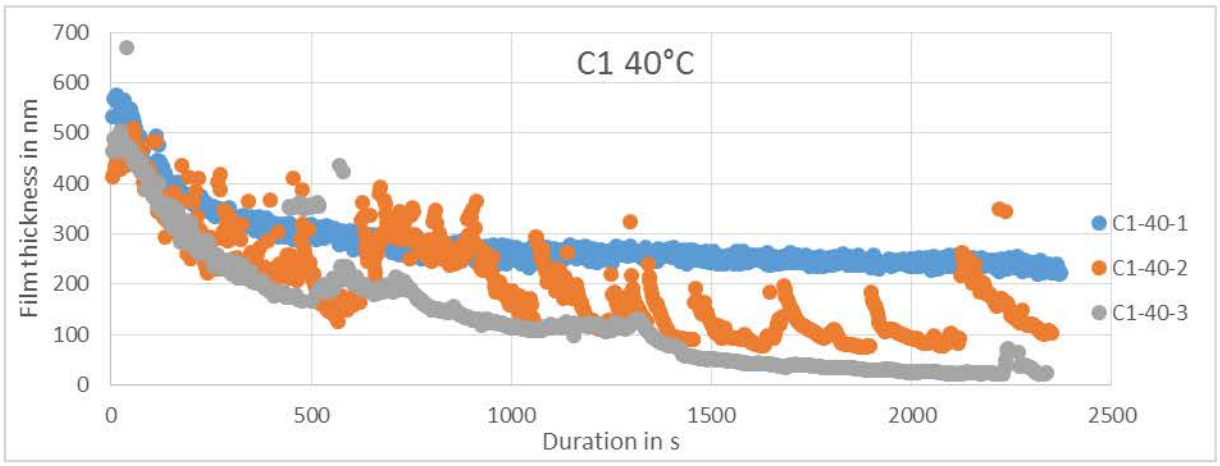


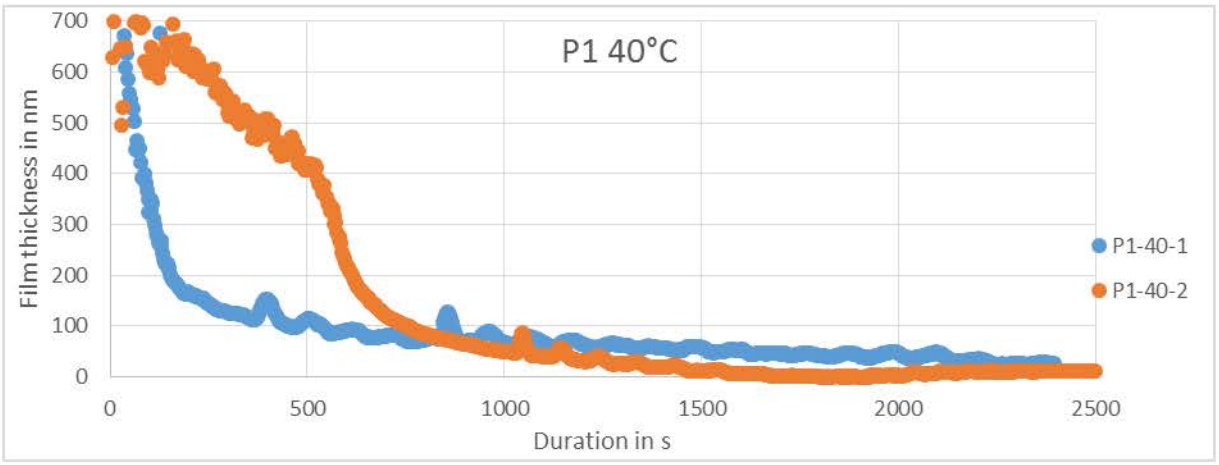


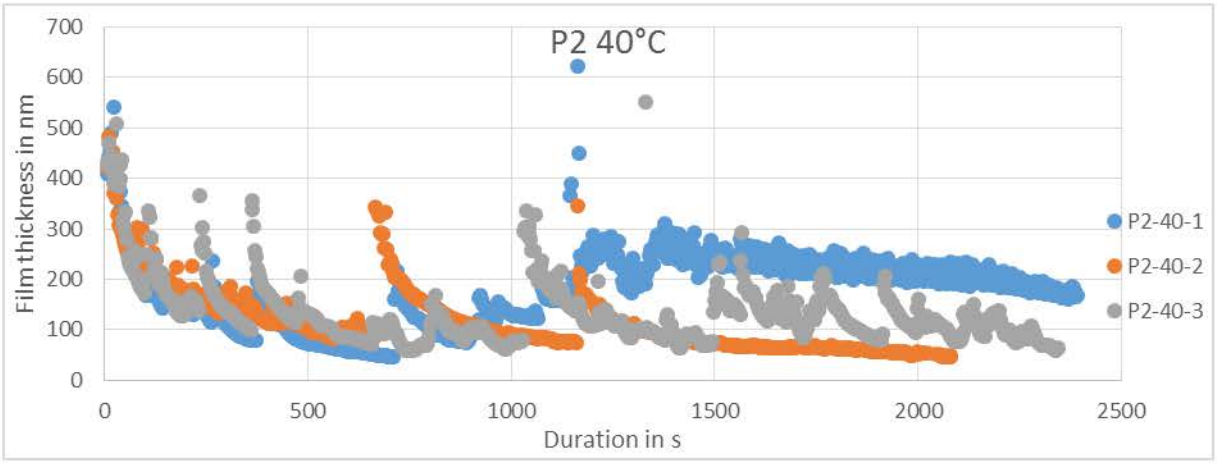

- Test under operating condition 10: grease behaviour along time – 80°C

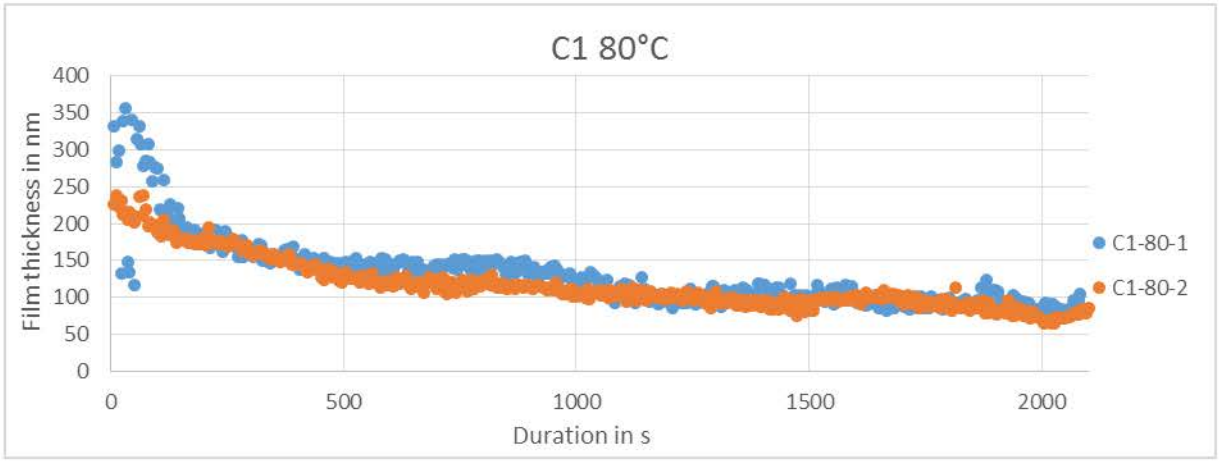


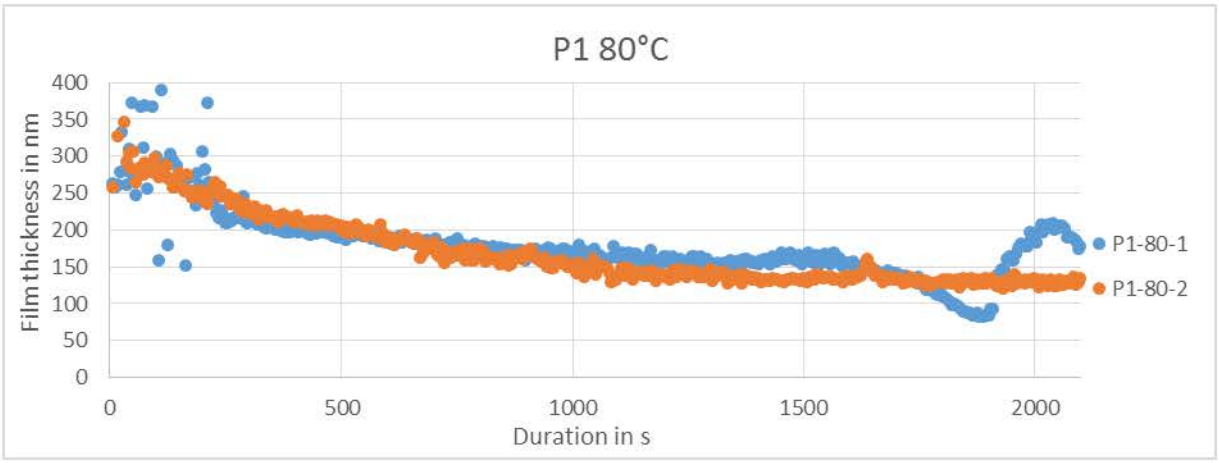


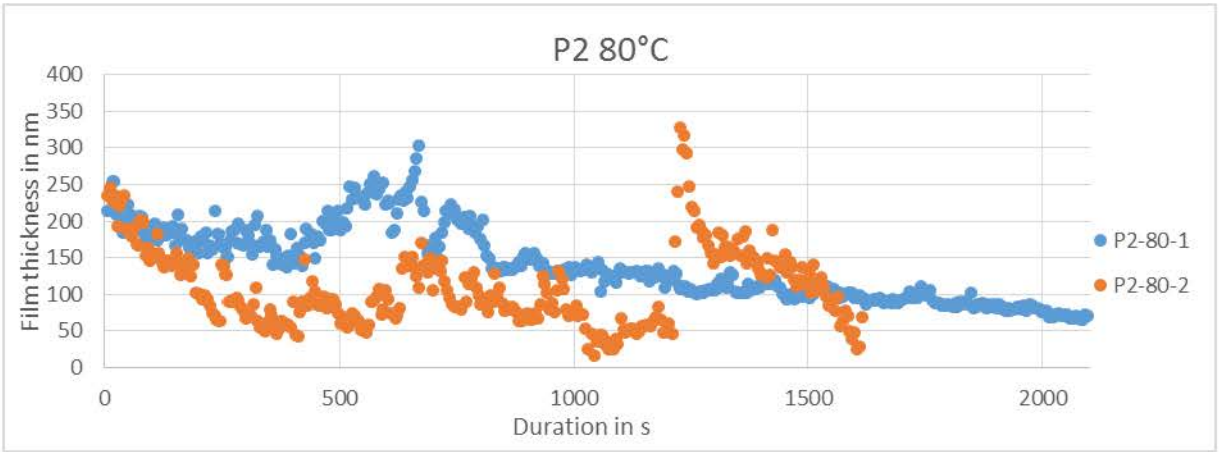

# BIBLIOGRAPHY

[1] Alfred H RZEPPA, “Universal Joint,” US1665280A, 1928.

[2] M. Orain, *Théorie générale et expérimentation des joints homocinétiques*. Glaenzer Spicer., 1977.

[3] Commissariat général au développement durable, “Chiffres clés du transport Édition 2018 Commissariat général au développement durable,” 2018.

[4] JAPAN AUTOMOBILE MANUFACTURERS ASSOCIATION, “2011 REPORT ON ENVIRONMENTAL PROTECTION EFFORTS Promoting Sustainability in Road Transport in Japan.” p. 35, 2011.

[5] United States Environmental Protection Agency, “Where the Energy Goes: Gasoline Vehicles,” 2018. [Online]. Available: https://www.fueleconomy.gov/feg/atv.shtml.

[6] GROUPE PSA, Transport and environment, France nature environnement, and Bureau Veritas, “Real world fuel economy measurements,” 2017.

[7] T. Yamamoto, T. Matsuda, and N. Okano, “Efficiency of Constant Velocity Universal Joints.” SAE Technical Paper 930906, 01-Mar-1993.

[8] P. Dinwiddy, “GKN Driveline’s Breakthrough countertrack™ Technology Saves Fuel | Business Wire,” 2009. [Online]. Available: https://www.businesswire.com/news/home/20090721006245/en/GKN-Driveline’s-Breakthrough-countertrack™-Technology-Saves-Fuel. [Accessed: 18-Sep-2018].

[9] Pierre GUIMBRETIÈRE, “Joints homocinétiques,” *Tech. l’ingénieur*, 1996.

[10] S. Serveto, J.-P. Mariot, and P. Diaby, “Joint tripode coulissant de transmission automobile. Effort axial généré : essais et modèles,” in *18eme Congrès Français de Mécanique*, 2007, p. 6.

[11] K. L. Johnson, “Normal contact of elastic solids – Hertz theory,” in *Contact Mechanics*, Cambridge: Cambridge University Press, 1985, pp. 84–106.

[12] G. INGLEBERT, T. DA SILVA BOTELHO, and I. LEMAIRE CARON, “Théorie du contact de Hertz - Contacts ponctuels ou linéiques,” *Tech. l’ingénieur*, vol. 1, pp. 270–271.

[13] C.-H. Lee and A. A. Polycarpou, “Assessment of Elliptical Conformal Hertz Analysis Applied to Constant Velocity Joints,” *J. Tribol.*, vol. 132, no. April, p. 3, 2010.

[14] B. J. Hamrock and D. Brewe, “Simplified Solution for Stresses and Deformations,” *J. Lubr. Technol.*, vol. 105, no. 2, pp. 171–177, 1983.

[15] R. Stribeck, *Die wesentlichen Eigenschaften der Gleit- und Rollenlager*. Berlin: Springer, 1903.

[16] B. J. Hamrock, “Fundamentals of Fluid Film Lubrication,” *NASA Ref. Publ.*, vol. 1255, p. 676, 1991.

[17] T. E. Tallian, “On Competing Failure Modes in Rolling Contact,” *A S L E Trans.*, vol. 10, no. 4, pp. 418–439, Jan. 1967.

[18] T. G. Mezger, *The rheology handbook : for users of rotational and oscillatory rheometers*. 2011.

[19] F. Cyriac, P. M. Lugt, and R. Bosman, “On a New Method to Determine the Yield Stress in Lubricating Grease,” *Tribol. Trans.*, vol. 58, no. 6, pp. 1021–1030, 2015.

[20] I. COURONNE-DARRAK, “Etude Experimentale du comportement de griasses lubrifiantes pour roulements à billes,” Université de Lyon, 2000.

[21] N. Brunetière, “Introduction à la Tribologie,” p. 118, 2016.

[22] ASTM International, “Standard Test Methods for Cone Penetration of Lubricating Grease.” 2017.

[23] R. N. Bolster and R. C. Little, “Dependence of Lithium Grease Dropping Points on Solubility Parameter of Oil Component,” *Ind. Eng. Chem. Prod. Res. Dev.*, vol. 5, no. 2, pp. 198–202, Jun. 1966.

[24] S. Beret, “Impact of base oil changes on grease performance,” *Spokesman, NLGI*, pp. 192–198, 1993.

[25] W. Dresel and R.-P. Heckler, “Lubricants, 8. Lubricating Greases,” *Ullmann’s Encycl. Ind. Chem.*, vol. 21, pp. 547–571, 2012.

[26] L. Liu and H. W. Sun, “Impact of polyurea structure on grease properties,” *Lubr. Sci.*, vol. 22, pp. 405–413, 2010.

[27] R. W. Bruce, *CRC Handbook of Lubrication: Theory and Practice of Tribology, Volume II: Theory and Design*. CRC Press, 2010.

[28] Dr. Gareth Fish, “The Effect of Friction Modifier additives on CVJ Grease Performance,” *NLGI Spokesm.*, vol. 66, pp. 22–31, 2002.

[29] P. C. H. Mitchell, “OIL-SOLUBLE MO-S COMPOUNDS AS LUBRICANT ADDITIVES,” *Wear*, vol. 100, pp. 281–300, 1984.

[30] M. Kato and T. Sato, “The Development of Low Friction and Anti-Fretting Corrosion Greases for CVJ and Wheel Bearing Applications,” in *SAE Technical Paper*, 1987.

[31] PCS INSTRUMENTS, “EHD2 Ultra Thin Film Measurement System,” 2019.

[32] V. Ripard, F. Ville, J. Cavoret, M. Ruzek, P. Charles, and M. Diaby, “Experimental Investigation of Sliding on Tripod Constant Velocity Joints,” *SAE Tech. Pap. 2019-01-5017*, 2019.

[33] C.-H. Lee and A. A. Polycarpou, “Experimental Investigation of Tripod Constant Velocity (CV) Joint Friction,” 2006.

[34] Esnault Francis, *Construction mécanique : transmission de puissance*. 2002.

[35] G. Knothe, “Evaluation of ball and disc wear scar data in the HFRR lubricity test,” *Lubr. Sci.*, no. April, pp. 35–45, 2008.

[36] P. Rabaso, “Nanoparticle-doped lubricants : potential of Inorganic Fullerene-like (IF-) molybdenum disulfide for automotive applications,” Université de Lyon, 2014.

[37] 3D Systems, “Fiche signalétique Accura ® ClearVue™,” 2016.

[38] C. H. Lee and A. A. Polycarpou, “A phenomenological friction model of tripod constant velocity (CV) joints,” *Tribol. Int.*, vol. 43, pp. 844–858, 2010.

[39] AFNOR, “Produits pétroliers et graisses lubrifiantes - Séparation d’huile au stockage des graisses lubrifiantes - Méthode sous pression - Conditions statiques,” *NF T60-191*. AFNOR, p. 12, 2011.

[40] S. Hurley and P. M. Cann, “IR Spectroscopic Analysis of Grease Lubricant Films in Rolling Contacts,” in *Lubrication at the Frontier*, D. Dowson et al., Ed. Elsevier Science, 1999, pp. 589–600.

[41] C. GROSSIORD, “Mécanismes tribochimiques de réduction du frottement limite : Cas des additifs au molybdène,” Ecole Centrale Lyon, 1998.

[42] C. Balan and J. M. Franco, “Influence of the geometry on the transient and steady flow of lubricating greases,” *Tribol. Trans.*, vol. 44, no. 1, pp. 53–58, 2001.

[43] L. Salomonsson, G. Stang, and B. Zhmud, “Oil/thickener interactions and rheology of lubricating greases,” *Tribol. Trans.*, vol. 50, no. 3, pp. 302–309, 2007.

[44] D. Gonçalves, B. Graça, A. V. Campos, J. Seabra, J. Leckner, and R. Westbroek, “Formulation, rheology and thermal ageing of polymer greases - Part I: Influence of the thickener content,” *Tribol. Int.*, vol. 87, pp. 160–170, 2015.

[45] I. Couronne, G. Blettner, and P. Vergne, “Rheological Behavior of Greases: Part I-Effects of Composition and Structure,” *Tribol. Trans.*, vol. 43:4, pp. 619–626, 2008.

[46] H. Cen and P. M. Lugt, “Film thickness in a grease lubricated ball bearing,” *Tribol. Int.*, vol. 134, pp. 26–35, Jun. 2019.

[47] P. M. Lugt, S. Velickov, and J. H. Tripp, “Tribology Transactions On the Chaotic Behavior of Grease Lubrication in Rolling Bearings On the Chaotic Behavior of Grease Lubrication in Rolling Bearings,” *Tribol. Trans.*, vol. 52, pp. 581–590, 2009.

[48] P. Svoboda, D. Kostal, J. Kunak, and I. Krupka, “Study of Grease Behaviour in a Starved Lubricated Contact,” *MM Sci. J.*, pp. 465–469, 2014.

[49] P. M. Cann, “Starvation and Reflow in a Grease-Lubricated Elastohydrodynamic Contact,” *Tribol. Trans.*, vol. 39, no. 3, pp. 698–704, Jan. 1996.

[50] P. M. E. Cann, “Thin-film grease lubrication,” *Proc. Inst. Mech. Eng. Part J J. Eng. Tribol.*, vol. 213, no. 5, pp. 405–416, May 1999.

[51] L. Huang, D. Guo, and W. Shizhu, “Film thickness decay and replenishment in point contact lubricated with different greases: A study into oil bleeding and the evolution of lubricant reservoir,” *Tribol. Int.*, vol. 93, pp. 620–627, Jan. 2016.

[52] J.-Y. K’NEVEZ, “Etude cinématique et dynamique d’une transmission automobile à joints tripodes,” Université du Maine, 2000.

[53] J. Giesbers, “CONTACT MECHANICS IN MSC ADAMS,” University of Twente, 2012.

[54] Y. Yamamoto and S. Gondo, “Friction and wear characteristics of Molybdenum Dithiocarbamate and Molybdenum Dithiophosphate,” *Tribol. Trans.*, vol. 32, no. 2, pp. 251–257, 1989.

[55] M. De Feo, C. Minfray, M. Bouchet, B. Thiebaut, and J. Martin, “MoDTC friction modifier additive degradation. Correlation between chemical changes and tribological performances,” *RSC Adv.*, vol. 5, p. 24, 2015.

[56] Wikipédia, “ZnDTP.” [Online]. Available: https://upload.wikimedia.org/wikipedia/commons/7/7f/Zn%28dtp%292.png. [Accessed: 28-Sep-2018].

# Résumé étendu en français

## Introduction

A l'heure actuelle, la durabilité des composants mais aussi le rendement de ces composants sont des données très importantes pour les constructeurs automobiles. Dans cette optique, les avancées de ces dernières années se sont concentrées non seulement sur la réduction des émissions de $CO_2$ mais aussi sur la réduction de la consommation de carburant, en travaillant principalement sur les moteurs et boîte de vitesses.

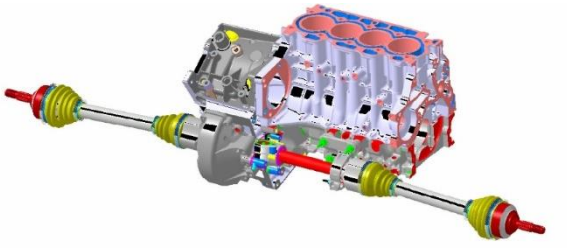

*Figure i: Vue de la transmission*

Ces travaux portent sur la transmission transversale présentée sur la figure i. Sa principale fonction est de transmettre le couple et la vitesse depuis la boîte de vitesse jusqu'à la roue. Elle est composée d'un joint homocinétique permettant, contrairement au joint de cardan, d'avoir la même vitesse sur les arbres d'entrée que de sortie. En plus, côté boîte de vitesse, un joint dit tripode est monté. Il permet de transmettre la vitesse en permettant un changement d'angularité entre les arbres d'entrée et de sortie ainsi que de réaliser un mouvement de translation. Ce mouvement permis grâce à des galets (figure ii), autorise une variation de la longueur des axes, essentielle pour le comportement de la voiture.

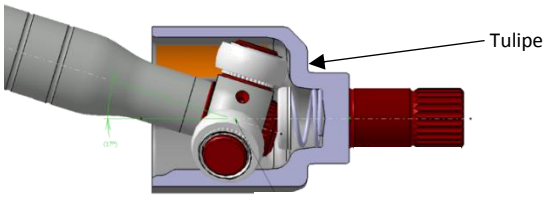


*Figure ii: Vue du joint côté boîte (tripode)*

Ces joints homocinétiques sont connus comme pouvant provoquer de l'usure qui induirait un problème de durabilité pour les clients. Cette usure peut apparaître sur les véhicules surélevés car ils présentent une plus forte angularité de la transmission se traduisant dans certains cas par des vibrations de la transmission.

Le fonctionnement cinématique assez complexe de la transmission induit ainsi des problèmes tribologiques au sein de ce tripode. Ces problèmes causés par l'architecture mécanique du joint peuvent alors se répercuter sur la lubrification avec comme résultante une usure des pièces.

L'objectif de cette thèse est alors de comprendre ces problèmes de lubrification dans le but de réduire l'usure des organes de transmission afin de garantir une durabilité satisfaisante, mais aussi de minimiser le frottement dans ce contact galet / piste de l'entraineur.

**Moyens expérimentaux utilisés**

Afin de mener à bien ces objectifs, une approche expérimentale a été utilisée. Elle repose sur des bancs d'essais de la société PCS Instruments (HFRR, MTM, EHD) mais aussi sur des bancs créés autour de la problématique, au sein des laboratoires accueillant les travaux de recherche.

- High Frequency Reciprocating Rig (HFRR)

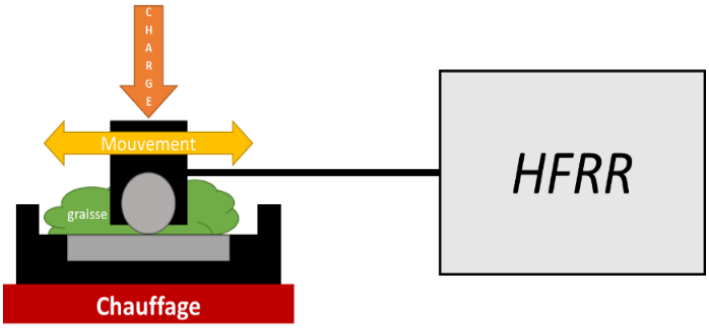


*Figure iii : Illustration de la HFRR*

Le principe de ce banc est illustré sur la figure iii. Il s'agit d'un tribomètre bille -plan fonctionnant en glissement pur. Il sera utilisé pour ses bonnes propriétés de reproductibilité afin de qualifier les propriétés tribologiques des graisses. La charge appliquée peut varier de 0,98 N à 9,81 N. L'échantillon supérieur est une bille de 6 mm de diamètre en 100 Cr6 tandis que l'échantillon inférieur est un disque en 100Cr6. Les échantillons sont polis avec un Ra < 20 nm pour le disque et Ra < 50 nm pour la bille. La température peut être ajustée jusqu'à 150°C. Il fonctionne sur une gamme de déplacement allant de 20 µm à 2 mm avec une fréquence allant de 10 Hz à 200 Hz.

Ce banc produit en résultats le coefficient de frottement du contact ainsi que la résistance électrique permettant de remonter à la séparation des surfaces.

- Mini Traction Machine (MTM)

Un autre banc utilisant le contact bille plan est la MTM (figure iv). Dans ce cas, elle permet de créer un contact de roulement avec glissement en contrôlant les vitesses de la bille et du disque indépendamment. La charge appliquée peut varier entre 0 N à 75 N. L'échantillon supérieur est une bille de 19.05 mm de diamètre en 100 Cr6 tandis que l'échantillon inférieur est un disque en 100Cr6. Les échantillons sont polis avec un Ra < 10 nm pour le disque et la bille. Un disque plus rugueux peut aussi être utilisé avec un Ra>100 nm. La température peut être ajustée jusqu'à 150°C. Il fonctionne sur une gamme de vitesses allant -4 à 4 m/s avec un slide to roll ratio (SRR) pouvant aller jusqu'à 100%. Enfin, afin de réalimenter le contact, un « grease scoop » peut être utilisé afin de réintroduire la graisse dans le contact et d'éviter la sous-alimentation (figure v).

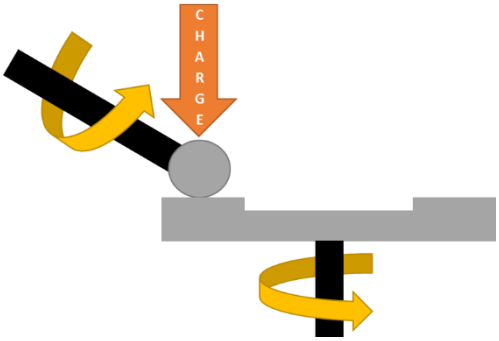


*Figure iv : Illustration de la MTM*

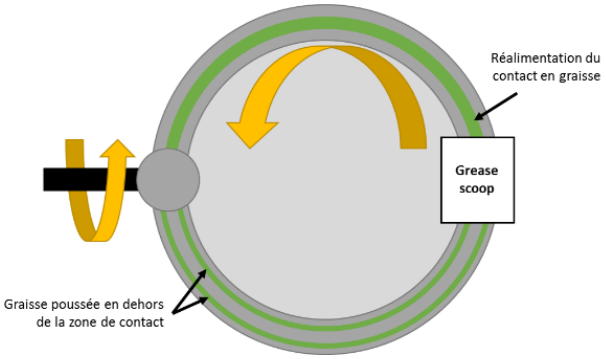


*Figure v : Fonctionnement du grease scoop*

- Ultra Thin Film Measurement System (EHD)

Ce tribomètre reprend en grande partie le principe de fonctionnement de la MTM. De plus, il est pourvu d'un mode « mesure de l'épaisseur de film » qui s'ajoute à la traditionnelle mesure du coefficient de frottement. Ce mode de fonctionnement est autorisé en remplaçant le disque en acier par un disque en verre ou saphir (figure vi). Cette mesure permet de connaitre l'épaisseur du film de lubrifiant jusqu'à 1 nm. L'interférométrie optique est utilisée afin d'obtenir ces valeurs. Les échantillons sont aussi en 100Cr6 dans le cas de l'acier avec un diamètre de bille de 19,05 mm. La charge peut aller de 0 à 50 N.

*Figure vi : EHD*

- Banc d'observation du contact

Afin de caractériser le contact entre le galet et la piste du joint tripode, un banc d'observation a été créé. La tulipe (figure ii) a été imprimée grâce à une imprimante 3D donnant comme résultat un plastique transparent. La majorité du banc a aussi été réalisée à l'aide de fabrication additive. En contrôlant la tige filetée sur la gauche (figure vii), il est aisément possible de définir avec précision l'angle de brisure de la transmission. Enfin, pour des raisons de sécurité avec des éléments tournants, la vitesse a été définie à 150 tours par minute.

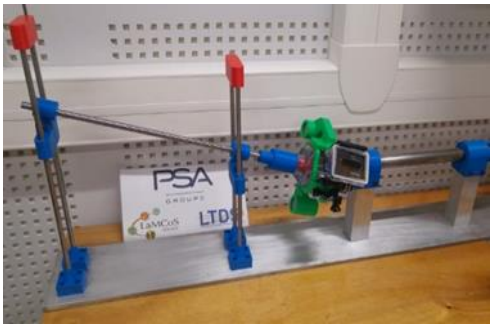


*Figure vii : Banc d'observation*

L'acquisition vidéo est réalisée par une caméra sportive embarquée (dont l'ensemble a été équilibré) et les fichiers sont alors post-traités dans un logiciel dédié créé pour cette application.

L'ensemble de ces moyens expérimentaux va donc pouvoir fournir des résultats fiables et reproductibles guidant la compréhension des phénomènes illustrés dans l'introduction.

**Caractérisation du contact**

Afin de faciliter la compréhension des mécanismes d'usure, une première approche est de calculer l'ensemble des conditions de fonctionnement du contact. A l'aide de la théorie de Hertz et des données du groupe PSA, la pression dans le contact a été calculée en fonction du couple transmis dans la transmission mécanique. Pour un couple de 250 N.m, il est obtenu une pression de Hertz d'environ 1,3 à 1,43 GPa en fonction des théories employées (section 3.1.1).

Ensuite, un modèle numérique utilisant un logiciel de la dynamique des solides a été créé. Il permet d'avoir, en fonction de l'angularité de la transmission, les distances de roulement des galets en considérant le contact comme étant en roulement pur. De plus, cela permet aussi d'évaluer les vitesses de rotation du galet dans la piste mais aussi sa vitesse dans l'axe de la piste. Ces informations seront alors très précieuses dans l'analyse de l'usure mais aussi dans les perspectives des travaux.

Enfin, le banc d'observation est utilisé afin de caractériser expérimentalement la part de glissement comparée au roulement dans le mouvement des galets. Dans un premier temps, pour s'assurer de la validité des résultats, une étude a été menée pour valider le comportement tribologique du couple plastique/acier à acier / acier dans les conditions expérimentales fixées (figure viii).

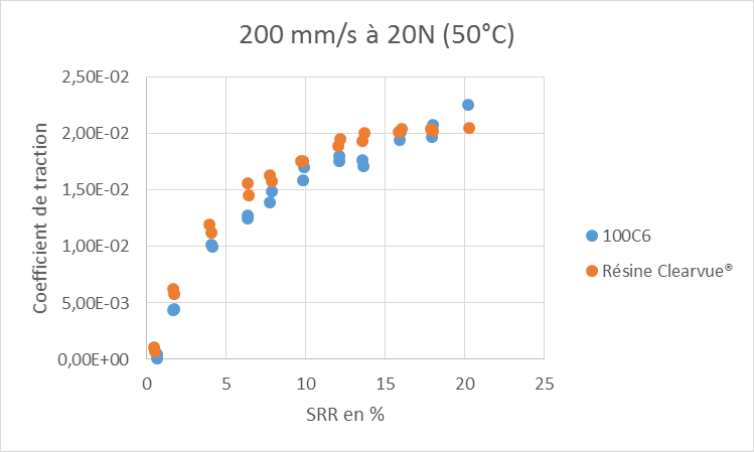


*Figure viii : Comparaison entre les disques en 100C6 et Résine plastique Clearvue®*

Les courbes de coefficients de frottement se superposent ce qui permet ainsi de valider le choix des matériaux du banc d'observation. Plusieurs facteurs sont ensuite évalués à l'aide du banc d'observation :

- Différence de glissement

Dans cette section, la différence de glissement entre les directions que peuvent prendre le galet a été étudiée. En effet, au cours d'une révolution complète du joint homocinétique, le galet réalise un aller-retour sur la piste de la tulipe. Les directions ont été définies comme dans la figure ix.

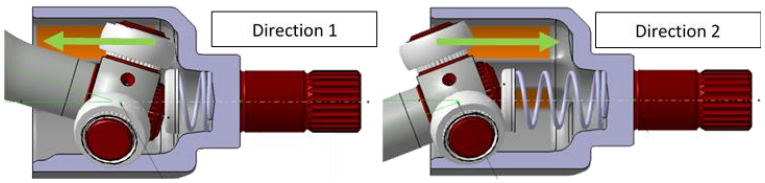


*Figure ix : Définition des directions du mouvement des galets*

Par la suite, de nombreux cas ont été étudiés. Les résultats majeurs sont ceux présentés en figure x et figure xi. La tulipe est graissée avec une quantité dite *série*, c'est-à-dire la quantité utilisée lors de la production en usine des joints homocinétiques. En effet, sur la figure x, il est possible de noter qu'avec cette quantité, le glissement est symétrique entre les deux directions.

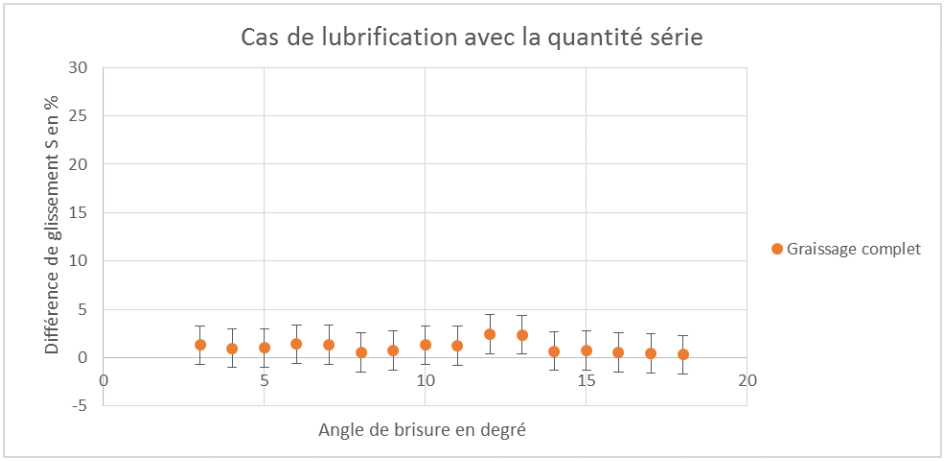


*Figure x : Résultats différence de glissement graissage complet*

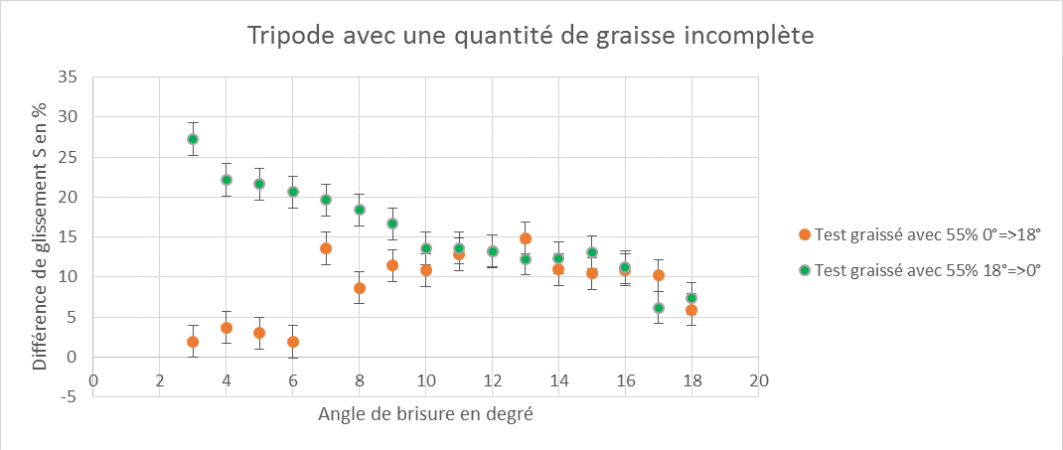


*Figure xi : Résultats différence de glissement graissage incomplet*

Au contraire du cas avec la quantité *série* de graisse, il est notable que le glissement n'est pas symétrique lorsque la quantité de lubrifiant est incomplète (figure xi). En effet, à 55 % de quantité en termes de masse, le comportement varie par rapport au cas précédent.

Tout d'abord, il y a une similitude avec des bas angles si l'acquisition est faite en augmentant les angles de brisure. Par la suite, un accroissement est présent avec un bond de cette différence.

A l'inverse, en faisant l'acquisition avec diminution des angles, cette différence de glissement ne fait qu'augmenter. Cela est dû à l'apparition de cavités. En effet, avec les grands déplacements des galets, la graisse est chassée loin du contact et ne permet pas une présence aux abords des galets. Ainsi, le contact n'est plus assez alimenté (section 3.2.2).

- Taux de glissement

En complément de la première étude qui montre l'importance de la bonne quantité de lubrifiant, une quantification de ce glissement a été effectuée avec une quantité de graisse série (figure xii).

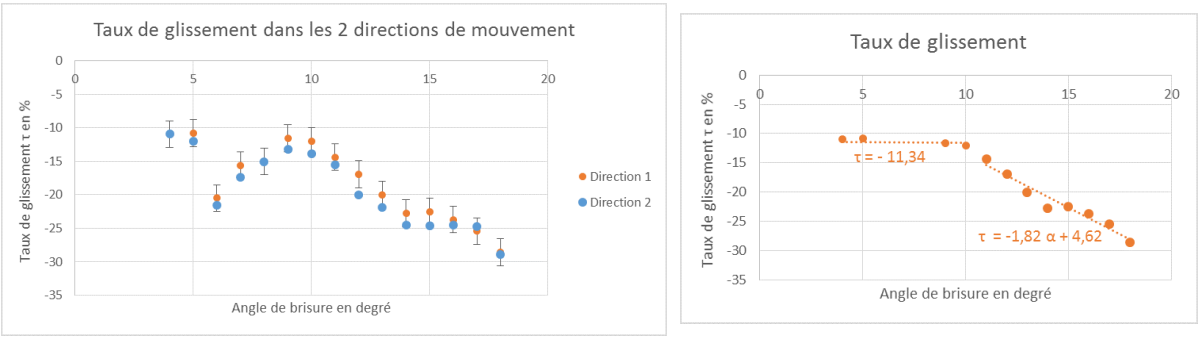


*Figure xii.a (gauche) et xii.b (droite) : Résultats taux de glissement graissage complet*

Sur la figure xii.a, il est possible de noter le comportement symétrique des galets en termes de glissement exposé dans la section précédente. En plus de ce comportement, il est à noter qu'un comportement répétable est présent entre 6 et 9 degrés. Cela peut être dû à une conception du joint tripode ou à une condition de lubrification particulière. Ce point sera investigué dans la suite du manuscrit. Enfin, il a été défini un taux de glissement constant entre 0 et 10° puis un taux sous forme de fonction affine quand l'angularité est supérieure à 10% (figure xii.b).

**Zoom sur les graisses utilisées pour lubrifier le contact**

D'un point de vue industriel, une graisse doit répondre à 2 critères pour les joints homocinétiques tripodes :

- Avoir un coefficient de frottement adapté à son angularité. Plus l'angularité sera haute, plus le coefficient de frottement devra être bas pour éviter trop de vibrations
- Protéger les surfaces et assurer une lubrification correcte afin d'avoir une durabilité ne nécessitant pas d'intervention sur les organes de transmission au cours de la durée de vie d'un véhicule.

Différentes graisses ont été utilisées (voir ci-dessous) : trois graisses issues de lots industriels (C1, P1 et P2) et un lot laboratoire pour pouvoir étudier l'influence de l'additivation de la graisse.

| | C1 | C2 | P1 | P2 |
|---|---|---|---|---|
| Huiles | Minérale + PAO | Minérale + PAO | Ester synthétique + PAO | Ester synthétique + PAO |
| Epaississant | Lithium / Calcium Complexe | Lithium / Calcium Complexe | Polyurée | Polyurée |
| Additifs | MODTC 0,28 | MODTC 1 | MODTC 1 | MODTC 1 |
| | | MODTP 0,4 | MODTP 0,4 | MODTP 0,4 |
| Grade de la graisse [22] | 2 | 2 | 1-2 | 1-2 |

Dans le but de corréler les résultats laboratoires à la réalité, des essais sur les organes de transmission ont été conduits au sein du Groupe PSA. Il consiste à tester les transmissions, puis les démonter à intervalles réguliers de durée pour mesurer l'usure des pistes. Pour des raisons de confidentialité, ces résultats ont été normés puis mis sous forme de pourcentage.

| Dommage sur les pistes en pourcentage | | | | | |
|---|---|---|---|---|---|
| Durée | C1 (%) | Durée | P1 (%) | Durée | P2 (%) |
| 200h | 14 | 200h | 17 | | |
| 400h | 23 | 400h | 35 | | |
| 600h | 32 | 600h | 53 | | |
| 800h | 31 | 800h | 100 | 730h | 5 |
| | | | | 1130h | 8 |

Pour étudier le comportement des graisses, la HFRR est utilisée. Pour cela, des conditions réalistes ont été transposées sur ce banc laboratoire afin de reproduire la part de glissement du galet dans la piste de la tulipe. Les températures des essais vont de 40°C à 80°C représentant une situation d'un véhicule froid et celle d'un véhicule chaud.

Pour commencer, il est important de noter que le comportement des graisses présenté ici est répétable (figure xiii et annexe B). A 40°C, les comportements sont grandement différents. Il est notable que le changement de concentration d'additifs dans la composition de la graisse permet ici de diminuer de 25% le coefficient de frottement (C1 & C2). De plus, le changement d'huile de base et d'épaississant permet de décroitre une nouvelle fois de 30% le coefficient de frottement (C2 &P1). Dans le cas d'un véhicule qui ne serait pas extrêmement « chaud », ces compositions font donc varier le coefficient de frottement du simple au double créant ainsi potentiellement des forces vibratoires deux fois plus grandes dans la transmission mécanique.

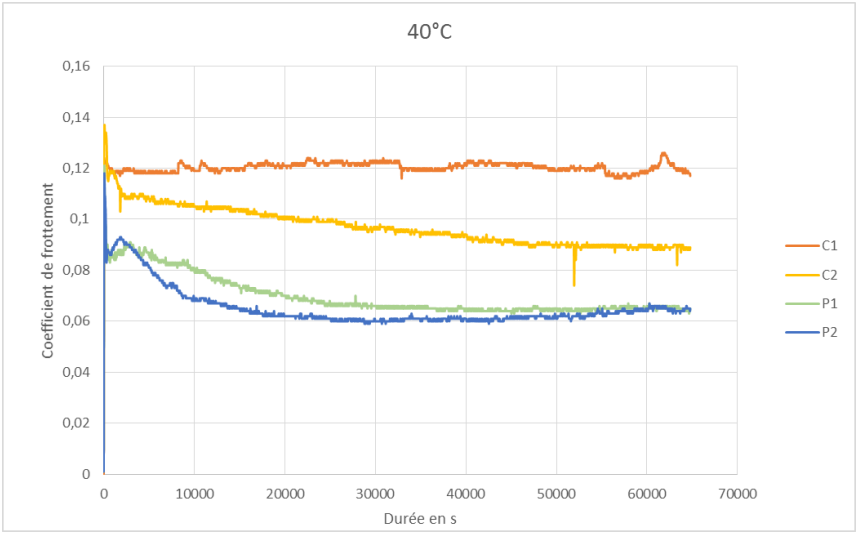


*Figure xiii : Résultats coefficient de frottement à 40°C*

Les résultats à 80°C diffèrent légèrement de ceux à 40°C (figure xiv). En effet, les coefficients de frottement de C1 & C2 convergent autour de 0.08 révélant ainsi une plus faible sensibilité du coefficient à la concentration en additif. Il est toujours à noter que les graisses P1 & P2 ont toujours un coefficient inférieur aux graisses C1 & C2 ce qui demeure intéressant dans le cas d'une application pour des joints homocinétiques fortement inclinés. Enfin, à l'aide d'une analyse XPS (X-Ray Photoelectron Spectroscopy), l'évolution du coefficient de frottement entre P1 & P2 est expliquée par une différence de forme chimique du molybdène dans le tribofilm.

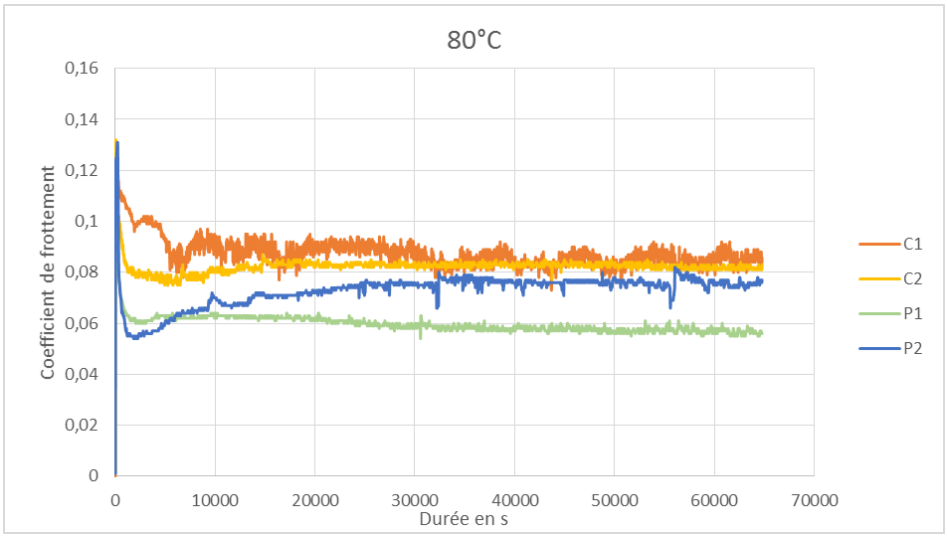


*Figure xiv : Résultats coefficient de frottement à 80°C*

En complément des résultats de frottement, des analyses par rugosimètre ont été menées sur les échantillons afin de qualifier l'usure. Les deux paramètres utilisés ont été la largeur de la trace d'usure et le volume de matière perdu à la suite du frottement (figures xv et xvi).

Les résultats présentés paraissent cohérents. Ils peuvent être directement liés aux résultats sur le coefficient de frottement. En outre, les deux facteurs choisis pour évaluer l'usure donnent les mêmes indicateurs. Cependant, en faisant un retour sur les résultats issus des bancs-organes transmission du Groupe PSA, les résultats en termes d'usure ne se corrèlent pas. La graisse P1 devrait largement se démarquer. Or ce n'est pas le cas. Cela prouve que les conditions ne reflètent pas encore exactement celles du véhicule car elles n'arrivent pas à engendrer le même endommagement des surfaces. C'est pourquoi une investigation spécifique de l'usure est conduite dans la suite des travaux.

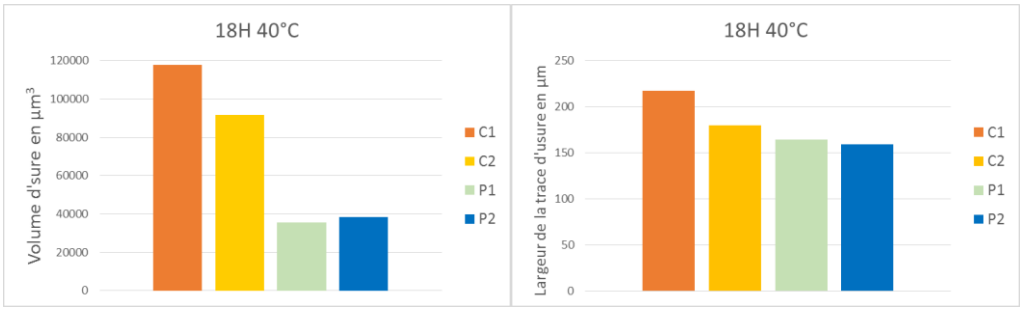


*Figure xv : Résultats usure à 40°C*

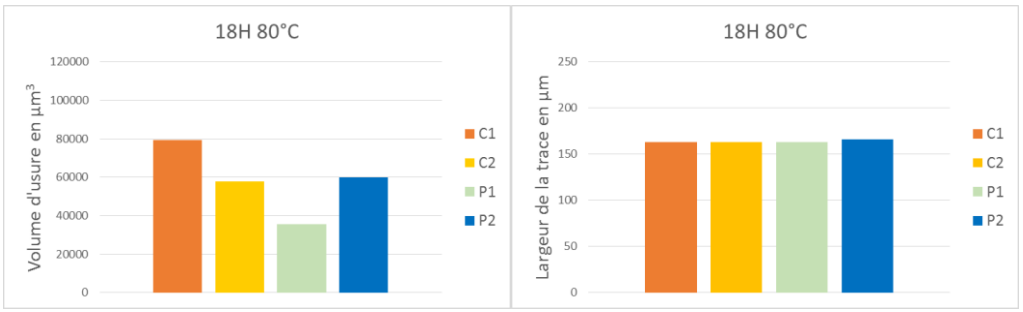


*Figure xvi : Résultats usure à 80°C*

**Investigation de l'usure**

Suite aux investigations précédentes, les conditions expérimentales sur la HFFR ont été modifiées dans le but d'amener la machine à la limite de son fonctionnement avec des conditions extrêmes. Ces conditions correspondent davantage à la vitesse de roulement des galets dans la piste. Les résultats de coefficient de frottement sont disponibles sur la figure xvii.

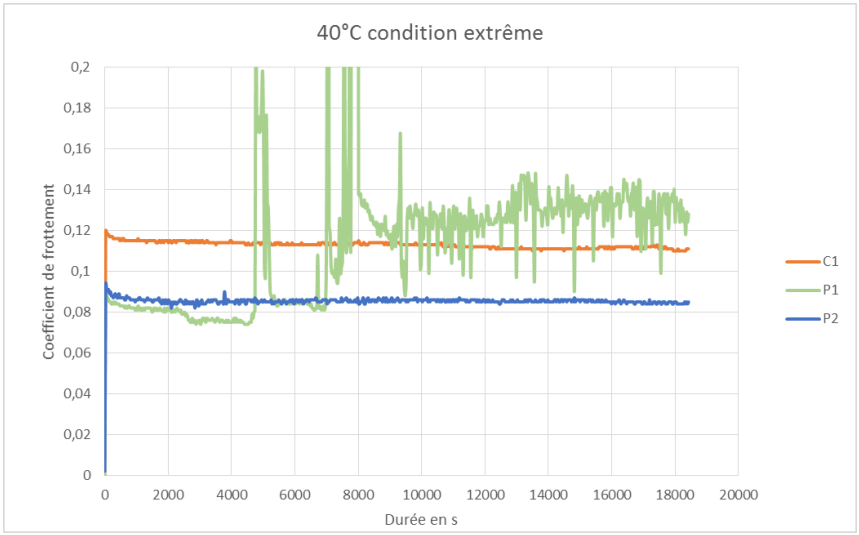


*Figure xvii : Résultats coefficient de frottement à 40°C sous condition extrême*

D'une façon générale, il est à noter qu'à 40°C, les graisses C1 et P2 se comportent comme avec les conditions précédentes, en prenant en compte les légères variations de pression et vitesse. Cependant, P1 se comporte totalement différemment. Au début de l'essai, la graisse se comporte normalement, mais après un peu plus d'une heure d'essai, le coefficient explose signifiant une défaillance dans la lubrification des surfaces. Cette défaillance est observable à l'œil nu (figure xviii) ou selon la même méthodologie que précédemment (figure xix).

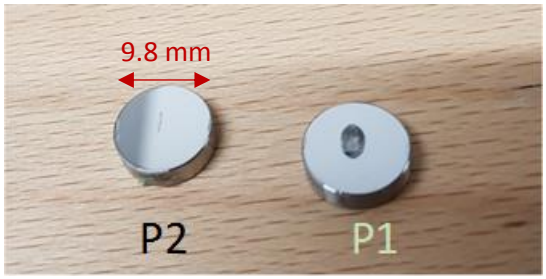


*Figure xviii : Echantillons HFRR 40°C condition extrême*

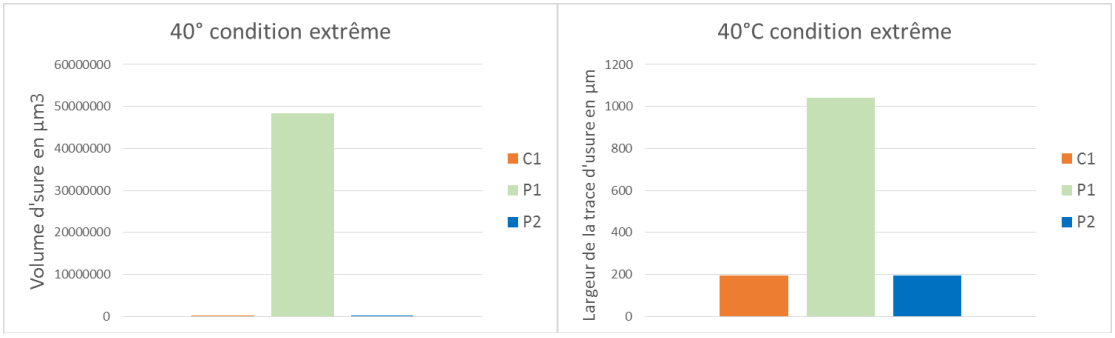


*Figure xix : Résultats usure à 40°C sous condition extrême*

En outre, lorsque la température est de 80°C, cette défaillance n'apparait pas, de même que l'usure engendrée par la défaillance (figure xx).

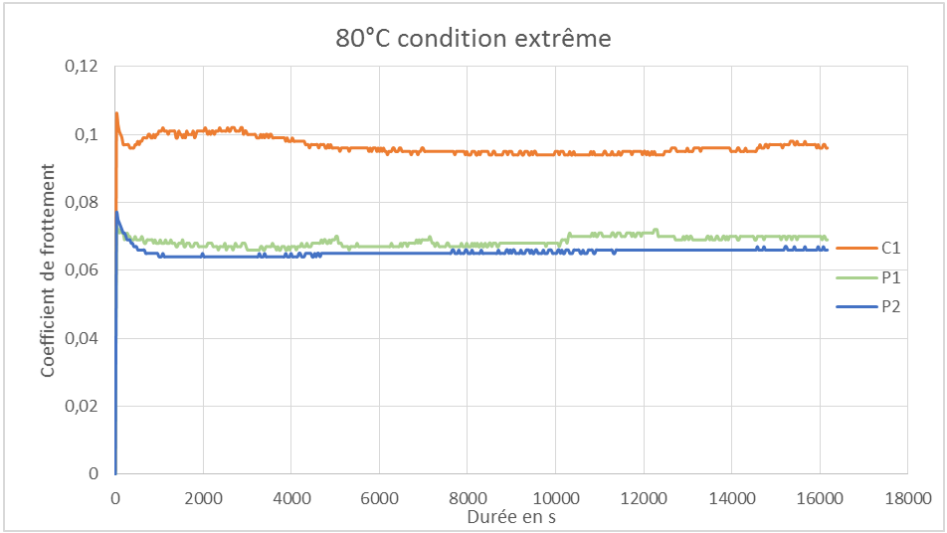


*Figure xx : Résultats coefficient de frottement à 80°C sous condition extrême*

Pour analyser cette défaillance, un essai HFRR a été interrompu dès le premier saut de coefficient de frottement. Par la suite, les échantillons (bille et disque) ont été analysés au profilomètre. Sur les figures xxi et xxii, les photos prises au profilomètre sont disponibles.

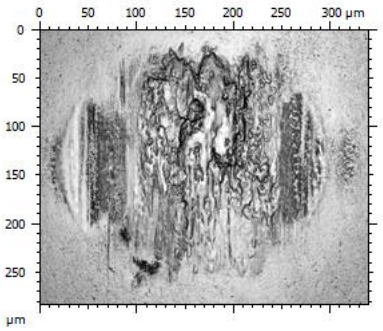


*Figure xxi : image de la bille*

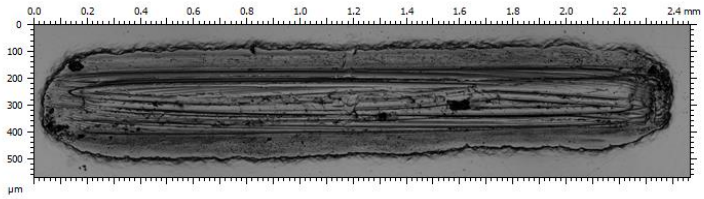


*Figure xxii : image du disque*

En complément de ces images, une image en interférométrie permet d'observer que les traces à la surface de la bille signalent un dépôt de matière (figure xxiii). De plus, le profil issu du disque indique que cette matière provient du disque (figure xxiv). Cela confirme alors que le phénomène critique est ici du grippage.

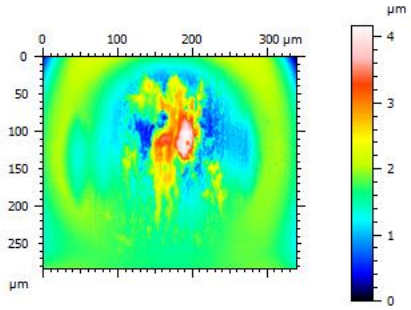


*Figure xxiii interférométrie de la surface de la bille*

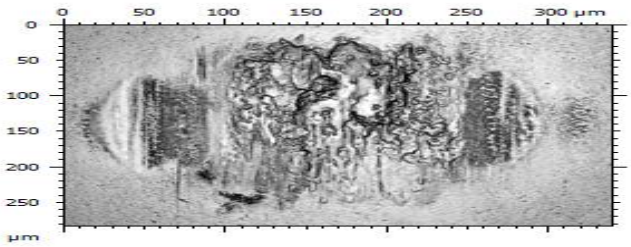


*Figure xxiv: profil de la surface du disque*

En revenant une nouvelle fois au challenge industriel, avec les nouvelles conditions expérimentales, l'usure sur banc transmission a été reproduite et le phénomène identifié. Le premier indice qui peut être déduit de ce test est l'impact de la température dans le processus d'usure. En effet, elle n'est pas générée à 80°C. Ainsi, l'explication de l'usure doit se trouver dans une propriété mécanique et non directement chimique de la graisse. C'est pourquoi la rhéologie de la graisse a été étudiée par la suite.

La rhéologie des graisses a donc été étudiée sur un rhéomètre à contrainte imposée. Des tests oscillants à 40°C ont été choisis (figures xxv, xxvi & xxvii) afin de caractériser le comportement des graisses à agir comme un solide ou un liquide représenté par le module de stockage G' et le module de perte G''.

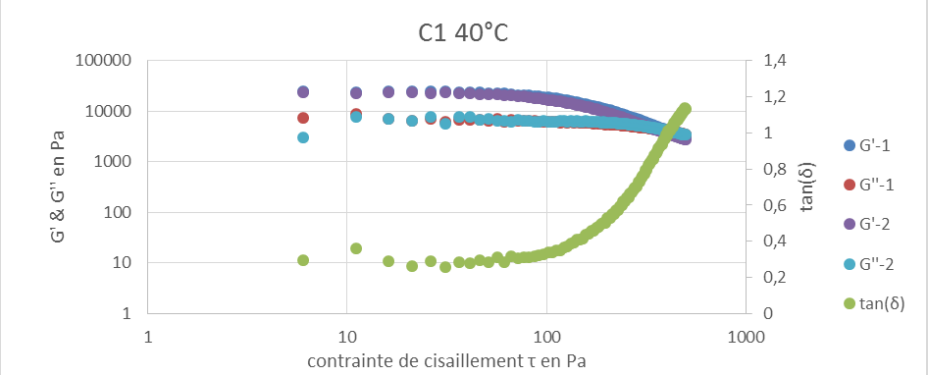


*Figure xxv : Résultats test oscillant C1 à 40°C*

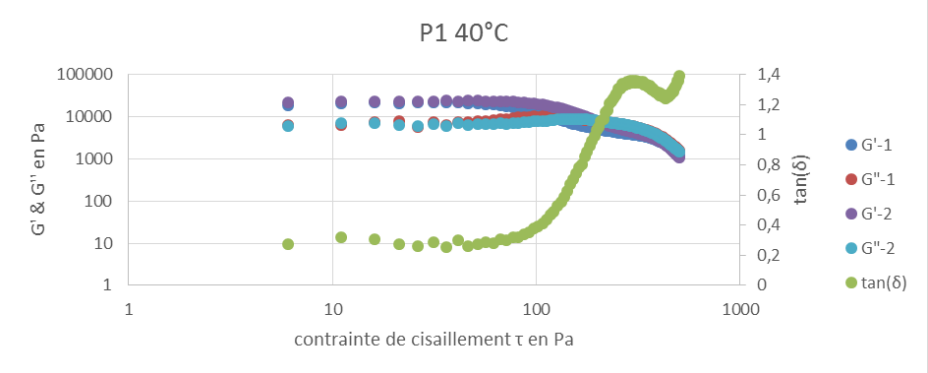


*Figure xxvi : Résultats test oscillant P1 à 40°C*

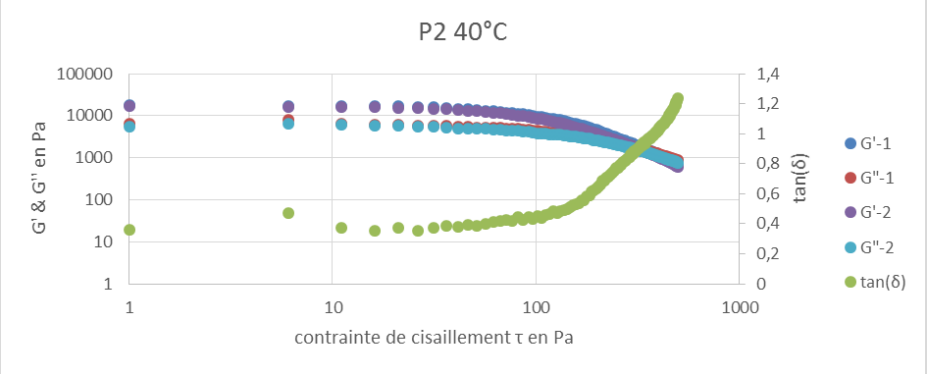


*Figure xxvii : Résultats test oscillant P2 à 40°C*

Il est notable que C1 & P2 ont un comportement similaire. En effet leur point d'écoulement est à peu près à la même valeur. De plus le module de stockage de P2 est plus faible que celui de P1 qui a pourtant la même huile de base. En outre, P1 a un point d'écoulement très inférieur aux autres graisses ce qui indique que la graisse arrête plus tôt d'agir comme un solide. Enfin, il est observable qu'une fois le point d'écoulement passé par P1, les 2 modules restent assez proches provoquant une difficulté à savoir comment se comporte la graisse en tant que matériau.

Pour compléter cette caractérisation, une étude de l'épaisseur de film est nécessaire. Elle permet de lier le comportement des graisses à une épaisseur du film qui, elle, est directement reliée à l'usure des surfaces.

Afin de réaliser ces mesures d'épaisseur de film, la machine EHD de PCS Instruments a été utilisée. Les échantillons ont été choisis afin de reproduire un contact elliptique. La vitesse des conditions extrêmes a été reprise en ajoutant un SRR de 10%. Les résultats sont représentés sur les figures xxviii, xxix, xxx à 40°C et 80°C.

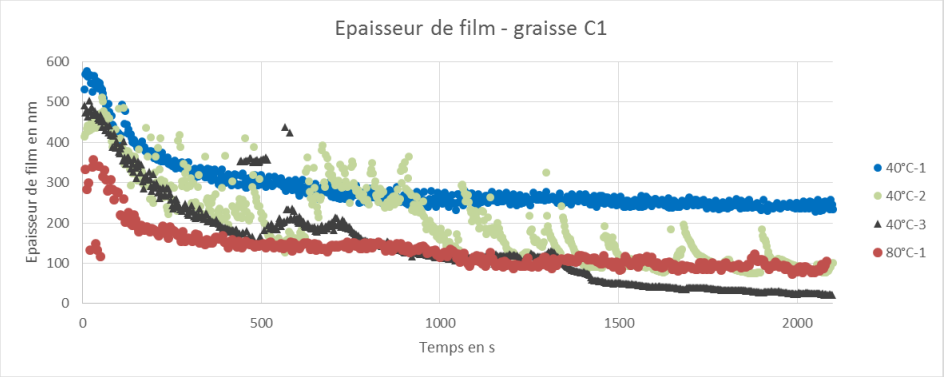


*Figure xxviii : Epaisseur de film C1*

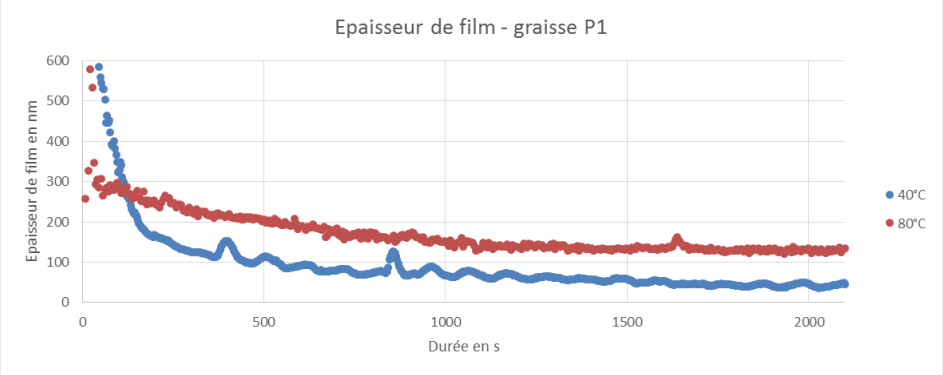


*Figure xxix : Epaisseur de film P1*

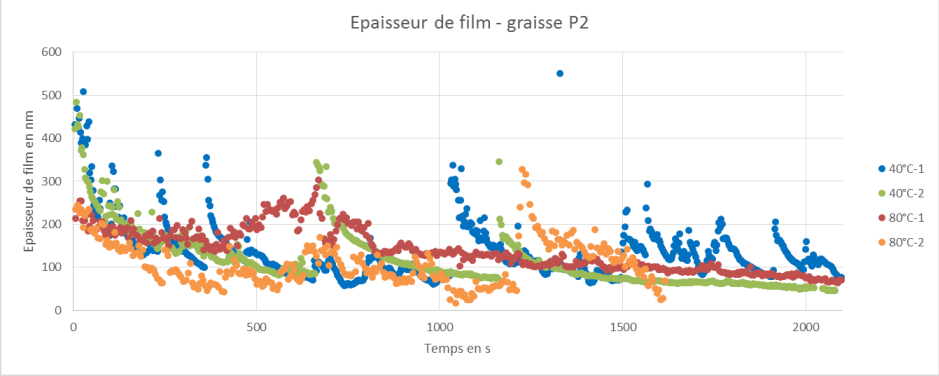


*Figure xxx : Epaisseur de film P2*

Premièrement, une graisse peut avoir plusieurs comportements répétables comme C1 à 40°C qui possède 3 comportements distincts. Le premier sépare correctement les surfaces aux alentours de 250 nm. Le second est à l'opposé, le film rétrécit et va à zéro endommageant le revêtement du disque en verre. Enfin le dernier oscille entre les 2. Ce comportement est très intéressant pour notre application. En effet, il signifie que le contact se réalimente en lubrifiant, protégeant ainsi les surfaces. Cette capacité est aussi présente pour la graisse P2 à 40°C et 80°C. Au contraire, ce comportement n'est pas visible en présence de la graisse P1. A 40°C, la graisse va assez rapidement à zéro sans jamais réalimenter le contact. A 80°C, à l'inverse des idées préconçues, la graisse P1 fournit un film plus épais qu'à 40°C. Ainsi, le processus d'usure peut être représenté par la figure xxxi.

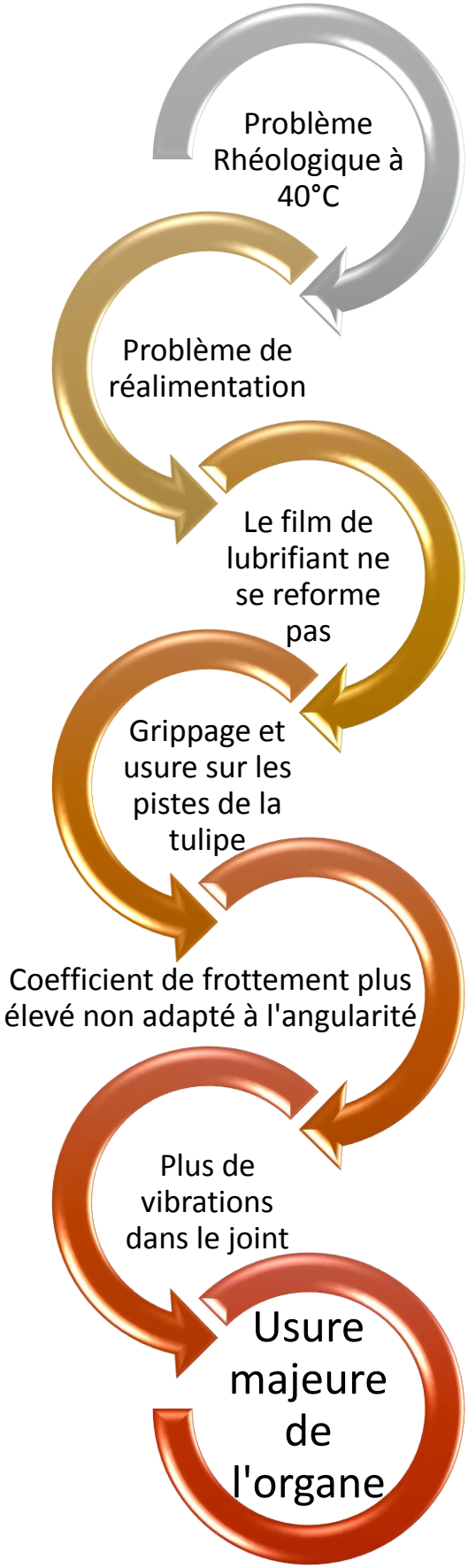


*Figure xxxi : Processus d'usure*

**Conclusions**

Un joint homocinétique reste une partie très importante du véhicule. Sa conception, utilisée depuis des années n'a pas beaucoup évolué. Par contre, les challenges relevés par les constructeurs automobiles ont, eux, évolué, notamment avec un changement de style avec une transformation des berlines vers des véhicules rehaussés type SUV en Europe. Ces changements ont demandé quelques modifications de la transmission avec notamment des angles de brisure de transmission plus élevés. En plus de l'objectif premier d'une durabilité accrue des transmissions, un autre paramètre est entré en jeu : celui du rendement des transmissions et de la chasse aux pertes. Ainsi apparait la nécessité de minimiser les frottements dans les joints homocinétiques.

Ce travail a été l'objet d'une approche expérimentale dont les moyens ont été exposés. Ils permettent de fournir des données répétables et fiables. De plus, un nouveau moyen expérimental a été créé pour cette étude afin d'observer le contact à l'intérieur de la tulipe tout en gardant son entièreté.

La caractérisation du contact a permis d'identifier les grandeurs. Pour commencer, la pression a été calculée à l'aide de la théorie de Hertz. Ensuite, la cinématique a été déterminée. Pour finir, afin de caractériser expérimentalement le glissement, l'exploitation du banc d'observation spécialement créé a été effectuée. Celui-ci a permis de prouver la nécessité d'avoir la bonne quantité de lubrifiant à l'intérieur du joint mais il a aussi permis de quantifier le taux de glissement en fonction de l'angularité de la transmission. Il permet alors un premier pas vers l'optimisation du rendement de la transmission.

Avec toutes ces données, il s'est avéré nécessaire de s'intéresser au lubrifiant lui-même. Quatre lubrifiants ont été étudiés afin de dissocier les différents facteurs. Grâce à des tests réalisés sur des organes entiers par le Groupe PSA, de vrais résultats d'usure étaient disponibles afin de réaliser et valider les essais laboratoires. La graisse a été étudiée à basse température mais aussi à une plus haute température correspondant davantage à un long roulage véhicule. Cela a permis d'identifier les rôles de chaque composé de la graisse dans le coefficient de frottement de cette dernière. De plus, ces essais ont prouvé que la cause de l'usure n'était pas directement liée à la composition chimique de la graisse. Cette différence entre les résultats d'usure banc-laboratoire et banc-organe PSA a conduit à une étude plus poussée de l'usure.

En s'appuyant sur les résultats précédents, un changement d'hypothèse a été considéré. Celui-ci a alors permis d'opérer un changement dans les résultats d'usure obtenus. En effet, à basse température, l'une des graisses montre des dégradations de surfaces répétables durant les essais, ce qui n'arrive pas sur les autres graisses ou à 80°C. Ces résultats corrèlent parfaitement à ceux issus du banc-organe du Groupe PSA. Il est alors envisageable d'explorer la rhéologie de la graisse afin de prouver qu'il s'agit du comportement mécanique de la graisse qui induit l'usure. En s'appuyant sur cette investigation, il a été montré un comportement particulier à 40°C de la graisse posant problème sur le test précédant. Cette dernière présente un seuil d'écoulement plus faible que les autres ainsi qu'une difficulté à passer du comportement solide à liquide. Afin d'observer ce que ce comportement implique dans la lubrification, une étude de l'épaisseur de film dans le contact a été mené en utilisant un tribomètre couplé à de l'interférométrie. Ces tests ont en particulier montré une incapacité de cette graisse à réalimenter le contact en huile à 40°C impliquant une absence de lubrification. C'est ce phénomène qui crée l'usure sur le véhicule.

**Perspectives**

Comme suggéré dans la conclusion, la perspective d'évolution des joints homocinétiques n'est pas très grande en raison notamment des contraintes de coûts du secteur automobile. De plus, les joints actuels remplissent très bien leurs fonctions. Cependant, un travail et une optimisation du lubrifiant est possible comme l'indique le travail mené précédemment. Pour éviter de nombreux essais coûteux, l'idée d'un banc dédié a émergé. Le concept du banc est de reprendre la cinématique d'un joint homocinétique tripode et de l'intégrer au sein d'un tribomètre. L'objectif de ce banc est de pouvoir observer la répartition de graisse dans le contact grâce à l'interférométrie. Il doit aussi pouvoir mesurer le coefficient de frottement afin de simuler les forces axiales générées par la transmission responsable de potentielles vibrations.

C'est pourquoi le banc XEHD a été développé et breveté.


*Figure xxxii: Banc XEHD*

Ainsi, 2 modes de fonctionnement ont été imaginés :

- Mode usure : en utilisant un disque en verre et un galet en acier, il est possible de détecter les sous-alimentations pendant un test, en regardant les vidéos qualitativement, en fonction de l'angularité,
- Mode qualification graisse : en utilisant un disque en acier et un galet en acier, il est possible d'obtenir le coefficient de frottement en fonction de l'angularité de la transmission.

Ce banc fournit alors un outil précieux aux fabricants de graisse et constructeurs automobiles pour concevoir les voitures de demain.

FOLIO ADMINISTRATIF

THESE DE L'UNIVERSITE DE LYON OPEREE AU SEIN DE L'INSA LYON

NOM : RIPARD DATE de SOUTENANCE : 25/10/2019

Prénoms : Valentin

TITRE : Tribological characterization of greased drive-shaft: evaluation of component durability

NATURE : Doctorat Numéro d'ordre : 2019LYSEI083

Ecole doctorale : MEGA N°EDA 162

Spécialité : Génie Mécanique

RESUME :
La modification des besoins clients amène les constructeurs automobiles vers de nouveaux challenges. En effet, en Europe notamment, les véhicules rehaussés type SUV sont de plus en plus populaires. Or, ces véhicules impliquent une modification de l'implantation des transmissions mécaniques. Ces dernières possèdent alors une angularité plus élevée que pour des berlines par exemple. Cette modification a alors 2 impacts : l'augmentation du glissement dans la transmission ainsi que son influence sur la durabilité des composants.
La modification de l'angularité demeure un des enjeux majeurs de ces dernières années pour les constructeurs. Son augmentation influe sur le rendement des transmissions. Or, avec des normes environnementales de plus en plus contraignantes mais aussi une hausse du prix du pétrole, cet axe d'amélioration représente un facteur d'attractivité pour les constructeurs.
De plus, la durabilité des organes reste primordiale. Une voiture se doit d'avoir une transmission fiable ne nécessitant, pour les joints homocinétiques, aucun entretien durant la vie du véhicule. C'est sur ce dernier axe que les travaux suivants ont majoritairement porté.
L'objectif de ce manuscrit est de comprendre le mécanisme d'usure des joints homocinétiques côté boîte, dit tripode. Une analyse de la cinématique a d'abord été menée afin de reproduire les contacts sur bancs d'essais. Elle s'est appuyée sur des données issues de la bibliographie mais aussi sur une simulation de la dynamique des solides. De plus, la création en fabrication additive d'un banc d'observation a permis d'obtenir de façon expérimentale le glissement dans cet organe de transmission.
Par la suite, une caractérisation des graisses de transmission a été effectuée afin de connaître les coefficients de frottement induisant le niveau de vibrations de la transmission pour un client. Ces derniers sont essentiels pour juger l'efficacité énergétique de l'organe.
Enfin, une étude de l'usure a permis d'expliquer les mécanismes de défaillance de la lubrification avec des graisses à partir des propriétés mécaniques. Cela permet alors de comprendre les données clés afin de choisir une graisse assurant une durabilité maximale des organes de transmission et remplissant alors un des deux enjeux cités ci-dessus.
Pour l'avenir, un banc de caractérisation des lubrifiants spécialement conçu pour les contacts de joint tripode a été créé. Il permettra ainsi de caractériser de façon plus complète les lubrifiants du futur pour cet organe essentiel d'une voiture.

MOTS-CLÉS :
Joint homocinétique, tripode, Automobile, Graisse, transmission mécanique, tribologie

Laboratoire (s) de recherche :
LaMCoS
LTDS

Directeurs de thèse :

Professeur Fabrice Ville
Professeur Fabrice Dassenoy

Président de jury :

Professeur Jorge Seabra

Composition du jury :

Agnes Fabre, Professeur Francesco Massi, Pierre Charles, Clotilde Minfray, Michal Ruzek